

## CATALYTIC ASPECTS OF SYNTHETIC FUELS FROM COAL

G. Alex Mills

Energy Research and Development Administration -  
Fossil Energy  
Washington, D. C. 20545

It is appropriate that this symposium honoring Dr. Storch should focus on catalysis, a field in which he made so many contributions and in which he published widely, most recently posthumously in the comprehensive review with Dr. William Wu (1). It was my privilege to know Henry Storch and to be greatly impressed by his high scientific standards and his creative research accomplishments. One of his greatest contributions was in attracting to the Bureau of Mines and training highly competent scientists and engineers who still constitute a research resource of great present national value and who, in a real sense, are continuing his research efforts.

I am greatly honored to be the recipient of the 1975 Storch Award for advancement of coal chemistry. Until 1968, my work involved primarily petroleum research. This year's award is a further sign of the integration of coal and petroleum chemistry into a single more fundamental field of the science of fossil fuel energy. Also, this award more than usually is a recognition of the contributions of my colleagues, particularly those in the Bureau of Mines Laboratories (now the Energy Research and Development Administration) since this is where recent experimental work was carried out.

The following papers in the symposium deal with specific topics of synthetic fuels and chemicals from coal. It is my privilege to discuss certain aspects of catalysis research which seem important to draw to your attention. For this purpose, research programs in which I have been involved will be used to illustrate ideas believed to be of catalytic significance including implications for the future.

Coal Liquefaction

Catalysis is vitally needed for the success of each of the four generic coal liquefaction processes--pyrolysis, solvent extraction, direct hydroliquefaction, and indirect synthesis (from CO + H<sub>2</sub>). Liquids produced by pyrolysis and by solvent extraction require catalytic refining to remove unwanted constituents (sulfur, nitrogen and oxygen) and to upgrade them to the proper boiling point and, if the desired product is gasoline, to provide the suitable octane number quality.

Pyrolysis

An early catalytic coal project concerned the cracking/refining of tar produced by low temperature pyrolysis of coal. It was found that active catalysts suitable for cracking petroleum produced very high coke yields but greatly improved results could be obtained by using

very low activity catalysts. This type of catalyst provided the best balance of reactions for cracking of coal tars, which have a high tendency to coke.

In a similar situation--cracking petroleum residua--the use of a low activity cracking catalyst was found to give the best products distribution including lowest coke. This was developed to a commercial scale--the Houdresid Process (2). In this case, a relatively large amount of steam was used with the reactants to assist in desorbing reactive fragments (3).

Now, it is important to recognize that frequently in the application of catalysis, it is necessary to balance the kinetics of several reactions proceeding simultaneously. For both coal and coal derived liquids, it is desired to carry out molecular cracking and yet to avoid polymerization (especially of asphaltenes) which lead to coke formation, Figure 1a and 1b. Thus, the functional properties of the catalyst must be balanced and conditions of operation, notably temperature, must be adjusted so as to accomplish cracking but avoid coking.

### Litol

Another experience in coal catalysis was the development of a catalyst to upgrade the "light oil" produced in conventional high temperature coking of coal. (Incidentally, it is of practical significance that one fifth of all coal mined in the United States is employed in the production of metallurgical coke, vital in the manufacture of steel.) The so called secondary light oil, boiling about the 140 - 300°F range, contains, beside benzene, higher aromatic homologs, sulfur containing compounds, especially thiophene, as well as paraffins. For high quality benzene required by the chemical industry, even 0.1 percent paraffins are too much and the sulfur content must be reduced to less than one ppm. In the LITOL process developed at the Houdry Laboratory, light oil and hydrogen are passed at high temperature and pressure over a fixed bed of catalyst. Sulfur compounds are converted to H<sub>2</sub>S (C<sub>6</sub>H<sub>4</sub>S thiophene + H<sub>2</sub> → C<sub>4</sub>H<sub>10</sub> + H<sub>2</sub>S), paraffins to gases (C<sub>4</sub>H<sub>16</sub> + H<sub>2</sub> → C<sub>3</sub>H<sub>8</sub> + C<sub>4</sub>H<sub>10</sub>) and some hydrodealkylation occurs (C<sub>6</sub>H<sub>5</sub>CH<sub>3</sub> + H<sub>2</sub> → CH<sub>4</sub> + C<sub>6</sub>H<sub>6</sub>).

The chemical constituents of a typical charge and product are given in Table 1 (4). The benzene product is of 99.94 percent purity or better and contains less than 0.05 ppm CS<sub>2</sub>. The kinetics and reaction mechanism sequence for hydrodealkylation as well as process engineering have been described (5).

Concurrent with process development, it was necessary to produce a catalyst with suitable activity selectivity and stability. Stability was a special problem because of the relatively high temperatures used.

As the result of systematic studies of the effect of variables outlined above plus some inventive ideas as how to prevent crystal growth (leading to inactivation), a catalyst was developed having performance life of several years and which is in commercial use internationally (cf. 6).

	<u>MOLES</u>	
	<u>FEED</u>	<u>PRODUCTS</u>
BENZENE	160.6	175.6
TOLUENE	23.7	17.1
XYLENE	6.6	1.4
STYRENE	2.4	
INDENE	1.8	
C <sub>9</sub> + AROMATICS	0.7	
PARAFFINS & OLEFINS	1.1	
THIOPHENE	2.1	
C <sub>1</sub> to C <sub>4</sub>		53.7
H <sub>2</sub> S		2.1

TABLE 1. LITOL PROCESS CHEMICAL BALANCE

The systematic research program measured and co-related preparational methods with physical, chemical, and catalytic properties. Preparational variations are:

- o major constituents  $\text{Cr}_2\text{O}_3$ ,  $\text{Al}_2\text{O}_3$  and minor, eg.,  $\text{Na}_2\text{O}$ ,  $\text{SiO}_2$
- o method of preparation - coprecipitation, dipping
- o conditions of drying and calcining - time, temperature, atmosphere
- o pellet formation

Physical and chemical properties include:

- o crystal structure, surface area, pore volume, pore size distribution
- o pellet strength
- o state of surface oxidation and of acidity by oxygen chemisorption, iodine and base titration

A further variation in control of surface chemistry, and hence of catalytic properties, is by the addition of compounds added while in process, sulfur, ammonia, water, halides, etc.

To correlate the effect of preparation variations with catalytic properties, standardized catalytic tests were carried out, tests designed to provide diagnostic information. Model compounds tested individually can be used to determine dehydrogenation properties--cyclohexane, isomerization-cyclohexene, and dehydrogenation/isomerization interaction - methyl cyclopentane (7). Test conditions are chosen to yield less than equilibrium products. These tests can be correlated with catalyst preparation variables and with physical and chemical tests.

The point to be made is that the "art" of catalysis, important to success, is to recognize, measure, and control the critical importance of, for example, drying a gel when enormous structural changes occur which determine the character of the catalyst just as importantly as overall composition. Only a few attempts have been made to describe in a methodical manner techniques in catalyst preparation.

#### Coal Hydroliquefaction

A comparison of the chemical composition of coal, petroleum, and gasoline (Table 2) and molecular structure quickly identified from a chemical viewpoint the changes which are required to transform coal to petroleum products. In fact, five changes or steps are needed. First, it is necessary to transform coal into a liquid form, second to remove inorganic matter (ash), and third to remove S, N, and O heteroatoms and transform asphaltenes, usually by means of hydrogenation. Fourth, molecular size must be reduced (cracking) and frequently a fifth step is needed to increase the octane number of the gasoline produced (reforming). Bringing coal to a liquid state is relatively rapid, but the product formed is high in asphaltenes. It is the hydrocracking of asphaltenes which is slow. In actual practice some overlapping of reactions occurs in a single process step, e.g., partial cracking and hydrogenation occur during liquefaction. Figure 2, taken

TABLE 2. CHEMICAL COMPOSITION OF SOME COALS AND PETROLEUM

	Anthracite	Medium volatile bit.	High volatile A bit.	High volatile B bit.	Lignite	Petroleum crude	Gasoline	Toluene
C	93.7	88.4	84.5	80.3	72.7	83-87	86	91.3
H	2.4	5.0	5.6	5.5	4.2	11-14	14	8.7
O	2.4	4.1	7.0	11.1	21.3			
N	0.9	1.7	1.6	1.9	1.2	0.2		
S	0.6	0.8	1.3	1.2	0.6	1.0		
H/C atom ratio	0.31	0.67	0.79	0.82	0.69	1.76	1.94	1.14

Coal analysis on moisture- and ash-free basis. Ash content of coal 3 to 15 percent.

C-fraction aromatic = 0.7. Aromatic rings per cluster--not over 3.  $H_{arom}/H_{aliph} = 0.23$ .

H/C atom ratio of petroleum residua: asphaltenes 1.18, resin 1.47, oil 1.67.

from a review (8) which emphasizes novel catalysts, also depicts how three types of liquefaction processes accomplish the required changes. Catalysts used by the Germans (9) as well as more modern petroleum catalysts are also specified.

#### Mechanism of Hydroliquefaction

An overall mechanism of catalytic hydroliquefaction of coal (10) which has much support for many catalyst systems views the primary step to be transformation of coal to asphaltenes. This can occur principally as a thermal reaction. The highly reactive fragments alternatively can polymerize or they can be hydrogenated to stable products if suitable catalytic circumstances are provided (Figure 3). The catalyst must be able to provide rapidly activated hydrogen to the fragments. Of course, additional transformations can occur on the catalyst surface, such as isomerization and/or cracking. According to this scheme, the amount of benzene insolubles, asphaltene and oil in the product depend upon the relative rates of splitting, hydrogenation-stabilization of fragments, and polymerization of fragments. The product distribution should correspondingly depend upon the presence of splitting catalysts, hydrogenation catalysts and high pressure hydrogen. Catalysts have been examined from this viewpoint as a means of determining how they function (10). The importance of knowing the actual at least major pathway is that it leads to ideas for improvements of key steps and control of proper transport, hydrogen accessibility, etc. The above pathway--thermal cracking and subsequent catalytic transformation--is consistent with the practice of using high hydrogen pressures (to provide for hydrogen availability) and avoidance of too high temperatures where the generation of reactive fragments would exceed the capability of the catalyst to handle them, especially as the rate of undesirable polymerization increases at a higher power.

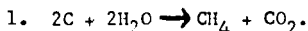
#### Synthoil

The growing capability to hydrotreat petroleum over fixed-bed catalysts, led to my suggestion that mixtures of coal in recycle oil could be directly liquefied over Co-Mo-Al<sub>2</sub>O<sub>3</sub> type catalysts. In the first experiments, to the surprise of some, runs of many hours were achieved without plugging the reactor and with promising conversion levels. Later concepts by others for operation with a reactor geometry and hydrogen flow rate so as to have gaseous turbulent flow demonstrated further advantages in catalyst stability and reactivity leading to the development of the Bureau of Mines Synthoil Process. A pilot unit capable of processing about eight T/D is being constructed. The development of the Synthoil process has been carried out vigorously by Aktar and Yavorsky (11) and their associates. They have described in detail the effect of process variables and provided an insight as to the reactions from the chemical/structural nature of the products.

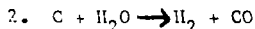
As far as the catalyst is concerned, some variations in composition and physical structure have been established, although it is fair to say that much remains to be established and there appear to be real opportunities for improvements.

Catalysis for the Integral Gasification  
Hydrocarbon Synthesis (IGHS)

The objective of the transformation of coal into hydrocarbons can be symbolized from a chemical viewpoint by the reaction

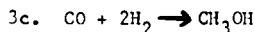
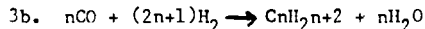
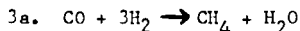


This reaction is balanced stoichiometrically and nearly so calorimetrically. However, as is well known, for the steam-carbon reaction to occur at sufficient speed to be of commercial interest requires a temperature of about 900°C. This high temperature results in primarily H<sub>2</sub> + CO as products since hydrocarbons are not sufficiently stable.



Reaction (2) is highly endothermic.

Three reactions between CO and H<sub>2</sub> which are of interest occur below about 500°C



These reactions are all exothermic.

If the steam-carbon reaction (1) could be accelerated so as to proceed sufficiently rapidly at 500°C, then products shown in reaction (3) could be produced simultaneously with improved thermal efficiency and also with lower equipment cost. Thus, there is a great opportunity for development of catalytic systems to speed up the steam-carbon reaction (12), (13).

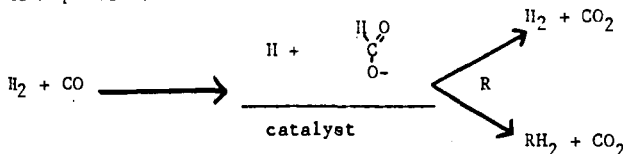
In our work on the Synthane coal gasification, the integrated gasification-hydrocarbon synthesis (IGHS) was accomplished to a substantial extent. This was achieved in part by the mechanical arrangement by using a fluid bed having two zones, the top or exit zone operating at about 1400°F as shown in Figure 4 (14). As an example, product gas from Illinois #6 coal on a mole percent basis is 17 CH<sub>4</sub>, 31 H<sub>2</sub>, 20 CO, and 32 CO<sub>2</sub>. On a CO<sub>2</sub>-free basis, the methane is 26 percent and is more than half the ultimate methane in the gas following methanation.

It is also believed that the mineral matter in the coal (Fe, Na, and Ca) plays a significant role in hydrocarbon synthesis. Haynes and Forney have shown the acceleration of gasification by adding inorganic salts (15). The rapid rate of gasification of lignite is at least partially attributable to its high alkali content. Possibly recirculation of high alkali ash will be a useful catalytic procedure.

An important objective should be to carry out coal gasification/hydrocarbon synthesis as a single integrated operation. While methane is desirable, it should also be possible to produce higher hydrocarbons (transportation of ethane and propane by pipeline is more economical than methane). It should also be possible to produce methanol and/or aromatic hydrocarbons integrated with coal gasification. The advantages

of manufacturing methane/methanol as co-products was previously pointed out (16).

An additional interesting point is that base catalysts are effective in the steam-carbon reaction. The petroleum industry rarely employs base catalysts. Base catalysts have many unusual characteristics, for instance, the nature of reactant/catalyst complex. Some evidence points to a formate ion intermediate, which results in either  $H_2 + CO_2$  or alternatively to a hydrogenated product  $RH_2$  if a hydrogen acceptor, R, is present. (CO-steam process)



Perhaps even more significant for coal chemistry is the concept that the catalyst is mobile. Normally in catalytic reactions, the reactants move to an active catalyst site. However, catalytic substances (alkali) having surface mobility or indeed having volatility can operate by moving the catalyst to solid char reactant. In a broad sense, this is an example of the unusual dynamic nature of catalysts proposed some years ago (17).

#### Future

There is a major recent national commitment to manufacture synthetic fuels from coal on a massive scale and in what must be regarded as essentially the immediate future. This commitment recognizes that a major research and development effort is vitally needed to accomplish the installation of processes which are of improved efficiency and cost. Federal funding is being provided and growing academic and industrial support. Several workshop meetings (18-22) have set forth the technical background, objectives, and priorities. Prominent in research recommendations are all aspects of catalysis. The importance in carrying out systematic diagnostic catalytic tests to follow variations in catalyst preparation seems to need more emphasis in comparison to the approach of fundamental knowledge of the physics of surfaces. At this stage of development, the reaction mechanism, including transport phenomenon, needs clarification in order to provide the basis for improving key slow steps. Also, new ideas are needed and must be tested in the areas of photo, bio or coordination, basic and mobile catalysts. Based on the advances made in applied catalysis in the last several decades in fuel chemistry, especially in the petroleum and petrochemical industry, it can be expected with confidence that major new catalytic developments will provide the technology for a highly effective synthetic fuels from coal industry.

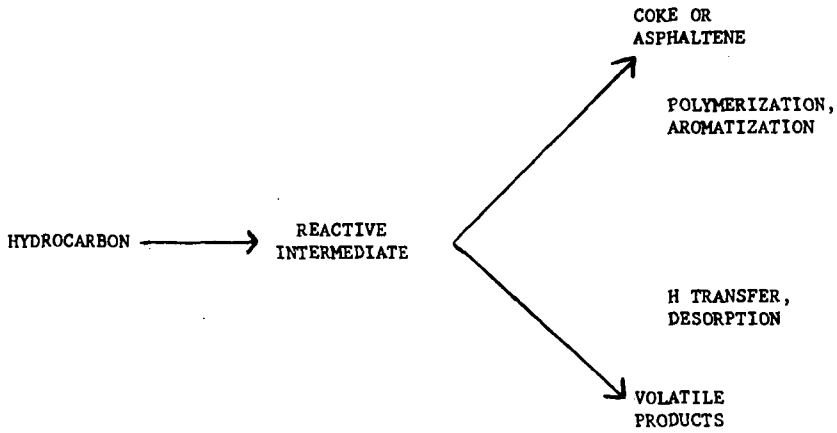


FIGURE 1a. ALTERNATE PATHS, REACTIONS CONTROLLING RELATIVE RATES

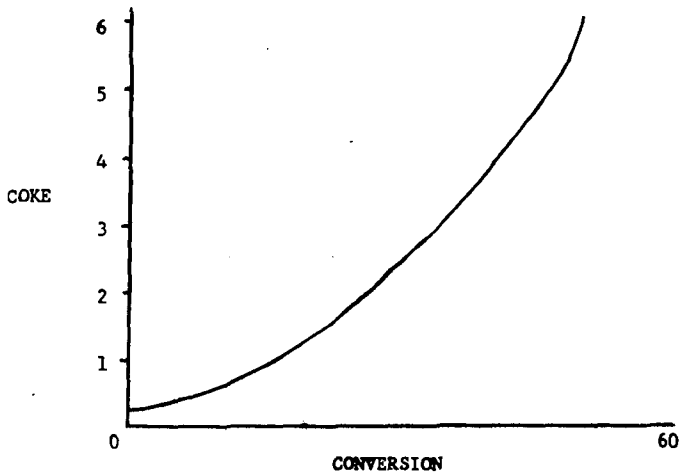


FIGURE 1b. INCREASE IN COKE IN CAT CRACKING

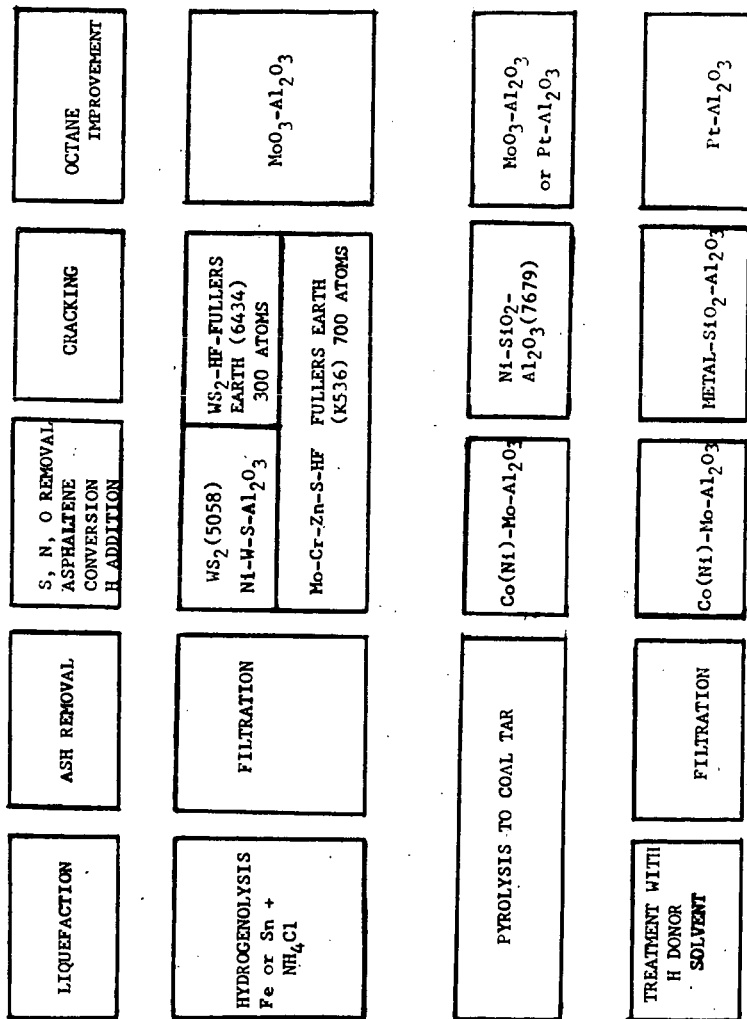


FIGURE 2. CONVERSION OF COAL TO GASOLINE

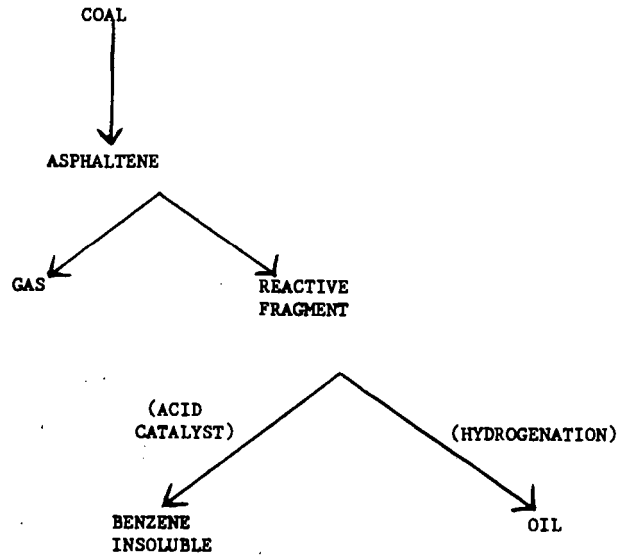


FIGURE 3. MECHANISM OF COAL CONVERSION

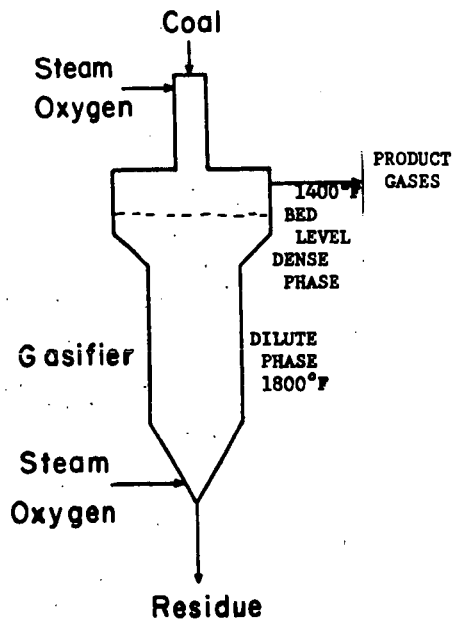


FIGURE 4.  
SYNTHANE GASIFIER TEMPERATURE PATTERN

## REFERENCES

- (1) Wu, W. R. K. and Storch, H. H., U.S. Bureau of Mines Bulletin 632, Washington, D. C., 1968.
- (2) Dart, J. C., Mills, G. A., Oblad, A. G., and Peary, C. C. "Houdresid Converts Crude Residua into Profitable Products." Oil and Gas Journal, May 1955.
- (3) Mills, G. A., Milliken, T. H., and Stevenson, D. H. "Cracking of Residual Oils Containing Asphaltic and Metallic Contaminants." U.S. Patent 2,914,459
- (4) Anon. Litol Process Hydrocarbon Processing.
- (5) Logwinuk, A. K., Friedman, L., and Weiss, A. H. "The Houdry Litol Process." Erdol and Kohle, July 1964.
- (6) Cornelius, E. B., Milliken, T. H., and Mills, G. A. "Stabilized Dehydrogenation Catalyst." 2,945,823
- (7) Mills, G. A., Heinemann, H., Milliken, T. H., and Oblad, A. G. "Houdriforming Reactions - Catalytic Mechanism." Ind. Eng. - Chem. 45, 134, 1953.
- (8) Mills, G. A. "Conversion of Coal to Gasoline - New Catalytic Concepts." Ind. Eng. Chem. 61, No. 7, 6, 1969.
- (9) Donath, E. E. "Chemistry of Coal Utilization." Lowry, H. H., Ed., Sup. Vol., Chapter 22, Wiley, New York, 1963.
- (10) Weller, S. W. "Catalysis." Emmett, P. H., Ed. Reinhold, New York, 1956.
- (11) Aktar, S. and Yavorsky, P.
- (12) Mills, G. A. "Future Catalytic Requirements for Synthetic Energy Fuels." Preprints, Division of Pet. Chem., ACS, Vol. 17, March 1972.
- (13) Mills, G. A. "Gas from Coal - Fuel of the Future." Environmental Science and Technology 5, No. 12, 1,178, 1971.
- (14) Mills, G. A. "Progress in Coal Gasification - U.S. Bureau of Mines." 3rd AGA Synthetic Gas Symposium, November 1970.
- (15) Haynes, W. and Forney, A.
- (16) Mills, G. A. and Harney, B. M. "Methanol--the New Fuel From Coal." Chem. Tech., p. 26, January 1974.
- (17) Milliken, T. H., Mills, G. A., and Oblad, A. G. "The Chemical Characteristics and Structure of Cracking Catalysts." Far. Soc. Symposium on Catalysis, p. 279, 1950.

- (18) Hightower, J., et. al. "Needs for Fundamental Research in Catalysis as Related to the Energy Problem." N.S.F., June 1974.
- (19) Libby, et. al. "Needs of the Department of Defense for Catalysis." RDA-TR-3501-002, 1973.
- (20) Boudart, M. "Catalysts as Materials." Center for Materials Research, Stanford University.
- (21) Weller, S. W., et. al. "Research in Coal Technology - the University's Role." OCR/NSF Workshop, 1974.
- (22) Gouse, S. W. and Rubin, E. S. "A Program of Research and Development and Demonstration for Enhancing Coal Utilization." Carnegie-Mellon, NSF-RANN, 1973.

CATALYTIC LIQUEFACTION OF COAL AND REFINING OF PRODUCTS. Alex G. Oblad, 209 Mineral Sciences Building, University of Utah, Salt Lake City, Utah, 84112.

The catalytic conversion of coal to liquids and hydrocarbon gases is an old art. It was practiced on a large scale in Germany prior to and during World War II. During the preceding years, the technology was largely developed by German scientists and engineers. Development has been active in other nations as well, including the United Kingdom, France, Italy, Poland, and others. The United States' effort goes back to 1936. Modern versions of these older catalytic coal liquefaction processes are in various stages of development. Some improvements have been made in processing steps and catalysts. Catalytic coal liquefaction is difficult, primarily because of numerous restraints such as transport, thermodynamic, kinetic, reactor environment and separation limitations. The present state of the technology and catalyst development will be discussed. An attempt will be made to indicate new process and catalyst possibilities for coal liquefaction.

## CATALYTIC SYNTHESIS OF CHEMICALS FROM COAL

Irving Wender

Pittsburgh Energy Research Center  
U. S. Energy Research and Development Administration  
4800 Forbes Avenue, Pittsburgh, Pennsylvania 15213

While the oil needed for the production of chemicals in the United States is only a small percentage of the total oil consumed, the manufacture and use of chemicals from oil has a tremendous impact on the economy of the country. A recent study by A. D. Little, Inc. (1) showed that the impact of a 15% decline in production of organic chemicals could result via a "multiplier" effect, in a loss of over 1,700,000 jobs and a \$65-70 billion loss in the production value of goods. One need only look around to see how pervasive and ubiquitous chemicals from oil are in our everyday life: our clothes, our automobile's interiors, all sorts of polymers, plastics, drugs and medicinals, tires, tubing (pipelines), building materials -- the list is very long and very important to the economic health and growth of the economy.

Another recent study (2) estimates that by the year 2000, perhaps as much as 42% of the projected U. S. petroleum and natural gas production (23.7 million barrels oil equivalent per day) will be needed to supply the projected U. S. demand for petrochemical feedstocks. Even if this projection is too high, there will still be a very large increase in the demand for petrochemicals. At present, only about 10% of our domestic oil and gas production would be needed to supply petrochemicals. But, the projected growth for petrochemicals is so large, Sherwin and Fuchs estimate that petrochemical demand in the year 2000 will require 10.3 million barrels oil equivalent per day. This is approximately equal to all of our present domestic production of crude oil.

To meet this demand for petrochemicals in the year 2000, it will be necessary to utilize non-conventional hydrocarbon sources, such as coal and shale oil, for the production of petrochemical feedstocks. Coal, which comprises over 80% of the known recoverable fossil fuel reserves in the United States, is the most likely candidate as the "chemical resource material of the future." Figure 1, part of which is from their paper, shows how primary and intermediate organic feedstocks can be produced starting from coal.

This paper is concerned chiefly with the catalytic synthesis of chemicals from coal. While it is not likely that coal or any other new source will be used for chemicals for possibly five or ten years (extensive manufacture of chemicals from coal, except via high-temperature carbonization, will not occur for at least a decade), this paper endeavors to point out the routes to chemicals from coal, emphasizing those that involve the use of catalysts.

The "Structure" of Coal

We have a good idea, after a vast amount of research, of the structures of the myriads of compounds found in crude petroleum. Coals, however, differ more widely in composition than do petroleum crudes. In addition, the physical disadvantages of coal relative to petroleum are that it is solid and has a high ash content, which ranges from a few percent to 20% or more. It will be of help to understand the constitution of coal; in this way, we will know how to process it to chemicals. What is surprising is that coal, in spite of its complexity, often behaves as you would expect an aromatic or hydroaromatic organic compound to behave.

Figure 1. Production of Primary and Intermediate Organic Chemicals From Coal

**GASIFICATION:** Synthesis gas,  $H_2 + CO \rightarrow$  Methanol  $\rightarrow$  Ethanol; Acetic Acid; Olefins, Paraffins, Aromatics  
 $\rightarrow$  Fischer-Tropsch synthesis of hydrocarbons and oxygenates

$\rightarrow$  Ethylene glycol + other polyols

$\rightarrow$  By-product Tar  $\rightarrow$  Benzene, Toluene, Xylenes

**LIQUEFACTION:** Syncrude  $\rightarrow$  Processed to Chemical Feedstocks

Aromatics from Hydrocarbonization

**OXIDATION:** Benzenepolycarboxylic Acids ("Coal Acids")  $\rightarrow$  Phthalic, Isophthalic and Terephthalic Acids

**CARBONIZATION:** High-temperature carbonization  $\rightarrow$  Aromatics, Phenols, Tar Bases

Low-temperature carbonization  $\rightarrow$  Aromatics, Phenols, Olefins

ACETYLENE from  
Calcium Carbide  
or Plasma Arc:

$C_2H_2 \rightarrow$  Chloroethylenes; Vinyl chloride; Vinyl acetate; Acrylonitrile

We know enough technology to be able to obtain chemicals from almost any carbon-containing material, from wood to carbon dioxide, and everything in between. But the nature of the substrate, in this case coal, will strongly influence its treatment to yield chemicals. So let us first look at the "structure" of coal.

There has been a very large effort made over many years to determine the structure of coal. The full weight of the traditional method; elemental analyses, qualitative chemical tests and degradative reactions, plus modern tools of instrumental analysis have been turned loose on coal. An examination of the literature reveals, however, that most of this attack has been aimed only at the constitution of bituminous coals, usually of 81 to 86% carbon on a moisture and ash-free (maf) basis. Very little is known about the structure of subbituminous coals or of lignite, although these constitute the major coal reserves of the United States. It is interesting to note that, while about three-quarters of our coal reserves are west of the Mississippi (mostly lower rank coals, subbituminous and lignite), about 70% of the coal presently used in the United States comes from the higher rank bituminous coals found east of the Mississippi.

Given (3) has developed a structural model which has the elementary composition of a vitrain of a carbon content of 82%. This model is a convenient visualization of certain analytical data. It is useful, especially for discussion purposes, and I would have hoped that the same type of convenient visualization could be done for higher and especially lower ranks of coal. However, I tend not to use the type of model discussed above. Instead, after working with coal for some time, I find myself choosing what amounts to a representative small portion of such a model for chemical guidance. Four ranks of coal are usefully distinguished in this way, with coals of intermediate rank having intermediate structure. I will only mention the fifth rank, anthracite. Anthracite has a large condensed polynuclear structure, usually contains little ash, and has a low oxygen and sulfur content. It makes an excellent fuel and is in great demand for combustion and metallurgical purposes. But it is an expensive coal, and found only in certain areas of the East. Because of its structure, it is not easily processed to chemicals; it can be gasified, but it is almost impossible to convert into a liquid.

The structures shown in Figures 2-5 are not coal models. But they represent, to me at least, a convenient way of cataloging the chemical structures so that the reactions of the various ranks of coals can be understood, at least in a preliminary way. They are useful as an aid to memory and a basis for prediction; they are, in short, frames of reference. The four ranks of coals given in Figures 2-5 are a low-volatile bituminous coal (coal A), a high-volatile A bituminous coal (coal B), a subbituminous coal (coal C) and a lignite (coal D). The analytical data given for each coal are the results of an analysis of an actual coal sample. It is possible to discuss a number of reactions of coal in terms of these representations. The structures help to understand the way the ranks of coal react under different conditions; we can also use some of the reactions to support or attack the validity of these structures. At various points in this paper, I shall refer back to these representations for the different ranks of coal.

#### Gasification of Coal to Synthesis Gas and Production of Chemicals from Syngas

There are five general routes available to convert coal to chemicals. The first that I wish to discuss is the production of chemicals from synthesis gas -- that is, mixtures of hydrogen and carbon monoxide. These gases are produced by the gasification of coal. After leaving the gasifier, the syngas mixture will be cleaned, catalytically shifted via the water gas shift reaction to the desired hydrogen-to-carbon monoxide ratio, and the carbon dioxide and hydrogen sulfide (and other sulfur compounds) removed to the levels needed for further catalytic reactions.

## Pocahontas No. 3 Bed, W. Va. (lvb)

	<u>dry</u>	<u>maf</u>
C	83.8	90.7
H	4.2	4.6
O	2.6	2.8
N	1.2	1.3
S	0.6	0.6
Ash	7.6	-
Volatile Matter	17.3	18.7
Btu per pound		15,660

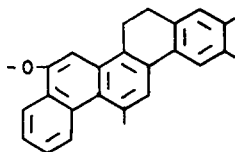


Figure 2 - COAL A  
Low-volatile  
bituminous

## Pittsburgh Bed (hvab)

	<u>dry</u>	<u>maf</u>
C	77.1	84.2
H	5.1	5.6
O	6.4	6.9
N	1.5	1.6
S	1.5	1.7
Ash	8.4	-
Volatile matter	36.5	39.9
Btu per pound		15,040

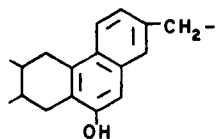


Figure 3 - COAL B  
High-volatile A  
bituminous

## Mammoth Bed, Wyo. (Subbituminous A)

	<u>dry</u>	<u>maf</u>
C	72.9	76.7
H	5.3	5.6
O	14.8	15.5
N	1.2	1.3
S	0.9	0.9
Ash	4.9	-
Volatile Matter	41.5	43.6
Btu per pound		13,490

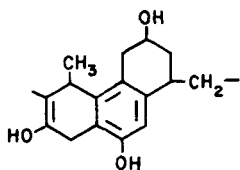


Figure 4.-COAL C  
Subbituminous coal

## Lignite, Beulah-Zap Bed, N. D.

	<u>dry</u>	<u>maf</u>
C	64.5	72.6
H	4.3	4.9
O	18.0	20.2
N	1.0	1.1
S	1.1	1.2
Ash	11.1	-
Volatile Matter	40.8	45.9
Btu per pound		12,150

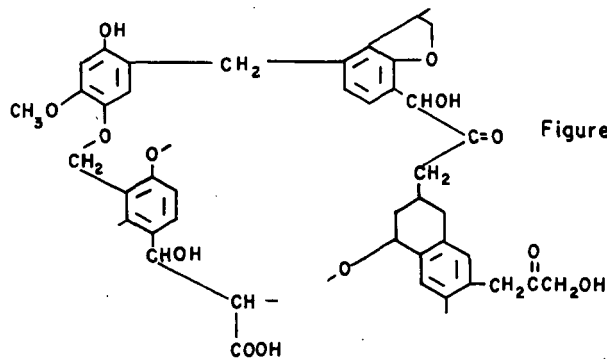


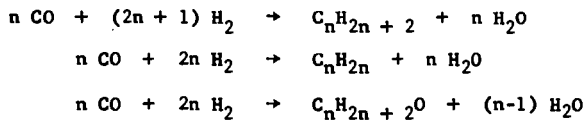
Figure 5.-COAL D  
Lignite

One large-scale, commercially proven route to take from here is the production of methanol. The present U. S. production of methanol is about 10,000 tons/day, using almost entirely syngas obtained by the steam reforming of methane over a nickel catalyst. A zinc chromite catalyst is used for methanol synthesis  $\text{CO} + 2\text{H}_2 \rightarrow \text{CH}_3\text{OH}$  at pressures near 4000 psi and temperatures near 350°C, or a copper-zinc oxide-on-alumina catalyst is used at lower pressures (800 to 1500 psi) and temperatures near 250°C (4). Given a clean synthesis gas derived from coal, it is anticipated that the large scale production of methanol from coal can be done in this way.

Because of the large production that will be called for as methanol produced from coal becomes necessary as a chemical feedstock, two improvements in methanol catalysts would be desirable. Both are being studied by various investigators. Zinc chromite and (especially) copper-zinc oxide-on-alumina are sensitive to sulfur poisoning. A methanol catalyst more tolerant to sulfur compounds in the feed gas would be very useful with coal-derived synthesis gas.

The methanol synthesis is a highly exothermic reaction. Studies are being made using a three-phase reactor where synthesis gas contacts the catalyst in the presence of an inert liquid which serves to remove the heat of reaction (5). In this way, it is hoped that larger conversions per pass could be obtained than in the conventional gas-solid fixed bed reactor. Also, by varying the liquid in this reactor, it may be possible to produce some useful derivative of methanol from syngas directly.

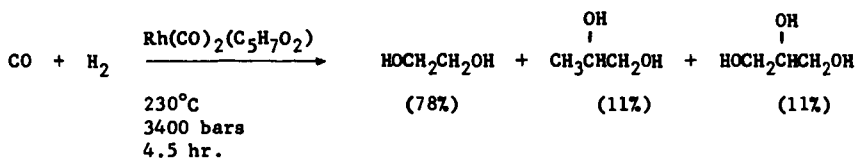
Another source of chemicals from coal-derived synthesis gas is the Fischer-Tropsch (FT) synthesis. This is being carried out in a small-scale commercial plant (5000 barrels/day) at SASOL in South Africa, mainly to produce fuels. In the FT synthesis as done at SASOL,  $\text{H}_2 + \text{CO}$  mixtures react over iron catalysts to produce mixtures of hydrocarbons and oxygenates. The reactions are



In the plant at SASOL, two types of reactors are used. One is a fixed bed reactor containing an iron catalyst and operates near 230°C and at pressures near 400 psi. The second is a "Synthol" entrained bed reactor operating at 330°C and 350 psi and uses a different type of iron catalyst specifically designed for this type of operation. As can be seen in Table 1, there is a great deal of difference in the product distribution from the different reactors (6). It is of interest to note that in their planned ten-fold expansion, SASOL intends to use only entrained bed reactors.

As shown by the data in Table 1, the choice of catalyst and operating conditions profoundly affects the product distribution in the FT synthesis. As a further example of this, in preliminary work at the Pittsburgh Energy Research Center of ERDA using an iron-on-silica-alumina catalyst, almost all of the hydrocarbons formed from syngas at 320°C were in the  $\text{C}_1$  to  $\text{C}_4$  range, primarily paraffins (7).

Ethylene glycol is another chemical which can be obtained by reacting equimolar amounts of carbon monoxide and hydrogen in the presence of rhodium dicarbonyl-acetylacetonate (8).



The polyols comprise 64% of the oxygenated products; the balance consists of methanol, water, and methyl formate. There is some evidence (9) that the pressure needed for this reaction can be lowered to at least 400 atmospheres, which would be a considerable improvement.

TABLE 1. Product distribution at SASOL from fixed bed and Synthol Fischer-Tropsch synthesis on iron catalysts

	Fixed bed reactor		Synthol reactor	
	Wt pct total	Wt pct olefins	Wt pct total	Wt pct olefins
Temperature, °C	220-240		320-340	
Pressure, bars	26		22	
H <sub>2</sub> /CO ratio in feed gas	1.7:1		3:1	
Primary products	Wt pct total	Wt pct olefins	Wt pct total	Wt pct olefins
C <sub>1</sub> .....	7.8	--	13.1	--
C <sub>2</sub> .....	3.2	23	10.2	43
C <sub>3</sub> .....	6.1	64	16.2	79
C <sub>4</sub> .....	4.9	51	13.2	76
C <sub>5</sub> -C <sub>11</sub> .....	24.8	50	33.4	70 <sup>a</sup>
C <sub>12</sub> -C <sub>20</sub> .....	14.7	40	5.1	60 <sup>a</sup>
> C <sub>20</sub> .....	36.2	~ 15	--	--
Alcohols, ketones .	2.3	--	7.8	--
Acids .....	--	--	1.0	--

<sup>a</sup> These fractions also contain appreciable amounts of aromatic compounds.

Mobil Research and Development Corporation under contract from ERDA is developing a catalytic process for converting methanol to gasoline. This will be a two-step process, in which methanol is first catalytically dehydrated to dimethyl ether. In the second step, over a zeolite catalyst, dimethyl ether is converted to hydrocarbons. Most of these hydrocarbons are in the C<sub>5</sub>+ range and the mixture contains appreciable quantities of aromatics. At present, the process is being optimized for gasoline production, but could conceivably be used as a means of producing chemical feedstocks starting with coal-derived methanol.

The reaction of methanol with carbon monoxide to form acetic acid is homogeneously catalyzed by either cobaltous iodide or an iodide-promoted rhodium carbonyl complex. The latter catalyst is more efficient since it allows the reaction to proceed at low pressures (200 psig), a temperature of 175°C, and a very high selectivity of methanol to acetic acid of 99% (10). The authors of this review paper state that "As coal replaces natural gas and petroleum as a source of petrochemical raw materials, the most important building block is expected to be synthesis gas... the methanol carbonylation route to acetic acid should enjoy an enviable raw material position in the transition from natural gas and petroleum to coal as a petrochemical raw material base."

The chemistry of this reaction has been studied in detail, and the reaction is believed to occur via the following steps. Methanol and hydrogen iodide react reversibly to form methyl iodide



which then reacts with the metal carbonyl, probably through oxidative addition, to form a methyl carbonyl complex



where M = Co or Rh and L is a ligand other than CO. The next step is the CO "insertion reaction"



This last complex then reacts with water to form  $\text{CH}_3\text{COOH}$ , HI, and regenerates the original complex,  $\text{M}(\text{CO})_x\text{L}_y$ .

The homologation of methanol to ethanol using synthesis gas and  $\text{Co}_2(\text{CO})_8$  as the catalyst was first reported in 1951 (11).

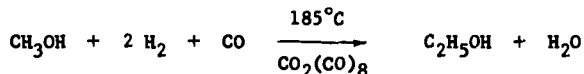


Table 2 gives reaction conditions and products formed in a batch autoclave experiment where 76% of the starting methanol had reacted. Work at the Pittsburgh Energy Research Center of ERDA is under way to improve the yields of this reaction (12). Gas chromatographic analysis of the reaction mixture shows that it can contain as many as 25 compounds. This indicates the need to find catalysts or conditions to make the reaction more selective; however, ethanol is the major constituent of the product, and would thus be a source of ethylene, based on coal-derived methanol as the raw material.

#### Chemical Refining of Coal Liquefaction Products

"Syncrude" obtained by the catalytic liquefaction (and hydrodesulfurization) of coal will also serve as a source of raw materials for the chemical industry. A review of coal liquefaction processes that can now be seriously considered as providing a supply of petrochemical feedstocks has been recently prepared (13). The processes can be divided into the following categories:

- Hydroliquefaction -- Solvent Refined Coal (SRC)
- Catalytic hydroliquefaction -- H-Coal, SYNTHOIL Process
- Pyrolysis -- COED
- Extraction (and hydrotreating) -- Cresap type plant
- Indirect -- Fischer-Tropsch (SASOL)

Products from these processes are broken down by boiling range (much in the way that petroleum fuels are considered) and, within each boiling range, hydrocarbon type analyses are given; light constituents are identified. One very important point that is mentioned is that coal liquids differ in their aromatic, naphthene and cycloparaffin content from similar petroleum fractions.

TABLE 2. Products from reaction of methanol with  $H_2 + CO$  at  $185^\circ C$  and 4000 psi using  $Co_2(CO)_8$  as the catalyst

	<u>Yields as percent of converted methanol</u>
Methyl formate .....	2.0
Methyl acetate .....	9.0
Ethyl alcohol .....	38.8
Ethyl acetate .....	6.3
Propyl alcohol .....	4.7
Propyl acetate .....	0.1
Butyl alcohol .....	0.9
Methane .....	<u>8.5</u>
Total .....	70.3
Water .....	90.8

Several specific petrochemicals which could be produced from these coal derived liquids are:

- Olefins, via steam cracking;
- BTX and naphthalene, recovered directly and via hydrocracking of heavy oils and extraction;
- Phenols, recovered directly; and
- Aromatic amines and N-bases, recovered directly.

O'Hara et al. present one possible scenario based on (economic) incentives to produce alternate petrochemical feedstocks from coal leading to the construction of a number of plants. This scenario requires facilities to process 100,000 tons per day (TPD) of coal in 1985, 270,000 TPD in 1990 and 570,000 TPD in 1995. They also present a conceptual scheme depicting a combination of process steps which include coking, hydrocracking, hydrodesulfurization, catalytic naphtha reforming, aromatics extraction, extraction and fractionation, and gas recovery and fractionation.

Table 3, taken from their paper, lists the potential for production of petrochemical feedstocks from coal, based on their assumptions in their studies. This estimate gives a potential supply of ethylene feedstock ranging from 20% in 1985 to 115% in 1995 of that used in 1974. Similarly, for naphtha feedstock, the range is from 82% (1985) to 470% (1995). Benzene production via coal liquefaction processes could range from 9% to 50% of 1974 volume. The authors summarize by stating that a significant portion of our petrochemical needs can be produced from coal liquefaction processes and that the potential should be further evaluated, and the economics should be studied in detail.

#### Chemicals by Oxidation of Coal to Benzenepolycarboxylic Acids and Their Selective Decarboxylation to Phthalic Acids

When coal is carefully oxidized, a mixture consisting largely of aromatic acids is produced. Two methods of oxidation have shown most promise, controlled air oxidation in the presence of alkali (14) and oxidation by nitric acid (15); the first method uses inexpensive oxidizing agents and is preferred. The oxidations were originally carried out to obtain structural information by examination of the fragments produced by oxidative cleavage of the large coal molecules.

TABLE 3. Examples of potential for production of petrochemical feedstocks from coal

Feedstock	1985		1990		1995	
	Millions of pounds per year	Percent of 1974 consumption	Millions of pounds per year	Percent of 1974 consumption	Millions of pounds per year	Percent of 1974 consumption
Ethane	2400	15	6500	40	13,700	90
Propane + LPG	3100	20	8300	55	17,600	115
Naphtha (Raffinate)	4500	80	12,100	220	25,500	470
Benzene	1000	9	2800	25	6000	50
Toluene	2800	40	7600	110	16,000	235
Xylenes	2100	45	5600	125	11,900	265

All aromatic compounds from toluene on up, on chemical oxidation, eventually yield benzenecarboxylic acids, which are then stable to further oxidation. Thus, toluene yields benzoic acid, p-xylene yields terephthalic acid, tetralin or naphthalene yield phthalic acid and anthracene yields pyromellitic acid.

Oxidative work has been used to show that coal has an essentially benzenoid structure. In going from coal structures D to A (Figures 2-5), the aromatic nature of the coal shows progressive development during natural maturing. It is not surprising that the ultimate yield of benzenepolycarboxylic acids (BPCA) is a function of the molecular structure of the coal. Coal A, a low-volatile bituminous coal with its highly aromatic structure containing some hydroaromatic linkages, would probably give the best yield of BPCA. Anthracite, with even more condensed polynuclear aromatic rings, would oxidize with greater difficulty to give a larger yield of mellitic acid (benzenhexacarboxylic acid). Coal B should oxidize at a greater rate than coal A with perhaps a lower yield of BPCA; aromatic rings containing phenolic groups tend to oxidize to quinones and then cleave. Coals C and D are more highly oxygenated, should oxidize rapidly but should not give acids with many carboxylic acid groups. See Table 4.

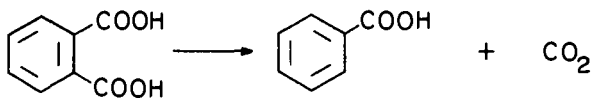
TABLE 4. Distribution of benzenepolycarboxylic acids from oxidation of coals with air and alkali

Percent carbon in coal, maf	Acids, percent			
	Tri	Tetra	Penta	Hexa
84	3	9	5	5
88	6	12	8	7
91	4	9	8	8
92	4	11	10	12
94.5	1	5	7	17

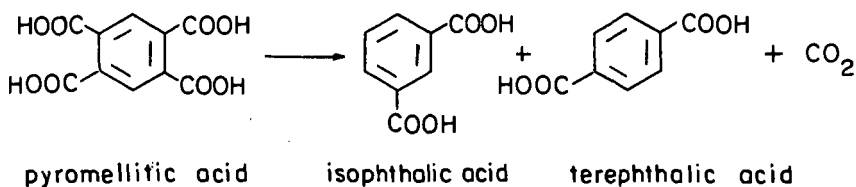
The product from the oxidation of coal with air and alkali was interesting enough for a large chemical company to do bench-scale work on oxidizing coal to coal acids (16). The product of this controlled air oxidation of a 90% carbon coal (coal A) consisted of a mixture of benzenepolycarboxylic acids (about 50% by weight of the coal) and other higher molecular weight, oxygenated materials of unknown structure. Potential uses were found for the whole mixture, but the crude product could not compete against the relatively pure compounds or mixtures usually demanded by our present sophisticated chemical industry. The possibility of using the benzenecarboxylic acids, once they had been separated from the rest of this material, has not been adequately investigated.

Though commercialization did not occur, interest in coal acids has remained high, and workers in laboratories scattered around the world have published on this topic in recent years (15-23). Analyses indicate that these coal acid mixtures may contain up to 95% benzenepolycarboxylic acid (BPCA), ranging all the way from phthalic acid to mellitic acid. Conversion of this complex mixture to a simple mixture with but few separable components would make oxidation of coal and its derivatives a promising route to valuable chemicals. This second step, the conversion of coal acids to a mixture rich in isophthalic and terephthalic acids, is feasible as a result of a catalytic reaction discovered at the U. S. Bureau of Mines (24).

Initially, it was found that when phthalic anhydride or phthalic acid was heated to 200°C in the presence of  $\text{Co}_2(\text{CO})_8$  and under pressure of synthesis gas ( $\text{H}_2 + \text{CO}$ ), it was converted quantitatively to benzoic acid.



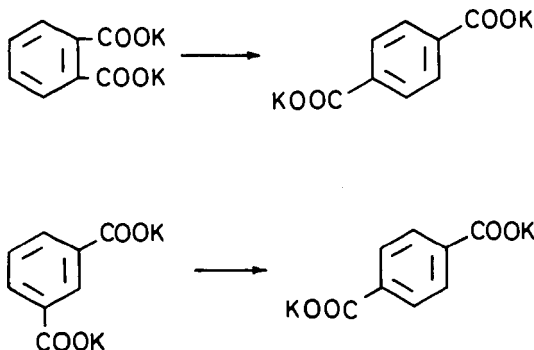
This contrasts with other decarboxylation procedures which yield only benzene from phthalic anhydride or acid. Further experiments established that benzenepoly-carboxylic acids, up to mellitic acid, could all be selectively decarboxylated by this same method to yield principally iso- and terephthalic acids, as shown for pyromellitic acid.



The decarboxylation occurs whenever there are two carboxyl groups on adjacent aromatic carbon atoms.

This decarboxylation provides a way of converting the previously mentioned mixture of aromatic polycarboxylic acids into a simple mixture containing large and recoverable amounts of isophthalic and terephthalic acids (17), both of which have expanding markets at the present time. The present source of these acids is the xylene fraction obtained by dehydrocyclization of petroleum feedstocks. Demands for low-lead, high-octane gasoline may result in shortages of xylenes. This factor, coupled with the shortage of domestic petroleum, may encourage the move to coal-based chemicals. Improved catalysts, formed by substituting tertiary alkylphosphine ligands for one or two of the carbon monoxides in  $\text{Co}_2(\text{CO})_8$ , have been found for the decarboxylation. These catalysts are more stable and more easily recoverable than is the unsubstituted catalyst (17). The decarboxylation has been carried out in the laboratory on several mixtures of coal acids obtained by alkaline oxidation of a low-volatile bituminous coal (coal A). Conversions of the BPCA to isophthalic and terephthalic acids have been high.

Another approach to the production of terephthalic acid from the BPCA is the Henkel Reaction, in which the dry potassium salts of the acids are heated to about 400°C in the presence of zinc or cadmium catalysts under 10 or more atmospheres of  $\text{CO}_2$ .



Yields approaching 95% have been obtained on a large scale. The process has been used on an industrial scale in Japan to produce terephthalic acid.

It is obvious that the oxidation of coal to BPCA is noncatalytic. But the two processes for obtaining individual compounds from the complex mixture involve intriguing catalytic reactions which merit further study. A review of the production of chemicals by oxidation of coal has been recently published (25).

#### Chemicals from the Carbonization of Coal

The traditional route to chemicals from coal, and the one first used, is to extract and purify the chemicals contained in the tars obtained by the coking of coal. The process is usually called coal carbonization and is carried out at temperatures of about 900-1000°C. Almost any coal heated to these temperatures will give the same products and we can consider coal carbonization to essentially be noncatalytic, although coal contains over 70 elements, with Na, K, Ca, Cl, Si, Fe and Ti present in significant amounts. Carbonization has been and still is an important source of chemicals since almost 90 million tons of coal were transformed into coke in 1974. (It is the second most important use of coal.) The most important chemicals obtained from coking processes are aromatic compounds (benzene, toluene, xylenes, naphthalene, phenanthrene, anthracene, etc.), phenols, and tar bases.

While coke is ordinarily obtained by carbonizing coal at 900-1000°C (high-temperature carbonization), low-temperature carbonization, ordinarily carried out at around 500°C, yields more tar and is a possible source of aromatic chemicals and olefins. Low-temperature carbonization was practiced in Europe and in this country some years ago but is not important today. The inorganic compounds in coal present may have some catalytic effect in low-temperature carbonization.

Of the many publications on carbonization products, review articles by Karr (26), Weiler (27), and Muder (28) are particularly worthwhile.

Acetylene from Coal

Acetylene can be made from coal via calcium carbide or in a plasma arc (29), both of which are noncatalytic processes. The chemistry of acetylene and the routes to various chemicals that can be made from acetylene (vinyl chloride, chloroethylenes, vinyl acetate, acrylonitrile, acrylates, etc.) are well known.

References

- (1) United States Petrochemical Industry: Impact Analysis, Arthur D. Little, Inc., November 1973, 15 pages.
- (2) M. B. Sherwin and W. Fuchs, Paper presented at the 79 National AIChE Meeting, Houston, Texas, March 16-20, 1975.
- (3) P. H. Given, Fuel, 39 147 (1960).
- (4) C. L. Thomas, Catalytic Processes and Proven Catalysts, Academic Press, New York, 1970, Chapter 14.
- (5) D. Blum and M. B. Sherwin, Paper presented at Division of Fuel Chemistry, 170th National Meeting American Chemical Society, Chicago, Illinois, August 1975.
- (6) C. D. Frohning and B. Cornils, Hydrocarbon Processing, 53 (11) 143-146 (November 1974).
- (7) R. A. Diffenbach, Pittsburgh Energy Research Center, ERDA, unpublished data.
- (8) W. E. Walker and R. L. Pruett, Belgian Patent 793,086 to Union Carbide.
- (9) A. M. Brownstein in Chem. Eng. News, March 31, 1975, pages 10-11.
- (10) R. P. Lowry and A. Aguilo, Hydrocarbon Processing, 53 (11) 103-113 (November 1974).
- (11) I. Wender, R. A. Friedel, and M. Orchin, Science, 113 206-207 (1951).
- (12) I. Wender, S. J. Metlin, and B. D. Blaustein, Pittsburgh Energy Research Center, ERDA, unpublished data.
- (13) J. B. O'Hara, N. E. Jentz, and J. E. Papso, Paper presented at the 79th AIChE National Meeting, Houston, Texas, March 1975.
- (14) R. C. Smith, R. C. Tomarelli, and H. C. Howard, J. Am. Chem. Soc., 61, 2398 (1939).
- (15) A. Benning, Brennstoff-Chemie, 36 38 (1965).
- (16) W. L. Archer, R. S. Montgomery, K. B. Bozer, and J. G. Louch, Ind. Eng. Chem., 52 849 (1960).
- (17) S. Friedman, S. R. Harris, and I. Wender, Ind. Eng. Chem. Prod. Res. Dev., 9 347 (1970).

- (18) J. E. Germain and F. Valadon, Bull. Soc. Chem. Fr. 1960, 11.
- (19) Aranda V. Gomez and Beltran F. Gomez, Combustibles, 22, 147 (1962).
- (20) Y. Kamiya, Fuel, 40 149 (1961).
- (21) J. Biner and A. Wieloposki, Koks-Smola-Gaz., 14 159 (1969).
- (22) C. Caneva and S. Fumasoni, Il Calore, 1966, 3.
- (23) E. I. Rukin, Khim. Tverd. Topl. 1969, 70.
- (24) S. Friedman, M. L. Kaufman, and I. Wender, Ann. N. Y. Acad. Sci., 145, 141 (1967).
- (25) A. E. Bearse, J. L. Cox, and M. Hillman, Production of Chemicals by Oxidation of Coal. Battelle Energy Program Report, March 31, 1975, 45 pages.
- (26) C. Karr, Jr., Low-Temperature Tar. Chapter 13 in Chemistry of Coal Utilization - Supplementary Volume, H. H. Lowry, editor, Wiley, New York, 1963.
- (27) J. F. Weiler, High-Temperature Tar. Chapter 14 in Chemistry of Coal Utilization - Supplementary Volume, H. H. Lowry, editor, Wiley, New York, 1963.
- (28) R. Muder, Light-Oil and Other Products of Coal Carbonization. Chapter 15 in Chemistry of Coal Utilization - Supplementary Volume, H. H. Lowry, editor, Wiley, New York, 1963.
- (29) R. Gannon and V. Krukonis, Final Report, Arc-Coal Process Development, Contract 14-01-0001-493, April 19, 1972, Office of Coal Research, Washington, D. C.

The Use of Catalysts in Coal Gasification. James L. Johnson, Institute of Gas Technology, 3424 S. State Street, Chicago, Illinois 60616.

There is substantial support for the view that catalysts will play an important role in future processes to convert coal to high-Btu gases and hydrocarbon liquids via gasification. Although processes currently being developed for conversion of coal to synthetic pipeline gas (methane) necessarily employ catalysts for shift and methanation external to direct gasification stages, experimental investigations have shown that catalysts can also significantly enhance reaction rates and product selectivity during actual gasification. The great majority of catalytic investigations, however, have been conducted at low pressures using relatively low reactivity carbonaceous solids without volatile matter, and only a limited amount of information is available related to catalysis of coals at elevated pressures. Certain aspects of available chemical information pertinent to direct coal gasification catalysis, as well as shift and methanation catalysis, are reviewed with a major objective of pointing out potentially useful areas for future research to aid in the development of improved coal gasification processes through the use of catalysts.

## FORM-COKE REACTIVITY AND IT'S EFFECT ON BLAST FURNACE OPERATION

Robert T. Joseph

FMC Corporation  
Chemical and Development Center  
Princeton, New Jersey 08540

A study was carried out to compare the effect of carbon reactivity on the operation of commercial iron blast furnaces. Two cokes, produced via by-product oven technology with a relative reactivity in carbon dioxide of one where contrasted with a carbon reductant produced as a form-coke briquet from an Intermountain, noncoking coal with a relative reactivity of twenty. The work was carried out both in a British and an American production blast furnace operating under commercial conditions across a protracted period. The information obtained by reflectance analysis offers an explanation of what appears to be an advantage for high reactivity form-cokes.

CLEAN COKE PROCESS: FLUID-BED  
CARBONIZATION OF ILLINOIS COAL

T. F. Johnson, K. C. Krupinski, and R. J. Osterholm

U. S. Steel Corporation  
Research Laboratory  
Monroeville, Pa. 15146

The CLEAN COKE Process is based on a conceptual plan, developed by United States Steel Corporation, for converting nonmetallurgical-grade coals to metallurgical coke, chemical feedstocks, and liquid and gaseous fuels (1). In accordance with the process, low-temperature carbonization of coal and coal hydrogenation are combined in a manner that affords an energy- and hydrogen-balanced process. Moreover, coke production—from initial carbonization to finished product—is implemented so as to avoid contamination of the atmosphere with pollutants.

The process is shown schematically in Figure 1. Mined coal is beneficiated, and a portion is sent to a low-temperature carbonization plant where pyrolysis occurs at pressures as high as 165 psia in a fluidized-bed system. A stream of cleaned, hydrogen-rich recycle gas serves as the fluidizing medium in the carbonizer vessel. The high partial pressure of hydrogen in the gas and the essential absence of sulfur impurities provide an effective hydrodesulfurization environment whereby the sulfur content of the coal is reduced from an initial level of more than 2 percent to below 0.5 percent in the resulting char. The char can then be pelletized with a process-derived binder oil, and the pellets can be cured and calcined to produce the low-sulfur metallurgical coke.

The second portion of the beneficiated coal is sent to a hydrogenation plant where the coal is slurried with a process-derived carrier oil and subjected to noncatalytic hydrogenation at elevated temperature and pressure. Liquid product is separated from unreacted coal and mineral matter in a vapor-stripping vessel where the hydrogenate is contacted countercurrently with a stream of hot process gases and the volatile matter removed. Residual solids pass through a lock system into a receiving vessel and are quenched and withdrawn from the system.

In the coke-preparation section, carbonization char and liquid binder, the latter obtained from liquids treatment, are combined in a disc pelletizer to form green pellets. These are then cured by heating in the presence of air to impart a degree of green strength, and the cured pellets are finally calcined at temperatures up to 2000 F (1100 C) to produce the hard metallurgical coke pellets.

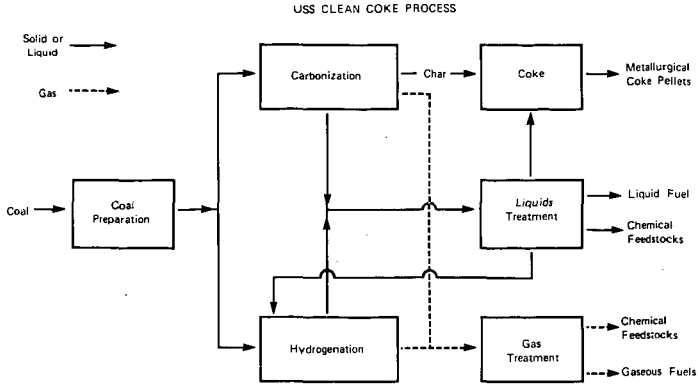


Figure 1

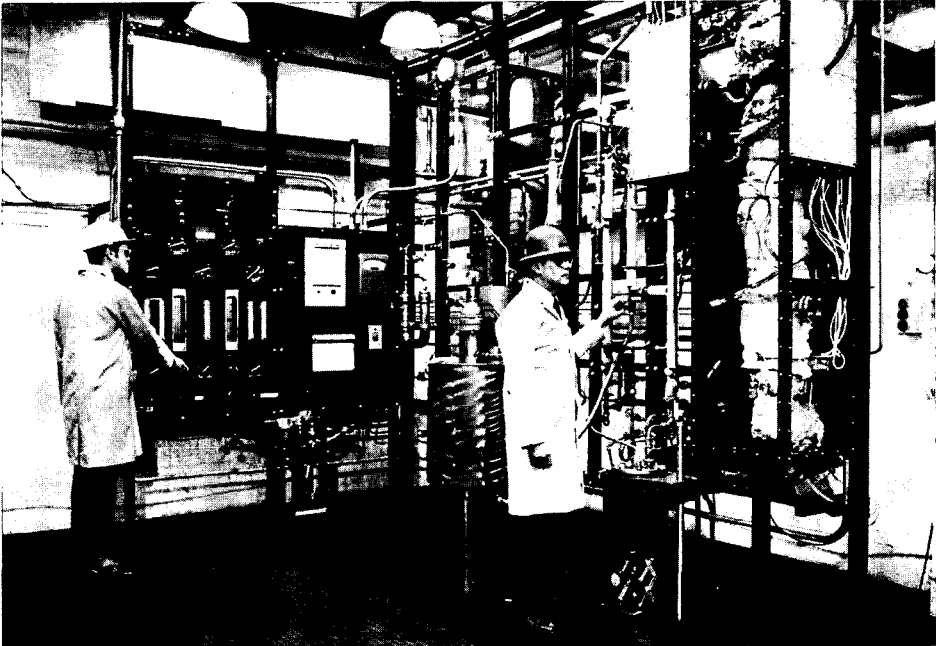


Figure 2 Three-inch bench-scale carbonizer.

This paper summarizes the results of studies on carbonization of Illinois No. 6 seam coal in a fluidized bed to produce the low-sulfur char that is ultimately converted to metallurgical coke. The objectives of the carbonization studies were to determine the efficiency of desulfurization of coal and to determine the effect of carbonization variables—temperature, pressure, reaction time, and feed pretreatment—on the desulfurization reaction (2).

#### Bench-Scale Carbonization Reactor

For this work, a special pressurized reactor was designed and fabricated to permit carbonization-desulfurization of coal in a closed loop with recycle of gas under pressure. The bench-scale unit, shown in Figure 2, has a temperature limit of 1400 F (760 C) and a pressure limit of 140 psia. The reactor section is constructed of 3-inch, Schedule 40, Type 316 stainless-steel pipe in the fluid-bed region and expands to 6-inch pipe above the fluid bed. A perforated stainless-steel plate serves both as a gas-distributor plate and as the bed support. The fluidizing gas is heated by an electric heater and the external heater windings on the reactor section. The hot gas leaving the reactor is cleaned of any coal or char particles by the Pyrex-wool filter. After removal of the solids, heavy oils are condensed from the gas in a water-cooled tar trap, and lighter oils are condensed in a dry-ice trap. Hydrogen sulfide is removed by the H<sub>2</sub>S absorber, which consists of a 2-inch stainless-steel U tube packed with Molecular Sieves. Gas flow is monitored by flow meters, and the gas is recycled by an air-driven Haskel AGD-4-C double-acting, single-stage gas booster pump. As additional gas is generated during a carbonization, a constant pressure is maintained by means of a gas accumulator. Water is released from the gas accumulator, thereby increasing the volume of the system; no gas is vented. Recycled gas is analyzed for hydrogen, methane, and carbon monoxide by a Greenbrier process gas chromatograph, which is permanently connected to the carbonizer.

#### Experimental Procedure

A typical test consisted of charging the reactor with 1 kg of coal or a blend of 400 g of recycle char and 400 g of coal; this gave an expanded bed height, during fluidization, of about 18 inches. A synthetic mixture of hydrogen, methane, and carbon monoxide (approximately the steady-state recycle-gas composition) was added to the reactor to the desired test pressure, and the gas flow rate was adjusted to give a superficial gas velocity of about 1.2 feet per second in the reactor. The recycle gas and the reactor were then heated to the desired temperature, and the fluid bed was maintained at that temperature for the specified residence time. After the reactor cooled, the reaction products were removed and analyzed.

Product water was separated from the carbonization tar by centrifugation to allow determination of the types and amounts of products available from the carbonization tar. The tar was distilled at a pressure of 200 torr by using a Vigreux column 2.5 cm in diameter

by 25 cm long. Three fractions were obtained: (1) a chemical oil, distilling to 385 F (195 C); (2) a middle oil, distilling at 385 to 635 F (195 to 335 C); and (3) a heavy oil (residue), distilling above 635 F. The chemical oil was further resolved into a tar-acid fraction, a tar-base fraction, and a neutral-oil fraction by extraction with aqueous caustic and acid.

The coal and char were analyzed by standard ASTM methods. The tars and derived oils were characterized by gas chromatography (GC); tar acids and bases were also determined by a potentiometric titration procedure. Mass spectroscopy and GC were used to analyze the gaseous products.

#### Results of Typical Carbonization of Illinois Coal

A typical carbonization of the coal feedstock resulted in removal of 80 percent of the contained sulfur and gave the following yield of products, in weight percent of the charge: char, 66.4; tar, 13.9; gas, 14.6; and water, 5.1. These results were obtained with a preoxidized feed coal and with the carbonizer operated at 1365 F (740 C) and a pressure of 80 psia for a 30-minute residence time. Efficiency of sulfur removal is illustrated by the reduction of sulfur content in the solid materials from 1.7 percent in the coal to 0.5 percent in the char product.

Figure 3 illustrates stream flow and product distribution in a typical carbonization test. Experimentally, the yields of char and gas are readily measured, but yield of liquids is difficult to measure quantitatively because of mechanical problems in removing water and tar from the unit. Consequently, handling losses were distributed proportionately between water and tar to provide overall material balance.

Results from analysis of the char product are presented in Table I, along with corresponding results for the feed coal. The sulfur content of the char (0.5%) is significant, since this indicates that the char can be converted to a coke product containing less than 0.5 percent sulfur. Of the sulfur removed from the coal, about 85 percent was converted to hydrogen sulfide, and the rest was separated as volatile organic sulfur compounds found mainly in the tar.

The gas product, after removal of hydrogen sulfide, had three major constituents: hydrogen, methane, and carbon monoxide in the molar ratio of 40:52:8. Small amounts of ethylene, ethane, propane, and carbon dioxide were also identified, although none was present in significant concentration.

To determine its chemical composition, the carbonization tar was distilled to divide it into 20 percent chemical oil, 37 percent middle oil, and 43 percent heavy oil. The chemical oil was then extracted to separate tar acids, tar bases, and neutral oil, and individual components were identified by gas chromatography. By

Table I

Analyses of Feed Coal and Product Char

<u>Analysis, wt %</u>	<u>Coal</u>	<u>Char</u>
Proximate		
Volatile matter	34.3	1.60
Fixed carbon	59.5	89.18
Ash	6.2	9.22
Ultimate		
Carbon	75.48	86.58
Hydrogen	5.21	1.64
Nitrogen	1.72	1.27
Oxygen	9.71	1.52
Sulfur	1.74	0.50
Ash	6.14	8.49

type of compound, the chemical oil consists of about 55 percent phenols, 20 percent benzenes, 7 percent each of tar bases and naphthalene, with the balance being naphthenes and heterocyclics.

The water produced during the carbonization reaction contains compounds typically found in waste water from conventional coke-oven operations. The component analysis of the water is given in Table II and shows a dissolved ammonia content of about 3 percent and a tar-acid content of almost 0.6 percent. Dissolved salts, including the thiocyanates, cyanides, sulfates, and sulfides, total about 3800 ppm. Cleanup of this stream will be necessary, but it will be simplified in this process by confining all the discharged water to a single stream.

Effects of Carbonization Reaction Conditions

A study was made to assess the effects of residence time, temperature, and pressure on the carbonization reaction and products. This study was limited by the relatively slow heat-up rate of the 3-inch unit, in which about 70 minutes was required to reach 1150 F (620 C) and about 100 minutes to reach 1365 F. For convenience in measuring times, heat-up periods were excluded, and residence times were measured only from that point at which the fluid bed reached the desired test temperature. However, it was recognized that intermediate temperatures above about 800 F (425 C) contributed an unmeasured, but significant, effect to residence time. To study the effect of heat-up time on coal desulfurization, a test was performed at nominal zero residence time, 1365 F, and 80 psia. The results from this test,

Table II

Analysis of Product Water From Carbonization

<u>Component</u>	<u>Parts per Million</u>
SCN <sup>-</sup>	1,171
CN <sup>-</sup>	74
SO <sub>4</sub> <sup>=</sup>	2,050
S <sup>=</sup>	562
NH <sub>3</sub>	33,320
Phenol	3,200
o-Cresol	700
m,p-Cresol	1,500
Xylenols	500

along with results obtained with the 30-minute residence time, are shown in Table III. Gas compositions and char yields were very similar for the two tests; the hydrogen content of the gas was about 38 percent, and the char yield was 66 percent. The sulfur content of the char at 0- and 30-minute residence times was 0.73 and 0.51 percent, respectively. The data indicate that the coal is devolatilized and significantly desulfurized during the heat-up period. However, increased desulfurization of the char is achieved by the additional residence time at the reaction temperature.

Table III

Effects of Time and Temperature on Desulfurization of Coal at 80 psia

Temperature, F	1365	1365	1150
Time at Temp, min	0	30	30
Fluidizing-Gas Composition, mole %			
H <sub>2</sub>	38	40	27
CH <sub>4</sub>	52	52	} 73
CO	10	8	
Sulfur Content, wt %			
Coal	1.76	1.76	1.76
Char	0.73	0.51	0.85

The effect of temperature on coal desulfurization was determined by carbonizing the preoxidized coal at 1150 F and 1365 F (80 psia and 30 minutes). The results of these tests, also in Table III, show the improvement in desulfurization and the hydrogen enrichment of the recycle gas with increasing temperature. However, in considering the slow rate of heat-up, it is seen that about 70 minutes of heating time is required to reach 1150 F, and 100 minutes is required for 1365 F. Therefore, a comparison of an 1150 F, 30-minute carbonization with a 1365 F, 0-minute carbonization may be more valid, since the total heat-up time plus residence time is the same. The sulfur content of the char produced at 1365 F and 0 minutes is 0.73 percent, which is lower than the 0.85 percent sulfur for the 1150 F, 30-minute char. This demonstrates that an increase in temperature does indeed improve desulfurization of the coal.

A series of three carbonizations of preoxidized coal was conducted at 1365 F and pressures of 30, 80, and 125 psia to study the effect of pressure on the desulfurization of the coal. Nominal residence time for these tests was 30 minutes. Desulfurization of the coal improved with increasing operating pressure, and steady-state gas data showed, as expected, decreasing hydrogen and increasing methane contents with increased operating pressure. Summary data for these carbonization tests at 30, 80, and 125 psia are presented in Table IV and demonstrate a definite advantage for higher-pressure operation with respect to desulfurization of the coal. Corresponding char products contained 0.77, 0.50, and 0.33 percent sulfur. The improvement in sulfur removal is the result of higher partial pressure of hydrogen, which of course increased in this series although the hydrogen concentration in the recycle gas decreased with higher pressures.

Table IV  
Effect of Pressure on  
Desulfurization of Coal at 1365 F

Pressure, psia	Recycle-Gas Composition, mole %			Sulfur Content, wt %	
	H <sub>2</sub>	CH <sub>4</sub>	CO	Dry Coal	Char
30	54.4	34.4	10.9	1.74	0.77
80	39.4	51.8	8.5	1.74	0.50
125	32.4	60.0	7.2	1.74	0.33

#### Studies on Modification of Feed Coal

Modification of the coal feed for fluid-bed carbonization tests was done to ensure that the fluid nature of the bed was not lost during the heat-up period. A fluid bed is essentially a suspension

of solid particles (coal or char or both) in a flowing gas stream. Because all the particles are in motion, a fluid bed exhibits many of the properties of a boiling liquid, including rapid heat transfer throughout the mass (3). Also, the fluid nature permits continuous addition of feed and withdrawal of product, which facilitates continuous operation. However, when a caking coal, such as Illinois No. 6 seam coal, is heated to about 750 F, the solid particles of coal become plastic and stick together in an agglomerated mass that destroys the fluid state.

Agglomeration of caking coals can be avoided by mild pre-oxidation to chemically alter the surface of the coal particles, or by blending the coal with a noncaking char, which physically separates the softened coal particles in the plastic region (4,5).

The effect of coal preoxidation on desulfurization and tar composition was determined by carbonizing unoxidized and preoxidized coal at 1365 F and 80 psia. Unoxidized coal was carbonized with an equal amount of recycle char to avoid agglomeration. For control purposes, a sample of the recycle char was carbonized neat to establish the extent of desulfurization and gasification that occurs under conditions of treatment. The results of the control test, given in Table V, show a reduction in sulfur content from 0.88 to 0.49 percent and a weight loss of 1.2 percent. The results of the test with a blend of unoxidized coal and recycle char are also presented in Table V, and show an apparent 88 percent desulfurization. On the assumption of no interactions between recycle char and feed coal, it is calculated that char produced from the coal portion of the carbonizer feedstock contained only 0.34 percent residual sulfur. Whether or not interactions between char and coal were actually occurring during carbonization, the char sulfur content was still at a low level and certainly did not exceed the 0.43 percent value determined for the total char.

A comparison of the carbonizations of unoxidized and pre-oxidized coal at 1365 F, 80 psia, and 30 minutes residence time is also given in Table V. Carbonization of the unoxidized coal gave apparently better desulfurization, less char, and more tar than carbonization of preoxidized coal; however, these results represent a single set of data and may only indicate the effect of small variations in reaction time and temperature.

Feed coal for these tests was preoxidized in the 3-inch carbonizer by using heated air as the fluidizing medium. Treating conditions included atmospheric pressure, a temperature of 350 F (175 C), and a residence time of about 10 minutes. When coal/char blends were used to prevent bed agglomeration, char from previous carbonizations were used in a weight ratio of 1 to 1.

Table V

Effects of Feed Modification  
on Desulfurization of Coal

	<u>Preoxidized Coal</u>	<u>Unoxidized Coal + Char</u>	<u>Char</u>
Yield Data, wt %			
Char	66.4	61.3	98.8
Tar	12.2	15.5	-
Water	3.3	5.0	-
Gas + loss	18.2	18.2	1.2
Sulfur Analysis, wt %			
Coal	1.76	1.79	-
Starting char	-	0.88	0.88
Final char	0.51	0.43	0.49

Continuous Carbonization of Coal in Two Stages

Both preoxidation of coal and blending of coal with recycle char effectively eliminated bed agglomeration in batch tests, which were limited by a rather slow heating rate of 10 degrees per minute. However, subsequent tests on continuous feeding of preoxidized coal to a hot fluid bed resulted in agglomeration of the bed, because continuous feed addition results in a much faster heating of the added coal. The heating rate in continuous operation appears to be about 10 degrees per second, which generates sticky tars at a rate faster than that at which tars can be vaporized away from the bed, and agglomeration results.

Subsequent tests on continuous feeding led to the development of a two-stage system, involving partial devolatilization of oxidized coal in a fluid bed operating at temperatures in the range 800 to 840 F (425 to 450 C), followed by carbonization in a fluid bed at temperatures of 1300 to 1400 F (700 to 760 C). A sample of 20- by 65-mesh Illinois coal was stage-carbonized in the 3-inch bench unit. In both devolatilization and carbonization stages, the coal was added to the top of the bed, using a rotary feed valve. Recycle gas was the fluidizing gas in both stages. During the first stage, 200 g of coal that had been oxidized at 350 F was added at the rate of 14 g per minute to a fluid bed of 800 g of coal which had been held at 840 F for 10 minutes. After all the coal was added, the bed was maintained at temperature for 20 minutes at 125 psia. The devolatilized coal (semichar) removed weighed 760 g and contained 16 percent volatile matter, an indication that about 218 g of volatiles had been removed from the coal; handling loss was about 18 g.

A portion (520 g) of the semichar was returned to the reactor and heated to 1380 F (750 C) at 125 psia. After a 15-minute hold, 200 g of the semichar was added to the fluid bed at 14 g per minute. When all the coal was added, the bed was maintained at temperature for 15 minutes.

The recovered char weighed 557 g and contained 1.86 percent volatile matter, an indication that about 104 g of volatiles was removed from the partially devolatilized coal; solids loss was about 50 g, which includes some handling loss and partial gasification of the fixed carbon.

Figure 4 is a summary of this staged carbonization and includes the yield of product at each stage, corrected for losses. The figure indicates that the yield of semichar was 78.2 percent of the preoxidized feed in the first stage, and about 63 percent of the volatile matter was removed. The product char from the second stage was obtained in 66.9 percent yield overall.

Results of proximate and ultimate analyses for the oxidized coal and the products of each stage of carbonization are presented in Table VI. Desulfurization was significant during the first stage, a decrease in sulfur content from 2.28 percent to 1.63 percent. The sulfur content of the char was 0.33 percent. The nitrogen content varied from 1.67 to 2.05 to 1.49 percent, an indication that nitrogen compounds react in the final carbonization stage almost exclusively.

Table VI  
Analysis of Products of  
Staged Carbonization of Coal

	<u>Preoxidized</u>	<u>Partially Devola- tilized</u>	<u>Carbonized</u>
Temperature, F	350	840	1380
Pressure, psia	15	125	125
Analysis of Products, wt %			
Proximate			
Volatile Matter	34.31	15.96	1.86
Fixed Carbon	58.72	74.50	87.43
Ash	6.97	9.54	10.71
Ultimate			
Sulfur	2.28	1.63	0.33
Carbon	72.96	74.80	86.29
Hydrogen	5.07	3.97	1.66
Nitrogen	1.67	2.05	1.49

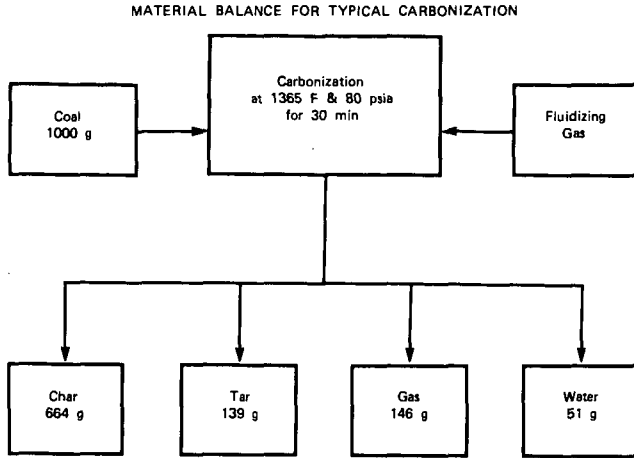


Figure 3

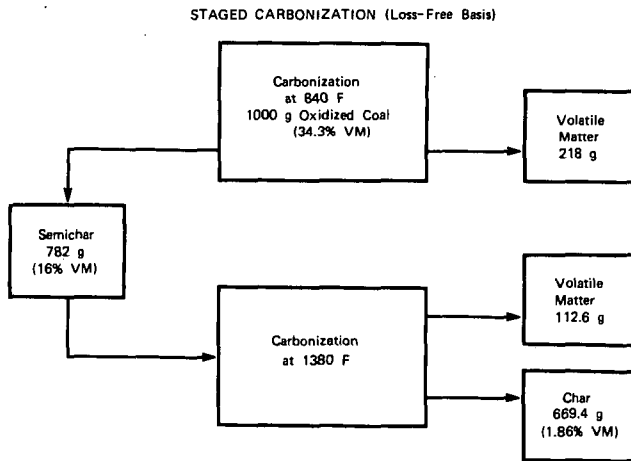


Figure 4

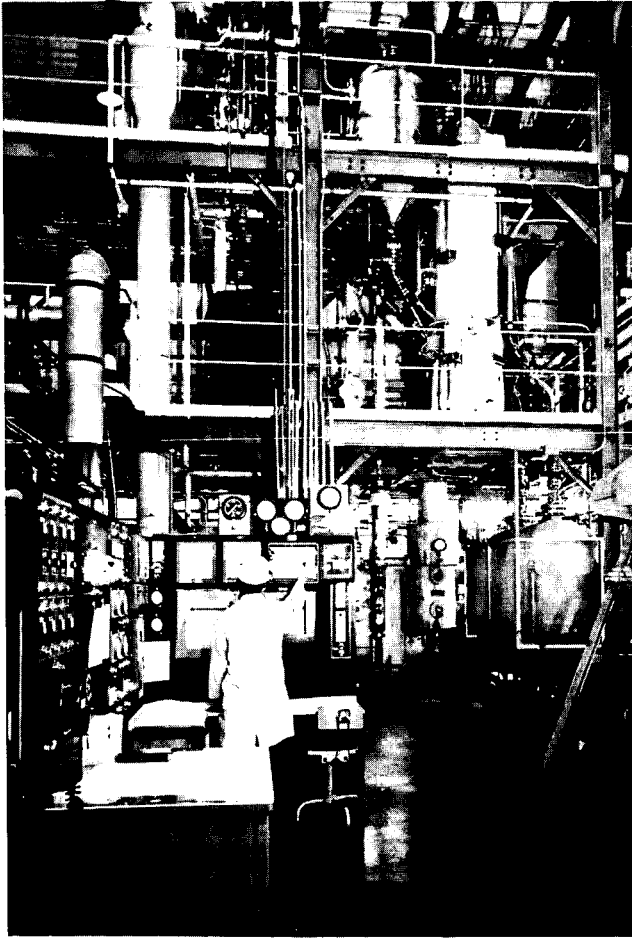


Figure 5 Carbonization process-development unit  
for CLEAN COKE project.

Current work on the CLEAN COKE Process is being conducted in a 500-pound-per-day process-development unit (PDU). The carbonization PDU, Figure 5, consists of a 10-inch-diameter fluid-bed reactor with lock hoppers for coal feed and char product, and gas-cooling and -scrubbing equipment for recovery of heat and tar from the recycle gas. Preliminary testing and shakedown runs in the PDU have been completed, and carbonization tests are now in progress to provide data on continuous operation in the unit. Results from these scale-up tests will be published when the work is complete.

The work described here is supported in part by the Energy Research and Development Administration, under contract No. 14-32-0001-1220.

#### References

1. K. A. Schowalter and N. S. Boodman, "The Clean Coke Process for Metallurgical Coke," Chemical Engineering Progress, Vol. 70, No. 6, June 1974.
2. USS Engineers and Consultants, Inc., "Clean Coke Process - Summary of Bench-Scale Studies," Interim report for period March 1972 - April 1974, Contract No. 14-32-0001-1220, Prepared for U. S. Department of Interior, Office of Coal Research, August 1974.
3. F. A. Zenz and D. A. Othmer, "Fluidization and Fluid-Particle Systems," Charles R. Wilke, Consulting Editor, Reinhold Publishing Corporation, New York, 1960.
4. P. J. Wilson and J. H. Wells, "Coal, Coke, and Coal Chemicals," McGraw-Hill, New York, 1950.
5. FMC Corporation, "Char Oil Energy Development," Final report for period June 1962 - December 1965, Contract No. 14-01-0001-235, Prepared for U. S. Department of Interior, Office of Coal Research, December 1965.

FORMCOKE PREPARATION IN  
CLEAN-COKE PROCESS

R. W. Shoenberger

Senior Research Engineer-Raw Materials Utilization Division

Research Laboratory  
U. S. Steel Corporation  
Monroeville, Pennsylvania 15146

For presentation at the Symposium on New Coke Processes  
Minimizing Pollution, Division of Fuel Chemistry, ACS,  
Chicago, Illinois, August 1975, and for publication as  
preprint for distribution in advance to Division members.

The Clean-Coke Process being developed by U. S. Steel under contract with the U. S. Government (Energy Research and Development Administration) has been described previously.<sup>1)\*</sup> Chemicals, fuels, and coke are the major products. However, an important phase of the Clean-Coke project is the ability to make an acceptable metallurgical coke from desulfurized char and heavy residual oils from the process. Of the various types of agglomeration (briquetting, pelletizing, nodulizing, or extrusion) considered, pelletizing appeared to have the best potential for more easily producing a superior product at the most reasonable cost by using char and binder derived from the process. The char as characterized in bench scale studies is low in density with a large percentage of cenospheres. Binder is available in large quantities. An advantage of producing coke by such a formcoke process is the reduction of pollution problems normally encountered in the conventional coke making process. The steps required for coke preparation will be carried out in a closed system with the off gases collected and returned to be processed through a common system. As a result, atmospheric pollution is practically non-existent.

Because the fluid-bed char-making unit was not yet constructed to produce desulfurized char at the time the coke-making phase of the process was initiated, char was produced in a

---

\* See References.

four-inch fluid-bed carbonizer using nitrogen as the fluidizing gas. Also, simulated binder was used because a binder was not available from the process in the quantity required for the coke-making studies. This paper presents the development of this method and shows some of the factors influencing the resultant coke properties.

#### Materials

Illinois No. 6 Seam coal, obtained from Franklin County, Illinois and washed at a 1.35 specific gravity, was charred in a fluid bed to a volatile matter content of 9 to 12 percent. This char was made by batch operation at a final bed temperature of 1150 F in an air-nitrogen fluidizing gas. Photomicrographs of the char are shown in Figure 1. The coal and char were nominally minus 10-mesh in size.

Various binders were used to determine how their properties would affect the resultant coke properties. The characteristics of these binders are listed in Table I. Some of the binders represent the type of binders available from the process whereas others represent binders from other sources having a wide range of properties.

#### Pelletization

A 24-inch pelletizing disc with a continuous-heated, (300 - 350 F) solids feeding system was used to study the pelletization of char fines with a heavy residual oil binder. The binder

was heated in a surge tank and sprayed on the solids to form the pellets. Figure 2 shows the equipment installed for the present work.

Strong green pellets of the desired size (2- by 3/4-inch) were produced from all test binders by regulating the disc conditions, the temperature of the binder and the solids, and by changing the properties of the binder. Test conditions for typical runs are listed in Table II. The percentages of binder required increased as the fineness of the solid material was increased and generally made up about 30 percent of the mix except for the pellets made with fluxed coal extract. The reason for the need to use 38 percent of the fluxed-coal extract binder with the minus 28-mesh char is not known. The recycle material was reduced to about 10 percent in the later runs. The pellets are soft as they are discharged hot from the disc, but they can fall 3 to 6 feet without changing their shape. When they cool they become hard and have a nominal 350-pound crushing strength. A test in the ASTM shatter machine showed no degradation of cold green pellets at room temperature when dropped four times.

Studies were conducted with coke fines and coal tar pitch to determine factors affecting pelletizing rate. It was necessary to provide multiple sprays and solid feeders for feeding the disc. In short runs, 3.5 pounds per minute of plus 3/4-inch green pellets were produced. Test data indicate that about 12 to 15 tons per hour could be produced on a 20-foot disc.

### Pretreatment and Carbonization of Pellets

With no pretreatment (curing) the green pellets agglomerated together during carbonization because the binder became soft and melted. In addition, any shearing action disintegrated the pellets to fines during the heating period while the pellets were soft. Preliminary studies showed that the pellets became soft at about 250 F and then hardened at about 900 F in the absence of oxygen. Tests also showed that pellets would harden permanently at 500 F in the presence of oxygen. Larger scale tests were then conducted in different types of equipment (such as a vertical retort, small test coke oven, and a stationary grate) to simulate the various methods that might be used for treating (curing) the pellets.

Pretreatment of the green pellets had to be initially conducted in shallow beds (two pellet depth) for long treating periods (3 to 5 hours). During these studies, it was found that mixing the pellets with an inert supporting medium reduced agglomeration, permitted deeper beds, and allowed faster heating rates to be used without cracking or destroying the pellets. Char fines or sized coke pellets (up to 3/4-inch top size) were used as media. The following methods were found effective in pretreating the green pellets:

- 1) Indirect heating in a Brennstoff Technik<sup>2)</sup> type coke oven which is relatively narrow (from 60 to 125 mm wide) and has walls made of iron, resulting in very fast heating rates. Pellets were heated from 900 to 1100 F in 1 and 3/4 hours. Agglomeration was prevented by mixing about 50 percent of 1/8 x 0 char as a supporting medium.
- 2) Direct heating in an intermittent vertical retort with 50 percent of a 1/2- by 1/4-inch supporting coke medium to 900 F in an inert atmosphere and to 500 F in an oxygen atmosphere for 1 and 3/4 hours (tested in bed depths up to 8-feet).
- 3) Direct heating on a grate with 50 percent of a 1/2- by 1/4-inch supporting coke medium to 900 F in an inert atmosphere and to 500 F in an oxygen atmosphere for 1-1/2 hours (tested in bed depths up to 18-inches).

Because shearing of the pellets is minimized in curing on a traveling grate, a grate using a 1/2- by 1/4-inch supporting coke medium and an oxygen atmosphere was selected as the most suitable equipment to use. A curing pot was installed for the present studies. Figure 3 is a diagram of the curing pot system.

When the pellets are cured or pretreated properly, they are sufficiently strong to withstand handling and will not soften upon further heating in the coking step. These treated pellets

have been successfully coked in a continuous coking kiln by using inert gases to coke the pellets. The coked pellets have a good appearance (very few cracks and a metallic, smooth surface) with 97 to 100 percent of the pellets being recovered after coking to 1800 F. The normal yield obtained after driving off the volatiles of the green pellets in both the pretreatment and coking steps is about 70 percent. A method was also found to coke green pellets to 1800 F by using 50 percent 1/8-inch by 0 supporting char medium in a Brennstoff-Technik type coke oven for 5-1/2 hours. However, such a method would be expensive and it would be difficult to control pollution when discharging and quenching the coke and medium. Therefore, a continuous vertical coking kiln was built for the present studies. This kiln is shown in Figure 4.

#### Properties of Coke Pellets

The tests used to evaluate the quality of the coke pellets were tumbler strength, crushing strength (total force on whole pellet), compressive strength, and apparent specific gravity. Because of the large quantity of sample required for the ASTM tumbler test, the number of tests was minimized. However a good relationship was found between crushing strength and the hardness value (plus 1/4-in.) determined from the tumbler test, Figure 5. A discussion follows on some of the factors affecting the resultant coke properties.

### Type of Binder

Table III shows some physical properties of formcoke produced from the various types of binders at similar conditions. The type of binder did have a significant effect on the properties of the resultant formcoke. It was possible to improve the effectiveness of some binders by using additives such as carbon black or coal or by air blowing. The strength of the formcoke generally increased as the carbon to hydrogen ratio and the Quinoline Insoluble content increased in the binder.

### Size Consist of Char

The effect of grinding the char to finer sizes is shown in Table IV. As noted, the strength of the formcoke increased as the char was pulverized more finely. When the char containing large cenospheres and an open structure (see Fig. 1) is used in preparing the pellets, a weak formcoke is obtained. However, when these char particles are crushed to eliminate the cenospheres and puffy structure, the coke is improved considerably.

### Type of Pretreatment and Carbonization

The type of pretreatment and carbonization did not appear to have a significant effect on the properties of the formcoke when the design conditions were used. A few typical results for the sample pellets treated in different ways are listed in Table V. From the data obtained to date, the final temperature within narrow ranges (1750 to 1950) had only a slight effect on coke properties.

Evaluation of Coke Pellets for Metallurgical Use

The method developed to produce a good quality coke pellet consisted of pelletizing finely ground char by spraying a heavy residual oil binder on a disc pelletizer. These green pellets are combined with 1/2 by 1/4 inch coke medium and then cured on a grate with an oxygen rich gas to 500 F in 1-1/2 to 2 hours. The cured pellets are then screened from the medium and coked to about 1800 F in a vertical coking kiln in 2-1/2 hours. A flow diagram of the coke preparation step is illustrated in Figure 6.

Using these conditions, several hundred pounds of formcoke pellets were produced; a sample of the pellets is shown in Figure 7. The physical and chemical properties of these formcoke pellets were tested for comparison with metallurgical coke and another type of formcoke that had been used successfully in a blast furnace test. The test results are listed in Table VI. From these test data, it can be concluded that these formcoke pellets will make a good blast furnace coke. The good quality of coke obtained in the Clean-Coke Process results from 1) the fine pulverization of the char to break it down to the denser wall sections, 2) the use of sufficient quantities of binder to wet the solid particles, and 3) the intimate distribution of char and binder to obtain maximum strength. The photomicrographs in Figure 8 show the good microstructure of the formcoke and the good distribution of the materials.

A unique method has been developed to process char and binder derived from the process into a good quality formcoke. Attaining a high grade product enhances the overall potential of the Clean-Coke Process. Currently, information from process-development units is being used in the design of a pilot plant capable of processing four tons of coal per hour.

#### References

1. K. A. Schowalter and N. S. Boodman, "The Clean-Coke Process for Metallurgical Coke," *Chemical Engineering Progress*, Vol. 70, No. 6, June, 1974, pp. 76-82.
2. D. C. Rhys Jones, "Briquetting," *Chemistry of Coal Utilization*, Sys. Vol. H. H. Lowry Ed., John Wiley and Sons, 1963, pp. 675-753.

Table I

## Selected Properties of Experimental Binders for Coke Pellets

	Asphalt		Coal-tar		Coal-		Fluxed		Pipe Line Enamelling Pitch
	AC 2000	RC 800	Pitch	CNBD*	Digestion Pitch	Coal Extract (De-ashed) Coal Blend)	Coal Extract (De-ashed) Coal Blend)		
Asphaltene Content, wt%	1.4	1.6	CNBD*	CNBD	CNBD	CNBD	CNBD	NA	
Viscosity @ 60 C poise	1900	634	167		Non- Newtonian	310		NA	
Softening Point, Ring and Ball, C	49.4	14.8	34.2	84.0		42.3		51.5	
Coking Value, wt %	19.4	17.6	36.4	29.4		29.9		NA	
Benzene Insoluble	0.1	0.1	13.9	22.3		19.2		10.5	
Quinoline Insoluble	0.0	0.4	6.5	CNBD		0.4		3.5	
Carbon/Hydrogen Ratio	0.67	0.66	1.60	1.38		1.37		NA	

\* Could not be determined.

NA = Not available on sample used.

Table II

Pelletizing Conditions to Produce Green Pellets

Solids, 100% minus Size, 100 mesh	Char					
	1/8 in.	28-mesh	100 mesh	28 mesh	100 mesh	
% Char or Coke	60	60	60	60	57	
% Pitch Coke	13	10	7	11	9	
% Binder	27	30	33	29	34	
Type Binder	Coal- Tar Pitch	Coal- Tar Pitch	Coal- Tar Pitch	Asphalt (AC2000)	Fluxed Coal Extract	Coal Digested Pitch
Temp of Binder	360	360	365	350	370	370
Disc Angle, degrees	41	40	38	42	40	38
Disc Speed, rpm	30	30	30	30	30	30
% Recycle (Minus 3/4-inch material)	NA	20	NA	10	12	4
Green Pellet App Sp Gr	1.05	1.18	1.25	0.91	NA	NA

NA = Not Available

75-H-424 (008)

Table III

Effect of Binder Type on Strength of Resultant Coke Pellet

Type of Binder	Coal-Tar Pitch		Asphalt RE800		Coal Digested Pitch		Fluxed Coal Extract	
	28 mesh	100 mesh	28 mesh	100 mesh	28 mesh	100 mesh	28 mesh	100 mesh
Size of Char, 100% minus	1800	1800	1800	1800	1800	1800	1800	1800
Final Coke Temperature, F	700	950+	210	475	475	915	470	820
Crushing Strength, lbs (whole Pellet, 1-in.)	67	86	ND	ND	ND	ND	46	84
Tumbler Strength, Hardness (Plus 1/4-in., 700 rev)	0.87	0.94	ND	0.75	0.86	1.10	0.76	ND

ND - Not determined.

Table IV  
Effect of Char Size on Strength of Resultant Coke Pellet\*

Char Pulverized to 98-100% minus	<u>1/8-inch</u>	<u>28-mesh</u>	<u>65-mesh</u>	<u>100-mesh</u>
Crushing Strength, lbs (whole pellet)	590	700	630	820
Tumbler Strength (1400 rev) Plus 1/4-inch Index	53	59	64	74
Apparent Specific Gravity	0.94	0.97	0.88	1.10

\* Pellets made from Illinois No. 6 seam char and coal-tar pitch. Carbonized in pilot test coke oven to 1800 F.

Table V

Effect of Method of Pretreating and Carbonizing on  
Strength of Resultant Coke Pellet

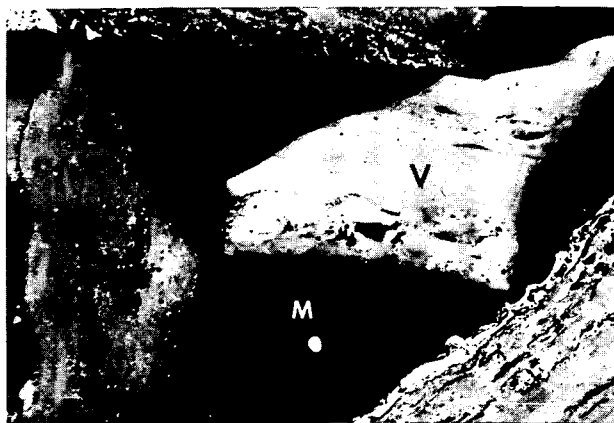
Type of Pretreatment	Type of Carbonization	Crushing Strength, lb (whole pellet)	Tumbler Strength Hardness*	Apparent Specific Gravity
A. Pellet Produced from Minus 28-mesh Char and Coal-tar Pitch				
1. Cured to 500 F (shallow bed at slow rate)	Pilot-Scale Coke Oven** (1800 F, no medium)	700	59	0.88
2. Preheated in Vertical Retort with Coke Medium to 900 F (Nitrogen Flow)	Pilot-Scale Coke Oven** (1800 F, no medium)	690	ND	0.81
3. None	Pilot-Scale Coke Oven** (with 1/8 in. x 0 coke fines, 1800 F)	750	59	ND
B. Pellets Produced from Minus 100-mesh Char and Coal-tar Pitch				
1. Cured to 500 F (Shallow Bed and slow rate)	Pilot-Scale Coke Oven** (1800 F, no medium)	835	74	1.13
2. Preheated in Vertical Retort with Coke Medium to 830 F	Pilot-Scale Coke Oven** (1800 F, no medium)	950	ND	1.10
3. None	Pilot Scale Coke Oven** (with 1/8 in. x 0 coke fines, 1800 F)	950	74	0.94
4. Preheated in Vertical Retort with Coke Medium to 830 F	Continuous Vertical Retort, 1800 F no medium	950	ND	1.10
* Plus 1/4-inch after 1400 rev.				
** Brennstoff Technik type coke oven.	75-H-424 (008)			80

Table VI  
Properties of Formcoke

	Metallurgical Coke <u>1-1/4 x 3/4</u>	Coke Pellet <u>1-1/4 x 3/4</u>	FMC Corp. Formcoke <u>1-1/4 x 1</u>
Tumbler Strength*			
Hardness, plus 1/4 inch	85	85	83
Crushing Strength, lbs	600	>1000	810
Compressive Strength, psi	2450	2150	3170
Bulk Density, lbs/ft <sup>3</sup>	29	32	32
Apparent Density	0.94	1.0	0.90
True Density	1.90	1.93	1.69
Porosity	50-1/2	48	47
<u>Chemical Analysis</u>			
V.M.	0.8	1.0	6.2
Fixed Carbon	92.2	91.5	87.1
Ash	7.0	7.5	6.7
Sulfur	0.7	0.5	0.75

\* 22 lb sample for 700 rev in ASTM Tumbler.

## ILLINOIS COAL



## CHAR

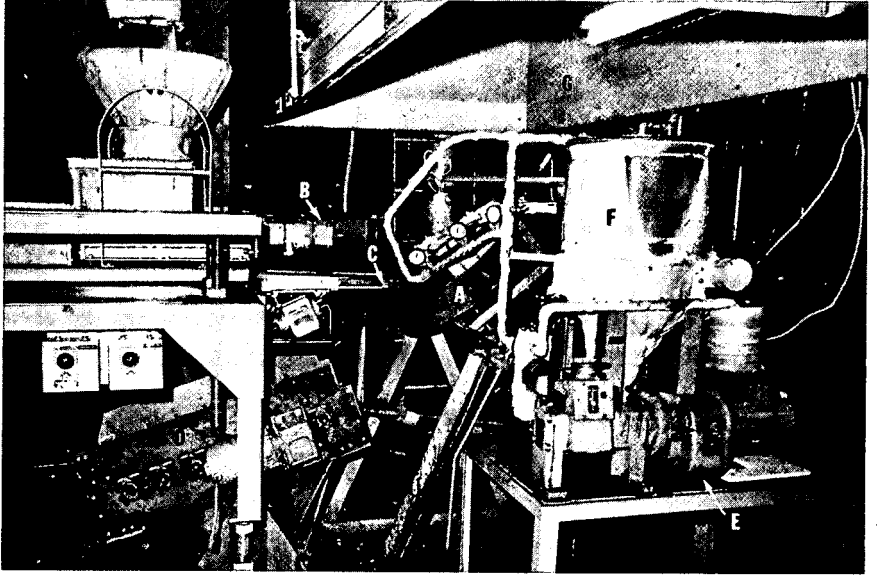


High-Volatile Char  
Approximately 12% VM



Low-Volatile Char  
Approximately 3% VM

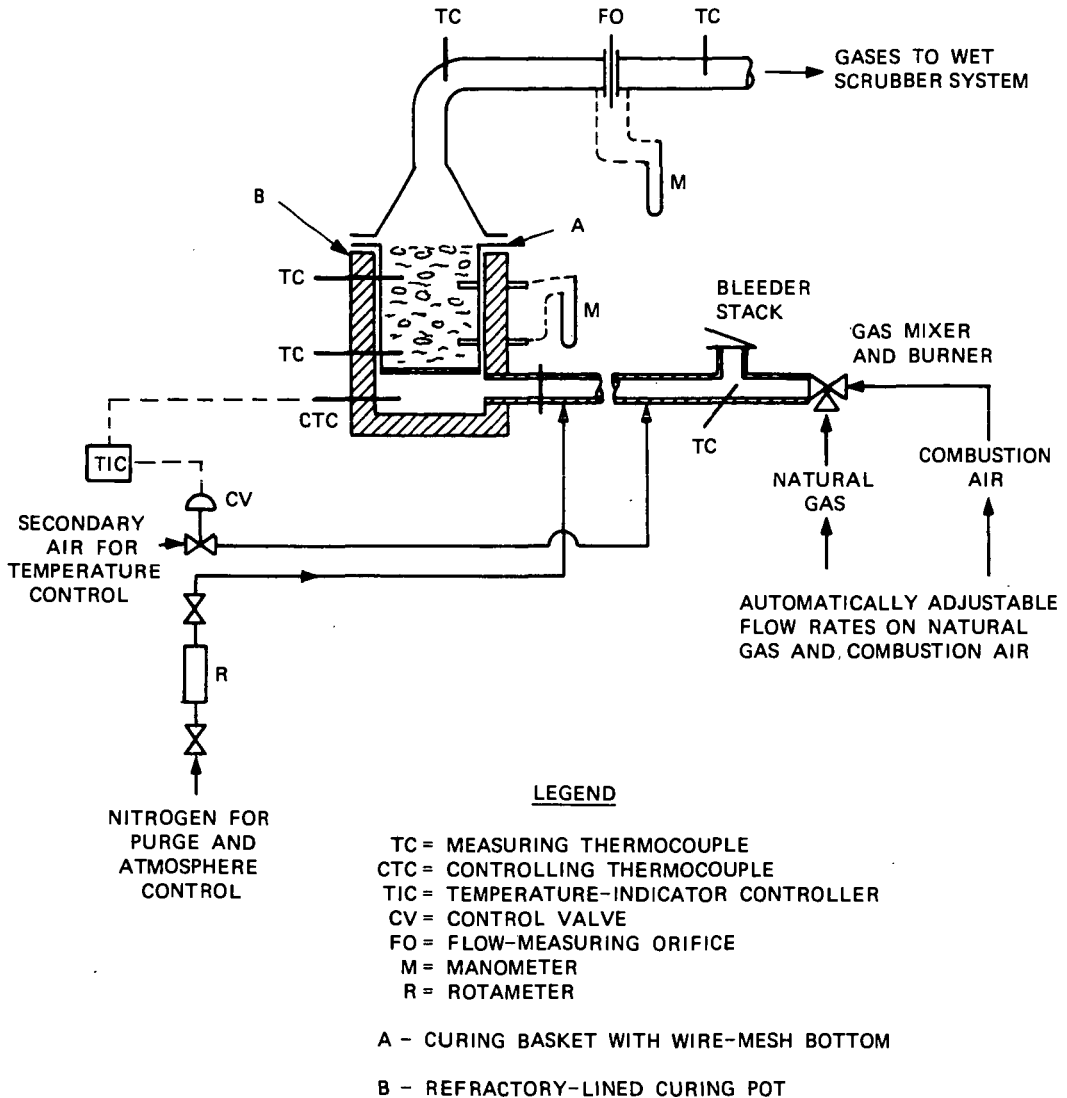
Photomicrographs showing typical appearance of Illinois No. 6 coal and the char product from coal which is used to make Formcoke pellets. (V) Vitrinoid (principal coal entity), (C) Char, (M) Mounting media, (P) Pores. Reflected light. X200



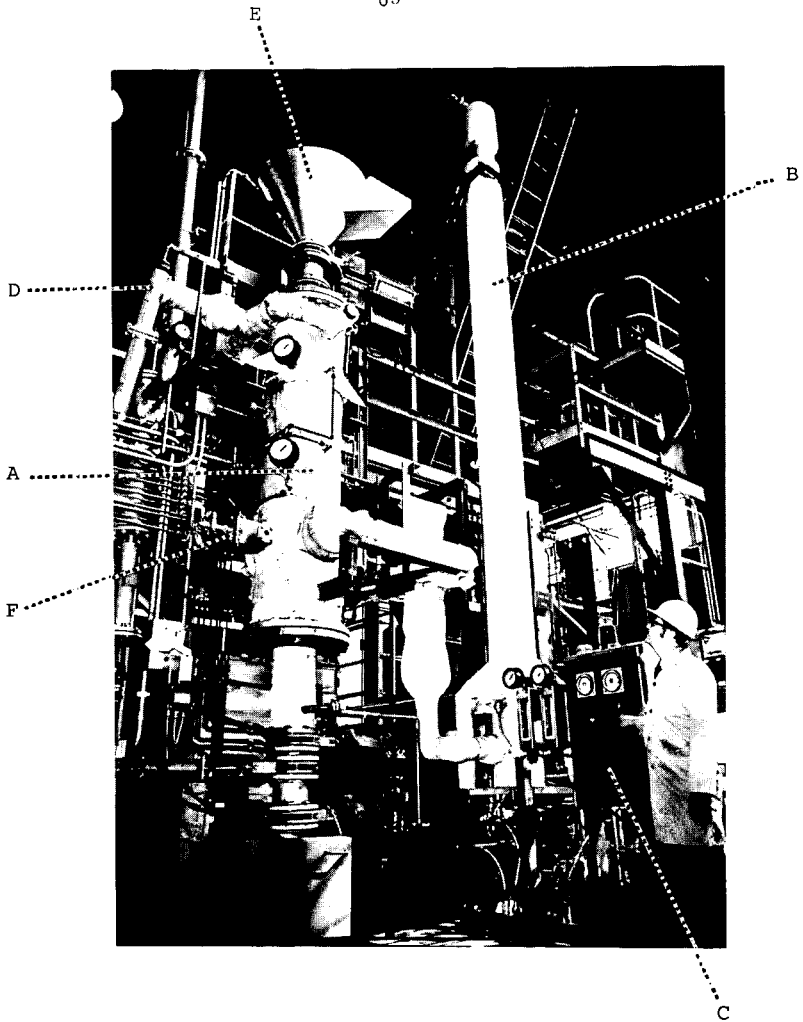
CHAR-PELLETIZING EQUIPMENT OF COKE-PREPARATION  
PROCESS-DEVELOPMENT UNIT

- A Two-Foot Pelletizing Disc
- B Char Screw Feeder
- C Char Distributor
- D Pellet Roller Screen
- E Binder Pump No. 1
- F Binder Surge Tank No. 1
- G Exhaust System

Figure 2

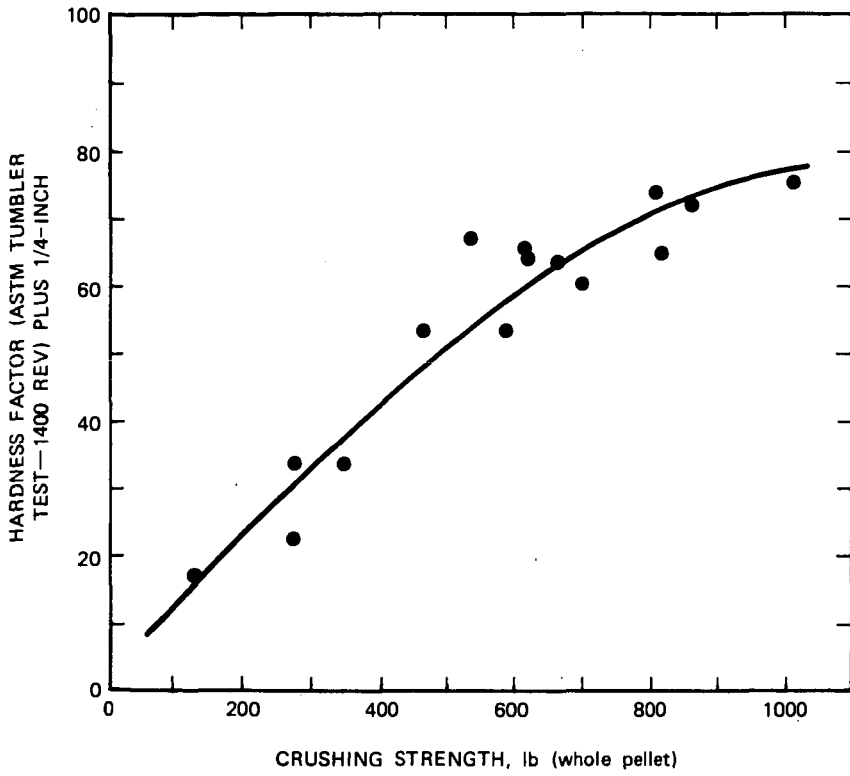


SCHEMATIC DIAGRAM OF CURING POT SYSTEM



Coking kiln and auxiliary equipment.

- A. Coking Kiln
- B. Kiln Gas Heater
- C. Heater Control Panel
- D. Kiln Gas Scrubber
- E. Pellet Surge Hopper
- F. Kiln Auxiliary Burner



RELATIONSHIP BETWEEN CRUSHING STRENGTH AND TUMBLER STRENGTH OF FORMCOKE PELLETS

Figure 5

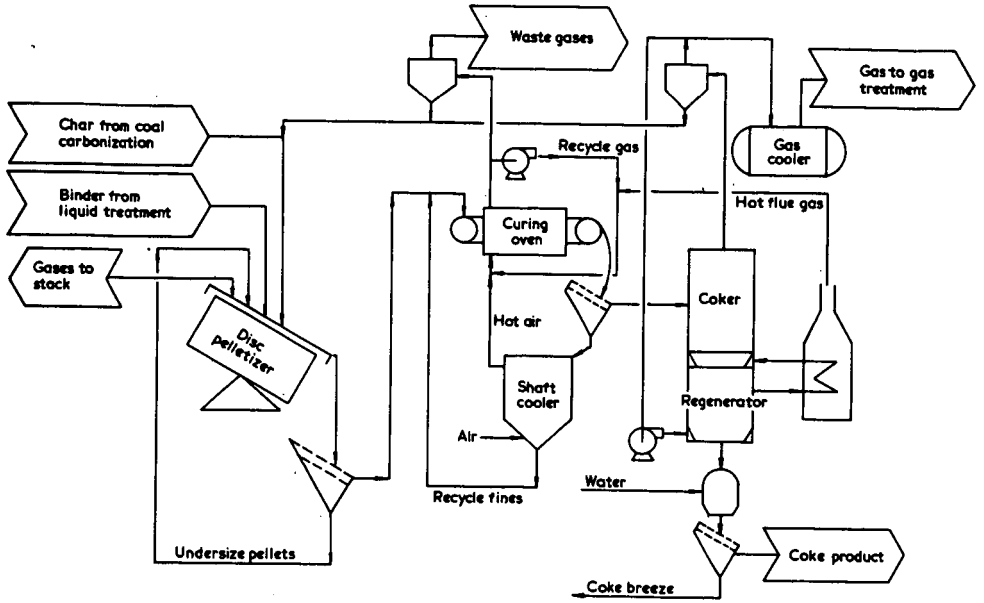
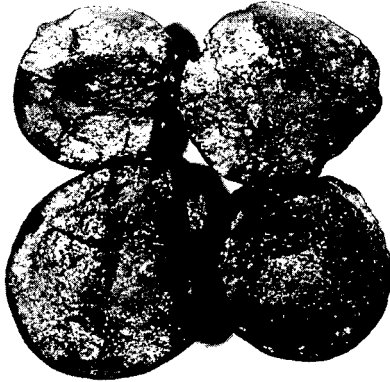


Fig 6. Illustration of equipment involved in the coke preparation during the Clean Coke Process

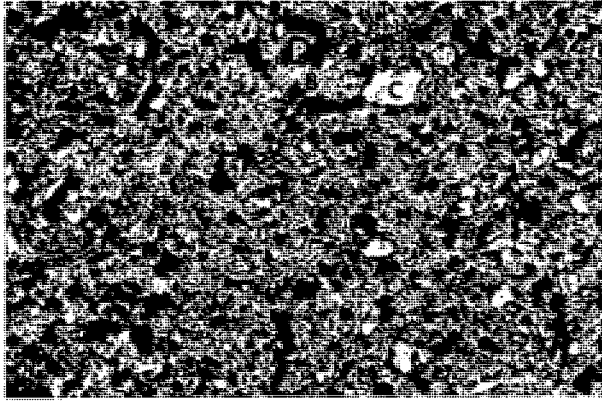


Broken Formcoke Pellets Showing Fracture Surfaces. X1.25

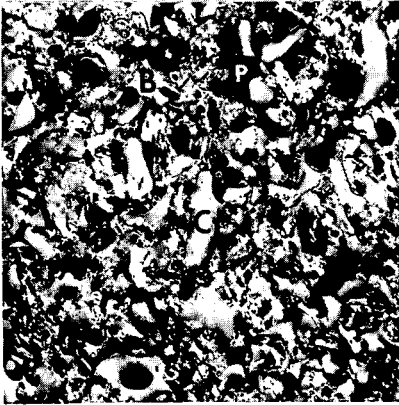


Formcoke Pellet Product

Photographs showing whole and broken of Formcoke pellets



Carbonized Formcoke Pellet Made From Minus  
28-Mesh Char. X25



Good Mixing. X100



Poor Mixing. X100

Photomicrographs showing Formcoke pellet structure at low magnification and variation in microstructure due to mixing at high magnification. (C) Char, (B) Binder, (P) Pores. Reflected light.

THE MANUFACTURE OF METALLURGICAL FORMED COKE ACCORDING  
TO THE BFL-HOT BRIQUETTING PROCESS

---

by

E. Ahland, J. Lehmann and W. Peters,  
Bergbau-Forschung GmbH., Essen

and

J. Langhoff,  
Ruhrkohle A.G., Essen

For the making of metallurgical coke, quite a number of continuous formed coke making processes have become known in the past years. It was the aim of these processes to produce lumpy coke suitable for blast-furnaces, above all from weakly or not caking coals. From a world-wide viewpoint, such coals are much more available than the prime coking coals from which conventional coke has been produced so far in slot-type recovery coke ovens.

Since 1962, Bergbau-Forschung GmbH., Essen, and the Lurgi Mineralöltechnik GmbH., Frankfurt, developed the so-called BFL-process which uses the hot briquetting of mixtures of coal and char in order to make formed coke. For the development of such a process for the thermal refining of hard coal, several years of testing and trial are indispensable. Subject of such a phase of trial are the process as such as well as the products made according to this process.

As for the trial and the process itself, the question arises first of all about the technical feasibility of the process. When this feasibility has been principally proven, questions of a suitable selection and set-up of machines and apparatus gained in importance, while the optimization of the overall process concludes the development. The necessary tests can be carried out in small-scale testing or trial plants or with physically similar models. Both methods of development are suitable and complement each other meaningfully. In this connexion, the question of the transferability of the results, first from small-scale plants to large-scale plants, and then, in case of model tests from the model to the large-scale realization, has an essential importance.

It is the objective of a testing and trial of the products to prove that the new product is at least equivalent to those hitherto used. A two-way procedure offers itself also for this stage of trial: on the one hand, trials can be run in small-scale plants as are available, e.g., to the West European metallurgical industry in the trial blast-furnace Ougrée, or, on the other hand, prediction about the behaviour of the product in practice can be made from the chemical, physical and technological properties obtained from the laboratory tests. It is a matter of course that - in order to establish the evidence of the formed coke for its suitability - a long-term trial in a practical blast-furnace for at least one month will be necessary. Without such a long-term trial nobody will risk to establish a commercial plant according to a new process, as the investments required therefor would be too high.

The BFL-process<sup>1)2)</sup> has already passed a considerable part of the lead time up to the unlimited application of the process in practice. For better understanding of the following expositions, however, the principle of the BFL-process will be described once more below.

#### Description of the process

As shown in Figure 1, hot and finely grained char with a temperature of about 750 °C is mixed with finely grained binder coal in a mechanical double screw mixer. The binder coal should be available in a size <1 mm. The ratio between binder coal and char is about 30:70. On account of this ratio and the temperature of the hot char, the temperature of the mixture is in the range of softening of the binder coal. The double screw mixer has the function to mix rapidly and intensively the char and the binder coal in order to attain a balance of temperature between the two flows at the end of the mixer. Thus, the binder coal has been heated up to a temperature of 450 °C and has become plastic. The mixture then gets into a pug mill from where it is conveyed to the double-roll press. This press gives the briquettes their shape. The briquettes leaving the press at a temperature of about 450 °C must be subjected to a careful cooling and are then eligible for use in the blast-furnace.

As Figure 2 shows, there are two methods for producing the necessary char. The more simple process and also that requiring less investments is the fluidized-bed carbonizer. Here, the fine coal fed into the reactor at a temperature of about 750 °C is carbonized in the fluidized bed. Part of the necessary heat can be supplied with the fluidizing gases, another part by the burning of char in the fluidized bed. The oxygen necessary for combustion is contained in the

fluidizing gases. The waste gas consists of a mixture of degasification gas and the fluidizing gases. Due to its high nitrogen contents, however, it has still only a low calorific value in the range of 1000 to 2000 kcal/m<sub>n</sub><sup>3</sup>.

The more expensive process circulating a heat carrier according to Lurgi-Ruhrgas, briefly called "the LR process", provides a separation of the heating-up process and of the degasification process with the result that a rich gas is obtained as a by-product. Circulating char at a temperature of about 750 °C and fine coal, in a ratio of 10:1, are supplied to a mechanical double-screw mixer. This mixture is then brought, with a temperature of 650 to 700 °C, into a subsequent degasifier from which the product gas on the one hand can be withdrawn and, on the other, the excess fine char. The excess fine char is supplied to the hot briquetting section, while most of the char remains in the circulation and is supplied to an airlift. In this airlift the char now used as a heat carrier is re-heated up to 750 °C either by partial combustion or by a bottom firing with fuel gas. In the collecting bin, the char is separated from the carrier gases and re-enters the process, while the flue gas, with its content of sensible heat, can be used for pre-heating the combustion air for the airlift and the drying of coal. The selection of the process for the production of a finely grained char is not without influence on the properties of the product.

The LR-process yields, as a whole, a denser char and, thus, also denser hot briquettes. Generally, all hard coals, from the anthracite to the long-flame coal, are suitable for char making. The binder coal, however, must fulfill certain requirements, viz. concerning the coking and the softening properties. Recent investigations in the laboratory and in our semi-technical plant showed that not only well-caking coal but also medium and weakly caking coal with a Swelling Index of ca. 3 can be used successfully as binder coal, provided part of the tar obtained during low-temperature carbonization and hot briquetting is admixed to the hot briquetting mixture. By adding about 6 to 9 % of tar to this mixture, the binding capacity of the coal is improved to such an extent that hot briquetting strengths are reached as with the sole use of a well caking coal as binder component.

#### Testing and trial of the process

The process has, so far, been tested and tried in four stages. Parallel to the investigations in the testing plants, individual problems of the development of the process were solved in a number of model tests. After reaching the next higher stage, however, the smaller-scale testing plants did not usually become superfluous as the duty to investigate several

times new coals necessitated each time tests and trials in the smaller-scale apparatus. Besides, the process itself is being further developed and improved continuously, as, e.g., now weakly or medium caking coals can be used as binder coal with the addition of tar or other binding agents to the hot briquetting mixture.

The smallest-scale plant, as shown in Figure 3, is a laboratory apparatus. This is, in fact, a discontinuously operated briquetting plant working with a small piston press. This press yields briquettes with a weight of about 12 g. From density and strength investigations a first statement can be made about the suitability of the used coals as well as about the presumably best operating conditions. In small coking ovens, the behaviour of these green briquettes during the subsequent heating-up can be investigated.

The next stage involves semi-technical plants with a throughput of 100 to 600 kg/h. These plants are working continuously with a double-roll press. For the production of char, an LR-plant as well as a fluidized-bed carbonizer are available. Figure 4 shows the building accommodating these plants. But even testing plants of this size do not yet permit to produce the quantities required for blast-furnace tests. This became possible only by a plant with a throughput of 5 t/h of hot briquettes shown in Figure 5. In this plant, quantities could be produced for blast-furnace tests with throughputs up to 7000 tons per test.

The presently last step of development are the large-scale testing plants. Messrs. Still of Recklinghausen established, by order of the Ruhrkohle AG, during 1973 and 1974 a 12.5 t/h hot briquetting plant on the area of the coke oven plant Prosper in Bottrop. This plant is operated by the "Arbeitsgemeinschaft Formkoks" formed by experts of Ruhrkohle AG and of Bergwerksverband GmbH., a subsidiary of the Bergbau-Forschung GmbH. Figure 6 will give you an impression of this plant which, compared with conventional coke oven plants, has been built much more to the height.

A further large-scale testing plant according to the BFL-process with an throughput per hour of 27 tons of hot briquettes is being built at present, by order of the British Steel Corporation, by the Lurgi Mineralöltechnik GmbH. in England.

These large-scale testing plants are to fulfil three duties:

1. Testing of the BFL-technology in a larger scale.
2. Making sufficient quantities of hot briquettes available for long-term blast-furnace tests.
3. Drawing-up of reliable material and heat balances to serve as a basis for economy calculations.

The flowsheet of the large-scale testing plant Prosper and its individual stages: drying, LR-low-temperature carbonization, hot briquetting, the cooling of briquettes and the purification of gases, can be seen from Figure 7.

The coals delivered by rail are stored separately, according to coal for char making and binder coal and are then dried after withdrawing through vibrating chutes into two parallel flash driers (1). The about 700 °C hot waste gases of the LR plant are used for drying. Afterwards, the moisture content of the coal is < 1 %.

The dried binder coal is crushed in an impact mill (2) to < 1 mm. As for the coal for char making, the sizes > 3 mm separated in a pneumatic deduster can also be subjected to crushing (2). According to our experience, however, crushing can be resigned on because of a sufficient crushing of the charring coal particles during the shock type heating-up during carbonization. The dried coal is bunkered for a while in the plant. The char is produced according to the LR-process. For this process, the coal for char making is proportioned, in a ratio of 1:10, to the circulating char, via a belt scale, in the double-screw mixer. By the following admixture of fresh coal, the temperature of the mixture decreases to about 700 °C. After a short residence in the degasifier shaft, the mixture is proportioned to the airlift to which the heat necessary for low-temperature carbonization is supplied, either by the combustion of char or the combustion of gas. In the ascension pipe, the char is heated up to 750 °C and conveyed into the collecting bin. The bulk of the char is returned to the circuit and, thus, into the mixer, while the excess char flows into the hot briquetting.

The waste gases of the airlift are passed, via a cyclone system (4), into a secondary combustion chamber where the residual coke dust and the combustible gases are burnt. The heat of the waste gases is utilized for the pre-heating of the air to the airlift and in the driers.

For hot briquetting, the binder coal is proportioned, via a belt scale, to the double-screw briquetting mixer (5) and is there intensively mixed with the hot char. In the subsequent pug mill (6) the final homogenization and degasification of the briquetting material take place which flows to the roll press by gravity (7).

The used briquetting rolls have a diameter of 1.4 m and a maximum contact pressure of 3.5 t/cm. Briquette sizes of 20 to 300 cm<sup>3</sup> can be produced.

Directly below the press, the grooves are separated from the briquettes by a fixed grate and are returned into the LR-plant.

The hot briquettes are cooled in a shaft cooler (8) by circulating gases, these gases being cooled themselves in a warm water cooler in order to avoid a condensing of water. At the end, the briquettes pass a water bath where the residual heat is discharged.

The carbonization gases from the LR-plant and the hot briquetting are subjected for purification to a several-stage condensing process where tar, oil and gas liquor from the carbonization are obtained, in addition to the gas.

As concerns environmental protection, the hot briquetting process can be considered as "non-polluting". All stages, from drying up to the cooling of the products, take place in closed containers and apparatus. Contrary to the presses in conventional briquetting processes, the hot briquetting press, too, is totally encased. This, however, hinders the attendance and the operating of the press by no means.

The dedusting of the waste gases from the drier and the collecting bin of the LR-plant takes place in an electrostatic precipitator down to a value - prescribed by the Mines Inspectorates - of  $150 \text{ mg/m}^3$ , after the residual CO and  $\text{H}_2$  have been burnt in a combustion chamber.

Desulphurized carbonization gas can be used for bottom firing of the LR-plant with the result that the dust gases, too, are free of sulphur.

All gases and water flows containing any contaminations are fully under control. As regards measuring and control, the entire plant has been conceived such as to be controlled from a central control room. No personnel needs to be present in the station, except for repair and attendance work. Thus, the demands placed on a modern hygiene at the working point have been realized to a wide extent.

The taking into operation of the demonstration plant Prosper began in May 1974 and has not yet been completed up today. Figure 8 containing schematically the individual sections with the ancillary plants, shows (in a dark colour) which components of the plant have been taken into operation so far.

A number of technical disturbances and standstills - not unusual for commissioning such a demonstration plant - caused considerable delays in the originally planned time schedule. Deficiencies in the conventional equipments formed a frequent source of defects and failures. E.g., the drying and re-heating phase of the refractory material required a much longer time as unexpected conditions of the Inspectorates with regard to the safety in operation had to be observed.

At the time when this report was written, the LR-cycling had been taken into operation and was well under control. The time schedule provides as a next step the taking into operation of the gas purification, which will be followed by the commissioning of the hot briquetting stage.

#### Testing of and trials with the products

A first indication on the suitability of different formed cokes for use in blast-furnaces is obtained from the data of analyses. The interesting properties are: size and shape, strength, density, reactivity and contents of volatile matter. These factors are much influenced by the control of the process, while other factors, such as the ash and sulphur contents, depend essentially on the type of input coals.

The size and shape of the briquettes can be freely selected during the briquetting process, the shape being subjected to a more stringent limitation than the size. In the 5 t/h plant, hot briquettes have been produced up to a maximum of 300 cm<sup>3</sup>. This large briquette, however, was not used in blast-furnaces, but in cupolas. Thorough model investigations about the flow resistance of formed coke led to new perceptions. Of decisive influence on the strength of burdens of formed coke is the purling of the burden into the void space of the formed coke.

For the lower part of the blast-furnace, e.g., the zone where the iron has been molten yet, a formed coke as lumpy as possible, is desirable in order to attain a low flow resistance. On the other hand, a lumpy coke can be disadvantageous before the tuyeres as well as in the shaft of the blast-furnace. In front of the tuyeres, the surface offered can be so low that the turn-over slows down with the blast. In the upper part of the blast-furnace, the finely grained sinter can purl into the void space to such an extent that the pressure loss will be higher than with small sizes of coke. Thus, there is an optimum size which always depends on the type of burden used. Generally, the optimum size is smaller when pellets are used than with the use of finely grained sinter. This know-how obtained first in model tests could be much confirmed in actual blast-furnace trials.

The strength of the formed coke plays an important part during trials in the blast-furnace. In order to be able to draw a comparison with the conventional coke, the drum test offers itself, as the crushing strength usual for briquettes cannot be applied to a conventional coke, because of the irregularity of the coke lumps. Figure 9 shows - besides other properties - some comparison strengths according to MICUM as well as according to IRSID. Attention must be paid, however, that the abrasion < 10 mm developing from formed coke is finer as when conventional coke is subjected to drum tests.

After the trials by Ledent<sup>4)</sup> in the Ougrée blast-furnace, the attention has been directed to the coke density and the porosity connected therewith. According to Ledent, formed coke should have, if possible, a similarly high porosity as conventional coke. An extremely dense coke is not suitable for use in a blast-furnace.

The reactivity of formed coke is, as a rule, higher than that of conventional coke. However, it is still within a range where it is without much influence on the operation of the blast-furnace.

Important in connexion with the behaviour of the hot briquettes in the blast-furnace was the question whether the burn-up of the green briquettes takes place from the outside or through the pore system in the inside of the green briquettes. In the latter case, the burn-up in the blast-furnace could have caused a decisive weakening of the green briquettes with the result that they could fall to pieces in the bottom part of the blast-furnace. Samples drawn from the tuyeres during blast-furnace tests showed, however, that the burn-up takes place wellnigh exclusively via the outside surface of the briquette and that the structure in the rest of the briquette remains nearly unchanged.

When using uncoked hot briquettes in the blast-furnace, a much higher content of volatile matter must be reckoned with as in the case of conventional coke, as is to be seen from Figure 9. As far as these volatile matters emit from the briquettes in form of gas, they will not interfere with the operation of the blast-furnace. The blast-furnace gas will be enriched thereby in its calorific value what was not even unwelcome in many of the works. The volatile matter must not contain any traces of tar, as otherwise operational defects could be caused by its condensation in the equipment subsequent to the blast-furnace. Tests run so far, however, gave not reason to such fears.

That this must not be expected from longer-lasting tests has been shown by comparable tests where steam coal nuts

(with 17.5 % Vol. Matter waf) were added to the coke (to the extent of 6:8 %) in operating blast-furnaces of the Youngstown Sheet and Tube Company); even after an operation of one year no depositions could be found in the subsequent pipelines.

Figure 10 gives a review of the blast-furnace tests and trials carried out in the meantime with BFL-formed coke. Green as well as calcined briquettes were tried, the hot briquettes being charged to the extent of 100 %, i.e. without admixing conventional coke. The strength of the hot briquettes proved to be sufficient for the transport processes outside the blast-furnace as well as for the mechanical stresses inside the blast-furnace. No breaking of the briquettes could hardly be observed. Dust development in the transport cars in front of the blast-furnace remained low. In the blast-furnace gas as well, the dust contents increased only a little, compared with the operation with conventional coke.

The tests and trials covered the period 1967 to 1973. They were run in Belgium, the Federal Republic of Germany and in England<sup>7)</sup>. The diameters of the hearth-casing of a blast-furnace reached from 1.4 m to 9.5 m, and the period of testing from one day to seven days. After the demonstration plant Prosper has been successfully taken into operation, it is provided to prove the definite suitability of the new fuel in blast-furnaces in long-term trials.

To close with, the advantages of the BFL-process will be summarized once more:

The process permits the use of coals otherwise not suitable for coking, thus enlarging essentially the coal basis for making coke.

The process can be considered to be "non-polluting", as the coking process takes place in closed apparatus from which the developing flows of waste gas can be got hold of fully and can be purified by conventional methods.

The entire plant can be started and stopped quickly. Thus, the process is most flexible and can be easily adjusted, if necessary, to a varying market for coke.

Thanks to the free selection in size and shape, the hot briquettes can be adjusted to different types of burdens with a view to a good permeability across the blast-furnace.

References

- 1) Ahland, E., J. Lehmann and W. Peters: Suitability of Coal for Production of Formed Coke. 31. Ironmaking Conference, Chicago 1972.
- 2) Schmalfeld, P. and R. Rammner: Results of the Development and Present Stage of the BFL-Hotbriquetting Process. 13<sup>th</sup> Biennial Conference of the Institute for Briquetting and Agglomeration, Colorado Springs, August 1973.
- 3) Schultz, H.-J. and O. Abel: Druckverluste in Koks-Sinter-Schichtungen und -Mischungen. Arch. Eisenhüttenwesen 45 (1974) No. 7, pp. 445-448.
- 4) Ledent, P., G. Burton and M. Marcourt: Die Entwicklung des INIEX-Verfahrens zur Erzeugung von Formkoks. Informationstagung der EGKS, Luxemburg, April 1970.
- 5) Harris, W. F., R. J. Tracey and D. L. Locier. Substitution of Coal for Coke in Blast Furnace Burdens. Paper presented at Eastern States Blast Furnace and Coke Oven Association, Pittsburgh, Pa., February 9, 1973.
- 6) Därmann, O., S. Henkel and K. D. Haverkamp: Die Verwendung von Heißbriketts und Formkoks im Hochofen. Stahl und Eisen (1970) pp. 1009-1012.
- 7) Holgate, J. K. and P. H. Pinchbeck: Use of Formed Coke: BSC Experience 1971/1972. J. of the Iron and Steel Institute 1973, pp. 547-566.

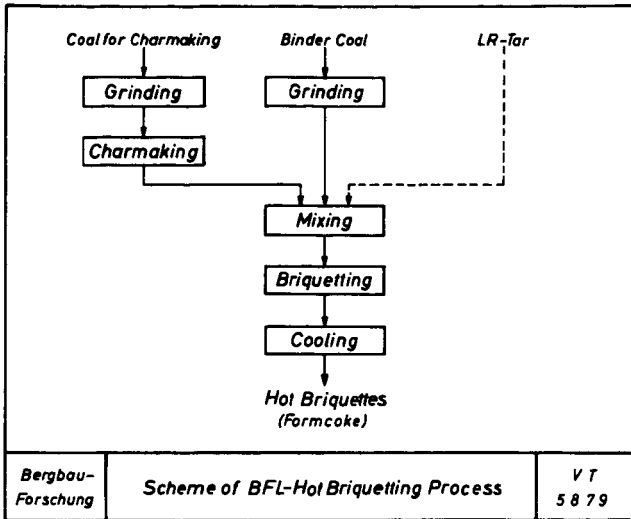


Figure 1

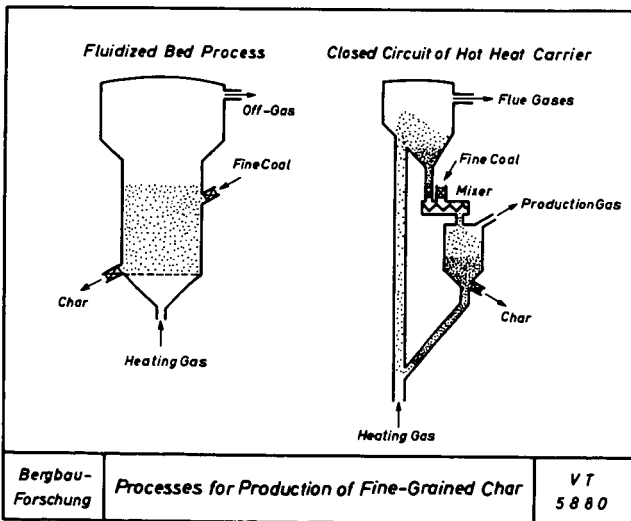


Figure 2

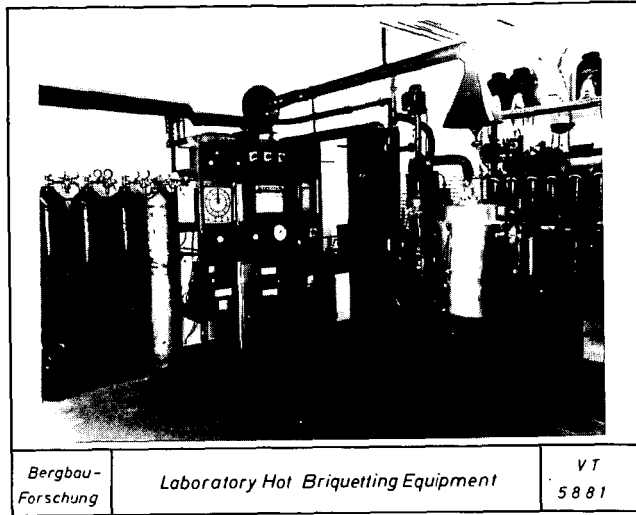


Figure 3

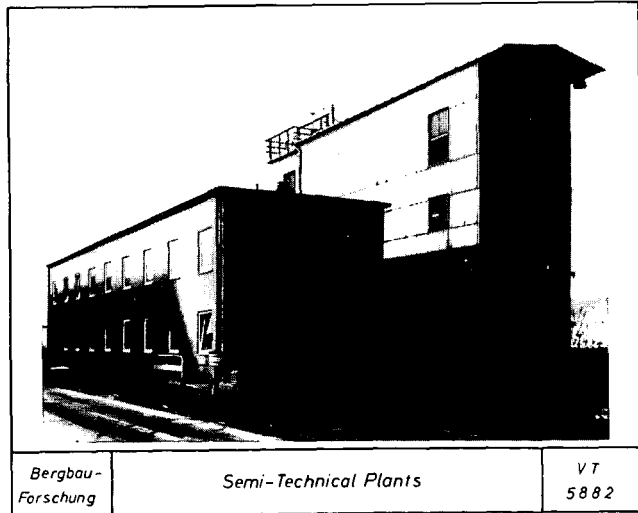


Figure 4

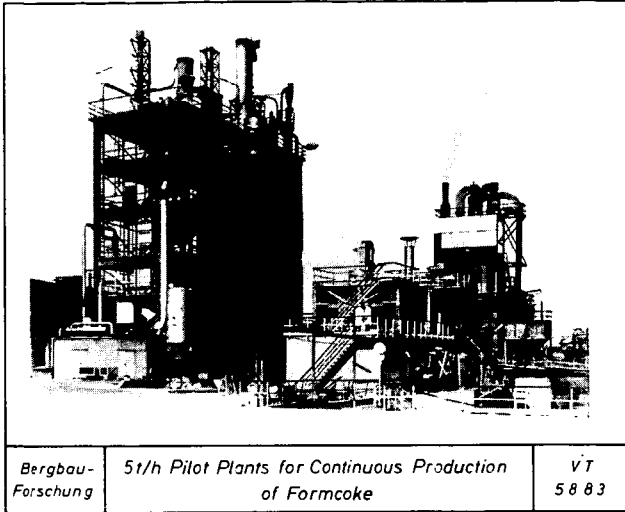


Figure 5

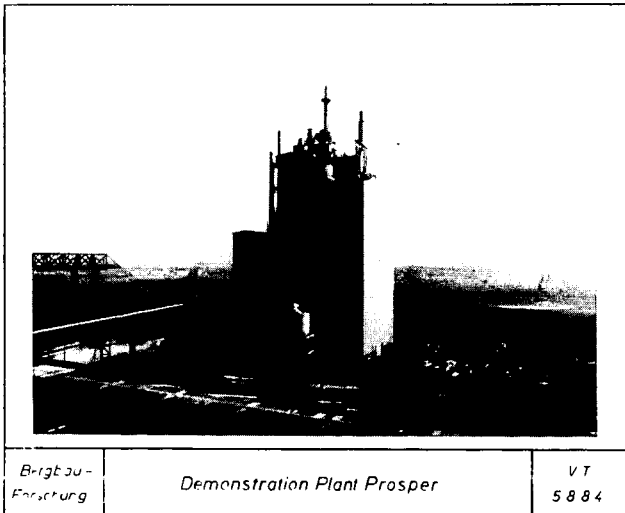


Figure 6

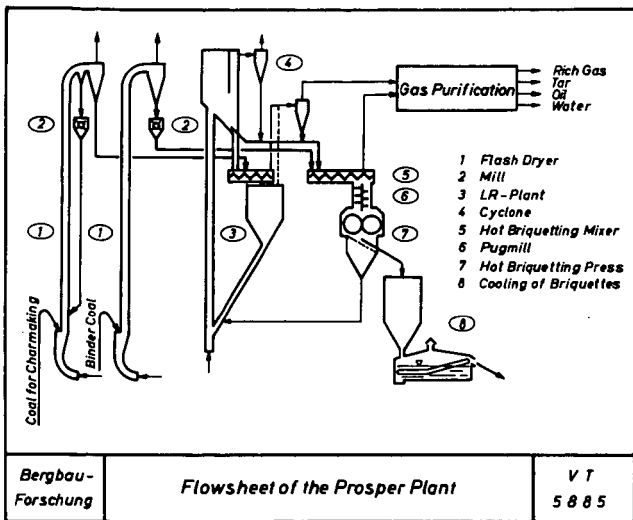


Figure 7

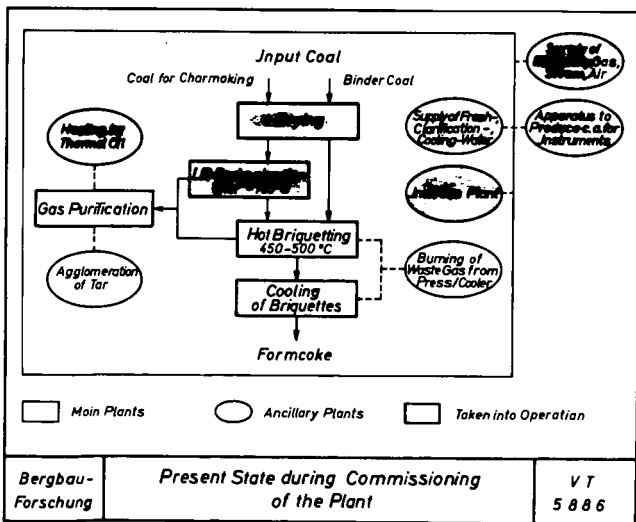


Figure 8

	BFL-HOT BRIQUETTES		BF COKE III
Weight per Piece.....g	101	48	—
Porosity.....%	39	49	50
Vol. Matter.....%	10,1	7,1	< 1
Ash.....%	6,8	7,0	8,6
Sulphur.....%	0,91	0,83	0,86
Bulk-Density.....Kg/m <sup>3</sup>	561	508	437
<b>STRENGTH</b>			
<b>MICUM [DIN 51717]</b>			
M <sub>40</sub> .....%	92,6	91,7	81,2
M <sub>10</sub> .....%	6,7	7,8	6,5
<b>IRSID</b>			
I <sub>20</sub> .....%	79,0		80
I <sub>10</sub> .....%	20,8		18
BF 1975	<b>PROPERTIES OF BFL-HOT BRIQUETTES AND CONVENTIONAL COKE</b>		5887

Figure 9

TEST	1	2	3	4	5	6
Year	1967	1969	1970	1970	1971	1973
Country	BEL	BRD	BRD	BRD	GB	BRD
Dio of Hearth-Casing..m	1,4	9,5	6,8	6,8	5,5	6,8
Tonnage.....t	500	1350	2700	7000	2650	1150
<b>PROPERTIES OF BRIQUETTES</b>						
Weight.....g	21	45	48	44	53	98
Volume.....cm <sup>3</sup>	26	49	55	51	58	106
<b>ABRASION M10</b>						
[DIN 51717].....%	6,7	7,0	7,8	7,1	12	10,4
Porosity.....%	57	54	49	59	43	45
Bulk-Density.....Kg/m <sup>3</sup>	415	558	508	495	507	495
Vol-Matter.....%	2,5	1,9	7,1	1,7	6,0	9,2
BF 1975	<b>BLAST FURNACE TESTS WITH HOT BRIQUETTES</b>					5888

Figure 10

RELATIONSHIP BETWEEN THE GASIFICATION  
REACTIVITIES OF COAL CHAR AND THE  
PHYSICAL AND CHEMICAL PROPERTIES OF  
COAL AND COAL CHAR

James L. Johnson

Institute of Gas Technology  
3424 S. State Street  
Chicago, Illinois 60616

## INTRODUCTION

A variety of experimental investigations have studied, at elevated pressures, the gasification kinetics of coal chars in hydrogen and in gases containing steam and hydrogen. The bulk of these investigations, however, have been primarily concerned with the characterization of gasification rates as a function of environmental conditions such as temperature, pressure, and gas composition, and have provided little systematic information concerning relationships between gasification reactivities and the physical and chemical properties of coal or coal char.

This study was therefore initiated to evaluate possible relationships between gasification reactivities and simple compositional parameters for coal chars derived from a wide variety of coals and coal-maceral concentrates. The internal structural changes that occur during the course of gasification of a few coal chars of varying rank were also explored. The gasification reactivities of individual coal chars were determined in hydrogen or in a 50:50 steam-hydrogen mixture at 35 atmospheres, using a high-pressure thermobalance. Most tests were conducted at 1700°F, although, in a special series of tests designed to investigate the catalytic effects of exchangeable cations on lignite char reactivities, temperatures were varied from 1400° to 1700°F. The following results are discussed in this paper:

- The relationship between the initial carbon content and the gasification reactivities determined in the hydrogen at 1700°F, for coal chars derived from 36 coals and maceral concentrates ranging in rank from anthracite to lignite.
- The effect of exchangeable cation concentrations (sodium and calcium) on gasification reactivities of lignites in hydrogen at 1700°F and in steam-hydrogen mixtures at 1400° to 1700°F.
- The surface area and pore volume variations that occur during gasification in hydrogen and in steam-hydrogen mixtures at 1700°F of coal chars derived from anthracite, metallurgical coking coal, high-volatile A bituminous coal, sub-bituminous A coal, and lignite.

## EXPERIMENTAL PROCEDURE

The high-pressure thermobalance used in this work to obtain gasification reactivity factors has been described previously (4). The main feature of this apparatus is that the weight of a small, fixed-bed sample of coal char (1/2 to 1 gram) contained in a wire-mesh basket can be continuously measured as it undergoes gasification in a desired gaseous environment at constant temperature and pressure. In all tests conducted, -20+40 U. S. sieve size particles were used, and gas flow rates in the reactor were maintained at sufficiently high values to result in negligible gas conversion. Under these conditions, coal-char gasification could be considered to occur under constant known environmental conditions. Coal chars were produced by initially exposing the raw coals to nitrogen at 1 atmosphere for

60 minutes, at the same temperature to be used during subsequent gasification in hydrogen or in steam-hydrogen mixtures. The weight loss versus time characteristics obtained during gasification in individual tests were then used as a basis for computing gasification reactivity factors, using a procedure described below.

Certain of the solid feeds and residues were analyzed for internal surface area, pore volume, and true density. Surface areas were computed from adsorption isotherms obtained with a Model 2100 Orr surface area-pore volume analyzer manufactured by the Micromeretics Corp., which was also used to obtain true densities in helium. Adsorption isotherms obtained in nitrogen at 77°K were interpreted with the BET equation to compute surface area, and isotherms obtained in carbon dioxide at 298°K were interpreted with the Dubinin-Polanyi equation as modified by Kaganer (7) to compute surface area. In general, surface areas computed from nitrogen and carbon dioxide adsorption isotherms were not in agreement, and values obtained in carbon dioxide were considered to be most reflective of equivalent internal surface area, which is consistent with the findings of other investigators (2, 3, 6, 7, 12). Apparently, the penetration of nitrogen into the microporous structure of coals or carbonized coal chars is severely limited by slow, activated diffusion processes at 77°K, leading to very low apparent surface areas; on the other hand, for partially gasified coal chars having more open microporous structures, capillary condensation of nitrogen can lead to unreasonably high apparent surface areas (1, 8). Adsorption isotherms obtained with carbon dioxide at the higher temperature of 298°K facilitate activated diffusion into microporous structures, and capillary condensation is inhibited by the lower relative pressures employed (0.003 to 0.02). Although there is some question concerning whether carbon dioxide adsorption isotherms should be interpreted in terms of micropore volume (8, 9, 10, 11) rather than micropore surface area (2, 3, 6, 7, 12), the distinction is not of importance in empirical correlations with gasification kinetic parameters. This is because the calculation methods used to compute numerical values of micropore volume and micropore surface area are virtually identical, differing only in the numerical constants used. Thus, reported values of micropore volumes can be converted to corresponding values of micropore surface area by a fixed constant. In this study we have chosen to compute surface area values, favoring the argument that carbon dioxide adsorption on a carbon surface should be restricted to a monolayer thickness, as a result of the quadruple interaction of the carbon dioxide molecules with the  $\pi$ -bonds of the carbon surface (2, 7).

An Aminco mercury intrusion porosimeter capable of a hydrostatic pressure of 15,000 psi was used to obtain pore volume distributions for pores having diameters greater than about 120 angstroms. Pore volume distributions for pores between about 12 and 300 angstroms were obtained from adsorption isotherms obtained in nitrogen at 77°K at relative pressures up to about 0.93. Good agreement was obtained with these two methods in the overlap region from 180 to 300 angstroms, similar to results reported by Gan *et al.* (3).

#### DEFINITION OF RELATIVE REACTIVITY FACTOR, $f_L$

Weight loss versus time characteristics obtained in individual thermobalance tests were interpreted to obtain relative reactivity factors for the coal chars used, based on a quantitative model developed previously at the Institute of Gas Technology to describe the gasification kinetics of bituminous coal chars as a function of temperature, pressure, gas composition, pretreatment temperature, and carbon conversion (4). The essential features of this model are described below.

Coal-char gasification in gases containing steam and hydrogen are assumed to occur via three main reactions:



where —

$f_o$  = reactivity factor dependent only on the inherent nature of the coal char

$T_p$  = pretreatment temperature, °R

$T$  = gasification temperature, °R.

Equation 3 is only applicable for  $T_p > T$ ; for  $T_p \leq T$ , then  $f_L = f_o$ .

At constant environmental conditions, Equation 1 can be integrated to yield —

$$M(X) = \int_0^X \frac{\exp(\alpha X^2)}{(1-X)^{2/3}} dX = f_L k_T \theta \quad 4)$$

Based on Equation 4, a plot of  $M(X)$  versus  $\theta$  should yield a straight line having a slope equal to the term  $f_L k_T$ . Values of  $M(X)$  can be computed from experimental thermobalance data, using Equation 2 to obtain values of  $X$  and using the defined value of  $\alpha$  to evaluate the integral in Equation 4. Note that, for tests conducted in pure hydrogen, the value of  $\alpha$  is 0.97; with this value, the term  $(1-X)^{2/3} \exp(0.97 X^2)$  is approximately equal to  $(1-X)$ , over nearly a complete range of  $X$ . For this case,  $M(X) = -\ln(1-X)$  and values of the specific gasification rate,  $(dX/d\theta)/(1-X)$ , are constant and equal to  $f_L k_T$ .

Figure 1 shows two types of behavior noted in this study in experimental plots of  $M(X)$  versus  $\theta$ . Line A is typical of the characteristics obtained with the majority of coal chars tested, with linearity exhibited over the complete range of base carbon conversion. The line shown does not extrapolate to the origin because char samples initially exposed to the gasifying environment in the thermobalance require 1 to 2 minutes to heat up to reactor temperature. A characteristic of the type shown for Case B was obtained with some coal chars, usually low-rank materials, indicating an initial period of transient reactivity, which decreased during the first 5 to 10 minutes and remained constant thereafter. For coal chars exhibiting this type of behavior, only the linear portion of the curve corresponding to constant reactivity was used to evaluate experimental values of  $f_L k_T$ .

Values of the reactivity factor,  $f_L$ , were then obtained by dividing the term  $f_L k_T$  by the value of  $k_T$  defined in the model (4) for the reaction conditions used.

## RESULTS

### Correlation of Reactivity Factors With Carbon Content in Raw Coals

The reactivity factors for coal chars derived from 36 coals and coal maceral concentrates were determined in hydrogen at 1700°F and 35 atmospheres. The distribution of coals used with respect to rank and lithotype is described in Table 1. In this study a variety of correlations were evaluated in attempting to quantitatively relate these reactivity factors with simple, compositional parameters included in ultimate, proximate, and petrographic analyses of the raw coals. The best success, however, was achieved with one of the simplest correlations considered — a relationship between reactivity factors and initial carbon contents. This correlation is illustrated in Figure 2, where the line drawn corresponds to the expression:

$$f_L = 6.2Y(1 - Y) \quad 5)$$

where -

$f_L$  = relative reactivity factor of coal char

$Y$  = concentration of carbon in raw coal (dry, ash-free), g/g coal.

Table 1. NUMBERS OF EACH COAL TYPE USED IN CORRELATION

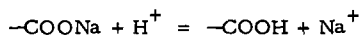
<u>Coal Rank</u>	<u>Whole</u>	<u>Vitrain</u>	<u>Fusian</u>	<u>Total</u>
Lignite	1	1	1	3
Subbituminous C	2	1	--	3
Subbituminous B	1	2	2	5
Subbituminous A	3	2	1	6
High-Volatile C Bituminous	1	2	1	4
High-Volatile B Bituminous	1	1	4	6
High-Volatile A Bituminous	4	2	--	6
Low-Volatile Bituminous	2	--	--	2
Anthracite	<u>1</u>	<u>--</u>	<u>--</u>	<u>1</u>
Total	16	11	9	36

For reasons discussed below, it should be emphasized that, for lignite coal chars, the correlation shown in Figure 2 is applicable only when the raw lignite is initially treated in acid to remove exchangeable cations.

The standard deviation of experimental reactivity factors shown in Figure 2 and of reactivity factors calculated from Equation 5 is about 0.1, which is equivalent to the reproducibility of experimentally determined reactivity factors. Interestingly, the correlation proposed does not uniquely distinguish between maceral types.

#### Effects of Exchangeable Cation Concentration on Lignite Char Reactivity

If reactivity factors determined for coal chars derived from untreated raw lignites were included in Figure 2, then a considerable amount of scatter would be apparent above the correlation line at low carbon concentrations. One phase of this study, however, showed that the reactivities of lignite chars obtained from lignites initially treated in HCl or HCl-HF acid were generally significantly less than the corresponding reactivities exhibited by lignite chars derived from untreated lignites. This was not observed with several bituminous and subbituminous coal chars. This behavior apparently resulted from a catalytic effect of exchangeable cations inherently present in raw lignites in carboxyl functional groups, which can be removed in acid by the following type of reaction:



With this explanation, one can reasonably expect that this catalytic effect would predominate in lignites and would decrease rapidly with increasing coal rank, corresponding to a rapid decrease in the amount of coal oxygen combined in carboxyl functional groups.

A series of tests were conducted to obtain a quantitative measure of the effects of exchangeable cation concentration (sodium and calcium) on char reactivity factors for gasification in hydrogen and in steam-hydrogen mixtures. These tests were conducted with lignite chars derived from raw lignites, with the lignite chars derived from raw lignites initially demineralized in hydrochloric acid to remove exchangeable cations and with the lignite chars derived from raw lignites initially demineralized in hydrochloric acid to which various amounts of calcium or sodium were then added by cation exchange in sodium acetate or calcium acetate solutions. Results of one

series of tests corresponding to gasification in hydrogen at 1700°F are shown in Figure 3. The results in Figure 3 were correlated with the expression:

$$f_L/f_L^0 = 1 + 54.7 Y_{Na} + 14.0 Y_{Ca} \quad (6)$$

where -

$f_L$  = reactivity factor of lignite to which sodium or calcium was added

$f_L^0$  = reactivity factor of acid-treated lignite ( $Y_{Na}, Y_{Ca} = 0$ )

$Y_{Na}, Y_{Ca}$  = concentration of exchangeable sodium or calcium in lignite before devolatilization in nitrogen, g/g fixed carbon.

Although the correlation given in Equation 6 was developed from data obtained with prepared lignites that did not contain both calcium and sodium at the same time, it does apply reasonably well to untreated lignites containing, in some cases, both calcium and sodium. This is demonstrated in Table 2.

Table 2. COMPARISON OF CALCULATED AND EXPERIMENTAL REACTIVITY RATIOS

Lignite	$Y_{Ca}$	$Y_{Na}$	$f_L/f_L^0$	
	g/g fixed carbon		Calculated	Experimental
Savage Mine, Montana (whole)	0.043	0.000	2.1	1.7
Savage Mine, Montana (vitrain)	0.019	0.004	1.5	1.7
Glenharold Mine, N. Dakota (whole)	0.031	0.009	1.9	2.0
Glenharold Mine, N. Dakota (vitrain)	0.019	0.002	1.3	1.2

A test series was also conducted to determine effects of exchangeable calcium and sodium concentrations on the reactivities on a Montana lignite char in steam-hydrogen mixtures at temperatures from 1400°F to 1700°F. Results obtained are illustrated in Figure 4, which plots values of the kinetic term,  $f_L k_T$ , as a function of temperature and cation concentration. Although these results have not yet been quantitatively correlated, they apparently show that sodium and calcium significantly enhance gasification in steam-hydrogen mixtures, even more so than for gasification in hydrogen alone. Figure 4 shows that the effect of calcium concentration on reactivities is substantially the same as the effect of sodium concentration at corresponding conditions (contrary to the behavior obtained in pure hydrogen), and that relative catalytic effects tend to decrease with increasing gasification temperature.

A significant additional result of the test series conducted with steam-hydrogen mixtures was that the reactivity of acid-treated Montana lignite ( $Y_{Ca}, Y_{Na} = 0$ ) remains constant for gasification in steam-hydrogen mixtures over a temperature range from 1400° to 1700°F. This is shown in Figure 5, which plots experimental values of  $f_L k_T$  versus values of  $k_T$  calculated from correlations developed to describe bituminous coal char gasification kinetics (4). The line drawn corresponds to a constant value of  $f_L = 1.3$ , which is about the same value obtained for gasification in pure hydrogen at 1700°F.

### Variations in Internal Char Surface Areas During Gasification

The variations in internal surface areas were measured for several chars at different stages of gasification in hydrogen or steam-hydrogen mixtures. The compositions of the coals from which these chars were prepared are given in Table 3. Figure 6 shows the variations in surface area measured in carbon dioxide with different base carbon conversion fractions for a series of tests conducted with Montana lignite chars. Figure 6 shows that the internal surface area of the Montana lignite char tends to remain constant over a major range of base carbon conversion fractions and is essentially independent of char pretreatment or gasification conditions. The apparent surface areas of carbonized chars ( $X = 0$ ) are lower than the nominal value of partially gasified chars. This difference may reflect that, even with carbon dioxide, penetration into the micropore structure is somewhat inhibited before the structure is opened up by partial gasification.

Figure 7 shows variations in apparent surface area measured in nitrogen for Montana lignite chars. The characteristics shown tend to support the suggestion made previously that, at low levels of conversion, nitrogen penetration into the micropore structure is severely inhibited, but that, at higher carbon conversions, unreasonably high apparent surface areas are obtained because of capillary condensation.

In Figure 8, variations in surface area measured in carbon dioxide ( $S_{CO_2}$ ) obtained with some other coal chars are compared with results obtained with Montana lignite chars. Although surface areas measured for char derived from anthracite, high-volatile bituminous coal, and lignite remained essentially constant during the course of conversion in hydrogen and steam-hydrogen mixtures, surface areas for the subbituminous coal char generally decreased with increasing carbon conversions during gasification in hydrogen. Interestingly, of the four coal chars tested, only the subbituminous coal char exhibited decreasing specific gasification rates during gasification with hydrogen that paralleled the decrease in surface area. This is shown in Figure 9. Although generalizations based on the kinetic behaviors exhibited by only four coal chars are not justified, these results do suggest that a form of kinetic correlation to describe coal-char gasification rates that is more meaningful than that derived from the Equation 1 may be the following:

$$\frac{dX}{d\theta} = \lambda S k_T (1 - X) \quad 7)$$

where —

$\lambda$  = relative reactivity per unit of internal surface area

$S$  = internal surface area per mass of carbon present.

With this interpretation, the constancy of the values of  $f_L$  and  $S_{CO_2}$  of anthracite, high-volatile bituminous, and lignite coal char during gasification in hydrogen corresponds to a constant value of  $\lambda$  for each char. For the subbituminous coal char,  $\lambda$  is also constant, although  $S_{CO_2}$  decreases with increasing carbon conversion, apparently because of the growth of crystallites. For the gasification temperatures used, this growth is probably unusual and not characteristic of most coal chars. This is particularly true if the first-order kinetics observed in a variety of previous studies of the gasification of a fairly large number of coal chars in hydrogen are assumed to correspond to constant values of  $\lambda$  and  $S_{CO_2}$  for the individual coal char tested.

Table 3. COMPOSITIONS OF COALS USED IN PHYSICAL PROPERTY STUDIES

Coal Identification	Pittsburgh No. 8 (Ireland Mine)		Brazilian Carvao Metallurgical		Rosebud, Colstrip Mine		Savage Mine (Montana)	
	Anthracite	Subbituminous A	Subbituminous A	Whole	Subbituminous A	Whole	Subbituminous A	Whole
Rank	Anthracite	Whole	Whole	Whole	Whole	Whole	Whole	Whole
Lithotype	Whole	Whole	Whole	Whole	Whole	Whole	Whole	Whole
Ultimate Analysis, mass %								
Carbon	83.40	69.47	66.70	66.70	69.60	69.60	65.13	65.13
Hydrogen	2.37	3.78	4.57	4.57	4.52	4.52	4.13	4.13
Oxygen	2.62	6.59	4.57	4.57	19.31	19.31	24.20	24.20
Nitrogen	0.84	1.39	1.22	1.22	0.99	0.99	0.89	0.89
Sulfur	1.03	3.75	1.90	1.90	0.65	0.65	0.57	0.57
Ash	9.74	15.02	21.04	21.04	4.93	4.93	5.08	5.08
Total	100.00	100.00	100.00	100.00	100.00	100.00	100.00	100.00
Proximate Analysis, mass % (dry)								
Volatiles Matter	6.77	22.70	31.80	31.80	42.10	42.10	43.62	43.62
Fixed Carbon	83.49	62.28	47.20	47.20	53.00	53.00	51.30	51.30
Ash	9.74	15.02	21.00	21.00	4.90	4.90	5.08	5.08
Total	100.00	100.00	100.00	100.00	100.00	100.00	100.00	100.00

Interestingly, in the kinetic model previously referred to, the value of  $\alpha$  in Equation 1 is approximately 1.7 for a variety of gas compositions containing steam and hydrogen at elevated pressures. Empirically, this value corresponds to decreasing values of  $\lambda$  with increasing carbon conversions when interpreted in terms of Equation 7. This occurs even when the total internal surface areas remain constant during conversion in steam-hydrogen mixtures, as was shown in Figure 6 for Montana lignite char.

Some additional evidence was obtained in this study that can be interpreted in terms of the formulation given in Equation 7. Figure 10 shows values of  $S_{CO_2}$  obtained during gasification of a coal char derived from Brazilian metallurgical coal, at various temperatures, with hydrogen and steam-hydrogen mixtures. With this material, the char surface area,  $S_{CO_2}$ , is not a function of carbon conversion level and is the same in hydrogen and in steam-hydrogen mixtures, but decreases with increasing gasification temperature. The reactivity factor,  $f_r$ , which is characteristic of results obtained at a specific temperature, also decreases with increasing temperature and is proportional to internal char surface area, as shown in Figure 11. This particular char then can be considered to have a constant value of  $\lambda$ , independent of temperature, conversion, or gasification medium, but does exhibit a decreasing internal surface area with increasing temperature, a feature that probably reflects its use as a metallurgical coking coal.

#### Variations in Char Pore Volumes During Gasification

Figure 12 illustrates typical pore-volume distributions of partially gasified coal chars. With the exception of untreated Montana lignite (Curve F), the features exhibited in Figure 12 appear to be generally similar to the distributions obtained by Stacy and Walker (9) with some coal chars resulting from a fluid-bed hydrogasification. Whereas Curves A through E tend to show a plateau at a pore diameter of about 55 angstroms, possibly indicative of the lack of development of significant transitional pores, Curve F shows a significant variation in pore volume through this range of pore diameters. It may be pertinent, therefore, that the gasification rates of untreated Montana lignite char in a steam-hydrogen mixture were about 7 times faster than the largest of the gasification rates obtained with chars corresponding to Curves A through E. It is thus possible that, with sufficiently large gasification rates, dynamic modifications that tend to occur within coal structures as carbon is removed are inhibited.

The plateau in pore-volume variations at a pore diameter of 55 angstroms exhibited by most coals tested has suggested the following simplified representation of pore-volume characteristics: Total pore volume accessible via pores less than 55 angstroms is defined as "micropore" volume, and pore volume accessible via pore openings having diameters between 55 and 20,000 angstroms is defined as "macropore" volume. Micropore and macropore volumes obtained with different coal chars are shown in Figures 13 and 14 as a function of the base carbon conversion fraction. Note that in these figures, volumes are represented per mass of initial base carbon rather than per mass of remaining carbon and, therefore, are proportional to volumes on a per particle basis. Figure 13 shows surprisingly little variation in macropore volume with increasing conversion for Curves A through E. In viewing these results, remember that the true density of base carbon in these coal chars is about 2 grams/cu cm, corresponding to a total volume of 0.5 cu cm/gram of initial base carbon. Thus, if the space initially occupied by gasified base carbon were added to the macropore volume, macropore volumes would increase significantly with increasing carbon conversion. The results shown in Figure 13, however, indicate that this is not generally the case, with the exception of Curve F, which does show a sharp increase in macropore volume up to conversions of about 0.8.

Figure 14 shows that micropore volumes tend to initially increase with increasing carbon conversion, reach a maximum, and then decrease with increasing conversion, approaching zero at complete conversion. Interestingly, the micropore-volume characteristics corresponding to untreated Montana lignite char gasified in a steam-hydrogen mixture are essentially identical to the characteristics for the other Montana lignite chars, as opposed to the behavior noted in Figures 12 and 13. Thus, the rapid gasification rates that evidently affect structural transitions at a "macro" level apparently do not affect structural transitions on a "micro" level. This is consistent with the results discussed previously, which showed an insensitivity in lignite-char-surface areas to initial acid treatment or to gasification conditions.

The variations in total particle volume with base carbon conversion measured with the mercury porosimeter are shown in Figure 15. The volumes represent the sum of solid volume plus pore volumes accessible via pore openings having diameters of less than 120 microns. As indicated in Figure 15, total particle volumes tend to decrease with increasing base carbon conversion fraction, particularly at conversions greater than about 0.5. Because these results were somewhat unexpected when initially observed, some additional tests were conducted to obtain photographic evidence of quantitative changes that occurred in individual external coal-char particle dimensions before and after gasification in hydrogen at 1700°F. In this series of tests, a few particles each of anthracite, high-volatile A bituminous coal, and Montana lignite were initially photographed in several orientations under optically calibrated conditions; were gasified in the thermobalance to relatively high levels of carbon conversion; and were then photographed again. Detailed examination of the photographs obtained did show a significant reduction in particle volumes, consistent with the results shown in Figure 15. The fraction of volume reduction of each type of char was independent of initial particle diameter in the range from about 200 to 800 microns. This fact and the fact that external topological characteristics remained unchanged except for a diminishment in size indicated that the observed shrinkage occurred throughout individual particles and was not the result of a "shrinking core" phenomenon.

#### SUMMARY AND CONCLUSIONS

The overall evidence obtained in this study suggests the tentative conclusion that gasification of coal chars with hydrogen and steam-hydrogen mixtures occurs primarily at char surfaces located within micropores. This conclusion is supported by the relationships indicated between specific gasification rates and internal char surface areas, particularly for gasification in hydrogen. With the majority of coal chars, internal surface area remains constant during gasification and is independent of gasification conditions, possibly indicating an invariance in average crystallite dimensions during the gasification process. With some coal chars, however, surface areas tend to decrease with increasing conversion or increasing gasification temperature, which would be indicative of a growth in crystallite dimensions.

Particle shrinkage occurs during coal-char gasification, due almost solely to contraction of the microporous phase (solids plus pores accessible via openings with diameters less than 55 angstroms), possibly because of the continuous re-orientation of individual carbon crystallites. Macropore cavities also shrink at higher levels of conversion, but in a manner analogous to cavities in a metallic solid undergoing thermal contraction. Although accessible macropore volumes may increase somewhat during the initial stages of conversion, this increase may correspond to an increasing accessibility of the macropore cavities present initially. Although there are some significant differences in the variations in surface areas and pore volumes for various coal chars during gasification, the different coal chars tested exhibit a surprising similarity in variations in average micropore diameter with increasing base carbon conversion. This is shown in Figure 16, which plots

values of the average micropore diameter,  $\bar{D}$ , versus the base carbon conversion fraction, X. The average micropore diameter was computed from the expression -

$$\bar{D} = \frac{4V}{S_{CO_2}}$$

where -

V = micropore volume (accessible pore-opening diameter <55Å).

Although the relative gasification reactivity factor,  $f_r$ , can be considered to be the product of two terms - "char surface area" and "reactivity per unit of char surface area" - this study has not produced enough data to evaluate correlations between these separate parameters and other coal properties.

The study has shown, however, that  $f_r$  itself correlates well with the initial carbon content of raw coals for most of the coal chars tested. Lignites represent a special case, because of the catalytic effects of exchangeable cations, particularly sodium and calcium, which predominate in lignites because carboxyl functional groups are present. This catalytic effect is greater for gasification in steam-hydrogen mixtures than in hydrogen alone and tends to decrease with increasing gasification temperature.

#### ACKNOWLEDGMENT

This work was conducted at the Institute of Gas Technology with primary support from the American Gas Association.

#### REFERENCES

1. Dubinin, M. M., "Chemistry and Physics of Carbon," Vol. II. (Ed. P. L. Walker, Jr.). Marcel Dekker, Inc., New York, 1966, p. 51.
2. Everett, D. H., Proc. Chem. Soc. 38, (1957).
3. Gan, H., Nandi, S. P. and Walker, P. L., "Porosity in American Coals," Stock No. 2414-00059, U.S. Government Printing Office, Washington, D.C. 1972.
4. Johnson, J. L., in Advances in Chemistry Series No. 131, "Coal Gasification," 1974.
5. Kaganer, M. E., Zh. Fiz. Khim. 33, 2202 (1959).
6. Marsh, H. and Siemieniewska, Fuel (London) 44, 355 (1965).
7. Marsh, H. and Wynne-Jones, W.F.K., Carbon 1, 281 (1964).
8. Spencer, D.H.T. and Bond, R. L., in Advances in Chemistry Series No. 55, "Coal Science," 724, 1966.
9. Stacy, W. O. and Walker, P. L., "Structure and Properties of Various Coal Chars," Stock No. 2414-00058, U.S. Government Printing Office, Washington, D.C., 1972.

10. Toda, Y., "Study on Pore Structure of Coals and Fluid Carbonized Products," Report No. 5 of the National Institute for Pollution and Resources. Japan, 1973.
11. Toda, Y., Hatauci, M., Toyoda, S., Yoshida, Y. and Honda, H., Fuel 50 (2), 187 (1971).
12. Walker, P. L. and Patel, R. L., Fuel 49 (1), 91 (1970).

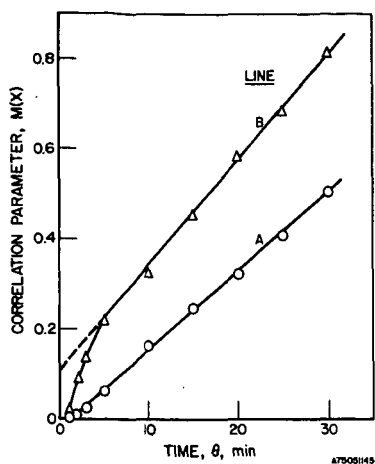


Figure 1. TYPES OF CORRELATION CHARACTERISTICS

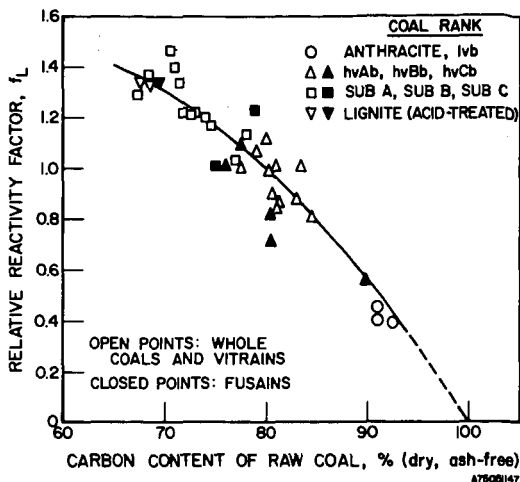


Figure 2. CORRELATION OF REACTIVITY FACTORS

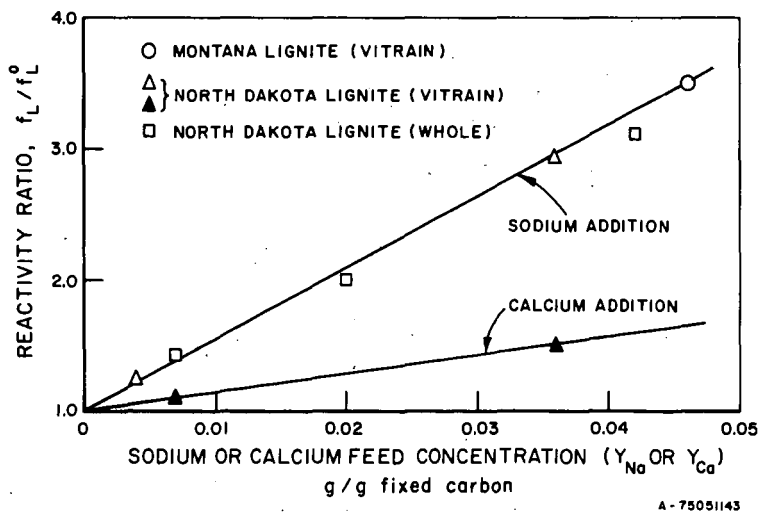


Figure 3. EFFECT OF CATION CONCENTRATION ON REACTIVITY OF LIGNITE CHAR IN HYDROGEN AT 1700°F AND 35 ATMOSPHERES

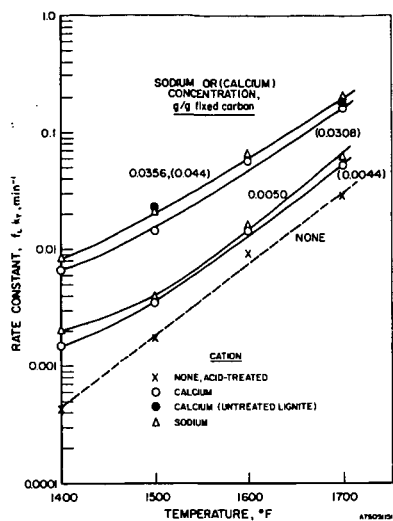


Figure 4. EFFECT OF CATION CONCENTRATION ON REACTIVITY OF MONTANA LIGNITE CHAR IN STEAM-HYDROGEN MIXTURES AT 1400° TO 1700°F AND 35 ATMOSPHERES

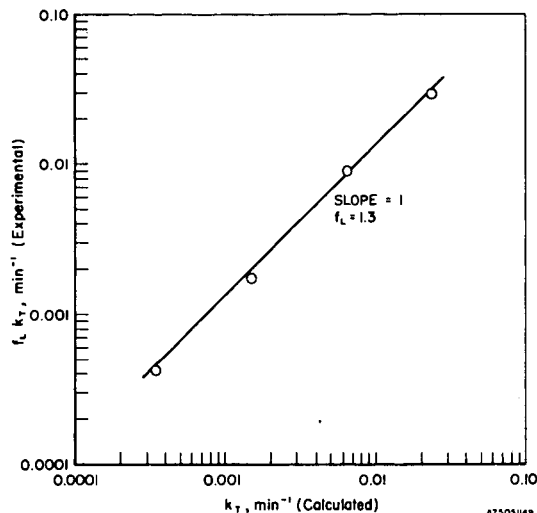


Figure 5. REACTIVITY OF ACID-TREATED MONTANA LIGNITE CHAR IN STEAM-HYDROGEN MIXTURES AT 1400° TO 1700°F AND 35 ATMOSPHERES

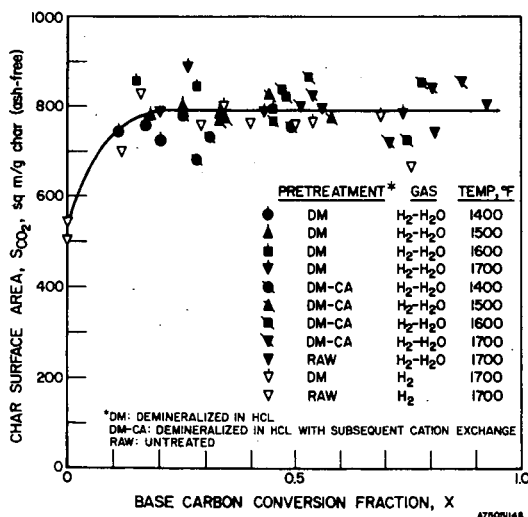


Figure 6. VARIATIONS IN SURFACE AREA MEASURED IN CARBON DIOXIDE ( $S_{CO_2}$ ) WITH BASE CARBON CONVERSION FRACTION FOR MONTANA LIGNITE CHARS GASIFIED AT VARIOUS CONDITIONS

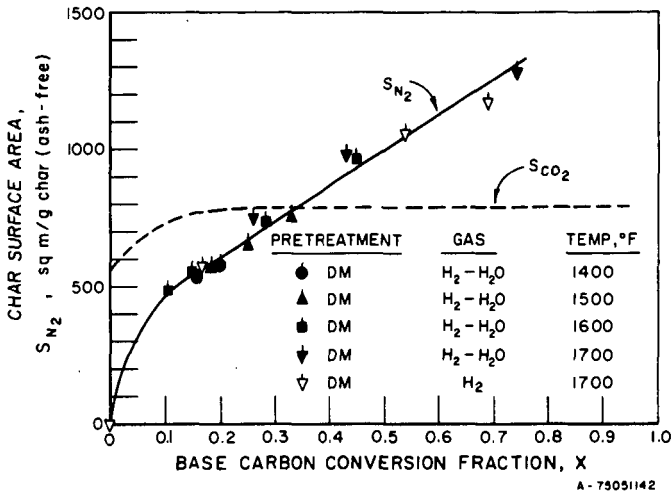


Figure 7. VARIATIONS IN APPARENT SURFACE AREA MEASURED IN NITROGEN WITH BASE CARBON CONVERSION FRACTION FOR MONTANA LIGNITE CHARS GASIFIED AT VARIOUS CONDITIONS

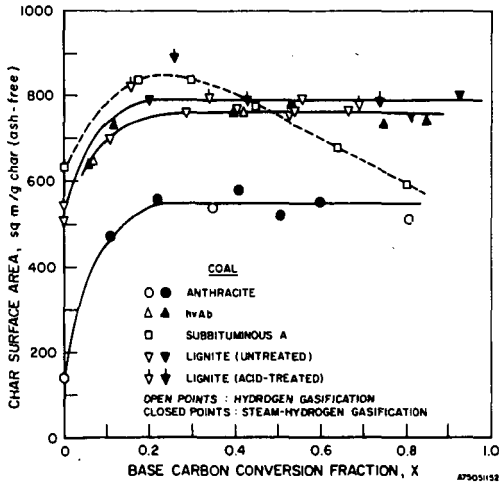


Figure 8. VARIATIONS IN  $S_{CO_2}$  WITH BASE CARBON CONVERSION FRACTION FOR DIFFERENT COAL CHARS GASIFIED IN HYDROGEN AND STEAM-HYDROGEN MIXTURES AT 1700°F AND 35 ATMOSPHERES

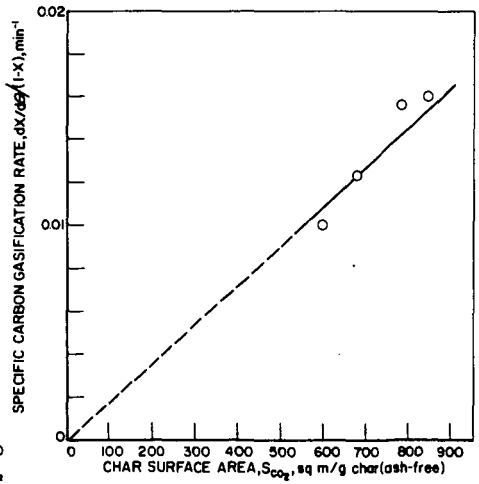


Figure 9. RELATIONSHIP BETWEEN SPECIFIC CARBON GASIFICATION RATE AND  $S_{CO_2}$  FOR GASIFICATION OF ROSEBUD SUBBITUMINOUS A COAL CHAR IN HYDROGEN AT 1700°F AND 35 ATMOSPHERES

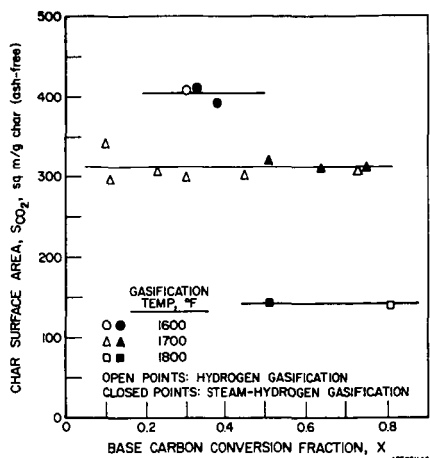


Figure 10. EFFECT OF GASIFICATION TEMPERATURE ON INTERNAL SURFACE AREA OF CARVAO METALLURGICAL COAL CHAR

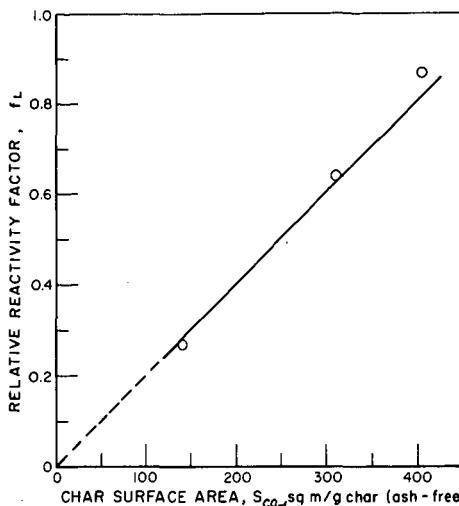


Figure 11. RELATIONSHIP BETWEEN REACTIVITY FACTOR,  $f_L$ , and  $S_{CO_2}$  FOR CARVAO METALLURGICAL COAL CHAR

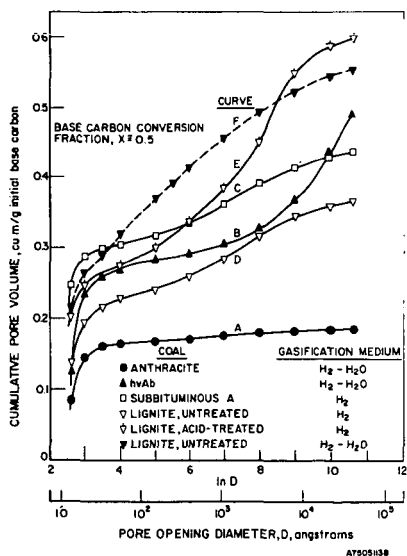


Figure 12. TYPICAL PORE VOLUME DISTRIBUTIONS FOR DIFFERENT COAL CHARS GASIFIED IN HYDROGEN AND STEAM-HYDROGEN MIXTURES AT 1700°F and 35 ATMOSPHERES

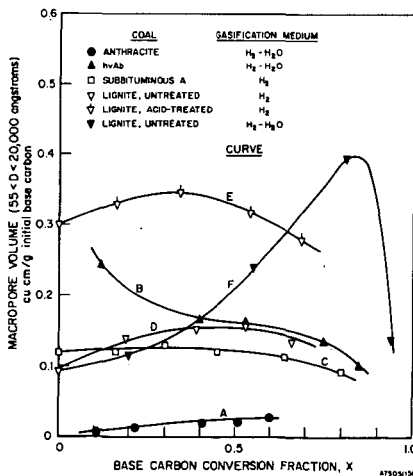


Figure 13. RELATIONSHIP BETWEEN MACROPORE VOLUME AND BASE CARBON CONVERSION FRACTION FOR DIFFERENT COAL CHARS

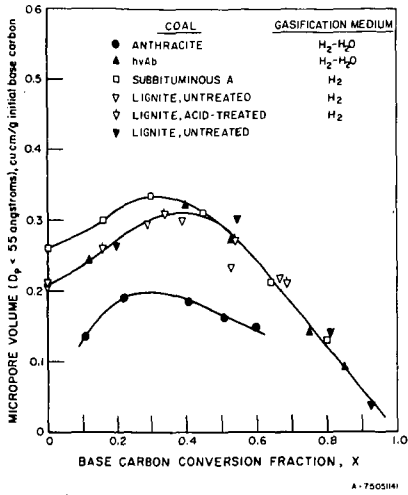


Figure 14. RELATIONSHIP BETWEEN MICROPORE VOLUME AND BASE CARBON CONVERSION FRACTION FOR DIFFERENT COAL CHARS

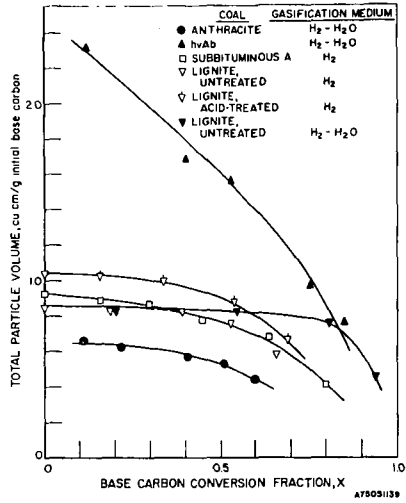


Figure 15. RELATIONSHIP BETWEEN TOTAL PARTICLE VOLUME AND BASE CARBON CONVERSION FRACTION FOR DIFFERENT COAL CHARS

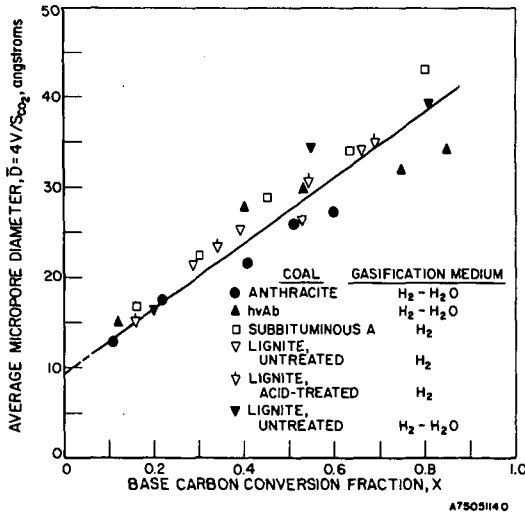


Figure 16. RELATIONSHIP BETWEEN AVERAGE MICROPORE DIAMETER AND BASE CARBON CONVERSION FRACTION FOR DIFFERENT COAL CHARS

**RAPID DEVOLATILIZATION AND HYDROGASIFICATION OF BITUMINOUS COAL.**

D.B. Anthony, H.C. Hottel, J.B. Howard, and H.P. Meissner, Department of Chemical Engineering, Massachusetts Institute of Technology, Cambridge, Massachusetts 02139

Rapid devolatilization and hydrogasification of a Pittsburgh Seam bituminous coal were studied and an approximate coal conversion (weight loss) model was developed that accounts for secondary char-forming reactions among volatiles. Approximately monolayer samples of small coal particles supported on wire mesh heating elements were electrically heated in hydrogen and hydrogen/helium mixtures. Coal weight loss was measured as a function of residence time (0.05-20 sec.), temperature (400-1100°C), heating rate ( $10^2 - 10^4$  °C/sec.), total pressure (0.001 - 100 atm), hydrogen partial pressure (0 - 100 atm), and particle size 50 - 1000 $\mu$ m). Rate of weight loss under these conditions appears to be controlled by thermal decomposition reactions that form volatiles and initiate a sequence of secondary reactions leading to char. Thermal decomposition is modelled as a large number of parallel first-order reactions having a statistical distribution of activation energies (20-89 kcal/mole). The contribution of secondary reactions to weight loss is described by a selectivity expression derived from the assumption that char formation by these reactions competes with hydrogenation reactions and diffusional escape of volatiles from the particle.

J. A. Gray, P. J. Donatelli, P. M. Yavorsky

U.S. Energy Research and Development Administration  
Pittsburgh Energy Research Center  
4800 Forbes Avenue  
Pittsburgh, Pennsylvania 15213

#### INTRODUCTION

Of the many processes currently under development which will convert coal to environmentally acceptable solid, liquid, and gaseous fuels utilizing pyrolysis, synthesis gas, solvent extraction, or hydrogenation techniques, the direct hydrogenation of coal to a raw gas that is easily upgraded to pipeline quality is a promising approach. Such a process is under development by the E.R.D.A., Pittsburgh Energy Research Center and is known as HYDRANE (1, 2).

Briefly, the HYDRANE flow sheet is as follows. Pulverized raw coal is fed to the top zone of the hydrogasifier, operated at 70 atm and 750°-900° C, where it falls freely as a dilute cloud of particles through a hydrogen-rich gas containing some methane from the lower zone. About 20 pct of the carbon in the raw coal is converted to methane, causing the coal particles to lose their volatile matter and agglomerating characteristics and to form very porous, reactive char particles. This char falls into the lower zone, operated at 70 atm and 900°-980° C, where hydrogen feed gas maintains the particles in a fluidized state and reacts with an additional 25 pct of the carbon to make methane. The product gas exists from the bottom of the dilute-phase zone and is cleaned of entrained solids, tars and oils, and some unwanted gases. After cleanup, catalytic methanation of the small amount of residual carbon monoxide gives a pipeline quality, high-Btu, substitute natural gas. Char from the lower zone of the hydrogasifier is reacted with steam and oxygen to make the needed hydrogen.

This process has the following advantages:

1. External hydrogen consumption per unit of methane produced is low because the hydrogen already in the coal is efficiently utilized,
2. Process costs associated with coal pretreatment, inherent in other coal conversion processes based on caking bituminous coal feedstocks, are eliminated,
3. 95 percent of the product methane is produced directly in the hydrogasifier thus requiring very little catalytic methanation,
4. Simple reactor design,
5. Produces low-sulfur char byproduct for hydrogen generation and low-sulfur tars, and
6. Utilizes sensible heat of the residual char from the hydrogasifier in the hydrogen generation plant.

Because of these advantages, coal and oxygen (the costliest items in gasification) requirements are minimized for the process, and thermal efficiency and carbon utilization are high at 78 pct and 44 pct, respectively (3, 4).

Much of the hydrogasification kinetic data on the laboratory scale, free-fall, dilute-phase reactor has already been published (5, 6) as well as data from a semiflow bench-scale reactor (7). In this paper we review previous and some recent kinetic data with regard to the type of reactor used to obtain the data, and the effect of the type of reactor on the conversion data. The conversion of the non-mineral elements in the coal during hydrogasification and the char yield are shown to be related to the carbon conversion regardless of the reactor geometry used, so that the constituent conversions can be calculated once the carbon conversion is known. This simplifies the reactor design in that only the carbon conversion need be kinetically defined for a particular reactor geometry.

#### EXPERIMENTAL REACTORS

##### "Hot-Rod" Reactors (HR)

In 1955 El Paso Natural Gas Company entered into a cooperative agreement with the then U.S. Bureau of Mines Synthetic Fuels Research Branch to investigate the hydrogenation of a subbituminous New Mexico coal to produce high-Btu gas and low-boiling aromatics. Part of the agreement called for tests in a reactor in which dry coal could be rapidly brought to the desired operating temperature and pressure. A normal autoclave required over an hour to reach temperature. Consequently, the effect of the heating and cooling cycles on the reaction could not be discerned. In late 1955, Hiteshue conceived the apparatus known as the "hot-rod" reactor and completed the El Paso project using it. The apparatus along with conversion data were first reported by Hiteshue, Anderson, and Schlesinger in 1957 (8) and again during 1960-1964 (9, 13).

The "hot-rod" reactor, shown in Figure 1, was a 70-inch long stainless steel tube (type 304) having a 5/16-inch inside diameter and a 5/8-inch outside diameter. A coal or char sample weighing 8 grams and screened to 30 x 60 U.S. sieve size was inserted into the tube between two porous stainless steel disks such that a 32-inch length was available to fluidize the sample. The tube was heated with electrical current by connecting it to a transformer that was capable of supplying 700 amperes at 9 volts. With this method of heating, the reactor, sample, and feed gas were heated from room temperature to 800° C in about 2 minutes and to 1200° C in about 4 minutes. At the end of the experiments, the reactor and sample were cooled to room temperature in about 10 seconds by spraying with cold water. The flowsheet of the entire apparatus is shown in Figure 2 and has been discussed in detail in the previously cited references.

##### Free-Fall Dilute Phase Reactor (FDP)

The agglomeration of bituminous coals in hydrogen is a major problem in designing a reactor for their continuous hydrogenation to produce a high-Btu gas. It has been shown that bituminous coals, both caking and noncaking, will agglomerate when rapidly heated in hydrogen at 500 psig and 500° C or at 6,000 psig and 500° to 800° C (10, 13, 14). Texas lignite agglomerated at 6,000 psig and 800° C but did not agglomerate at 500 psig and 500° C. Chars produced from carbonizing bituminous coals, cokes, graphite and anthracite, and a highly oxidized hvAb coal did not agglomerate. Feldmann (6) observed that at least 10 pct of the volatile matter in Pittsburgh seam hvAb coal, originally containing 36 pct volatile matter, had to be removed to obtain a char that would not agglomerate at 1,000 psig and 800° C in hydrogen in subsequent "hot-rod" reactor tests.

Lewis and Hiteshue (15) designed an entrained flow reactor for continuously hydrogenating both caking (hvAb) and noncaking (hvCb) coals. They believed that if the suspension of coal in the feed gas was dilute enough (dilute phase), particle-

particle collision and subsequent agglomeration could be avoided. The reactor was a 1/8-inch inside diameter, 60-foot long helical tube, and was operated at 600 psig and 800° C. The coal was entrained at a rate of 60 gms/hr in hydrogen where the hydrogen velocity was 2 fps. Experiments with the helical reactor were unsuccessful because of solids plugging at about the 500 to 550° C zone in the helical tube. Changing to a straight, horizontal tube reactor having an internal diameter of 5/16 inches and a length of 20 feet did not alleviate the plugging problem.

A 4-inch diameter vertical reactor where the coal particles would not contact the reactor wall during devolatilization was found to operate very successfully. It was further shown that reducing the diameter to less than 3 inches caused plugging, again due to coal particles contacting the reactor wall. Figure 3 shows the laboratory dilute-phase reactor that evolved from these studies.

A large amount of kinetic data has been reported for this reactor using Pittsburgh seam hvAb and Illinois #6 hvCb coals (5, 6, 16, 17). Details of the laboratory reactor and method of operation are discussed in the previous references.

The present FDP reactor is a 3.26-inch inside diameter pipe that is heated through the wall and contained in a 10-inch diameter pressure shell. Coal is injected into the top of the reactor through a 5/16-inch inside diameter, water-cooled nozzle using a rotary feeder and part of the feed gas. The coal free-falls through a 5-foot long reactor concurrently with the feed gas at a particle residence time of less than a second. Agglomeration is avoided because the rapid heating devolatilizes the particles before many particle collisions with the wall or other particles can occur. The char product is recovered from a cooled hopper after each experiment and is analyzed. Gas flows and compositions are measured over steady state periods of the experiment so that mass balances can be calculated.

#### Two-Stage Integrated Reactor

In order to react fresh dilute phase char with hydrogen as in the integrated reactor system described previously, and to measure reactivity and methane yield at carbon conversion levels expected in a commercial reactor, a two-stage laboratory hydrogasifier was built consisting of a dilute-phase reactor integrated with a second stage reactor that could be operated as either a moving-bed or fluid-bed reactor. Figure 4 illustrates the version using a fluid-bed second stage. Because the diameter of the coal particles increased substantially due to swelling and some agglomeration during devolatilization, a char crusher was used to reduce the particle size to a level acceptable for fluidization. In the moving-bed version, no crusher was used as shown in Figure 5.

The true composition of product gas from the individual stages could not be determined directly because a large amount of mixing occurred between gas near the bottom of the dilute phase reactor and gas near the top of the second stage reactor. The overall methane yield for the two-stage unit was determined in some cases, and these yields were compared to yields from previous dilute phase reactor experiments. The mixing problem was not unexpected since there was no gas seal leg used between the two reactors because of the small scale of the equipment. The mixing was caused from convection currents created from the falling char particles and the hot reactor walls. The operation of the two-stage hydrogasifier is described in much greater detail elsewhere (18).

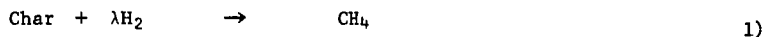
#### KINETIC MODEL

Within about the first few inches of free-fall in the FDP reactor, the coal particles are rapidly heated and devolatilized yielding a "popcorn" char (19). It is generally accepted that during the period of devolatilization, chemical bonds

such as methylene bridges, oxygen bonds, and side chains are easily broken resulting in evolution of hydrogen rich volatile matter and a large number of free radical structures (5, 20, 21, 22). These free radicals can react with hydrogen forming hydrocarbon gases and solid species that are active for further hydrogenation to volatile material or combine by polymerization to form a highly aromatic, unreactive char structure. During free-fall, but after rapid devolatilization has occurred (after about 6 inches), the solid carbon is very reactive in behavior as though not enough time has elapsed for significant polymerization to proceed (5). However, when the char is further reacted with hydrogen in a second-stage reactor such as a fluidized-bed or moving-bed, the hydrogasification rate is about two orders of magnitude slower (1, 18). Thus, the coal structure and reactivity change constantly during reaction.

Feldmann (5) has proposed that for kinetic modeling purposes the carbon in the raw coal can be divided into three types during hydrogasification. Type 1 carbon is the highly reactive species which is flashed off almost instantaneously during rapid heat-up and devolatilization, Type 2 is the solid carbon which readily hydrogasifies during most of the particle free-fall, and Type 3 is the low-reactivity carbon contained in the remaining, polymerized char structure. Johnson (23) has proposed a very similar model.

In developing a reaction rate expression for the hydrogasification of coal in the FDP reactor (5), the Type 1 carbon is assumed to devolatilize instantaneously and the remainder of hydrogasification occurs with Type 2 carbon. The reaction can be written as



for the data at high hydrogen partial pressures ( $P_{\text{H}_2}$  50-60 atm) (5), and as,



for data at lower hydrogen partial pressures (6). An empirical correlation of  $\lambda$ , the stoichiometric coefficient, has been developed from the high pressure data and is

$$\lambda = \begin{cases} 1.0 & \text{for } x < 0.45 \\ 8x - 2.6 & \text{for } 0.45 \leq x \leq 0.55 \\ 1.8 & \text{for } x > 0.55 \end{cases} \quad 3)$$

where  $x$  is the total fractional carbon conversion.

The oil yield has been as high as 5% for Pittsburgh seam hvAb coal and 6% for Illinois #6 hvCb coal. A small amount of carbon oxides are produced (usually less than 4% of the product gas) and are in equilibrium according to the water-gas shift reaction as shown in Figure 6.

The hydrogasification of Type 2 carbon follows the rate equation

$$\frac{dx}{dt} = k P_{\text{H}_2} (\alpha - x) \quad 4)$$

where  $x$  is the fractional carbon conversion,  $P_{\text{H}_2}$  the hydrogen partial pressure,  $\alpha$  the

fraction of the carbon which is available for reaction in the regime being considered and  $k$  the reaction rate constant. Another way of writing Equation 4 where the devolatilized carbon is not included in the fractional carbon conversion is

$$\frac{dZ}{dt} = k P_{H_2} (\beta - Z) \quad 5)$$

where  $Z = (x-E)/(1-E)$  and  $\beta = (\alpha-E)/(1-E)$ .  $E$  corresponds to the fraction of carbon that was devolatilized. Assuming the coal particles being fed to the dilute phase reactor attain terminal velocity and the same temperature as the reactor wall almost immediately, Equation 4 may be applied to the FDP reactor as

$$U_T \frac{dx}{dL} = k P_{H_2} (\alpha - x) \quad 6)$$

where  $U_T$  is the particle terminal velocity. Equation 6 is integrated over the reactor length yielding

$$\int_E^x \frac{dx}{\alpha - x} = k P_{H_2} \frac{L}{U_T} \quad 7)$$

In the integration,  $P_{H_2}$  is assumed constant and equal to the hydrogen partial pressure in the product gas because extensive backmixing occurs due to the hot reactor walls and the downward flow of char. The fraction of Type 1 carbon is accounted for as  $E$  in the integration. Within the constraint that  $0 < \alpha \leq 1$ , the best fit of carbon conversion data from the FDP reactor is obtained when  $\alpha = 1$  (2). This means that essentially all of the carbon is available for hydrogasification.

The hydrogasification of char in a "hot-rod", moving-bed, or fluid-bed reactor follows the same rate expression given by Equation 4, however, the reaction is much slower because most of the carbon that is reacting is of the Type 3 variety. Application of Equation 4 to fluid-bed and moving-bed reactors has been discussed elsewhere (18).

The rate expression does not take into account transitions between the various reactive types of carbon in the coal nor mass transfer resistance. In fact the hydrogasification of char is so complex because of the change in carbon structure during reaction, that the above simple classification of carbon may not apply in all cases. Johnson's model (23) takes into account the continuous deactivation of the char but also adds another constant into the model which must be evaluated using experimental data. Generally the more constants there are in a model, the better the model will fit regardless of the accuracy of the proposed reaction mechanism, and the more experimental data is needed to evaluate the constants. For this reason, Equation 4 was kept simple so that data from various reactors could be easily compared. With this perspective, the data from each of the reactor systems will now be discussed.

## EXPERIMENTAL RESULTS

### FDP Reactor

Using Equation 7 and a terminal velocity of 9 fps, Feldmann (5) determined  $E$  and  $k$  values for carbon conversion data at 900° C and 725° C. These values are listed in Table 1. In a later publication, Feldmann (2) reanalyzed the 725° C data as a function of hydrogen partial pressure and presented recent 850°-900° C (total

TABLE 1.- FDP Reactor kinetic data (5)

Reactor Wall Temp., °C	Total Reactor Press., atm	E, %	$k$ $\text{atm}^{-1}\text{hr}^{-1}$
725	103,205	22	6
900	205	14	21

TABLE 2.- Ultimate and proximate analyses of feeds

Run Series	Coals				Chars	
	HR-1	HR-2	FDP	HR-1C	HR-2C	
Wt. %	Pgh hvAb	Pgh hvAb	Pgh hvAb	Ill. #6 hvCb	Pgh hvAb	Ill. #6 hvCb
C	74.2	74.1	78.1	74.4	78.8	83.9
H	5.1	5.1	5.3	5.2	1.9	2.8
N	1.5	1.5	1.6	1.7	1.6	---
S	1.9	1.5	1.1	1.3	1.1	---
O	8.8	7.6	8.2	11.5	1.9	---
Ash	8.5	10.2	5.7	5.9	14.7	10.2
	100	100	100	100	100	---
Moisture	1.9	1.4	1.2	1.4	0	0.9
VM	33.9	35.3	36.4	36.8	---	26.0
FC	56.5	53.1	56.7	55.9	---	---

TABLE 3.- FDP Reactor kinetic data

Reactor Wall, Temp., °C	Total Reactor Press., atm	E, %	$k$ $\text{atm}^{-1}\text{hr}^{-1}$
725	103,205	23.1	5.3*
725	103,205	9.4	14.7
850-900	69-108	21.5	24.7*
850-900	69-108	12.2	33.0

\*Total carbon conversion.

pressure 69-108 atm) data (6). The ultimate and proximate analyses of the feed coals are shown in Table 2 for the FDP and "hot-rod" reactors. Figures 7 and 8 show the carbon conversion data as total carbon conversion and as carbon conversion to equivalent methane (carbon in methane and ethane).

The difference between total carbon conversion and carbon conversion to methane is due mainly to the production of carbon oxides and oil. Some experimental error is also introduced in measuring the flowrate and composition of the feed and product gases, and in recovery and analysis of the solid and liquid products. Often the run times were not long enough to collect enough oil so the yield could be accurately measured (2). These errors become obvious when the carbon and ash recoveries are much lower than 100 pct. Figure 9 indicates that the hydrogen partial pressure as well as reactor temperature greatly influences the amount of oil produced, especially below a partial pressure of 30 atm. The increase in oil yield with decreasing hydrogen partial pressure agrees with the divergence of the two carbon conversion curves in Figures 7 and 8. Apparently the higher hydrogen partial pressures enhance the hydrocracking of the oil products. Residence time of the hydrocarbon vapors in the reactor also affects the oil yield causing lower amounts of oil at increasing residence time as shown in Figure 10. As indicated in Figure 5, the oil yield was determined by recovery from the gas sample and main tail gas streams. However, some of the oil was lost by condensation on the char receiver wall and to some extent on the char in the receiver. Therefore the oil yield data are now being reexamined where the yield in the gas sample stream is multiplied by the ratio of the total product gas flowrate to the sample gas flowrate in order to estimate total oil yield. These values will probably be higher than the reported values.

The values of the kinetic parameters in Equation 7 for the data in Figures 7 and 8 are listed in Table 3. These parameters were evaluated both for total conversion and for carbon conversion to equivalent methane. The value of  $\alpha = 1$  gave the best fit of the total carbon conversion data and was subsequently used to fit the carbon conversion to methane data. The terminal velocity of a single char particle was calculated using the equation

$$U_T = \left[ \frac{3.1g(\rho_s - \rho_g)\bar{d}_p}{\rho_g} \right]^{1/2} \quad 8)$$

for  $500 < Re_p = \frac{\bar{d}_p U_T}{\nu_g} < 200,000$  (24), and correcting this value for the effect of the cloud of particles (25). Table 4 lists the parameters used for calculating the terminal velocities. A terminal velocity of 16.5 fps was used for the 850°-900° C data and 10.7 fps (average of 9.9 and 11.5) for the 725° C data.

The total reactor pressure has a large influence on the terminal particle velocity because the pressure determines for the most part the size of the char particles produced and hence the bulk and particle densities. This is illustrated in Figure 11 where the char bulk density is plotted versus total reactor pressure. As the pressure increases, the bulk density increases. The bulk density is higher when the feed gas contains about 50 pct methane instead of pure hydrogen. Apparently, increasing the reactor pressure dampens the explosive emission of gases during the rapid devolatilization reaction. A high concentration of hydrogen in the reactor causes more of the carbon to be reacted out of the particle structure resulting in a lower bulk density char (and lower particle density) than is obtained when the reactor feed gas contains about 50 pct methane. Some char particle size data is listed in Table 5 showing how increases in reactor temperature and pressure cause decreases in the mean char particle diameter.

TABLE 4.- Parameters used to calculate terminal velocity

Temperature, ° C	725	725	900	900
Pressure, atm	205	103	205	69
W, lb/hr ft <sup>2</sup>	165	128	145	207
d <sub>p</sub> , in.	0.0521	0.0667	0.0345	0.0660
ρ <sub>b</sub> , lb/ft <sup>3</sup>	13.33	8.0	12.29	5.8
ρ <sub>s</sub> <sup>*</sup> , lb/ft <sup>3</sup>	36.8	22.1	33.9	16.0
ρ <sub>g</sub> , lb/ft <sup>3</sup>	1.408	0.7074	1.199	0.4035
μ <sub>g</sub> , lb/ft hr	0.05745	0.05745	0.06409	0.06409
U <sub>TS</sub> , fps	3.3	4.1	2.8	4.6
Re <sub>p</sub>	1264	1010	542	573
U <sub>T</sub> /U <sub>TS</sub> <sup>**</sup>	3.0	2.8	3.0	3.6
U <sub>T</sub> , fps	9.9	11.5	8.4	16.5

\* Estimated by the ratio of bulk densities and particle density of 16.0 lb/ft<sup>3</sup> (26) for char produced at 850°-900° C and 69 atm, e.g.,  $\frac{13.33}{5.8} \times 16 = 36.8$ .

\*\*Ratio of terminal velocity to single particle terminal velocity at a specific mass feed rate per unit area (25).

TABLE 5.- Effect of reactor temperature and pressure on average char particle size

Press., atm/Temp., ° C	Average Char Particle Diameter*, in.			
	750	800	850	900
69	---	0.0735	0.0628	0.0537
83	---	---	0.0566	0.0501
103	0.0667	---	---	0.0485
205	0.0521	0.0492	0.0529	0.0345

$$\bar{d}_p = \left[ \sum_i \frac{x_i}{d_{p_i}} \right]^{-1}, \text{ Pittsburgh seam hvAb coal, 50 x 100 mesh feed.}$$

The effect of feed rate per unit reactor cross section on the average char particle diameter is shown in Figure 12. As the feed rate is increased for a fixed reactor diameter, the number of particle collisions increase and hence the mean char particle size increases due to agglomeration. At a mass feed rate of 221 lb/hr ft<sup>2</sup>, Pittsburgh seam coal yielded an average char particle diameter of 1.70 mm (0.0669 inches) compared to 0.487 mm (0.0192 inches) for char produced from Illinois #6 hvCb coal under identical reactor conditions. The maximum capacity in the dilute-phase section of the two-stage integrated reactor is limited by the size of the char produced in the dilute phase section that may be fluidized adequately in the second-stage fluid-bed section. Therefore, the dilute-phase reactor capacity will be much higher for Illinois coal than for Pittsburgh coal because of the smaller size char particles produced.

The feed rates per unit area in Figure 12 are probably low because the coal is not completely distributed across the dilute-phase reactor cross section before rapid heat-up and devolatilization, when the coal is susceptible to caking. As mentioned earlier, the coal is fed by a 5/16 inch diameter tube into a 3.26 inch diameter reactor. The particles hit the wall of the reactor about 12 inches down from the end of the feed nozzle. If devolatilization is completed within 6 inches from the end of the nozzle, a feed rate calculated to be 300 lbs/hr ft<sup>2</sup> of reactor cross section actually corresponds to a rate of 1000 lbs/hr ft<sup>2</sup> of cross-sectional area occupied by the particles. Data from a free-fall carbonizer (27), 12 inches in diameter, at the Morgantown Energy Research Center, show that Pittsburgh coal was processed at 1000 lbs/hr ft<sup>2</sup> and yielded char with a mean diameter of about 0.508 mm (0.02 inches). The feed coal was 70 pct through 200 mesh.

The reaction rate constants for the FDP reactor are shown on an Arrhenius plot in Figure 13. The relatively low activation energy of 15.1 kcal/mole of carbon reacted appears to indicate that the reaction may be controlled by mass transfer of hydrogen to the reaction sites and not by the rate of hydrogasification. Feldmann (2) has suggested that in the higher temperature range the rate may be better described as proportional to  $k_g P_{H_2}$ , where  $k_g$  is a mass transfer coefficient for hydrogen through the gas film surrounding the particle. This seems reasonable since a straight line could have just as easily fit the total carbon conversion data in Figures 7 and 8. The activation energy for carbon hydrogasification in an entrained flow reactor was determined by Zahradnik and Glenn (21) to be 15 kcal/mole, in agreement with the value obtained in this work. They suggest that this activation energy represents the difference in activation energy between the hydrogasification and polymerization reactions. An Arrhenius plot of Feldmann's (1) in which he calculates  $k$  by integrating Equation 7 from zero to  $x$  instead of from  $E$  to  $x$ , shows some low temperature FDP data. The activation energy is 29.8 kcal/mole for temperatures below 580° C, and decreases to 6.4 kcal/mole for temperatures above 580° C. The  $k$  values were calculated this way because  $E$  could not be determined from the available data and because  $P_{H_2}$  was approximately constant. This change in activation energy supports Feldmann's suggestion that the reaction is mass transfer controlled. More comments will be made on these results after reviewing some low-temperature "hot-rod" reactor data.

The data presented for the FDP reactor are based mainly on Pittsburgh seam hvAb coal. This coal was studied extensively because of its extreme swelling and agglomerating properties. If the reactor could process badly caking coal than surely it could easily handle mildly caking coals. Illinois #6 hvCb coal is mildly caking and FDP results on this coal are shown in Figure 14. The conversion of Illinois coal has not been studied over a wide range of hydrogen partial pressure as has the Pittsburgh coal, but does appear to be more reactive based on comparison of the two coals in Figure 14 at the same reactor conditions.

"Hot-Rod" Reactors

The results from the "hot-rod" reactor tests of Hiteshue, Friedman, and Madden (7) will be referred to as HR-1 series when coal is used as the starting reactant and HR-1C when char is used. Unpublished data of Feldmann and Williams will be referred to as HR-2 and HR-2C series. The weight loss and carbon conversion data are shown in Figures 15 and 16, respectively, for the HR-2 series experiments. In most of the HR-2 tests the reactor temperature was maintained low enough that Type 2 carbon conversion appeared to occur over a period of about 6 minutes. Once the temperature exceeded about 600° C, Type 3 carbon was rapidly formed. The conversions at which the curves in Figure 15 or 16 appear to level off correspond to the transition points at which the hydrogasification occurs predominately with Type 3 carbon. For the tests at 800° C, the devolatilization and Type 2 carbon conversion both occur in less than a minute. This is more clearly visible when the rate constants are plotted on the same Arrhenius graph with the FDP data in Figure 13. For the data up to 600° C, Equation 4 was integrated starting from zero carbon conversion, and the values of  $k$  and  $\alpha$  were determined from a least-squares fit of the data ( $E$  was found to be very close to zero in the regression analysis for temperatures below 520° C). For the 800° C data, the integration was started from  $E$  with  $\alpha = 1$ , and again  $k$  and  $E$  were determined from a least-squares analysis of the data. The values of these parameters are listed in Table 6. The model was also fit to the total weight loss data in Figure 15. As is obvious in Figure 16, the carbon conversions calculated from the carbon analyses were not consistent at 425° C and 69 atm with either the total conversion data in Figure 15 or data at 35 atm. Therefore, the carbon gasification rate constant at 425° C was calculated by extrapolating the line obtained when  $k$  is plotted versus  $k_T$  (rate constant for total conversion). The  $k$  value at 425° C can also be estimated by assuming the curve must pass through 0.0588 (average of two data points) at 6 minutes. This method gives a  $k$  value of  $0.255 \text{ atm}^{-1} \text{ hr}^{-1}$  compared to  $0.383 \text{ atm}^{-1} \text{ hr}^{-1}$  by extrapolation.

In the Arrhenius plot of Figure 13, the low temperature "hot-rod" reactor data appears to be consistent with the dilute-phase reactor data. Unfortunately, low temperature FDP data is very difficult to obtain in order to verify the low temperature "hot-rod" reactor data because of agglomeration and plugging. The high temperature "hot-rod" reactor data cannot verify the FDP data because the heat-up rate and residence times are such that they operate in different carbon conversion regimes. The key difference between the FDP reactor and the "hot-rod" reactor is the coal heat-up rate. In the FDP reactor this rate is on the order of 1000° C/sec whereas in the "hot-rod" reactor the rate is about 7° C/sec. By achieving reaction temperature quickly enough, the kinetics of Type 2 carbon hydrogasification can be observed.

The carbon conversion data for the HR-1 series experiments are shown in Figure 17. In these tests the devolatilization and Type 2 carbon conversion occurred in less than a minute because of the high temperatures. Therefore the curves for the most part represent Type 3 carbon conversion. Johnson (23) has observed in thermobalance experiments that devolatilization and Type 2 carbon conversion are essentially complete within 2 minutes at temperatures above about 800° C. The heat-up rate in the thermobalance tests was about the same as in the "hot-rod" reactor tests. The HR-1 series data were fit using Equation 4 with  $\alpha = 1$  and integration starting from  $E$ . The kinetic parameters are listed in Table 7. Choosing  $\alpha = 1$  simply means that essentially all the carbon beyond the fraction  $E$  is Type 3. Here  $E$  represents the sum of Types 1 and 2 carbon.

Figure 18 illustrates the effect of the reactor temperature on the amount of carbon that can be hydrogasified as Types 1 and 2. High temperatures and hydrogen

TABLE 6.- Kinetic parameters for HR-2 series data

Temp., ° C	P <sub>H<sub>2</sub></sub> , atm	$\alpha$	E	k atm <sup>-1</sup> hr <sup>-1</sup>	$\alpha_T^{**}$	k <sub>T</sub> <sup>**</sup> atm <sup>-1</sup> hr <sup>-1</sup>
425	69	.071*	0	0.383*	.099	0.510
470	69	.189	0	0.447	.261	0.594
490	69	.199	0	0.625	.278	0.838
520	69	.179	0	1.47	.264	2.07
600	69	.232	0	0.976	.272	1.08
600	69	1.0	.175	0.00751	---	---
800	69	.315	0	1.22	.344	1.66
800	69	1.0	.243	0.0123	---	---

\* Extrapolated using total conversion k<sub>T</sub> values. By another method, the k value is 0.255 atm<sup>-1</sup>hr<sup>-1</sup>.

\*\* Subscript T indicates total conversion parameters (total weight loss).

TABLE 7.- Kinetic parameters for HR-1 series data

Temp., ° C	P <sub>H<sub>2</sub></sub> , atm	$\alpha$	E	k atm <sup>-1</sup> hr <sup>-1</sup>
800	18.0	1.0	.252	0.0282
800	35.0	1.0	.355	0.0154
800	69.0	1.0	.450	0.0169
1200	4.4	1.0	.298	0.363
1200	18.0	1.0	.377	0.137
1200	35.0	1.0	.514	0.350

TABLE 8.- Effect of hydrogen partial pressure on carbon conversion in the hot rod reactor

Test	Temp., ° C	P <sub>H<sub>2</sub></sub> , atm	Carbon Conversion, pct		
			1 min.	2 min.	5-6 min.
HR-1	800	18	---	---	30.7, 25.7
HR-1	800	35	---	---	39.4, 40.4
HR-1	800	69	---	---	52.0, 55.5, 52.6, 54.6
HR-2	500	35	9.10	12.1	---
HR-2	490	69	10.4	14.5	---
HR-2	600	35	17.6	18.4	---
HR-2	600	69	17.5	17.9	---
HR-2	700	35	---	21.0	---
HR-2	800	35	23.7	24.3	31.2
HR-2	800	69	25.6	25.8	33.9

partial pressures result in a large amount of carbon being hydrogasified in the Types 1 and 2 regime. In fact Moseley and Paterson (22) have shown that at a hydrogen partial pressure of 500 atm and 900° C, the carbon is rapidly gasified to completion.

There is a large difference in the level of Types 1 and 2 carbon conversion between the HR-1 data at 800° C and the corresponding HR-2 tests. This discrepancy is shown in Table 8 and is especially noticeable at 800° C and 69 atm. Under these conditions the conversions from the HR-1 tests range from 52 to 54.6 pct at a residence time of 5 minutes whereas the corresponding conversions for the HR-2 tests ranged from 31.2 to 33.9 pct at a residence time of 6 minutes. The lack of response of conversion to changes in hydrogen partial pressure in the HR-2 tests suggests that the reaction rate was strongly mass transfer controlled. This can be verified by comparing the gas velocities in the HR-1 and HR-2 experiments in Table 9. In the HR-1 tests the superficial hydrogen feed gas velocity was 36 cm/sec compared to a velocity of 1 to 2 cm/sec in the HR-2 tests. Apparently the gas velocity was low enough in the HR-2 tests that at the higher temperatures the mass transfer resistance through the particle gas film was significant. In addition, the slower particle heat-up rate may have contributed to the difference in conversions. Anthony (28) has demonstrated, however, that varying the heating rate from 180 to 10,000° C/sec has no effect on the coal conversion. He found smaller particle sizes and more highly dispersed samples to be extremely important because the flux of volatiles emerging from the coal particle may limit the counter diffusion of hydrogen into the particle. This restriction makes it difficult for the hydrogasification reaction to compete with polymerization reactions that produce a relatively inactive char.

In Table 10 the Types 1 and 2 carbon conversion for FDP and "hot-rod" reactor tests are compared. The HR-2 tests were definitely mass transfer controlled whereas it is difficult to conclude this in the FDP tests compared to the HR-1 tests because of the large difference in residence time. In the FDP reactor the residence time was less than 1 second and in the "hot-rod" reactor it was two orders of magnitude greater. Anthony (28) has shown that Types 1 and 2 carbon conversions are complete after about 3 seconds at 69 atm, 900° C, and a heating rate of 750° C/sec. His starting coal particle size was 70 microns compared to about 220 microns in the FDP experiments. Therefore Types 1 and 2 carbon conversion in the FDP tests probably did not reach completion.

Photographs of some of the chars under a scanning electron microscope reveal the porous structure produced in the FDP and "hot-rod" reactors under various conditions. Figure 19 compares chars produced in the FDP reactor at 725° C, 205 atm (top-left), and at 850° C, 69 atm (bottom-left). The char produced at 69 atm appears to be much more porous and less dense than the char made at 205 atm. As discussed previously, this effect shows up as a large difference in bulk density.

Figure 20 compares chars produced in the "hot-rod" reactor at 600° C, 69 atm (bottom) and at 800° C, 69 atm (top) at different residence times. The low temperature char has much larger pores while the high temperature char has a larger number of very small pores. This difference in the pore size is probably related to the higher emission rate of volatile matter from the particles reacted at 800° C. In addition, the superficial hydrogen velocity in the 600° C test was 0.9 cm/sec versus 1.1 cm/sec in the 800° C test. Both these conditions (high volatiles emission, low gas velocity) limit counterdiffusion of hydrogen into the char structure resulting in less competition for the polymerization reaction. Comparison of the FDP and "hot-rod" char samples indicates that the pore structure of the FDP char is more highly developed with pores having thin walls. The samples in Figure 20 were crushed to 100 pct thru 60 mesh so that the gross pore structure is not as clear as possible.

TABLE 9.- Effect of hydrogen velocity on carbon conversion  
in the hot rod reactor at 800° C

<u>Series</u>	<u>Sample</u>	<u>P<sub>H<sub>2</sub></sub>, atm</u>	<u>H<sub>2</sub> velocity cm/sec</u>	<u>Average Carbon Conv., %</u>	<u>Residence Time, min.</u>
HR-1	Pgh. hvAb Coal	35	36.6	39.9	5
HR-2	Pgh. hvAb Coal	35	2.19	31.2	6
HR-1	Pgh. hvAb Coal	69	36.6	53.7	5
HR-2	Pgh. hvAb Coal	69	1.11	33.9	6
HR-1C	Pgh. hvAb Char	69	36.6	31.4	15
HR-2C	Ill. #6 hvCb Char	69	1.11	31.2	15

TABLE 10.- Comparison of types 1 and 2 carbon conversion  
in the FDP and "Hot-Rod" Reactors

<u>Tests</u>	<u>P<sub>H<sub>2</sub></sub>, atm</u>	<u>Carbon Conv., %</u>
FDP*	35.0	27.2
FDP*	69.0	32.2
HR-1**	35.0	33.2, 32.8
HR-1**	69.0	38.5, 40.3
HR-2**	35.0	23.7
HR-2**	69.0	25.6

\*From Figure 8, 850°-900° C.

\*\*800° C.

TABLE 11.- Kinetic parameters for HR-1C series data

<u>Temp., ° C</u>	<u>P<sub>H<sub>2</sub></sub>, atm</u>	<u>α</u>	<u>E</u>	<u>k atm<sup>-1</sup>hr<sup>-1</sup></u>
800	18.0	1.0	.009	.0234
800	35.0	1.0	.027	.0178
800	69.0	1.0	.144	.0110
800	69.0	1.0	.136	.0137*

\*HR-2C data.

Figure 21 shows the char samples from FDP tests at 850° C and 69 atm using a lignite coal feed. The pore structure appears very undeveloped compared to the structure obtained with bituminous coal. Because of the lack of particle swelling with lignite (coal particle also in Figure 21), the penetration of hydrogen into the particle is poorer compared to bituminous coal. Consequently, particle size should have an even stronger influence on the hydrogasification of lignite than with bituminous coals.

The char data in Table 9 are very interesting because the superficial hydrogen velocity had no effect on the carbon conversion. The mass transfer rate into the char particles must be large compared to the char-hydrogen reaction rate. This is not surprising since the reaction rate of Type 3 carbon is very slow, probably much slower than the diffusion rates of hydrogen and gaseous reaction products.

The results of HR-1C series experiments with char produced from Pittsburgh seam hvAb coal are shown in Figure 22. The carbon conversion is of the Type 3 species except for a small amount of rapid initial conversion. The kinetic parameters for these data are listed in Table 11. The results of the HR-2C series experiments are also shown in Table 11 and Figure 22, and agree well with the HR-1C data. The two chars are different in that the HR-2C char was produced from Illinois #6 hvCb coal in the dilute phase reactor at 585° C whereas the HR-1C char was produced from Pittsburgh seam hvAb coal by batch carbonization for 2 hours in helium at 600° C. The HR-2C char contained about 26 pct volatile matter compared to the original 36.5 pct volatile matter in the starting coal. Despite these differences, except for the nearly equal devolatilization temperatures, the reactivities of the two chars are essentially the same. A significant difference in the devolatilization temperatures could have resulted in the chars having differing reactivities (23, 29).

The Arrhenius graph in Figure 13 summarizes the results for all the coals and chars tested and includes some of Johnson's data (23) which was adjusted to calculate k values according to Equation 4. Assuming that it is valid to represent the low temperature "hot-rod" reactor data by the same Arrhenius line as the FDP data, the activation energy for hydrogasification of Type 2 carbon is 15.1 kcal/mole of carbon gasified. The hydrogasification rate of Type 3 carbon is about three orders of magnitude lower than the rate of hydrogasification of Type 2 carbon. The activation energy for the HR-1, HR-1C, and HR-2C data is 24.7 kcal/mole of carbon gasified (Type 3 carbon) compared to a value of 47.1 kcal/mole obtained by Johnson (23) using a thermobalance. At 600° and 800° C, the HR-2 data was complicated by the transition to Type 3 carbon conversion and a significant amount of mass transfer resistance. At these higher temperatures the apparent activation energy falls off considerably as shown in Figure 13.

#### Two-Stage Integrated Reactor

The results of the two-stage tests where the first-stage was a FDP reactor and the second-stage either a moving-bed or fluid-bed reactor have been presented elsewhere (18). The kinetic results are summarized in Tables 12, 13, and 14 and are also plotted in Figure 13. Because heat transfer limitations within the char particles caused the true particle temperature to be higher than the measured temperature, the activation energy of the moving bed data is low, and the rate constant values are relatively high at the lower reactor temperatures.

#### Correlation of Char Yield and Coal H, N, S, and O Conversion Data

In order to predict the conversion of other constituents in the coal during hydrogasification besides carbon conversion, results from ninety-five experiments

TABLE 12.- Kinetic results from two-stage integrated reactor  
experiments (18) at 69 atm

<u>Run</u>	<u>Total C</u> <u>Conv., X</u>	<u>Moving</u> <u>Bed C</u> <u>Conv., Z*</u>	<u>Fluid</u> <u>Bed C</u> <u>Conv., Z*</u>	<u>Bed</u> <u>Temp., °K</u>	<u>k</u> <u>atm<sup>-1</sup>hr<sup>-1</sup></u>
2	0.552	---	0.378	1158	0.0145
3	0.536	---	0.356	1158	0.0284
5	0.558	---	0.345	1158	0.0316
11	0.608	---	0.419	1073	0.0450
12	0.551	---	0.335	1118	0.0202
13	0.556	---	0.383	1113	0.0218
14	0.537	---	0.357	1183	0.0139
33	0.620	0.457	---	1178	0.0573
37	0.392	0.131	---	1173	0.0360
38	0.485	0.264	---	1148	0.0396
39	0.417	0.167	---	918	0.0449
43b	0.430	0.186	---	1038	0.0395
44b	0.391	0.130	---	923	0.0260
45b	0.406	0.151	---	933	0.0307
46a	0.399	0.151	---	957	0.0305
48	0.511	0.301	---	1073	0.0299
49	0.536	0.337	---	988	0.0358

TABLE 13.- Hydrogasification of Illinois #6 hvCb coal in a two-stage reactor at 1000 psig - run conditions

Test	46		48		49	
Reactor Zone	FDP*	MB*	FDP	MB	FDP	MB
Temp., ° C	850	684	850	800	850	715
Coal or Char Rate, lb(dry)/hr	10.51	6.68	10.26	5.08	10.32	5.01
Bed Height, in.	---	0	---	36	---	36
Residence Time, min.	---	0	---	10.4	---	10.4
Feed Gas, SCFH	164.4	141.4	181.7	152.0	166.2	150.7
Vol. Pct. H <sub>2</sub>	56.2	99.4	52.0	99.0	50.9	98.6
CH <sub>4</sub>	37.2	---	42.1	---	42.8	---
N <sub>2</sub>	1.05	0.50	1.10	1.00	1.50	1.30
He	5.45	---	4.70	---	4.70	---
Product Gas, SCFH**	168.6	141.4	179.0	124.6	169.8	130.3
Vol. Pct. H <sub>2</sub>	34.8	99.4	32.4	54.2	30.1	58.0
CH <sub>4</sub>	55.1	---	57.2	43.5	58.0	39.0
Run Time, min.	187		193		187	

\* FDP: free-fall dilute phase reactor (3 foot heated length); MB: moving-bed reactor.

\*\*For runs 48 and 49, the individual product gas flowrates and the composition of the MB product gas prior to mixing were estimated using the helium tracer data.

TABLE 14.- Hydrogasification of Illinois #6 hvCb coal in a two-stage reactor at 1000 psig - results

Test HY	46	48	49
Conversion, wt. pct.			
MAF Coal	43.1	60.2	60.4
C	33.0	50.7	53.6
H	75.4	96.4	93.4
S	66.7	74.8	76.3
N	59.4	89.7	86.4
O	91.0	99.6	90.0
Gas Yields, SCF/lb dry coal			
CH <sub>4</sub>	3.01	7.80	7.58
C <sub>2</sub> H <sub>6</sub>	0.11	0.17	0.13
CO	0.43	0.69	0.80
CO <sub>2</sub>	0.10	0.09	0.11
H <sub>2</sub>	-3.21	-11.63	-10.31
H <sub>2</sub> S*	0.04	0.03	0.07
Oil Yield, lb/lb dry coal	0.048	0.041	0.026
Carbon to Gas and Oils, wt. pct.	24.3	47.7	44.2
Mean Char Particle Diameter, mm	0.433	---	0.397

\* About 50% of the converted sulfur appears in the gas product after water scrubbing.

in the FDP reactor and FDP-Fluid Bed integrated reactors were correlated with carbon conversion to yield Figures 23-26. The correlations in Figures 23-25 show that char yield and removal of coal hydrogen and nitrogen can be accurately calculated from carbon conversion, independent of reactor conditions and possibly geometry. For carbon conversions above 20 pct (essentially devolatilization) the oxygen removal usually exceeds 90 pct and can be considered to be complete. The data for sulfur removal are very scattered, possibly because of the error in determining changes in small amounts of sulfur in the coal and char samples. In addition, the hydrogen sulfide that is formed may be in equilibrium with sulfur in the char such that a simple correlation with carbon conversion is not possible.

In Figure 27, the char yields have been recomputed in terms of MAF conversion so that the relationship between carbon conversion and MAF conversion can be shown. A curve is drawn through the data such that it bows away from the unit slope line and passes through (0,0) and (100,100). The data in Figures 23-25 only covered the carbon conversion range 22-55 pct so that for simplicity a straight line was used to fit the data. As the range is widened, however, it becomes obvious that a curve gives a better correlation of the data.

The carbon conversion range covered by the HR-1 and HR-2 series experiments is complete, ranging from 0 to 95 pct. In Figure 28, the MAF conversion is plotted versus carbon conversion and essentially the same curve as used in Figure 27 fits these results. Based on these curves it appears that the correlations of coal constituent conversions with carbon conversion are not only independent of reactor conditions, but also reactor geometry. Figure 29 shows a similar MAF-carbon conversion plot for the HR-1C and HR-2C series char tests. The carbon conversion in Figure 29 does not include the carbon that was lost during devolatilization of the coal to prepare the char.

The conversion of coal H, N, and S in the HR-1 and HR-2 series experiments are shown in Figures 30-32. In Figures 30 and 31, the straight line fits of the H and N data determined previously are shown to be inadequate over a very wide range of carbon conversion. These sets of data are both fit best with curves that are concave downward, similar to the MAF curves. Despite the scatter in the data, the correlation with carbon conversion still appears to be valid. Unlike in the FDP and Two-Stage reactor experiments, ultimate analyses were not run on the coal feed for each test, but only on the entire batch of coal. Consequently, some segregation in the feeds could have occurred causing scatter in the calculation of the H, N, and sulfur conversions. These constituents are present in relatively small amounts and thus their calculated conversions are very sensitive to fluctuations in the feed composition. The sulfur data in Figure 32 shows a more definite trend with carbon conversion than was evident in Figure 26 and shows the latter correlation to be conservative. Work is planned to extend the linear correlations in Figures 23-26 to a regression curve that will fit all of the data, i.e., FDP, HR-1, HR-2, and the Two-Stage reactors. These relationships are very valuable in scale-up design calculations because the displacement of the volatile elements in the coal and the char yield can be accurately predicted for the plant flowsheet.

## NOMENCLATURE

- $\alpha$  fraction of the carbon that is available for reaction in the regime being considered.
- $\alpha_T$  fractional weight loss that can be achieved in the reaction regime being considered.
- $\beta$  same as  $\alpha$  except the Type 1 carbon is excluded.
- $\lambda$  stoichiometric coefficient for the char-hydrogen reaction.
- $\mu_g$  gas viscosity, lb/ft hr.
- $\rho_b$  char bulk density, lb/ft<sup>3</sup>.
- $\rho_g$  gas density, lb/ft<sup>3</sup>.
- $\rho_s$  char particle density, lb/ft<sup>3</sup>.
- $\bar{d}_p$  mean char particle diameter, in.
- $E$  fraction of carbon instantaneously devolatilized.
- $g$  gravitational acceleration, ft/sec<sup>2</sup>.
- $k$  char-hydrogen reaction rate constant, atm<sup>-1</sup> hr<sup>-1</sup>.
- $k_T$  weight loss reaction rate constant, atm<sup>-1</sup> hr<sup>-1</sup>.
- $L$  reactor length, ft.
- $P_{H_2}$  partial pressure of hydrogen, atm.
- $Re_p$  char particle Reynolds number.
- $t$  time, sec.
- $U_T$  free-fall velocity of char particles, fps.
- $U_{TS}$  single char particle terminal velocity, fps.
- $W$  coal mass feed rate, lb/hr ft<sup>2</sup>.
- $x$  fractional carbon conversion based on total coal carbon.
- $z$  fractional carbon conversion based on starting char carbon.

References

1. Feldmann, H. F., C. Y. Wen, W. H. Simons, and P. M. Yavorsky. Supplemental Pipeline Gas From Coal by the HYDRANE Process. Presented at the 71st National AIChE Meeting, Dallas, Texas, Feb. 20-23, 1972.
2. Feldmann, H. F. and P. M. Yavorsky. The HYDRANE Process. Presented at the 5th AGA/OCR Synthetic Pipeline Gas Symposium, Chicago, Illinois, Oct. 29-31, 1973.
3. Wen, C. Y., C. T. Li, S. H. Tscheng, and W. S. O'Brien. Comparison of Alternate Coal Gasification Processes for Pipeline Gas Production. Presented at the 65th Annual AIChE Meeting, New York, New York, Nov. 26-30, 1972.
4. Wen, C. Y., coworkers. Optimization of Coal Gasification Processes, Research and Development Rept. No. 66, Interim Rept. Nos. 1 and 2, O.C.R., U.S. Dept. of the Interior, Wash., D. C.
5. Feldmann, H. F., W. H. Simons, J. A. Mima, and R. W. Hiteshue. Reaction Model for Bituminous Coal Hydrogasification in a Dilute Phase. Preprints of Fuel Division, ACS, v. 14, No. 4, Part II, Sept. 1970, pp. 1-13.
6. Feldmann, H. F., J. A. Mima, and P. M. Yavorsky. Pressurized Hydrogasification of Raw Coal in a Dilute-Phase Reactor. Fuel Gasification, Advances in Chem. Series 131, ACS, Washington, D. C., 1974, pp. 108-125.
7. Hiteshue, R. W., S. Friedman, and R. Madden. Hydrogasification of High-Volatile A Bituminous Coal. U.S. Bureau of Mines Report of Investigation 6376, 1964.
8. Hiteshue, R. W., R. B. Anderson, and M. D. Schlesinger. Hydrogenating Coal at 800° C. Ind. & Eng. Chem., 49 (Dec., 1957), pp. 2008-10.
9. Hiteshue, R. W., P. S. Lewis, and S. Friedman. Gaseous Hydrocarbons from Coal. Paper presented at the A.G.A. Operating Section Conference, 1960 (CEP-60-9).
10. Hiteshue, R. W., S. Friedman, and R. Madden. Hydrogenation of Coal to Gaseous Hydrocarbons. U.S. Bureau of Mines Report of Investigation 6027, 1962.
11. Friedman, S., R. W. Hiteshue, and M. D. Schlesinger. Hydrogenation of New Mexico Coal at Short Residence Time and High Temperature. U.S. Bureau of Mines Report of Investigation 6470, 1964.
12. Hiteshue, R. W., R. B. Anderson, and S. Friedman. Gaseous Hydrocarbons by Hydrogenation of Coals and Chars. Ind. & Eng. Chem., 52 (July, 1960), pp. 577-9.
13. Hiteshue, R. W., S. Friedman, and R. Madden. Hydrogasification of Bituminous Coals, Anthracite, and Char. U.S. Bureau of Mines Report of Investigation 6125, 1962.
14. Kawa, W., R. W. Hiteshue, W. A. Budd, S. Friedman, and R. B. Anderson. Agglomeration Studies in the Low-Pressure Hydrogenation of Coal in a Fluidized Bed. U.S. Bureau of Mines Bulletin 579, 1959.
15. Lewis, P. S. and R. W. Hiteshue. Hydrogenating Coal in the Entrained State. Ind. & Eng. Chem., 52 (Nov., 1960), pp. 919-20.
16. Lewis, P. S., S. Friedman, R. W. Hiteshue. High Btu Gas by the Direct Conversion of Coal. Fuel Gasification Advances in Chem. Series 69, ACS, Washington, D. C., 1967, pp. 50-63.

17. Hiteshue, R. W. The Hydrogasification of Raw Coal. Paper presented at the Amer. Gas Assoc. Symposium on Synthetic Pipeline Gas, Pittsburgh, Pa., Nov. 15, 1966.
18. Wen, C. Y., S. Mori, J. A. Gray, and P. M. Yavorsky. Application of the Bubble-Assemblage Model to the HYDRANE Process Fluid-Bed Hydrogasifier. Paper presented at the 67th Annual AIChE Meeting, Wash., D. C., Dec. 1-5, 1974.
19. Feldmann, H. F., W. H. Simons, C. Y. Wen, and P. M. Yavorsky. Simulation of a Reactor System for the Conversion of Coal to Methane by the HYDRANE Process. Paper presented at the 4th International Congress of Chem. Eng., Marianske Lazne, Czechoslovakia, Sept. 11-15, 1972.
20. Given, P. H. The Distribution of Hydrogen in Coals and Its Relation to Coal Structure. *Fuel*, 39 (1960), pp. 147-153.
21. Zahradnik, R. L. and R. A. Glenn. The Direct Methanation of Coal. *Fuel* 50, No. 1, (1971), pp. 77-90.
22. Moseley, F. and D. Paterson. The Rapid High-Temperature Hydrogenation of Coal-Chars Part 2: Hydrogen Pressures up to 1,000 Atmospheres. *J. Inst. of Fuel*, 38 (Sept., 1965), pp. 378-391.
23. Johnson, J. L. Kinetics of Bituminous Coal Char Gasification with Gases Containing Steam and Hydrogen. *Fuel Gasification, Advances in Chem. Series 131*, ACS, Wash., D. C., 1974, pp. 145-178.
24. Kunii, D. and O. Levenspiel. *Fluidization Engineering*. John Wiley & Sons, Inc., New York, 1969, p. 76.
25. Wen, C. Y. and J. Huebler. Kinetic Study of Coal Char Hydrogasification, Rapid Initial Reaction. *Ind. & Eng. Chem. Design & Develop.*, 4 (April, 1965), pp. 142-147.
26. Feldmann, H. F., K. D. Kiang, and P. M. Yavorsky. Fluidization Properties of Coal Char. *Preprints of Fuel Division, ACS*, v. 15, No. 3, Sept. 1971, pp. 62-76.
27. Quarterly Technical Progress Report, Morgantown Energy Research Center, Morgantown, West Virginia, September-December, 1969, p. 2.
28. Anthony, D. B. Rapid Devolatilization and Hydrogasification of Pulverized Coal. Sc.D. Thesis, Dept. of Chem. Eng., M.I.T., Cambridge, Mass., Jan., 1974.
29. Blackwood, J. D., B. D. Cullis, and D. J. McCarthy. Reactivity in the System Carbon-Hydrogen-Methane. *Aust. J. Chem.* 20 (1967), pp. 1561-70.

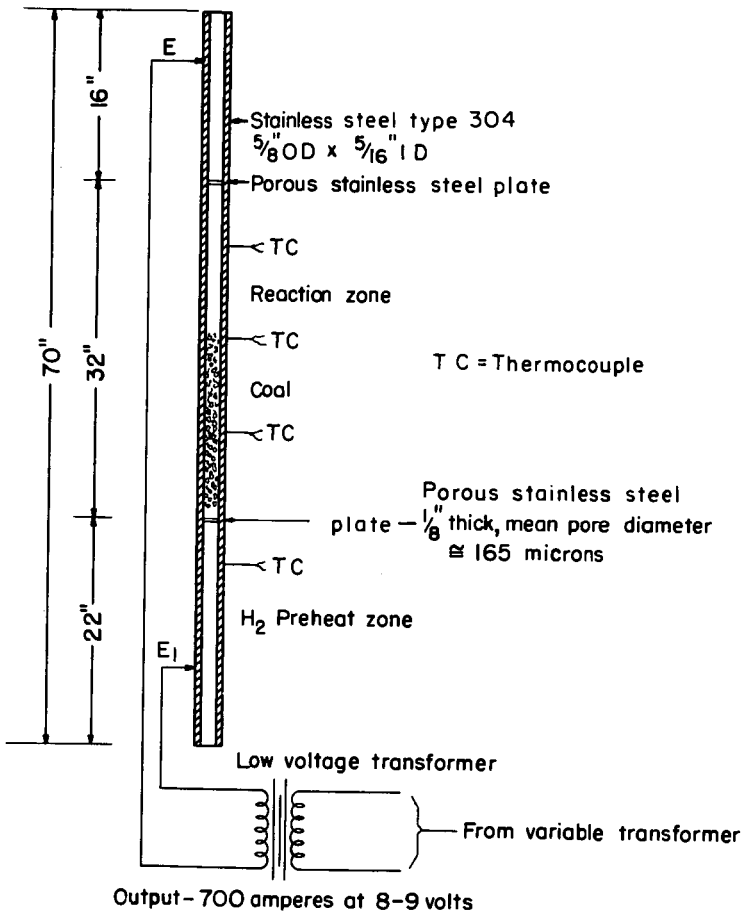


Figure 1 - "Hot-rod" reactor.

L 4753  
12-12-56

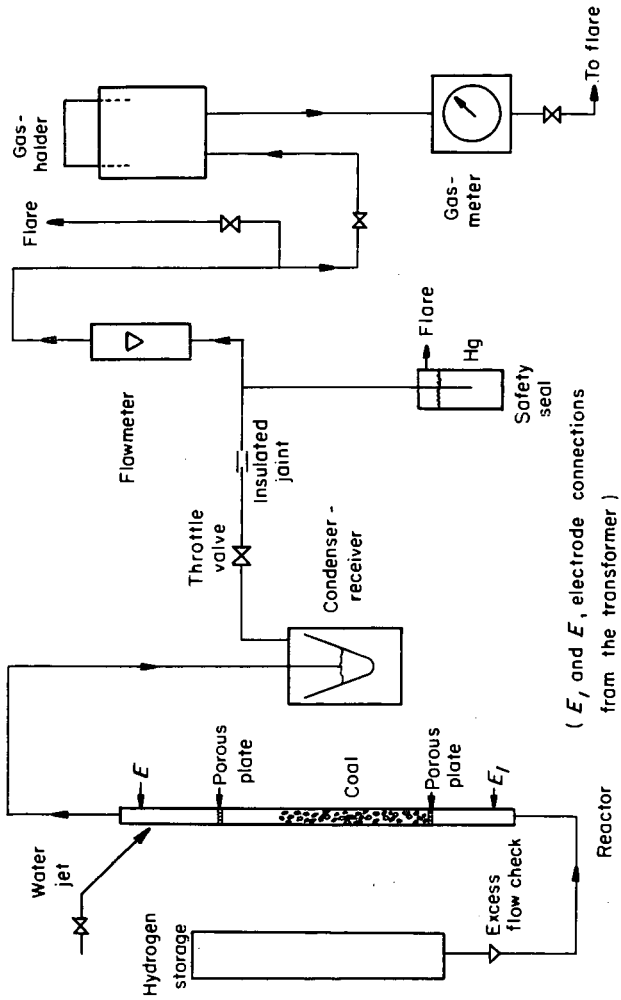


Figure 2 - Flow sheet of "hot rod" apparatus .

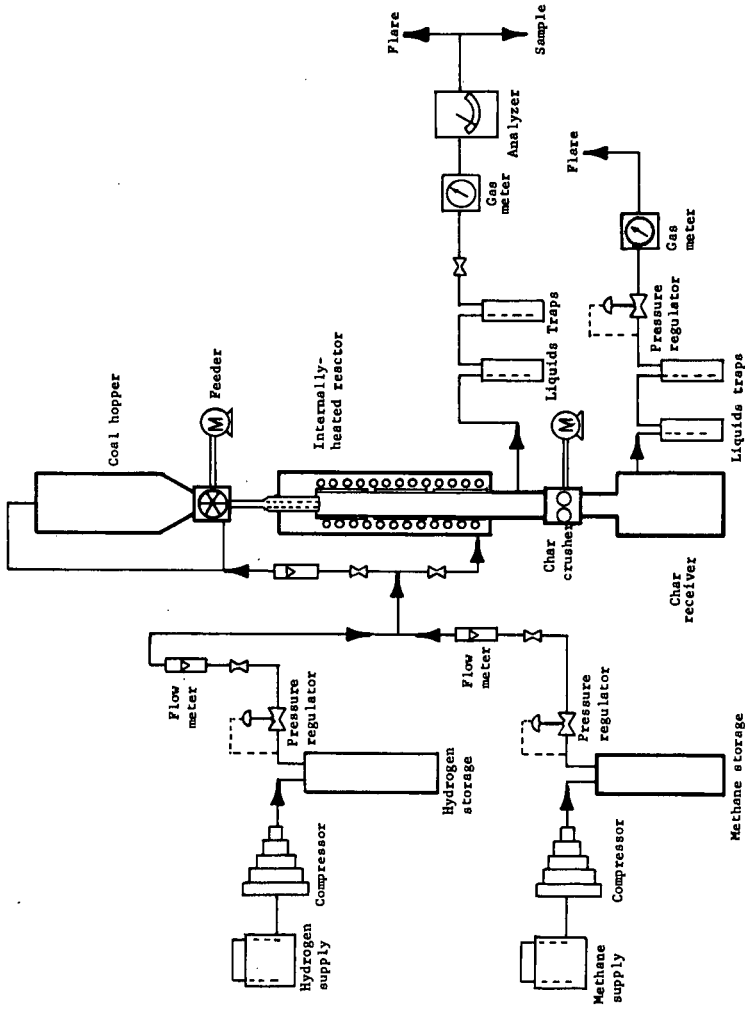


FIGURE 3.- Simplified Flowsheet: Hydrogasification of Coal in Dilute Phase. L-12449

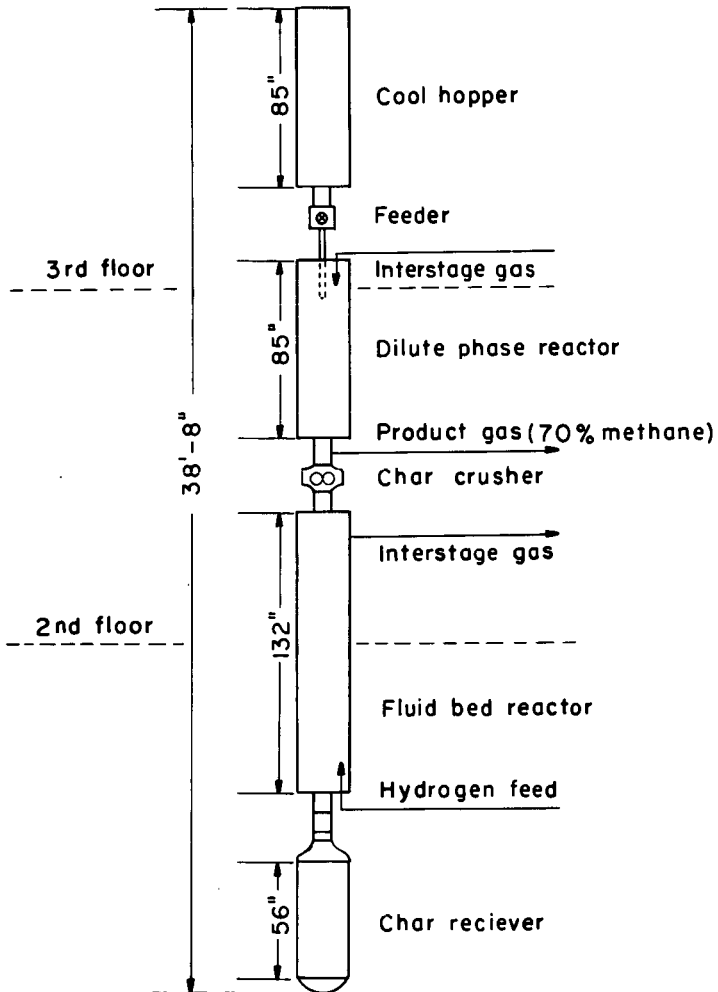


Figure 4 - Integrated hydrogasification unit.

L- 12914

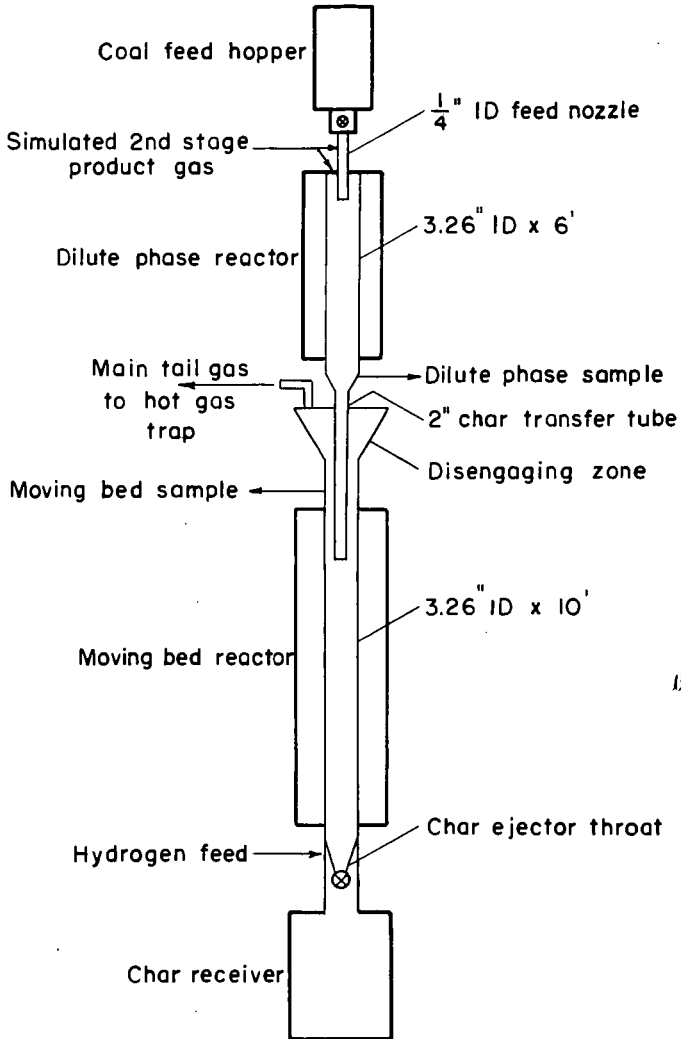


Figure 5 — Integrated two-stage hydrogasifier

L-13753



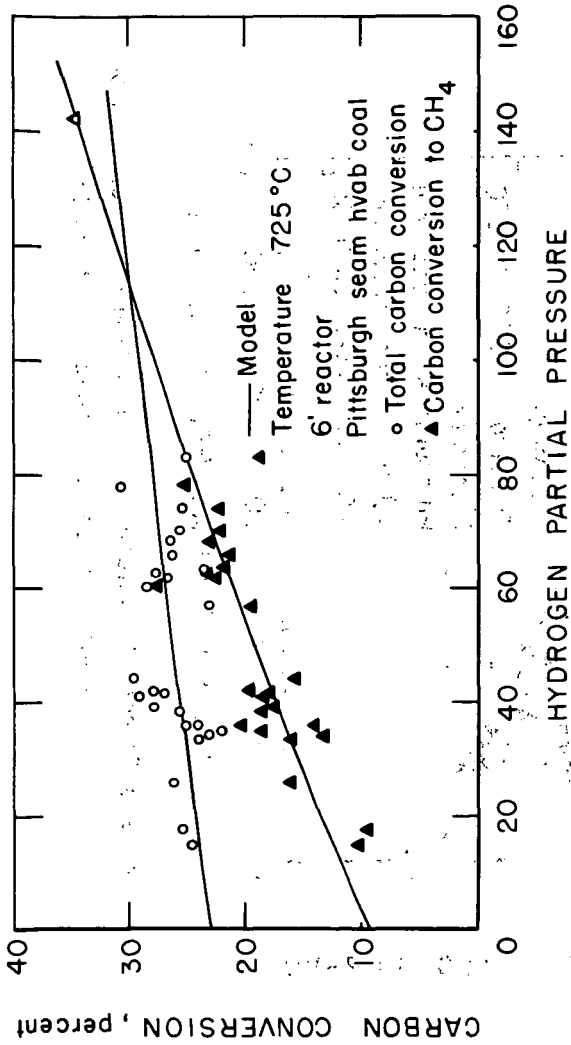


Figure 7 - Effect of hydrogen partial pressure on total carbon conversion and carbon conversion to methane.

5-15-75 L-14296

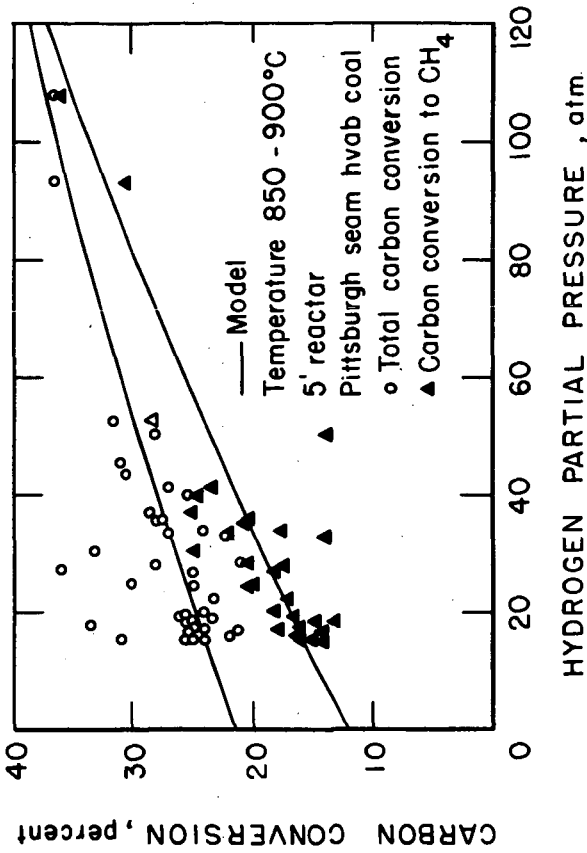


Figure 8-Effect of hydrogen partial pressure on total carbon conversion and carbon conversion to methane.

5-16-75

L-14295

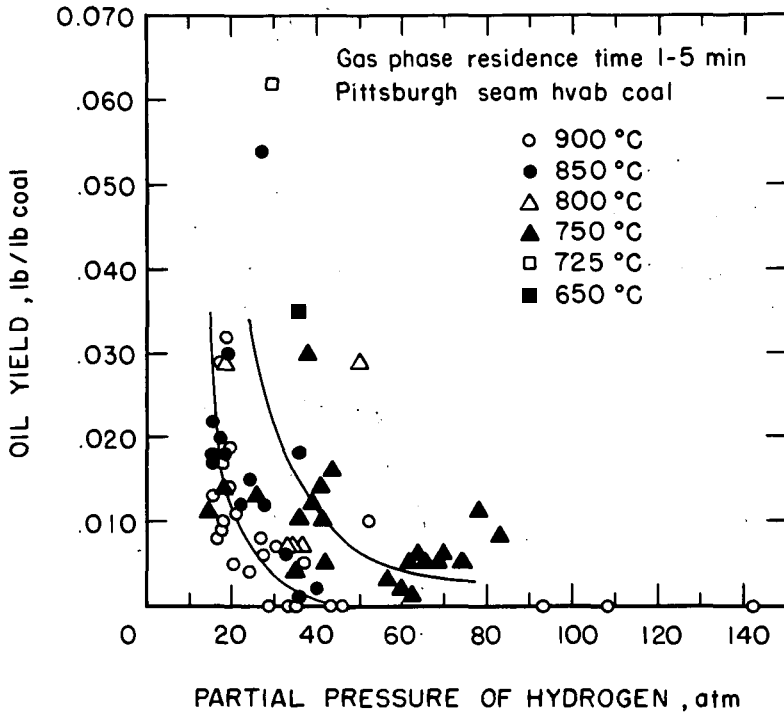


Figure 9 - Effect of hydrogen partial pressure on oil yield.

5-20-75

L-14294

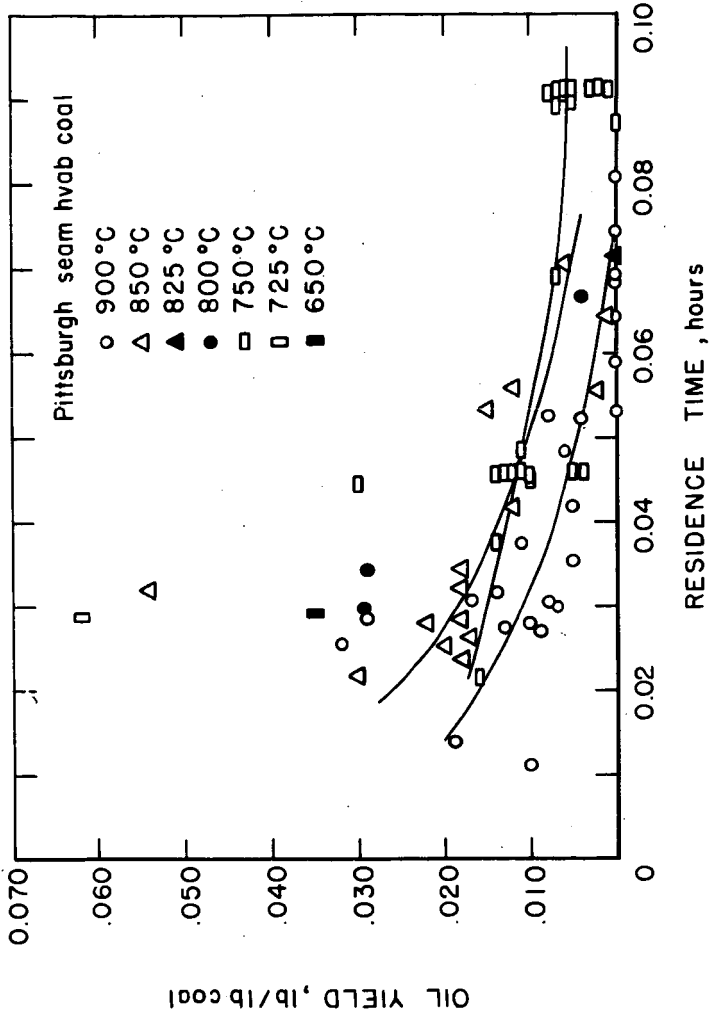


Figure 10-Effect of gas phase residence time on oil yield.

5-21-75

L-14297

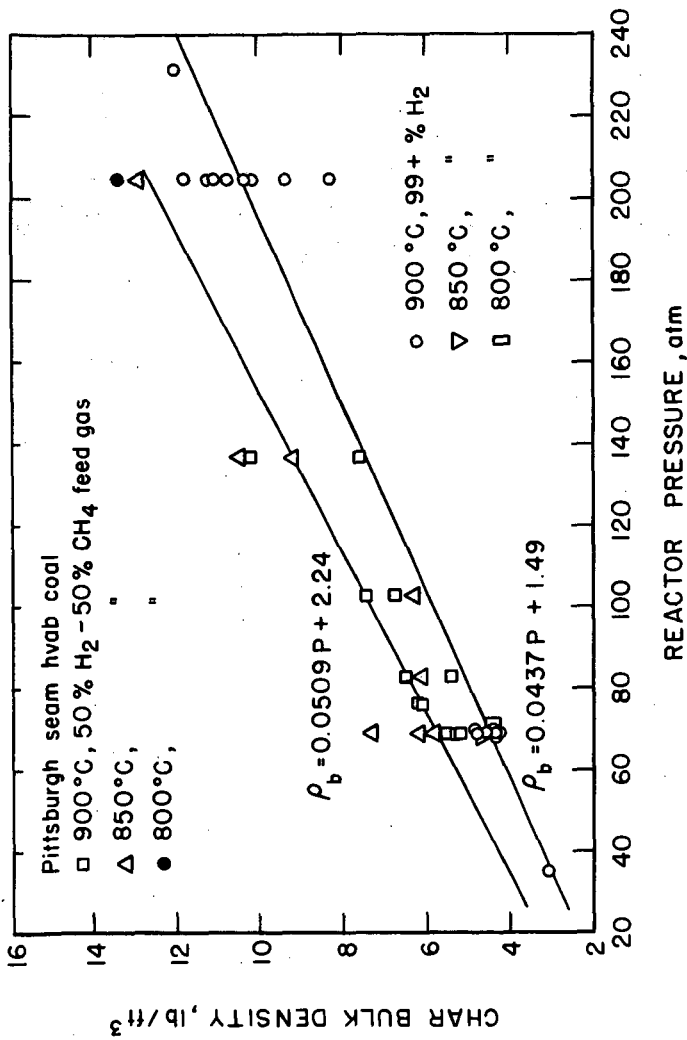


Figure 11 - Effect of total reactor pressure on char bulk density.

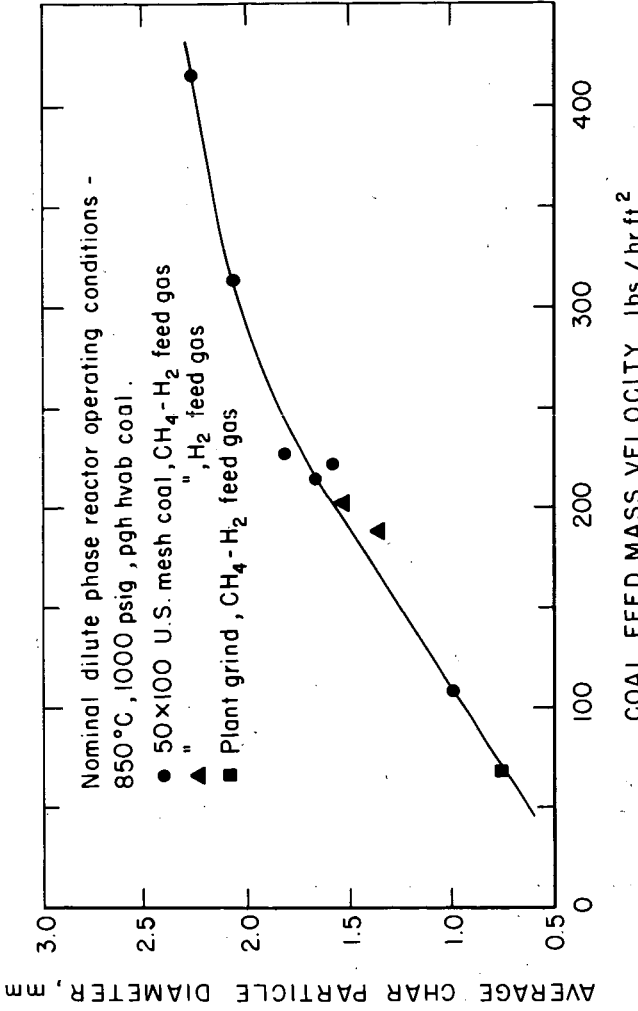


Figure 12-Effect of dilute phase reactor loading on the average diameter of the char product.

L-14084

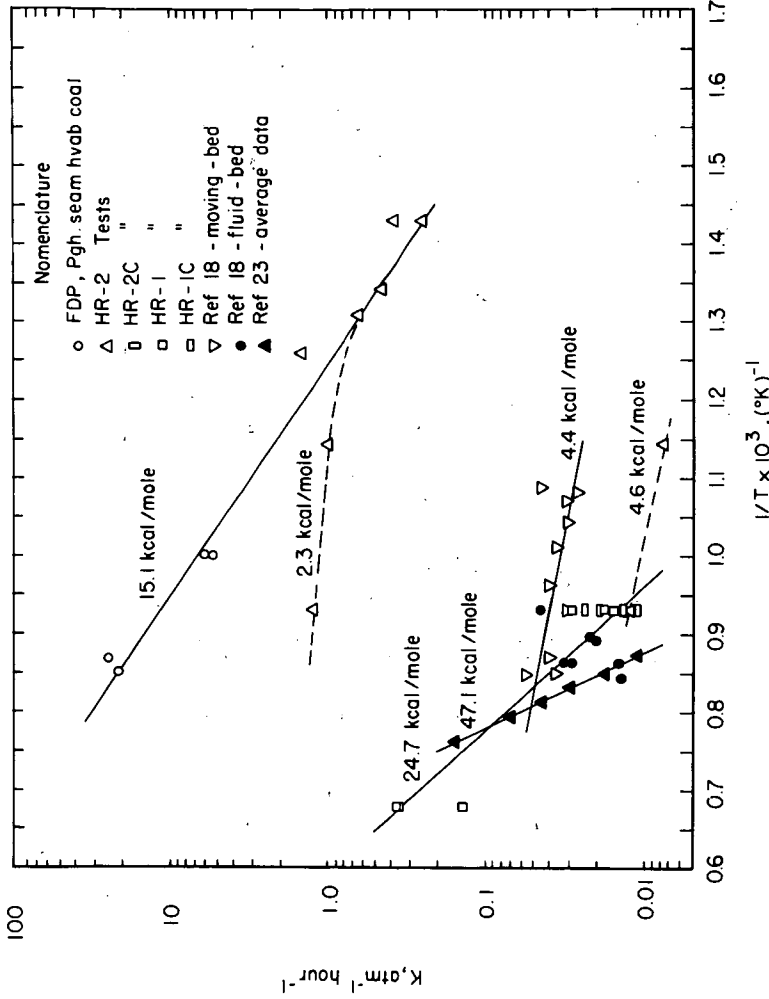


Figure 13 - Temperature dependence of the hydrogasification reactor rate constants for coal and char.

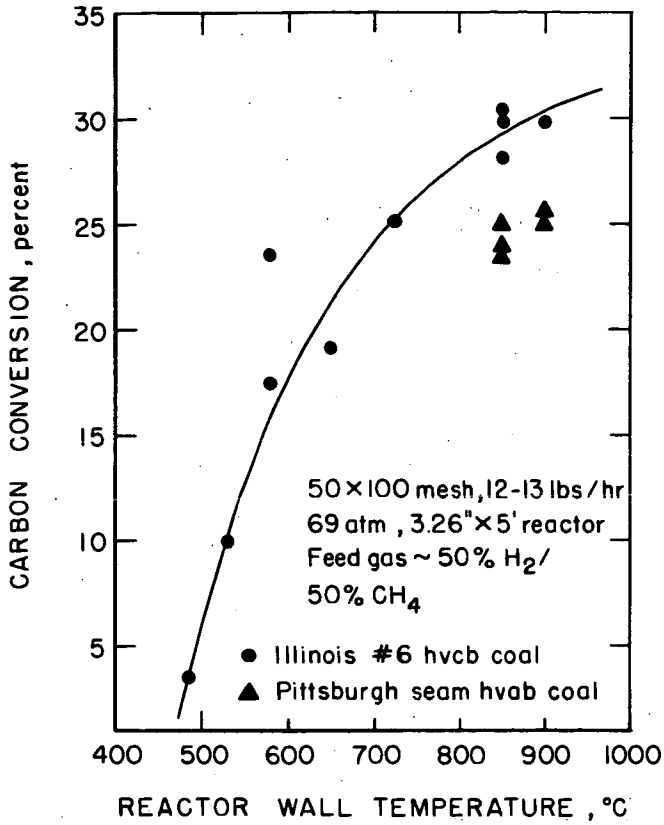


Figure 14 - Carbon conversion in the FDP reactor for Illinois #6 hvcb coal.

5-16-75

L-14292

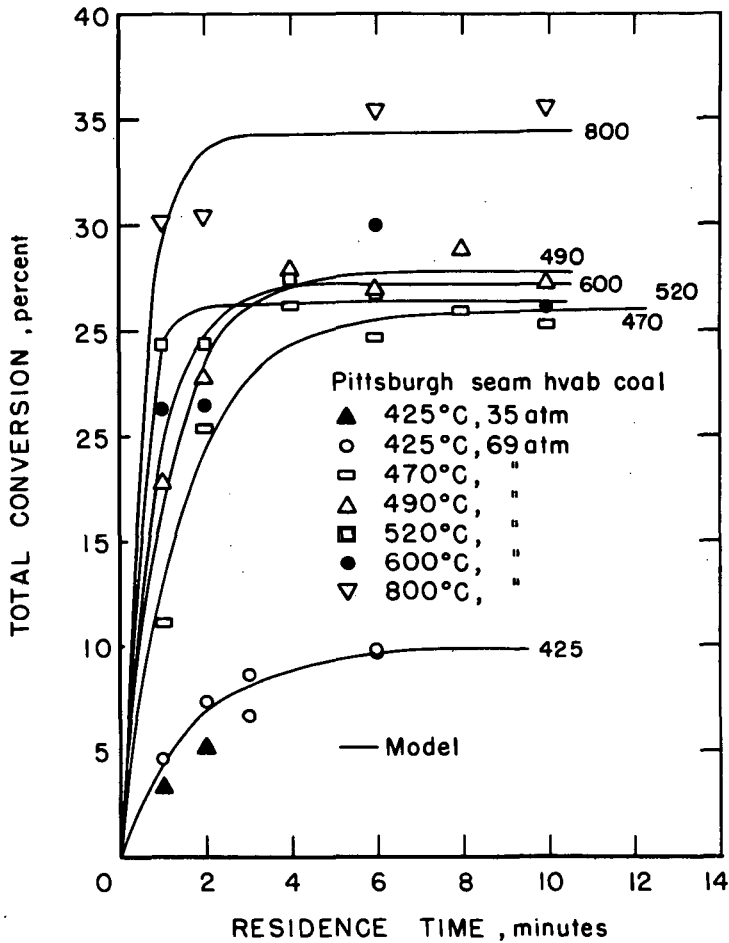


Figure 15 - Effect of temperature and time on total conversion in "hot rod" reactor, HR-2 tests.

5-22-75 L-14300

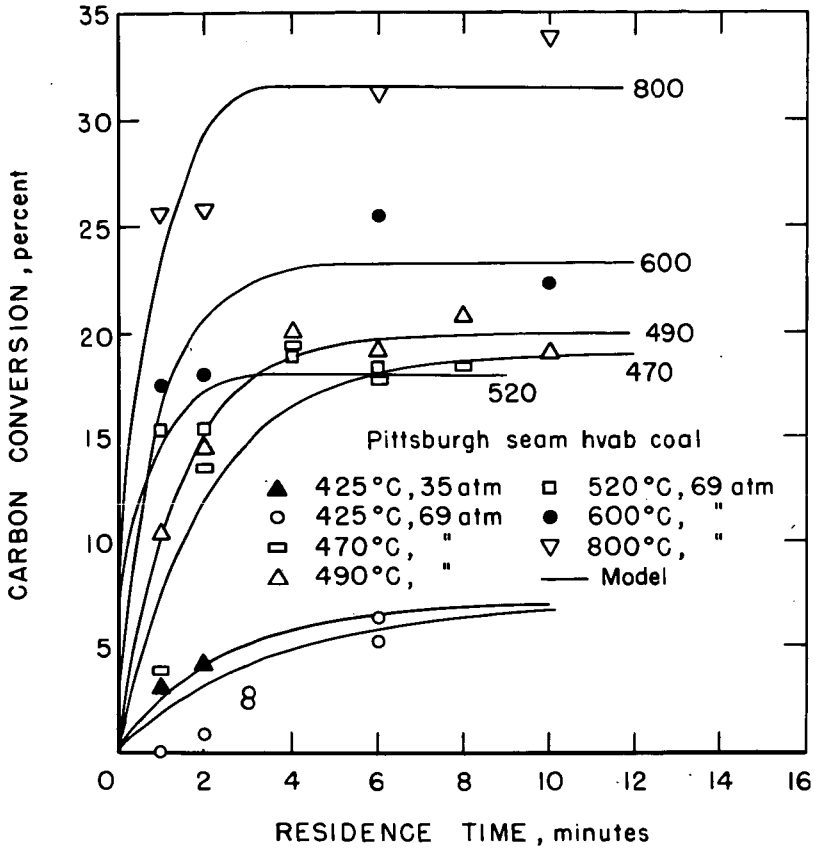


Figure 16- Effect of temperature and time on carbon conversion in "hot rod" reactor, HR-2 tests.

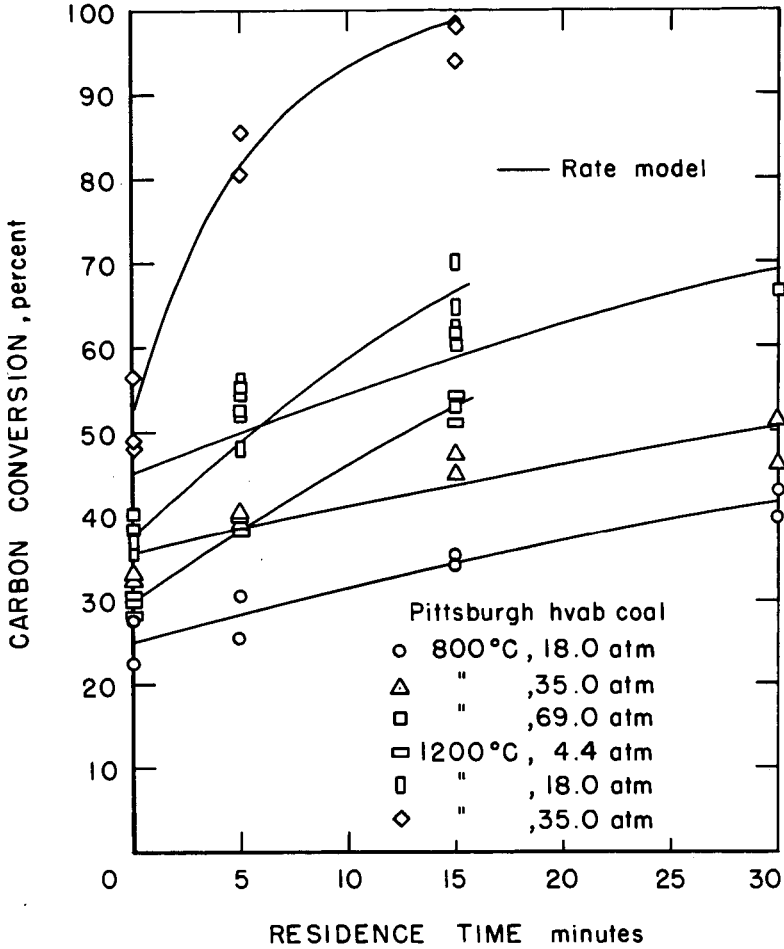


Figure 17- Carbon conversion data for the HR-1 series experiment .

5-21-75 L-14299

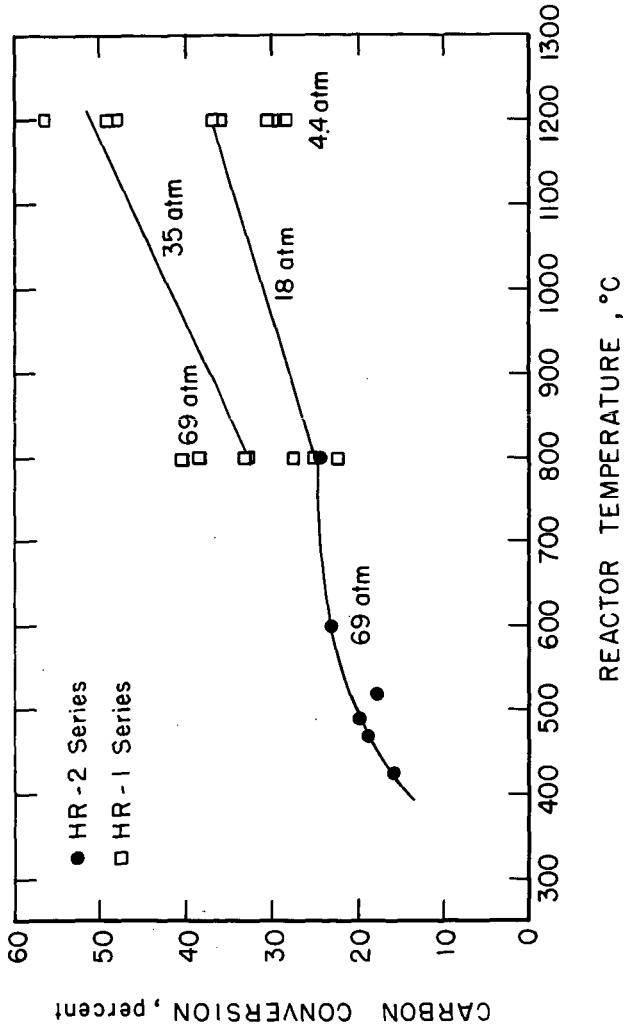


Figure 18-Effect of reactor temperature on types 1 & 2 carbon conversion.

5-15-75 L-14289

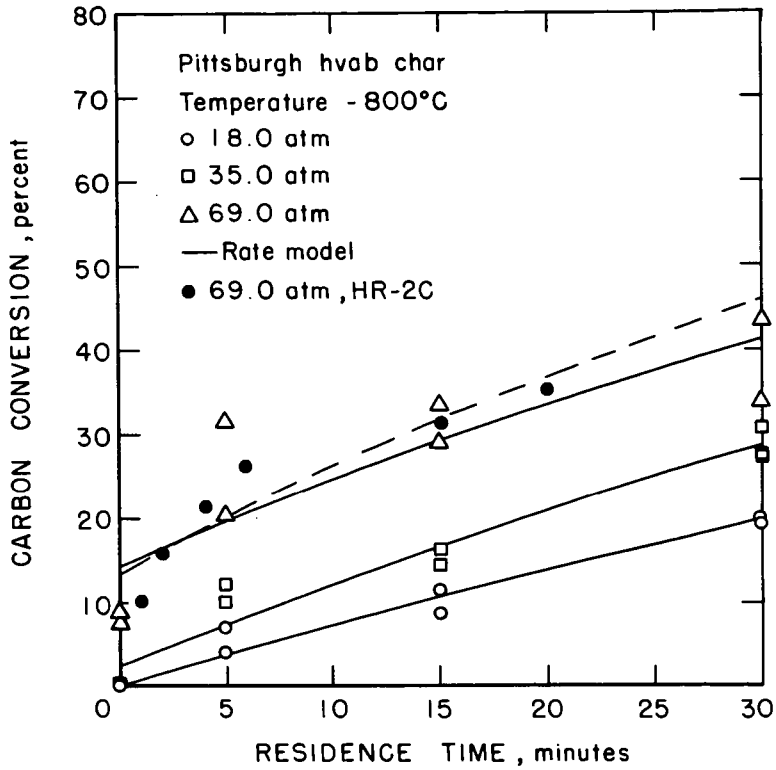


Figure 22- Carbon conversion data for the HR-1C series experiments.

5-15-75

L-14290

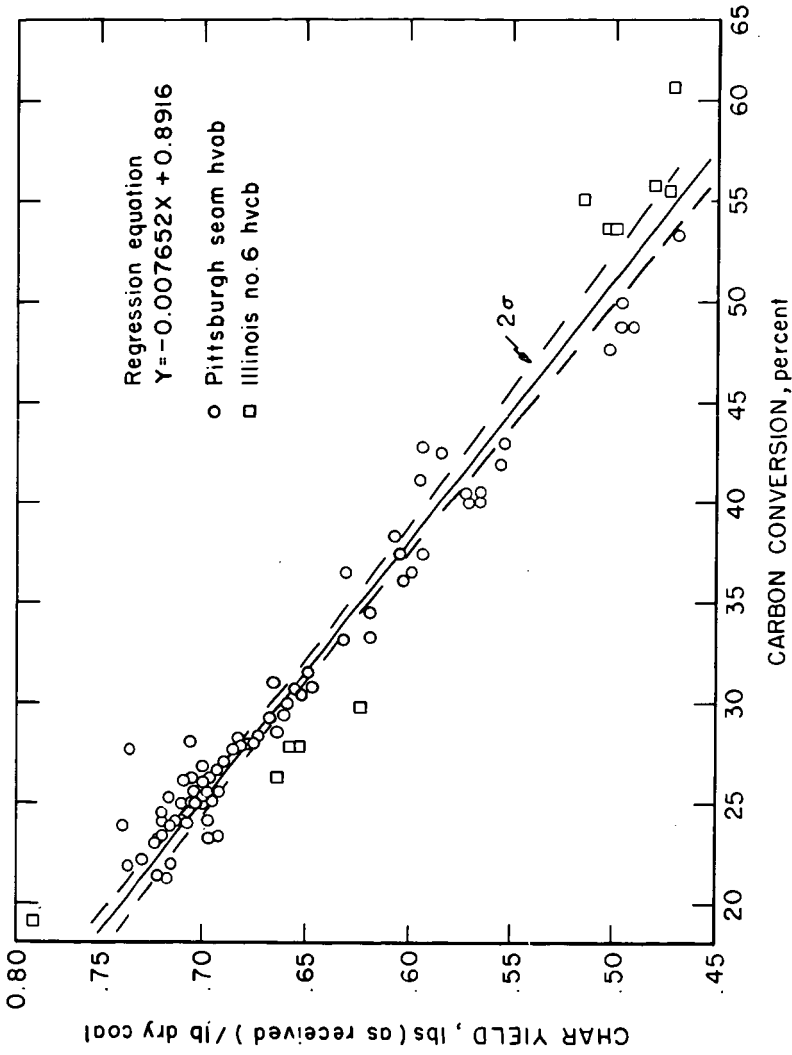


FIGURE 23 - Char yield as a function of carbon conversion during hydrogossification.

L-13708



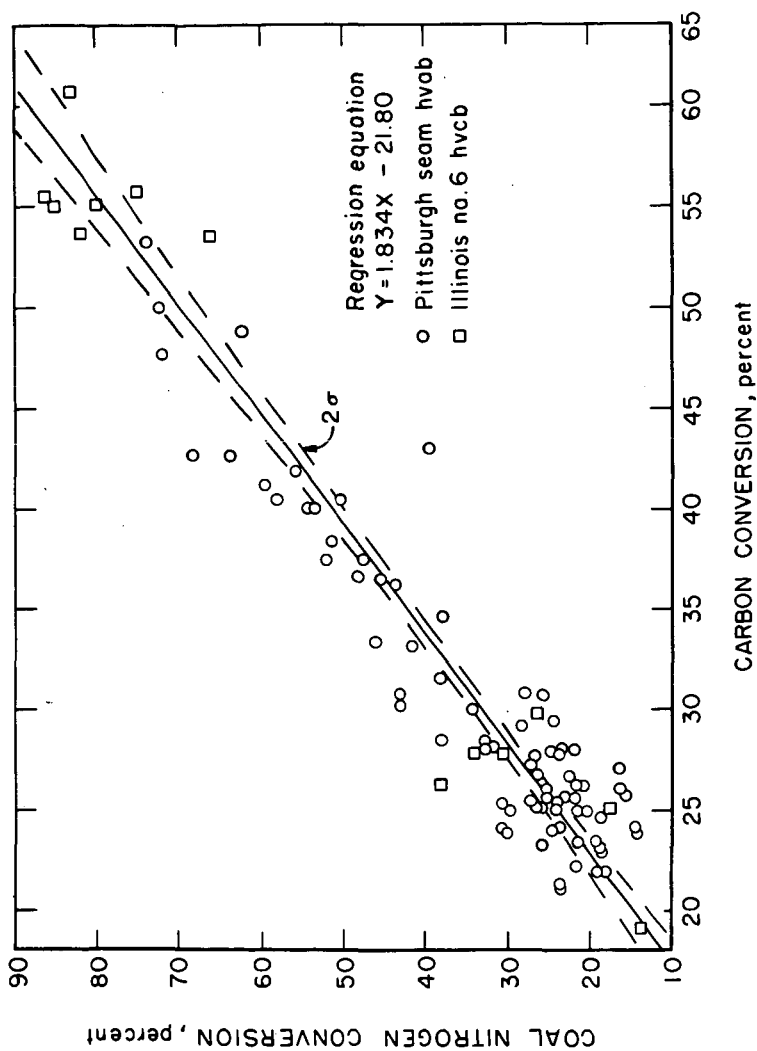


FIGURE 25-Cool nitrogen conversion as a function of carbon conversion during hydrogasification.

L-13712

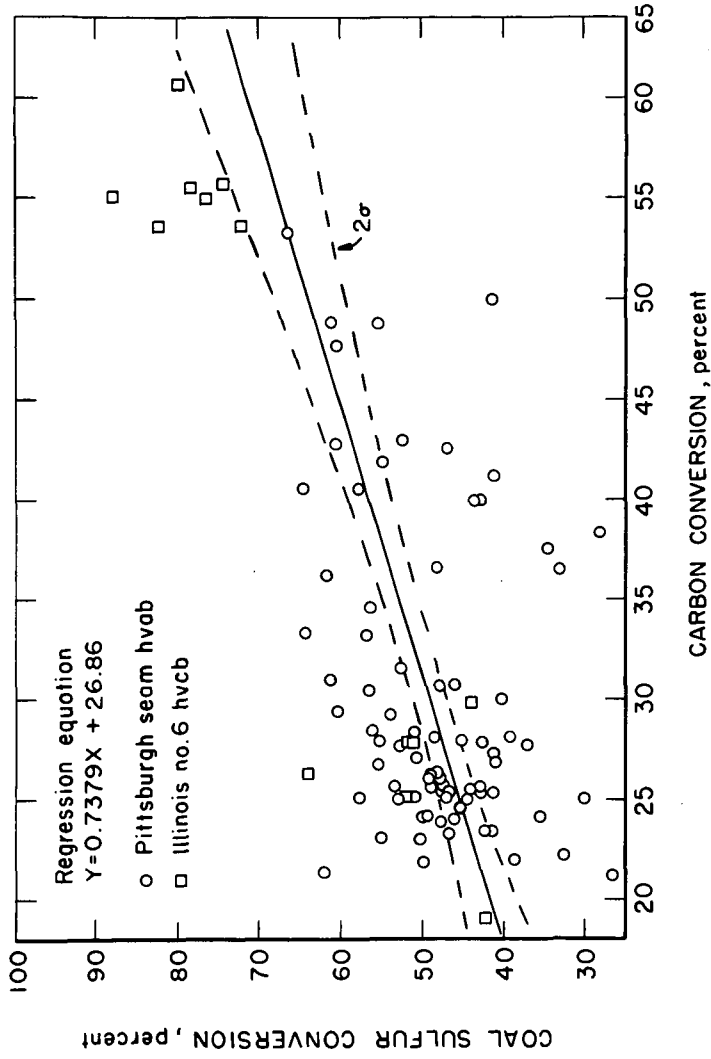


FIGURE 26-Sulfur conversion as a function of carbon conversion during hydrogossification.

L-13710

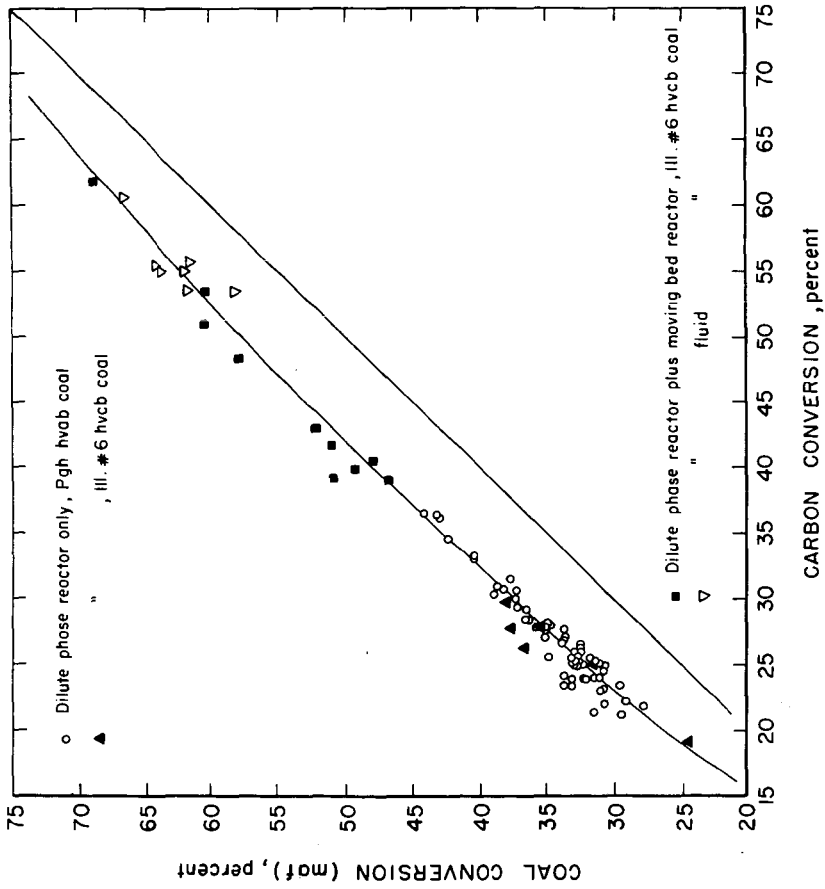


Figure 27-COal conversion (maf) as a function of carbon conversion during hydrogasification.

5-23-75 L-14305

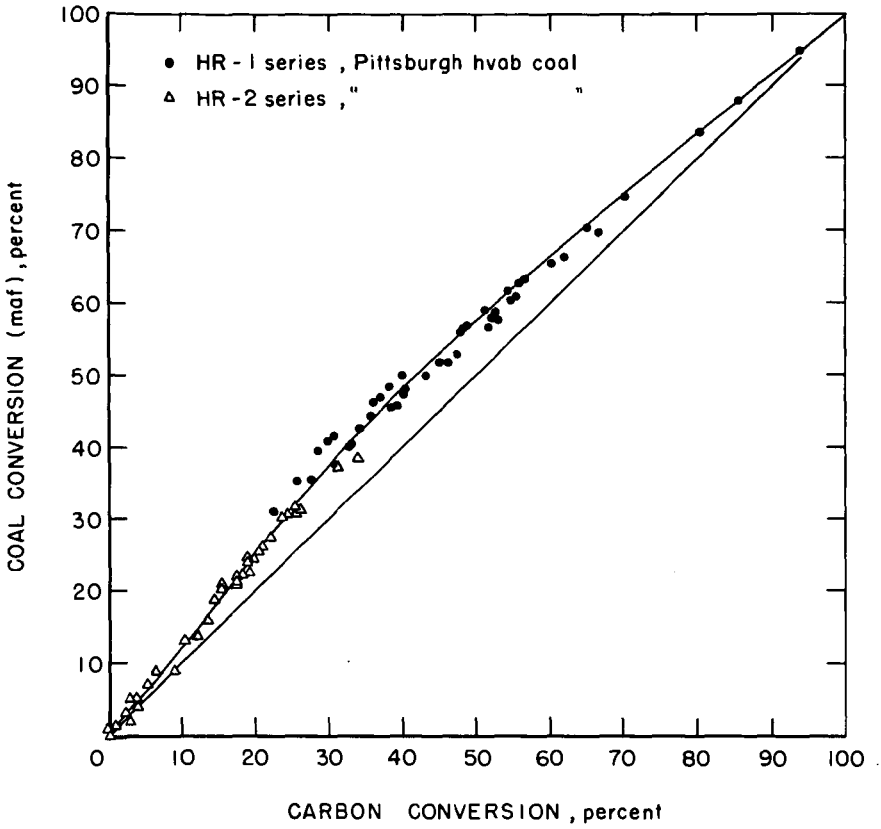


Figure 28 - Coal conversion (maf) as a function of carbon conversion during hydrogasification.

5-16-75

L-14306

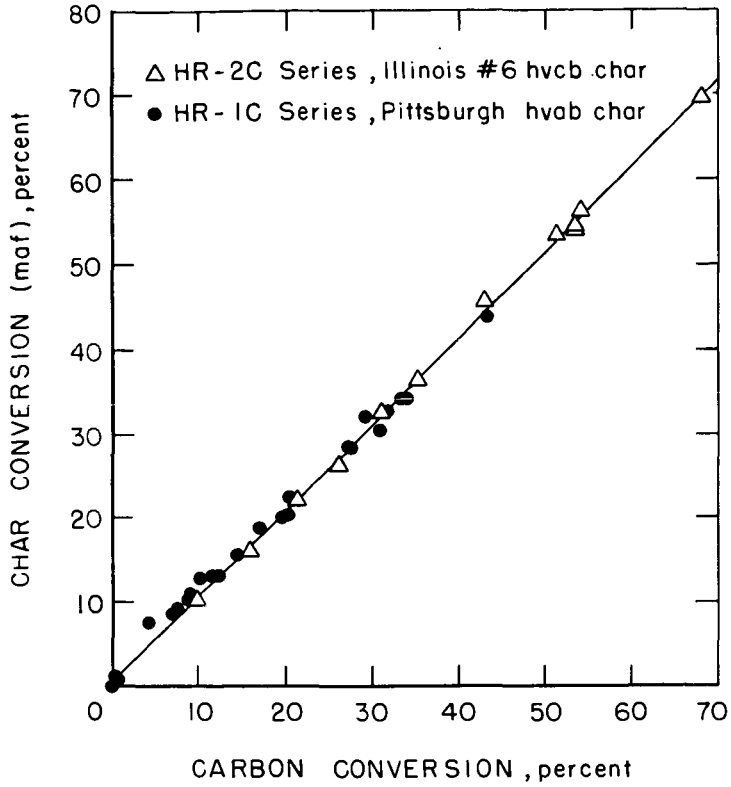


Figure 29- Char conversion (maf) as a function of carbon conversion during hydrogasification.

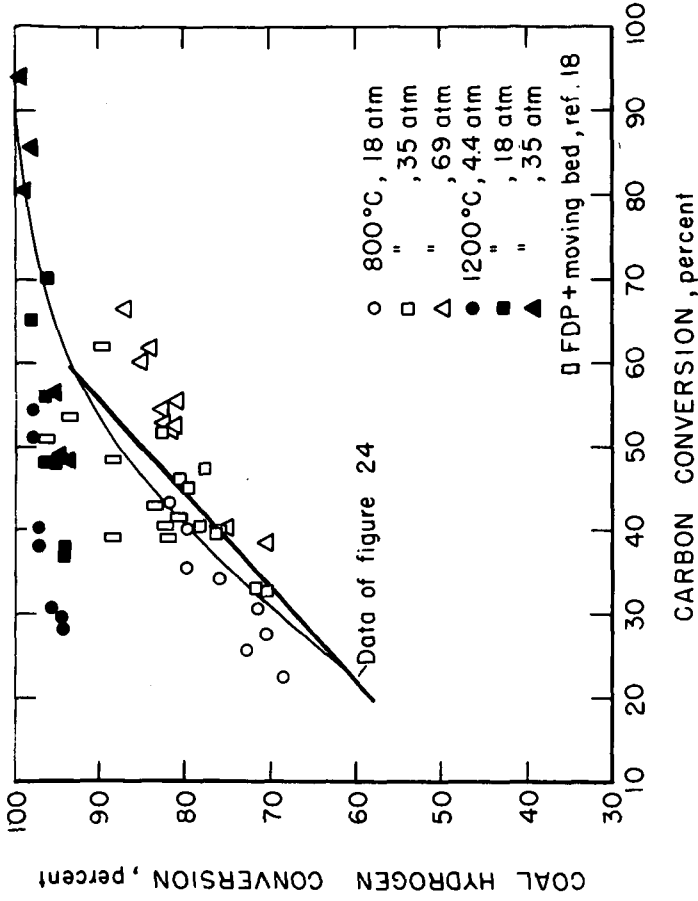


Figure 30-Conversion of coal hydrogen in HR-I tests.

5-20-75

L-14302

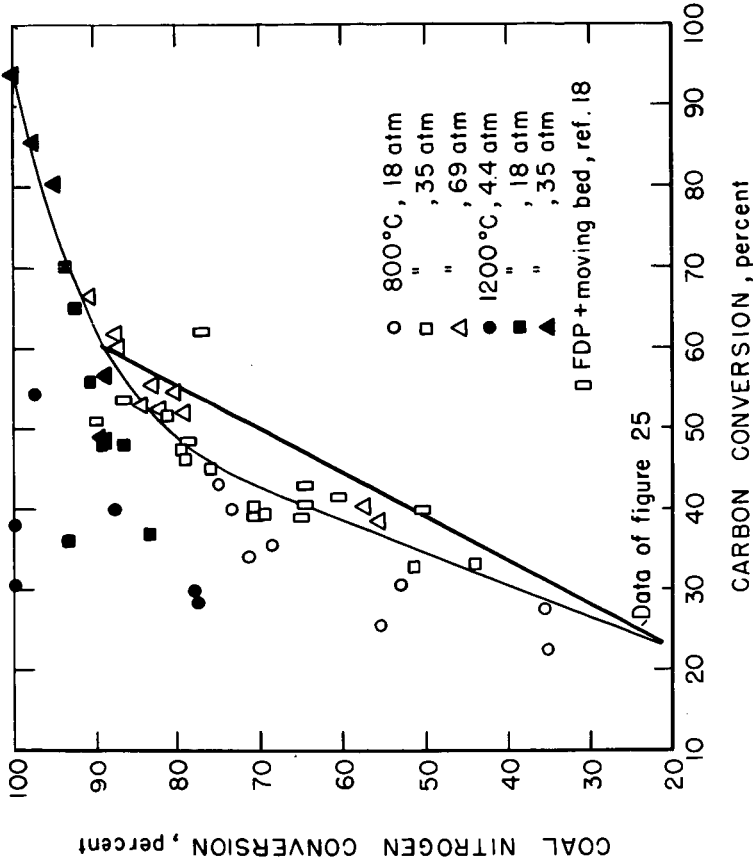


Figure 31- Conversion of coal nitrogen in HR-I tests

5-21-75

L-14303

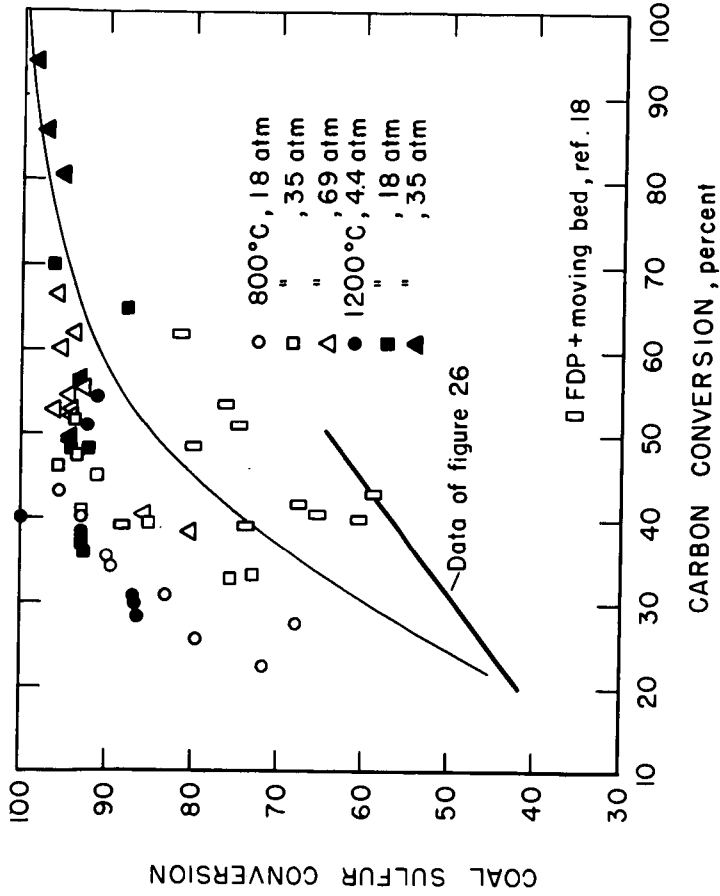
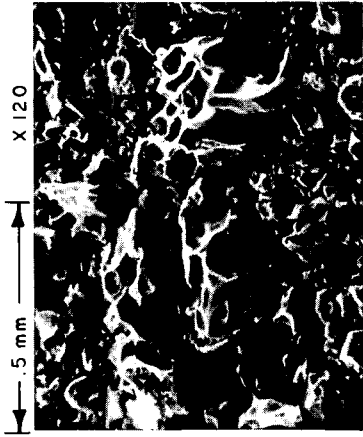


Figure 32 - Conversion of coal sulfur in HR-1 tests

5-20-75

L-14304



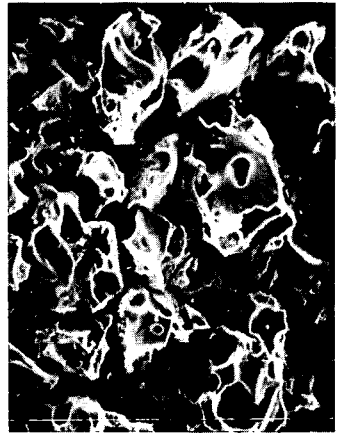
800°C- 2 min.



800°C- 10 min.



600°C- 2 min.

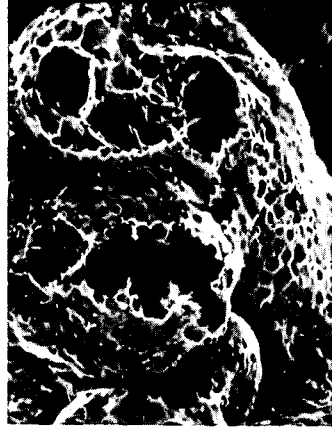


600°C- 10 min.

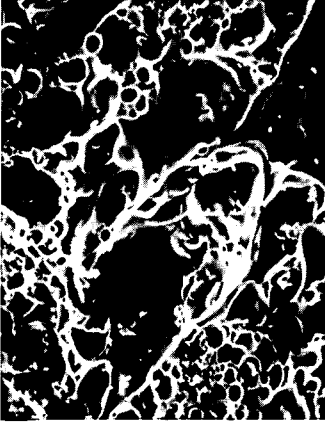
Figure 20 - SEM PHOTOGRAPHS OF 'HOT' ROD CHAR AT VARIOUS TEMPERATURES  
(69 atm) X 120



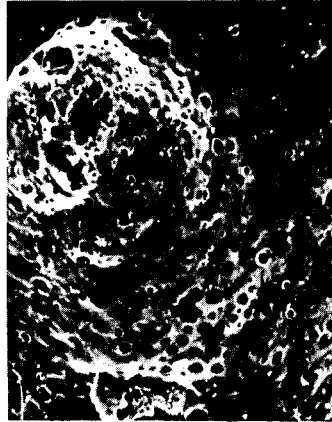
850°C- 137 atm



900°C- 35 atm



725°C- 205 atm



850°C- 69 atm

Figure 19 - SEM PHOTOGRAPHS OF FDP CHAR AT VARIOUS PRESSURES , X 120

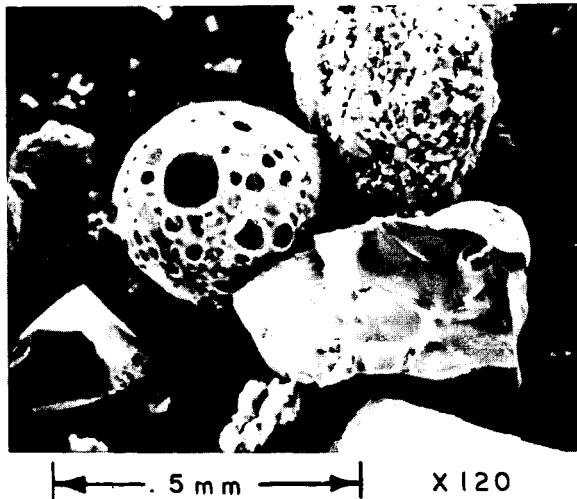
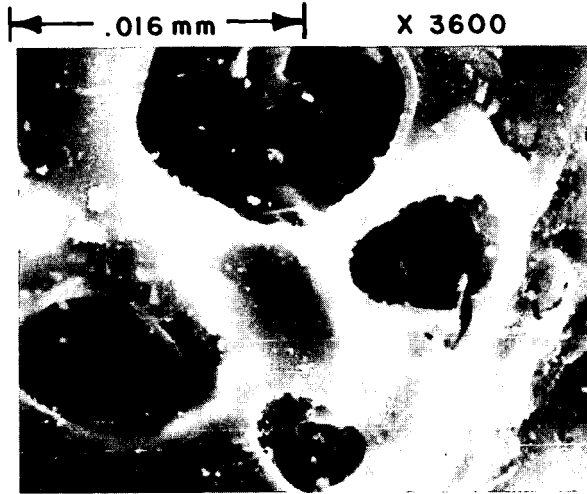


**Figure 21 - SEM PHOTOGRAPHS OF FDP CHAR (LIGNITE) ,  
(850°C, 69 atm)**

HYDROGASIFICATION OF HYDRANE CHAR IN FLUIDIZED AND  
MOVING BEDSC. Y. Wen,\* S. Mori,\* J. A. Gray,\*\* and P. M. Yavorsky\*\*\*West Virginia University  
Morgantown, West Virginia\*\*U.S. Bureau of Mines  
Pittsburgh Energy Research Center  
Pittsburgh, Pa. 15213ABSTRACT

To satisfy future pipeline gas requirements, considerable process development work is being aimed at gasifying coal to produce substitute natural gas (SNG). The heart of many of the gasification processes being developed is a fluid-bed gasifier in which char is reacted with steam/oxygen or hydrogen. In the HYDRANE process, being developed at the U.S. Bureau of Mines, Pittsburgh Energy Research Center, char is reacted directly with hydrogen in the fluid-bed stage of the hydrogasifier. In order to scale-up the fluid-bed reactor to pilot plant or commercial size with confidence, a fluid-bed reactor model has been developed using the bubble-assemblage concept and has been shown to fit existing data reasonably well. Data from moving-bed reactor experiments and the corresponding model were compared to the fluid-bed results and illustrate the differences between plug-flow and well-mixed solid-gas reactors.

INTRODUCTION

In order to satisfy future pipeline gas requirements and alleviate current shortages, considerable process development work is underway for gasifying coal to produce substitute natural gas (SNG). The heart of many of the gasification processes under development is a fluid-bed gasifier in which char is reacted with steam/oxygen or hydrogen. In the HYDRANE process (figure 1), being developed at the U.S. Bureau of Mines, Pittsburgh Energy Research Center, raw coal of bituminous or lower rank is reacted directly with hydrogen in a two-stage hydrogasifier to produce 95% of the product methane. The lower stage of the hydrogasifier is a fluidized bed of char in which hydrogen is the fluidizing gas. Conceptually,

the gas exiting the bed contains about 46% methane, and the char leaving the fluid bed contains about half the carbon initially fed to the hydrogasifier in the raw coal. Prevention of agglomeration is of great importance because most of the eastern and midwestern American coals soften, swell, and become sticky at temperatures above 400° C., especially in the presence of hydrogen, and are therefore impossible to process in a fluid bed without some pretreatment or dilution. Thus, the top stage of the hydrogasifier is a dilute-phase, free-fall reactor in which the raw pulverized coal is fed in a dilute cloud concurrently with the gas produced in the bottom stage, rendering the particles nonagglomerating and producing a very porous, reactive char. Approximately 20% to 30% carbon conversion occurs in this stage, and the product gas contains about 70% methane.

Experimental data have been obtained from a 12 lb./hr. process development unit in which the bottom stage of the hydrogasifier has been operated as either a fluidized bed or a moving bed reactor. In designing a scaled-up version of the fluid-bed reactor, a model describing the movement of gas and solids in the reactor and a reaction rate model is needed. The reactor model is then integrated with the reaction rate equation yielding reactor size and product gas composition. In this paper a fluid-bed reactor model has been developed using the bubble-assemblage concept originally developed by Kato and Wen (1) and is shown to describe some experimental data reasonably well. A moving-bed reactor model is also developed and used to model experimental data as well as illustrate the differences between plug-flow and well mixed solid-gas reactors.

#### Apparatus and Procedure

The two-stage laboratory hydrogasifier is shown in figure 2. It consists of a dilute-phase reactor integrated with a second stage which can be operated as either a moving-bed or fluid-bed reactor. The dilute-phase reactor is a 3-inch-diameter, schedule 10, type 304, stainless steel pipe 6-feet long. The pipe is heated in three 2-foot-long sections containing six 1,000-watt strip heaters

mounted directly on the pipe wall. The pipe is wrapped in fiberfrax insulation and is contained in a 10-inch-diameter, schedule 160, carbon steel pipe which acts as the pressure shell. Pulverized coal is fed into the reactor by gravity via a 1/4-inch nozzle which protrudes one foot into the reactor. When the second stage was operated as a fluid bed, the char leaving the dilute-phase reactor was crushed to reduce the particle size to a level acceptable for fluidization. The average diameter of char particles leaving the dilute-phase reactor can be as much as six times the average diameter of the pulverized feed coal particles owing to swelling and particle agglomeration and consequently, prevent adequate fluidization unless the particles are crushed. An example of particle swelling is shown in table 1. The second stage reactor is also a 3-inch-diameter pipe, but is 10-feet long and has five heated zones. A sleeve having a 2-inch inside diameter is inserted into the 3-inch-diameter pipe for fluidized-bed experiments. Temperatures reported for the dilute-phase and fluid-bed reactors correspond to reactor pipe wall thermocouple measurements. In the moving-bed experiments, reported temperatures correspond to thermocouples suspended directly into the char bed.

Two fluid-bed reactor schemes were used and are shown in figure 3. In scheme A, hydrogen was fed without preheating into the bottom of the bed by two gas nozzles, and residual char was removed at the bottom of the bed. A small amount of fines was carried over in the interstage gas. The bed level was measured by three pressure differential probes which were continually purged with a nitrogen flow of about 6 s.c.f.h. Some typical temperature profiles are shown in figure 4 and indicate that about 30 cm. of the fluid bed is required to heat up the hydrogen feed gas and attain a uniform bed temperature. In scheme B, the hydrogen was preheated to reactor temperature and was fed through a distributor plate at the bottom of the reactor. The preheater temperature and hence hydrogen feed temperature was controlled closely by a cooling water coil inside the preheater itself and extending the full length of the preheat zone.

TABLE 1.- Typical Particle Data for Dilute-Phase Char  
(Illinois #6 h.v.C.b.) Before Crushing\*

Run No.	162	163	164
<u>U.S. Mesh Size</u>	<u>Wt. %</u>	<u>Wt. %</u>	<u>Wt. %</u>
On 1/4"	0.05	0.03	0.05
1/4" x 4	1.16	0.57	0.49
4 x 6	8.96	4.89	5.62
6 x 8	17.35	14.77	10.27
8 x 10	12.09	12.09	10.81
10 x 12	8.47	8.91	8.51
12 x 14	8.34	8.89	9.40
14 x 20	17.35	19.34	20.00
20 x 30	13.27	13.78	17.76
30 x 50	9.52	10.52	14.31
50 x 100	3.11	5.47	2.45
100 x 200	0.18	0.47	0.18
Thru 200	0.15	0.25	0.18
$\bar{d}_p$ , mm.	1.031	0.866	0.897
$\rho_b$ , gm./cm <sup>3</sup>	0.109	0.141	0.111

\*Feed Coal 50- x 100-mesh (U.S. Sieve Size),  $\bar{d}_p$  = 0.223 mm.

The residual char was carried out of the reactor with the product gas via an overflow pipe and was separated from the gas. A baffle was inserted at the top of the reactor to prevent short-circuiting of feed char directly to the overflow pipe. Typical temperature profiles for this mode of operation are illustrated in figure 5. Again about 30 cm. of bed was needed to achieve a uniform temperature because too much cooling water was circulated through the preheater.

The reactor scheme for the moving-bed experiments is shown in figure 6. The char from the dilute-phase reactor dropped into the second-stage reactor which consisted of a free-fall zone and a moving-bed zone. Hydrogen was fed into the bottom of the moving-bed zone and flowed countercurrent to the movement of char. Char was removed from the bottom of the reactor by a starwheel crusher and the residence time was varied by changing the char bed height. Typical temperature profiles for this scheme are shown in figure 7.

In all experiments except HY-3, the carbon conversion was determined from an ultimate analysis of the char product and the composition of the initial coal assuming 100% ash recovery. In some experiments, the recovery of carbon, ash, and hydrogen were checked and were usually better than 95%. The moving-bed product gas composition was not known accurately because product gas from the dilute-phase reactor, containing about 70% methane, mixed with the moving-bed product gas near the sampling point. This yielded inflated values of methane concentration. Therefore, methane yields based on the moving-bed product gas analysis were not used. The mixing effect is shown in figure 8 where actual and calculated methane concentrations are shown. Carbon conversion for the overall two-stage unit based on the solids analysis was checked by calculating carbon conversion based on the total product gas and oil yields.

The ultimate analyses for the Illinois #6 h.v.c.b. coal and the char product for the fluid-bed tests and the char particle data are tabulated in table 2. The

TABLE 2.- Ultimate Analysis (As-received) of Illinois #6 h.v.c.b. Coal and Char,  
and Char Particle Data for Fluid-Bed Tests

Run No.	2		3		5		11		12		13		14	
	Coal	Char	Coal	Char	Coal	Char	Coal	Char	Coal	Char	Coal	Char	Coal	Char
C	70.8	75.1	71.8	67.7	70.9	66.0	63.8	53.7	62.4	54.8	64.7	61.6	63.8	59.7
H	5.1	2.0	5.1	2.1	4.8	1.6	4.3	0.7	4.3	0.9	4.4	0.8	4.3	0.9
N	1.7	0.8	1.6	1.1	1.7	0.9	1.4	0.5	1.4	0.4	1.4	0.4	1.4	0.5
S	1.4	0.4	1.2	0.7	1.3	0.7	1.4	0.6	1.3	0.6	1.3	0.6	1.4	0.5
O	12.8	2.3	11.7	9.7	10.0	7.0	8.9	1.1	9.4	1.8	12.0	1.9	10.4	0.6
Ash	8.2	19.4	8.6	18.7	11.3	23.8	20.2	43.4	21.2	41.5	16.2	34.7	18.7	37.8
VM	34.7	6.1	34.4	6.6	34.4	3.8	30.8	3.1	30.4	1.1	30.5	2.8	36.8	1.5
Moisture	3.0	6.0	2.5	5.7	1.0	5.3	1.1	0.4	0.7	0.4	1.4	2.3	1.7	0.7
U.S. Mesh Size														
6 x 12														
12 x 20	0.5		0.7		0.2		8.3		2.7		10.0		4.7	
20 x 30			3.4		2.8		26.8		20.9		31.4		22.7	
30 x 50			26.5		23.7		19.3		18.6		16.3		17.4	
50 x 80			27.4		27.1		22.6		29.8		22.7		30.8	
80 x 100			8.5		8.2		13.1		17.8		9.7		16.2	
100 x 140			4.8		5.5		4.0		4.3		2.4		3.8	
140 x 200			3.1		2.3		3.3		3.5		2.0		2.5	
-200			25.6		30.3		1.0		0.9		0.9		0.9	
d., mm.			0.135		0.124		0.406		0.356		0.442		0.401	
p <sub>s</sub> , gm./cm. <sup>3</sup>			0.171		0.160		0.131		0.112		0.123		0.188	

corresponding run conditions and conversion data are listed in table 3. The carbon conversion in the dilute-phase reactor for tests HY-2, 3, 13, and 14 was assumed to be about 28% based on previous dilute-phase data with Illinois #6 coal (2), and the remaining conversion occurred in the fluid bed. For tests HY-5, 11, and 12, essentially pure hydrogen was used as the feed gas instead of a hydrogen-methane mixture so that an additional 4.5 to 5% carbon conversion occurred bringing the dilute-phase value to 33%. The conversion of the other coal constituents in the dilute-phase reactor can be calculated using the correlations given in figures 9-12, which are based on 95 coal hydrogasification experiments in the HYDRANE PDU. The data for sulfur removal are scattered because of the error in determining changes in small amounts of sulfur in the coal and char samples. Oxygen removal, which usually exceeds 90% for carbon conversions above 20%, can be considered to be complete. The calculated constituent conversions in the dilute-phase reactor for 28% and 33% carbon conversion are shown in table 4.

The ultimate analyses for the Illinois #6 h.v.C.b. coal used in the moving-bed tests and the analyses of the char product are shown in table 5. These data are presented on a dry basis for convenience in calculating conversions.

#### Reaction Rate of Coal-Char Hydrogasification

It has been demonstrated by a number of investigators (3,4,5,6,7,8) that coal consists roughly of two portions greatly differing in reactivity: a highly reactive portion relating to the volatile hydrocarbons present in coal, and a relatively low reactivity residual carbonaceous matter, coke. In the presence of hydrogen, the initial phase of extremely rapid reaction is presumably due to pyrolysis followed by hydrogenolysis of the intermediates that are derived from essentially aliphatic hydrocarbon side chains and oxygenated functional groups. The remainder of the carbon in the char is converted to methane much more slowly, apparently at the char surface almost stoichiometrically according to the graphite-hydrogen reaction.

TABLE 3.- Solids Conversion For Fluid-Bed Tests, 50- x 100-Mesh  
Illinois #6 h.v.C.b. Coal, 1,000 p.s.i.g.

Run	2	3	5	11	12	13	14
Coal Rate, gms./hr. (Dry)	2270	2724	4631	5448	3087	2951	3042
<u>Dilute-Phase Reactor</u>							
Temp., ° C	850	850	850	850	900	900	900
Feed Gas, s.c.f.h.	234	185	260	167	108	110	110
% H <sub>2</sub>	45	56	94.5	93	92.6	53.4	47.8
CH <sub>4</sub>	48	35	0.2	0	0	38.0	39.0
Ar(He*)	6	8	4.3	7	7.4	7.3*	11.0*
N <sub>2</sub>	1	1	1.0	0	0	1.2	1.2
<u>Fluid-Bed Reactor</u>							
Feed Gas, s.c.f.h.	310	215	320	330	249	240	240
% H <sub>2</sub>	97	94	99	91	91.1	88	88
N <sub>2</sub>	3	6	1	9	8.6	12	12
<u>Total Conversion</u>							
C	55.2	53.6**	55.8	60.8	55.1	55.6	53.7
H	88.2	79.9	89.8	92.7	89.6	94.0	90.1
S	87.9	71.8	74.4	80.1	76.4	78.4	82.3
N	80.1	66.3	74.9	83.4	85.4	86.7	82.3
O	97.2	77.8	88.1	95.6	91.6	100	100
Fluid-Bed Height, cm.	143	143	143	122	122	122	122
Char Yield, gm./gm. dry coal	0.436	0.499	0.480	0.471	0.514	0.473	0.503

\*\*Calculated based on char recovered.

TABLE 4.- Calculated Constituent Conversion in  
the Dilute-Phase Reactor

<hr/>		
Conversion, %		
C	28.0	33.0
H	65.2	69.6
S	47.5	51.2
N	29.6	38.7
O	92.5*	93.0*
Char Yield, gm./gm. dry coal	0.677	0.639

\*Estimated from Figure 13.



During the initial phase of the coal-hydrogen reaction, the coal particles are quickly softened, become metaplastic giving off volatile matter, and erupt in a manner somewhat similar to popping of popcorn. Wen and Huebler (7) presented a kinetic model for this initial rapid reaction of coal hydrogasification. In the free-fall reactor of the HYDRANE process, the initial phase of hydrogasification of coal takes place leaving a small portion of volatile matter in the char. This char is then reacted with hydrogen in a fluidized-bed reactor in the HYDRANE process. The reaction rate in this second phase of hydrogasification has been described elsewhere (7,9,10).

For the second phase reaction,



where  $\lambda$  is a stoichiometric coefficient obtained by an empirical correlation (9,11)

$$\lambda = \begin{cases} 1.0 & \text{for } X < 0.45 \\ 8X - 2.6 & \text{for } 0.45 \leq X \leq 0.55 \\ 1.8 & \text{for } 0.55 < X \end{cases} \quad (2)$$

and the average value of  $\lambda$  is obtained as follows:

$$\bar{\lambda} = \int \lambda \, dX / \int dX \quad (3)$$

The rate of hydrogasification of char is given by

$$\frac{dZ}{dt} = k(1-Z)P_{\text{H}_2} \quad (4)$$

where  $Z$  is the carbon conversion in the second phase reaction and is equal to  $(X - X_0)/(1 - X_0)$ . Here  $X$  is the carbon conversion based on the raw coal,  $X_0$  is the carbon converted in the first phase reaction or in the pretreatment,  $P_{\text{H}_2}$  is the partial pressure of hydrogen and  $k$  is the reaction rate constant.

The above equation can be written in the following form as

$$\frac{dZ}{dt} = K(1-Z) Y_{\text{H}} \quad (5)$$

where  $Y_{\text{H}} = P_{\text{H}_2} / P_{\text{H}_2}^{\circ}$ ,  $K = k P_{\text{H}_2}^{\circ}$  and  $P_{\text{H}_2}^{\circ}$  is the partial pressure of hydrogen at the inlet.

Feldmann et al (12) presented the following correlation for the reaction rate constant:

$$\ln k = -10.45 \times 10^3 \left( \frac{1}{T} \right) + 7.08, \quad k: \text{atm.}^{-1} \text{hr.}^{-1}, \quad T: K$$

As will be shown later, the values of  $k$  and activation energy calculated from experimental carbon conversions using the Bubble Assemblage model or moving bed model developed are significantly smaller than those calculated from the above equation.

#### Simulation of Fluidized-Bed Hydrogasifier

##### 1. Minimum Fluidization Velocity

It has been shown by Feldmann et al (12,13) that the minimum fluidization velocity of coal chars with popcorn-like structure is greater than that calculated from the Wen-Yu correlation (14) which is applicable only to nonvesicular particles. The empirical correlation proposed by Feldmann et al (13) has the following form:

$$\frac{u_{mf} \rho_f d_p}{\mu} = 0.0135 \left[ d_p^3 \frac{\rho_f (\rho_s - \rho_f)}{\mu^2} g \right]^{0.73} \quad (6)$$

where  $d_p$  is particle diameter,

$\rho_f$  is gas density,

$\rho_s$  is particle density,

$\mu$  is gas viscosity

$g$  is gravitational acceleration, and

$u_{mf}$  is the minimum fluidization velocity.

##### 2. Fluidized-Bed Model

In the fluidized bed hydrogasifier, the second-phase reaction takes place either countercurrently, concurrently, or with overflow as schematically described in figure 13. The Bubble Assemblage model (1,15,16,17,18) is used to simulate the hydrogasification of coal char. The essential features of the Bubble Assemblage model are summarized as follows:

- The fluidized bed is divided into a number of compartments, each of which has a height that is uniquely determined by the diameter of the bubble at the corresponding height.
- Each compartment is composed of the bubble phase and the emulsion phase. The solids and gas in the emulsion phase and the bubble phase of each compartment are completely mixed with some exchange of gas between the two phases.
- The volume of the bubble phase is assumed to be equal to the volume of the bubbles in this paper. It is also assumed that no solids exist in the bubble phase.

Figure 14 depicts the Bubble Assemblage Model under various modes of flow arrangement.  $P_c$  is an index of solid flow arrangement and is equal to unity when solids flow countercurrent to the gas. Under this condition,  $q_1 = 1 + q_2$ , where  $q_1$  and  $q_2$  are the ratio of solids downflow rate and solids upflow rate to the solid feed rate, respectively.

When solids are fed from the top and withdrawn from the top of the bed (overflow type),  $P_c$  is 0 and  $q_1 = q_2$ .

From the material balance of  $H_2$  around the  $n$ -th compartment in the bed, the following equations can be written for the bubble phase and emulsion phase.

$$W_{HO} (Y_{Bn-1} - Y_{Bn}) + V_{Bn} Y_{HO} F_{On} (Y_{en} - Y_{Bn}) = 0 \quad (7)$$

$$V_{Bn} Y_{HO} F_{On} (Y_{Bn} - Y_{en}) - V_{en} k_b Y_{en} (1 - Z_n) = 0 \quad (8)$$

where  $k_b$  is an apparent reaction rate constant for  $H_2$  consumption in the emulsion phase and can be written as

$$k_b = \alpha_c (1 - \epsilon_{mf}) \rho_{CO} Y_{CO} K \quad (9)$$

$\alpha_c$  is the number of moles of  $H_2$  reacted with one gram of carbon in char and is related to  $\bar{\lambda}$  as  $\alpha_c = \bar{\lambda}/12$ .

From a material balance of carbon in the char around the  $n$ -th compartment, excluding  $n=1$  and  $N$ , the following equation can be obtained,

$$q_1 W_{SO} Y_{CO} (Z_{n+1} - Z_n) + q_2 W_{SO} Y_{CO} (Z_{n-1} - Z_n) = -v_{en} k_b Y_{en} (1-Z_n) / \alpha_c \quad (10)$$

For the top compartment of the bed ( $n=N$ ), we get  $Z_{N+1} = 0.0$  and the following equation is obtained:

$$-q_1 W_{SO} Y_{CO} Z_N + W_{SO} Y_{CO} \left[ q_2 Z_{N-1} - (1-P_c) Z_N \right] = -v_{eN} k_b Y_{eN} (1-Z_N) / \alpha_c \quad (11)$$

For the first compartment ( $n=1$ ), the following equation can be written for the overflow type and the countercurrent type:

$$W_{SO} Y_{CO} (q_1 Z_2 - P_c Z_1) - q_2 W_{SO} Y_{CO} Z_1 = -v_{e1} k_b Y_{e1} (1-Z_1) / \alpha_c \quad (12)$$

From equations (7) and (8) we obtain:

$$Y_{Bn} = Y_{Bn-1} \left[ 1 - \frac{\alpha_2 (1-Z_n)}{1 + (1+\alpha_1) \alpha_2 (1-Z_n)} \right] \quad (13)$$

$$Y_{en} = -(Y_{Bn} - Y_{Bn-1}) / \alpha_2 (1-Z_n) \quad (14)$$

where  $\alpha_1 \equiv F_t / V_{Bn} F_{on}$  and  $\alpha_2 \equiv v_{en} k_b / W_{HO}$ .

From equations (10), (11), (12), and (14) we get:

$$Z_{n+1} = \left[ (q_{11} + q_{21}) Z_n - q_{22} Z_{n-1} + \alpha_3 (Y_{Bn} - Y_{Bn-1}) / \alpha_2 \right] / q_{12} \quad (15)$$

where  $Z_0 = Z_{N+1} = 0.0$ ,  $\alpha_3 \equiv v_{en} k_b / \alpha_c W_{SO} Y_{CO}$  and the values of  $q_{ij}$  are given in table 6.

If the solid particles in the bed are assumed to be completely mixed, the basic equation can be simplified as follows:

$$Z_n = Z_{1F} = \text{constant}$$

$$Y_{BN} = \prod_{j=1}^n \left[ 1 - \frac{\alpha_2 (1-Z_{1F})}{1 + (1+\alpha_1) \alpha_2 (1-Z_{1F})} \right] \quad (16)$$

where  $Z_{1F}$  is the conversion in the bed and at the outlet.

From an overall material balance, another equation relating  $Y_{BN}$  and  $Z_{1F}$  can be obtained as follows:

TABLE 6.-  $q_{ij}$  in equation (15)

	$q_{11}$	$q_{12}$	$q_{21}$	$q_{22}$
$n \neq 1, N$	$q_1$	$q_1$	$q_2$	$q_2$
$n = 1$	$P_c$	$q_1$	$q_2$	0.0
$n = N$	$q_1$	1.0	$1 - P_c$	$q_2$

$$Z_{1F} = \alpha_3 (1 - Y_{BN}) / \alpha_2 \quad (17)$$

From Hovmand and Davidson (19), if the value of  $G_f \equiv (u_o - u_{mf}) / 0.35 \sqrt{g D_t}$  is less than 0.2, the bed can be kept in freely bubbling condition. When the value of  $G_f$  is greater than 0.5, the bed is in a slug flow condition. When  $G_f$  is between 0.2 to 0.5, the bed is in a transition condition between bubbling flow and slug flow.

Recently, Mori and Wen (17,18) presented a new correlation of bubble growth for a bubbling bed as follows:

$$D_B = D_{BM} - (D_{BM} - D_{BO}) \exp(-0.3 h / D_t) \quad (18)$$

where  $D_{BM}$  is the maximum bubble diameter,  $D_{BO}$  is the initial bubble diameter and  $h$  is the elevation above the distributor.

Since the fluidized gasification unit used has a large bed height to diameter ratio ( $L_f \gg D_t$ ), equation (18) can be simplified as follows:

$$D_B \sim D_{BM} = 0.652 \{A_t (u_o - u_{mf})\}^{0.4} \quad (19)$$

Then, the height of each compartment in the bed,  $\Delta h_n$ , also can be approximated as:

$$\Delta h_n = D_B = D_{BM} \quad (20)$$

From Kato and Wen (1), the gas interchange coefficient,  $F_{on}$ , is given by

$$F_{on} = 11 / D_B \quad (21)$$

Based on the two-phase theory, volume fractions of bubble phase and emulsion phase in each compartment are given as follows, respectively:

$$\epsilon_{Bn} = V_{Bn} / \Delta h_n A_t = (u_o - u_{mf}) / u_B \quad (22)$$

$$V_{en} = (1 - \epsilon_{Bn}) \Delta h_n A_t \quad (23)$$

Since the solid particles may be assumed to be transferred upward in the wakes behind the bubbles, the volumetric flow rate of solids upward can be written as  $f_w (u_o - u_{mf}) (1 - \epsilon_{mf}) A_t$ , where  $f_w$  is the volume ratio of the wake and the bubble.

Thus,  $q_2$  can be rewritten as,

$$q_2 = \frac{(u_o - u_{mf}) f_w (1 - \epsilon_{mf}) A_t}{W_{so}/\rho_{co}}$$

Using equations (19), (20), (21), (22), (23) and (24) the values of  $V_{Bn}$ ,  $V_{en}$ ,  $F_{on}$ ,  $q_2$  and  $\Delta h_n$  can be calculated for a set of operating conditions. Thus, numerical solutions of equations (13), (14), and (15) are obtained simultaneously by an iterative method. A computer logic diagram is shown in figure 15.

#### Results of Fluidized-Bed Performance Simulation

In table 7, the calculated reaction rate constants are shown based on the experimental carbon conversions. The values of reaction rate constants from the Bubble Assemblage Model and those from the simplified Bubble Assemblage Model with complete mixing of solids are compared. As for the axial solids mixing, the large height to diameter ratio of the experimental reactor used results in a relatively small degree of solid mixing. The following equation derived by Miyauchi (20) for a backflow mixing model is used to estimate the Peclet number for counterflow case,

$$\frac{1}{N_{Pe}} = \frac{E_{zp}}{(W_{so}/\rho_{co}) A_t} L_f = \frac{1}{2N} + \frac{q_2}{N} \quad (25)$$

where  $N$  is the total number of compartments. For the overflow case, an analogy of equation (25) is used to calculate the Peclet number:

$$\frac{1}{N_{Pe}} = \frac{q_2}{N} \quad (26)$$

In table 8, the values of  $\frac{1}{N_{Pe}}$  are tabulated and vary between 0.3 to 1.2, considerably different from the large values obtained for complete mixing. As can be seen from table 7, the  $k$  values of countercurrent operation calculated from the Bubble Assemblage model with partial mixing of solids differ very little from the Bubble Assemblage model with complete mixing of solids indicating that the solid mixing does not affect carbon conversion significantly. The reaction rate constants are plotted on an Arrhenius Plot shown in figure 16 based on

TABLE 7.- Comparison of Reaction Rate Constants Calculated  
from Bubble Assemblage Models

Run No.	Solid Flow	$X_{1F}$ observed	$Z_{1F}$ observed	Bed temp. K	$k_{cal.}, atm^{-1} hr^{-1}$	
					Solid partial mixed	Solid complete mixed
11		0.608	0.419	1073	0.0450	0.0515
12	counter current	0.551	0.335	1118	0.0202	0.0220
13		0.556	0.383	1113	0.0218	0.0248
14		0.537	0.357	1183	0.0139	0.0152
2		0.552	0.378	1158	0.0145	0.0123
3	over- flow	0.536	0.356	1158	0.0284	0.0140
5		0.558	0.345	1158	0.0316	0.0223

TABLE 8.- Estimated Solid Mixing in Fluidized-Bed Hydrogasifier in Terms of Peclet Number

Run No.	N	$q_2$	$1/N_{pe}$
11	32	19.9	0.64
12	34	25.1	0.76
13	39	20.3	0.53
14	41	25.8	0.64
2	38	46.4	1.22
3	54	16.0	0.30
5	40	20.5	0.51

N = total number of compartments.

$N_{pe}$  = Peclet number of axial solid mixing in the fluidized bed.

the average temperatures of the bed. The data include the results of I.G.T. experiments (7) shown in table 9 for countercurrent and concurrent fluidized-bed hydrogasification experiments. The complete mixing model is used for calculation of the reaction rate constants for the I.G.T. experiments. The reaction rate constants calculated from moving-bed data are also plotted in figure 16.

An empirical relation for the temperature effect on the rate constant can be expressed as,

$$\ln k = -4.36 \left( \frac{1}{T} \right) \times 10^3 + 0.28 \quad (27)$$

where  $k$ :  $\text{atm.}^{-1} \text{ hr.}^{-1}$ , and  $T$ : K .

An activation energy of 8.63 Kcal/mole is estimated which is very much smaller than 15-16 and 21 Kcal/mole reported by Feldmann et al (12).

The rate constants calculated from the moving-bed data are considerably larger than those from the fluidized bed, particularly in the low temperature region. An explanation of the deviation is presented in the moving-bed section. In figure 17, the carbon conversions calculated using equation (27) are compared with experimental conversions. The scatters of the points shown in figures 16 and 17 are partly due to the nonuniformity and time dependency of temperature along the bed axis.

#### Moving-Bed-Reactor Model

In this model the gas and solid are assumed to move in a plug flow manner and the temperature profile of the bed is averaged to approximate an isothermal reactor. The movement of char through the moving bed,  $V_s = \frac{dh}{dt}$ , is assumed to be constant and can be combined with equation (3) to yield an equation describing the carbon conversion in terms of position in the moving bed ( $h = 0$  at top of bed),

$$V_s \frac{dZ}{dh} = k P_{H_2} (1-Z) \quad (28)$$

The carbon conversion in the countercurrent moving bed can be related to the change in methane content of the gas by the carbon balance equation,

TABLE 9.- Operating Condition of I.G.T. Experiments  
[Wen and Huebler (1965)]

Operation . . . . .	Countercurrent	Concurrent
Char. . . . .	Consolidation Coal Co. Bituminous coal char	
$d_p$ . . . . .	60/325 mesh	
$D_t$ , cm. . . . .	4.88	4.3(equivalent)
T, K . . . . .	905 - 958	992 - 1189
$U_{mf}$ , cm./sec. . . . .	1.83	
$W_{CO}$ , g./sec. . . . .	0.61 - 1.07	0.28 - 1.05
$F_t$ , cm <sup>3</sup> /sec. . . . .	57 - 111	29 - 54
$P_T$ , atm. . . . .	137 - 141	
$L_f$ , cm. . . . .	214	143, 225

$$Y_{co} W_{so} \frac{dZ}{dh} = - \frac{d}{dh} (W_g Y_M) \quad (29)$$

where  $W_{so}$  is the dry coal feed rate to the dilute-phase reactor (gm./hr.),  $X_o$  fractional carbon conversion in the dilute-phase reactor,  $Y_{co}$  the gm. moles of carbon per gram of dry coal,  $W_g$  the molar gas rate (gm.-moles/hr.), and  $Y_M$  the mole fraction of methane in the gas. We have made the assumption that the conversion of carbon to CO or CO<sub>2</sub> in the moving bed will be negligible. Previous work with char appears to support this assumption (6,21). The partial pressure of hydrogen is given by

$$P_{H_2} = (n - Y_M) P_T \quad (30)$$

where  $P_T$  is the total pressure and  $n$  is the combined mole fraction of hydrogen and methane in the gas. The difference of  $n$  from unity represents the mole fraction of inerts in the gas. The net change in the molar gas rate is

$$\frac{dW_g}{dh} = (\lambda - 1) Y_{co} W_{so} \frac{dZ}{dh} \quad (31)$$

Equations (29) and (31) may be integrated over an arbitrary distance  $h$  starting at the top of the moving bed resulting in the equations

$$W_{go} Y_{Mo} - W_g Y_M = Y_{co} W_{so} Z \quad (32)$$

$$W_g - W_{go} = Y_{co} W_{so} \int_0^Z (\lambda - 1) dZ \quad (33)$$

Evaluation of equations (32) and (33) using the boundary conditions  $Z = Z_H$ ,  $Y_M = 0$  and  $W_g = W_{gH}$  at  $h = H$  yields values for  $W_{go}$  and  $Y_{Mo}$ . Once  $W_{go}$  and  $Y_{Mo}$  are known,  $Y_M$  and  $W_g$  can be evaluated at any point in the moving bed. Thus, the mole fraction of methane at any position  $h$  is given in terms of the carbon conversion as

$$Y_M = \frac{W_{go} Y_{Mo} - Y_{co} W_{so} Z}{W_{go} + Y_{co} W_{so} \int_0^Z (\lambda - 1) dZ} \quad (34)$$

Henceforth the integral in the denominator will be written as  $F(Z)$ . Substitution of equations (30) and (34) into equation (28) and integrating over the length of the bed,  $H$ , yields the following relationship for the reaction rate constant  $k$ :

$$k = \frac{1}{P_T \theta} \int_0^{Z_H} \frac{[1 - BF(Z)] dZ}{[A + B(1-Z) - nBF(Z)][1-Z]} \quad (35)$$

where  $\theta = v_s/H$

$$A = n - Y_{Mo} - B$$

$$B = - \frac{Y_{co} W_{so}}{W_{go}}$$

Equation (35) can be solved analytically in one, two, or three parts, depending on the evaluation of  $\lambda$  in equation (1). The solution of equation (35) is shown in Appendix A.

#### Moving-Bed Results

The conversion of the coal constituents are plotted in figure 18 versus residence time in the moving bed. Zero residence time corresponds to solid material free-falling through the dilute-phase reactor followed by free-fall through the empty moving-bed reactor. Such a condition should approximate the conversion in the dilute-phase reactor plus that in the free-fall portion of the moving-bed reactor when a char bed level is maintained. Char conversion in the free-fall section of the moving-bed reactor is probably low because the reactivity is much lower compared to the starting coal and the residence time is less than a second. Zero residence time tests yielded a carbon conversion of 30%, and this value is used as  $X_o$  in the moving-bed model calculations. These results are summarized in table 10 and the rate constants are shown on figure 16 as an Arrhenius plot. The effect of temperature on the moving-bed rate constant values can be described by the

TABLE 10.- Countercurrent Moving-Bed Kinetic Data, Illinois #6

Run	Total C** Conv.	Moving Bed C Conv.	Dry Coal Rate, gm./hr.	Feed Gas Rate, mole/hr.	Product Gas Rate, mole/hr.	Total Pressure, atm.	Residence Time, min.	Rate Const. atm. <sup>-1</sup> hr. <sup>-1</sup>	Temp. °C
	X <sub>H</sub>	Z <sub>H</sub>	W <sub>SO</sub>	W <sub>GH</sub>	W <sub>GO</sub>	P <sub>T</sub>	θ	k	T
33*	.620	.457	3178	133.9	116.0	69.0	20	.0573	905
37	.392	.131	6497	173.5	173.5	68.6	3.8	.0360	900
38	.485	.264	5262	163.2	161.8	68.7	7.3	.0396	875
39	.417	.167	6170	191.9	191.9	68.4	4.0	.0449	645
43b	.430	.186	4654	177.9	177.9	68.4	5.1	.0395	765
44b	.391	.130	4985	178.5	178.5	68.7	5.1	.0260	650
45b	.406	.151	4998	176.9	174.9	68.7	5.1	.0307	660
46a	.399	.151	4772	173.6	173.6	68.7	5.1	.0305	684
48	.511	.301	4540	177.0	173.3	68.7	10.5	.0299	800
49	.536	.337	4685	176.6	168.8	68.1	10.0	.0358	715

\*n = 0.67; other tests, n = 1

\*\*X<sub>O</sub> = 0.300, Z = (X - X<sub>O</sub>)/(1 - X<sub>O</sub>)

equation

$$\ln k = -2.21 \left(\frac{1}{T}\right) \times 10^3 - 1.19 \quad (36)$$

The discrepancy between the moving-bed and fluid-bed data in figure 16 was first believed to be a result of hydrogen mass transfer resistance between the bulk gas and the char particle surface. The Reynolds number for the moving-bed tests ranged from 0.882 to 1.146 while the Schmidt number varied from 0.569 to 0.933. Using these values and available mass transfer correlations, the mass transfer coefficient,  $k_g$ , was estimated to be 0.119 to 0.132 moles  $H_2$ /hr.cm.<sup>2</sup>atm. Correction of these values to the same form as  $k$  yielded mass transfer coefficients in excess of 1,400 atm.<sup>-1</sup>hr.<sup>-1</sup> confirming that particle film resistance was not a significant factor. The discrepancy is believed to be a result of heat transfer resistance from the char particles to the bulk gas phase resulting in the particle temperature being higher than the temperature of the gas and the measured bed temperature. This can be verified by a simple heat transfer model if we assume the reaction rate, the average particle temperature, and the average gas temperature in the bed are constant, and the heat generated by reaction is distributed uniformly within the particles. A heat balance around a particle gives the equation

$$\frac{dT_p}{d\eta} = \frac{h A \theta}{\rho_p \bar{C}_{ps}} (T_g - T_p) + \frac{A_T H}{\bar{C}_{ps} \bar{W}_s} Q_T \quad (37)$$

where the equation for the heat generation rate per unit volume of bed,  $Q_T$  is

$$Q_T = \frac{(-\Delta H) Z_1 Y_{CO} W_{SO}}{A_T H} \quad (38)$$

Using the boundary conditions  $T_p = T_g$  when  $\eta = 0$  ( $t = 0$ ) and  $T_p = T_{p1}$  when  $\eta = 1$  ( $t = \theta$ ) the solution of equation (37) is,

$$\frac{T_{p1}}{T_g} = \left(1 + \frac{\beta}{\delta}\right) - \left(\frac{\beta}{\delta}\right)e^{-\delta} \quad (39)$$

$$\text{where } \delta = \frac{6h_f(1-\epsilon)\theta}{\rho_b T_{ps}^2}$$

$$\beta = \left[ \frac{Z_1 Y_{CO} (-\Delta H)}{T_g T_{ps}} \right] \frac{W_{so}}{W_s}$$

Evaluation of equation (39) using the parameter values listed in table 11 yields

$T_{p1}/T_g = 1.2$  and  $T_{p1} = 1120$  K. This means the temperature of the particles at  $t = \theta = 30.6$  sec. is 187 K above the temperature of the gas, which is 933 K.

The log-mean average temperature of the particles is  $990^\circ$  K, so that on the average the difference in temperature between the gas and particles is 57 K for this case. Thus, the moving-bed  $k$  values at the lower temperatures in figure 16 should be more toward the left since the particle temperature was probably higher than the gas temperature. The measured temperature approximates the gas temperature since the gas channels along the thermocouple sheath sweeping its surface to a large extent. The contact area between the char particles and the thermocouple sheath is small compared to the area swept by the gas.

#### CONCLUSIONS

Hydrogasification reaction rate constant values were calculated using partial mixing and complete mixing versions of the Bubble Assemblage model of the fluidized bed. These results indicated that solid mixing did not have a significant effect on the carbon conversion. This was not unexpected because the carbon conversions in the bed were under 40%. Thus, the reactor was operating in a regime where changes in axial mixing exhibit only a minor influence on conversion. The  $k$  values for the complete mixing model with countercurrent operation are slightly higher than the values for the partial mixing model because the carbon content in the

TABLE 11.- Parameter Values Used in Equation 39

$u_o$	2.5 cm./sec.	$C_{pf}$	3.5 cal./gm. K
$T_g$	933 K	$Z_1$	0.10
$\theta$	30.6 sec.	$Y_{co}$	0.68
$d_p$	0.04 cm.	Pr	12.6
$\rho_b$	0.15 gm./cm. <sup>3</sup>	Re	1.11
$\bar{C}_{ps}$	0.4 cal./gm. K	Nu	0.01
$\rho_f$	$4 \times 10^{-3}$ gm./cm. <sup>3</sup>	$h_f$	$2.5 \times 10^{-5}$ cal./cm <sup>2</sup> sec. K
$\mu_f$	$3.6 \times 10^{-4}$ poise	$\delta$	1.0
$k_f$	$1.0 \times 10^{-4}$ cal./cm.sec. K	$\beta$	$0.3 \frac{w_{so}}{w_s} \sim 0.3$
$-\Delta H$	$1.5 \times 10^3$ cal./gm. carbon reacted		

completely mixed bed is lower than in most locations in the partial mixed bed, thus, requiring a larger rate constant in order to obtain the same amount of conversion. In the case of overflow operation of the fluid bed, larger  $k$  values are obtained for the partial mixing case than for complete mixing because some of the char particles have a very short retention time in the bed before overflowing out. The  $k$  values must then be larger in order to obtain the same conversion as the complete mixing case.

Mixing was important, however, from the standpoint of heat removal from the char particles and maintaining an approximately isothermal bed. The importance of heat removal was very evident in the moving-bed results where heat transfer from the char particles was apparently poor, causing the particle temperature to be higher than the measured temperature. This effect was dominant in the low-temperature region where moving-bed  $k$  values were significantly larger than fluid-bed  $k$  values. This heat transfer problem may be the reason why Feldmann, et al (12) obtained large values of  $k$  and a large activation energy when they fit the kinetic model given by equation (3) to the moving-bed data of Lewis, et al (21). Obviously, hydrogasification data is best obtained in a fluidized bed or in a thermobalance such as that used by Johnson (22) where the reaction heat can be removed so the char temperature is equivalent to the gas temperature and is isothermal.

#### NOMENCLATURE

$A_p$	specific surface area, $A_p \approx (1-\epsilon) \frac{6}{d_p}$ , $\text{cm}^2/\text{cm}^3$
$A_t$	cross sectional area of the bed, $\text{cm}^2$
$\bar{C}_{pf}$	average heat capacity of gas, $\text{cal}/\text{gm} \cdot \text{K}$
$\bar{C}_{ps}$	average char heat capacity, $\text{cal}/\text{gm} \cdot \text{K}$
$d_p$	particle diameter, $\text{cm}$ .
$E_{zp}$	axial solid dispersion coefficient, $\text{cm}^2/\text{sec}$ .

$F_{on}$	gas interchange coefficient per unit volume of bubble phase in $n$ -th compartment, $\text{sec.}^{-1}$
$F_t$	volumetric gas flow rate in the bed, $\text{cm.}^3/\text{sec.}$
$h$	axial distance along bed, cm.
$H$	moving-bed height, cm.
$h_f$	heat transfer coefficient, $\text{cal./cm.}^2 \text{ K. sec.}$
$\Delta h_n$	length of the $n$ -th compartment, cm.
$-\Delta H$	heat of reaction, $\text{cal./gm. carbon}$
$k$	reaction rate constant of carbon, $\text{atm.}^{-1} \text{ hr.}^{-1}$
$L_f$	fluid-bed height, cm.
$N$	total number of compartments
$n$	$n$ -th compartment or one minus inerts mole fraction
$P_{H_2}$	hydrogen partial pressure, atm.
$q_1, q_2$	ratio of solid downflow rate and solid upflow rate to the solid feed rate, respectively
$Q_T$	heat generated in the moving bed, $\text{cal./sec. cm.}^3$
$t$	time, sec.
$T$	average bed temperature, K.
$T_g$	average gas temperature, K.
$T_p$	average particle temperature, K.
$u_o$	superficial gas velocity, $\text{cm./sec.}$
$u_B$	bubble rising velocity, $\text{cm./sec.}$
$u_{mf}$	superficial gas velocity at minimum fluidization, $\text{cm./sec.}$
$V_{Bn}, V_{en}$	volume of the bubble and emulsion phase at the $n$ -th compartment, $\text{cm.}^3$
$V_s$	downward char rate in moving bed, $\text{cm./sec.}$
$W_g, W_{gO}, W_{gH}$	total gas rate through the bed, moles/sec.
$W_{Ho}$	feed rate of hydrogen gas, moles/sec.

$W_{so}$	coal feed rate, gm./sec.
$\bar{W}_s$	average char rate in moving bed, gm./sec.
$X$	total fractional carbon conversion
$Y_{Bn}, Y_{en}$	nondimensional partial pressure of hydrogen in bubble and emulsion phase at $n$ -th compartment, respectively
$Y_{Ho}$	hydrogen concentration in feed gas, mole/cm. <sup>3</sup>
$Y'_{co}$	initial carbon content in feed coal, $Y'_{co} = Y'_{co}(1-X_o)$
$Y_M$	methane concentration, mole/cm. <sup>3</sup>
$Z$	carbon conversion based on the feed char, $Z \equiv (X-X_o)/(1-X_o)$
$Z_1, Z_{1F}$	outlet carbon conversion from moving bed and fluidized bed, respectively
$\alpha_c$	number of moles of hydrogen reacted with one gram of carbon, mole/gm.
$\epsilon_{mf}$	void fraction in emulsion phase
$n$	nondimensional time
$\theta$	residence time in moving bed, sec.
$\lambda$	number of moles of hydrogen reacted with one mole of carbon, mole/mole
$\rho_b$	char bulk density, gm./cm. <sup>3</sup>
$\rho_p$	char particle density, gm./cm. <sup>3</sup>
$\rho_{co}$	density of feed coal, gm./cm. <sup>3</sup>

Subscript

$O$	inlet
$1$	outlet
$B$	bubble phase
$e$	emulsion phase
$n$	$n$ -th compartment

BIBLIOGRAPHY

1. Kato, K. and C. Y. Wen. Chem. Engrg. Sci. 24, 1351 (1969).
2. Feldmann, H. F., J. A. Mima and P. M. Yavorsky. Coal Gasification. Advances in Chemistry Series, 131, A.C.S., Wash., D.C., p. 108 (1974).
3. Chermin, H. A. G. and D. W. VanKrevelen. Fuel, 36, 85 (1957).
4. Van Krevelen, D.W., C. Van Heerden and F. J. Huntjens. Fuel, 30, 253 (1951).
5. Pitt, G. J. Fuel, 41, 267 (1962).
6. Feldkirchner, H. L. and H. R. Linden. I. & E.C. Process Design and Development, 21, 153 (1963).
7. Wen, C. Y. and J. Huebler. I. & E.C. Process Design and Development, 4, 142 and 149 (1965).
8. Wen, C. Y., R. C. Bailie, C. Y. Lin, and W. S. O'Brien. Coal Gasification, Advances in Chemistry Series, 131, A.C.S., Wash., D.C., p. 9 (1974).
9. Feldmann, H. F., W. H. Simons, J. A. Mima and R. W. Hiteshue. A.C.S. Div. of Fuel Chem. Preprints, v. 14, No. 4, Part II, p. 1, Sept. 1970.
10. Feldmann, H. F. and P. M. Yavorsky. Paper presented at the 5th A.G.A./O.C.R. Synthetic Pipeline Gas Symposium, Chicago, Ill., Oct. 1973.
11. Feldmann, H. F., W. H. Simons, C. Y. Wen and P. M. Yavorsky. Paper presented at the 4th International Congress of Chem. Engrg., Chemical Equipment, Design and Automation, Marianske Laxne, Czechoslovakia, Sept. 1972.
12. Feldmann, H. F., C. Y. Wen, W. H. Simons and P. M. Yavorsky. Paper presented at the 71st National Meeting, A.I.Ch.E., Dallas, Tex., 1972.
13. Feldmann, H. F., K. D. Kiang and P. M. Yavorsky. A.C.S. Div. of Fuel Chem. Preprints, v. 15, No. 3, p. 62, Sept. 1971.
14. Wen, C. Y. and Y. H. Yu. A.I.Ch.E. J., 6, 220 (1960).
15. Yoshida, K. and C. Y. Wen. Chem. Engrg. Sci., 25, 1395 (1970).
16. Ishida, M. and C. Y. Wen. Chem. Engrg. Sci., 23, 125 (1968).
17. Mori, S. and C. Y. Wen. Paper presented at the 67th A.I.Ch.E. Annual Meeting,

- Wash., D.C., Dec. (1974).
18. Mori, S. and C. Y. Wen. Paper submitted in I. & E.C. Process Design and Development (1974).
  19. Hovmand, S. and J. F. Davidson. Fluidization, Chapt. 5, Academic Press (1971).
  20. Miyauchi, T. Chem. Engrg., Tokyo, 26, 999 (1962).
  21. Lewis, P. S., S. Friedman and R. W. Hiteshue. Fuel Gasification, Advances in Chemistry Series, 69, A.C.S., Wash., D.C., p. 50, (1967).
  22. Johnson, J. L. Coal Gasification, Advances in Chemistry Series, 131, A.C.S., Wash., D.C., p. 145 (1974).

#### APPENDIX A

##### Solution of Equation (35)

The function  $F(Z)$  in equation (35) has three different forms as defined by equations (2) and (34) depending upon the total fractional carbon conversion. When the total fractional carbon conversion,  $X$ , is less than 0.45,  $\lambda$  has the constant value 1.0 and  $F(Z) = 0$ . The integral for this case is then very simple. When  $X$  is between 0.45 and 0.55,  $\lambda$  has a value that varies linearly with  $X$  and  $F(Z)$  turns out to be a parabolic function. For this case the integral of equation (35) is evaluated in two steps: first, for  $X$  up to 0.45 and  $F(Z) = 0$ ; and second, for 0.45 up to the measured value of  $X$  and  $F(Z)$  as a parabolic function. Thus  $k_1$  and  $k_2$  correspond to the values of the first and second parts of the integral. When  $X$  is larger than 0.55,  $\lambda$  has the constant value 1.8 and  $F(Z)$  is a linear function of  $Z$ . For this case the same procedure as used previously results in three parts for the integral corresponding to  $k_1$ ,  $k_2$ , and  $k_3$ . These results are summarized by the following equations.

Case 1:  $X < 0.45$   
 $F(Z) = 0$

$$k = \frac{1}{P_T \theta A} \ln \left[ \frac{1 - \frac{BZ_H}{A+B}}{1 - Z_H} \right] \quad (A1)$$

Case 2:  $0.45 \leq X \leq 0.55$   
 $F(Z) = aZ^2 + bZ + C$

where  $a = 4(1 - X_0)$   
 $b = 8X_0 - 3.6$   
 $c = 4(0.45 - X_0)^2 / (1 - X_0)$   
 $k = k_1 + k_2$

$$k_2 = \frac{1}{P_T \theta} \left\{ -\frac{1}{2n} \ln \left[ \frac{\bar{Z}}{Z_1} \right] - \left( \frac{1 - BC'}{2\bar{C}} \right) \ln \left[ \frac{(1 - Z_H)^2}{(1 - Z_1)^2} \left( \frac{\bar{Z}_1}{\bar{Z}} \right) \right] + \left[ \frac{\bar{b}}{2n} + Bb' + \frac{B(1 - BC')}{2\bar{C}} \right] \frac{2}{\sqrt{q}} \left[ \tan^{-1} \left( \frac{2\bar{a}(1 - Z_H) + \bar{b}}{\sqrt{q}} \right) - \tan^{-1} \left( \frac{2\bar{a}(1 - Z_1) + \bar{b}}{\sqrt{q}} \right) \right] \right\} \quad (A2)$$

where  $\bar{a} = -4nB(1 - X_0)$   
 $\bar{b} = B(1 - nb')$   
 $\bar{C} = A - nBC'$   
 $q = 4\bar{a}\bar{C} - \bar{b}^2, q > 0$   
 $b' = -(2a + b)$   
 $C' = (a + b + C)$   
 $Z = \bar{a}(1 - Z_H)^2 + \bar{b}(1 - Z_H) + \bar{C}$

$$\bar{z}_1 = \bar{a}(1 - z_1)^2 + \bar{b}(1 - z_1) + \bar{c}$$

$$z_1 = 1 - (0.45 - X_0)/(1 - X_0)$$

Case 3:

$$X > 0.45$$

$$F(Z) = 0.8Z + (0.8X_0 - 0.40)/(1 - X_0)$$

$$k = k_1 + k_2 + k_3$$

$$k_3 = \frac{1}{P_{T\theta}} \left\{ \frac{D}{G} \ln \left[ \frac{J + G(1 - Z_H)}{J + G(1 - Z_2)} \right] + \frac{E}{J} \ln \left[ \frac{J + G(1 - Z_H)}{J + G(1 - Z_2)} \cdot \frac{1 - Z_2}{1 - Z_H} \right] \right\} \quad (A3)$$

where  $D = 0.80B$ 

$$E = 0.8B - B(0.8X_0 - 0.40)/(1 - X_0)$$

$$G = (1 + 0.8n)B$$

$$J = A + n(E - 1)$$

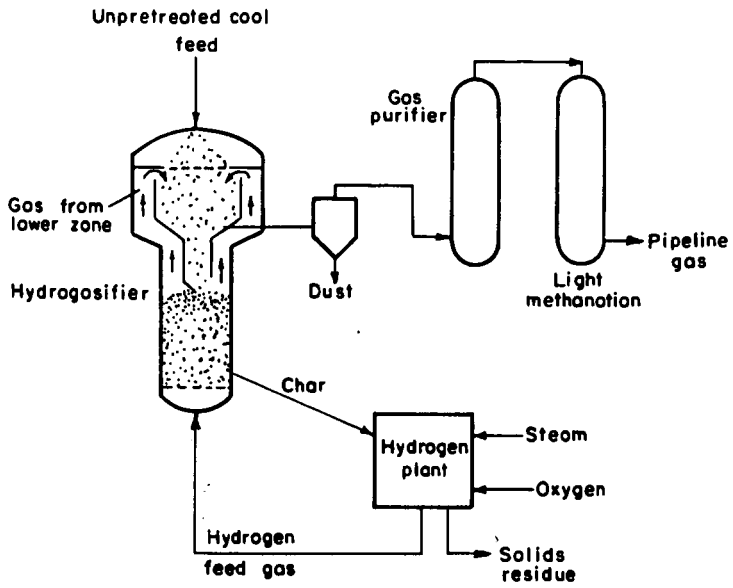


FIGURE 1 - The hydrane process for producing high BTU gas by the direct reaction of coal with hydrogen .

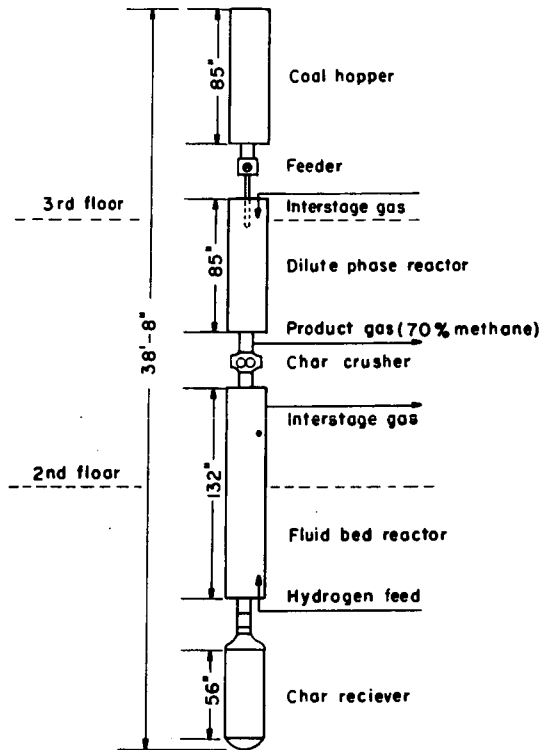


Figure 2 - Integrated hydrogasification unit.

L-12914

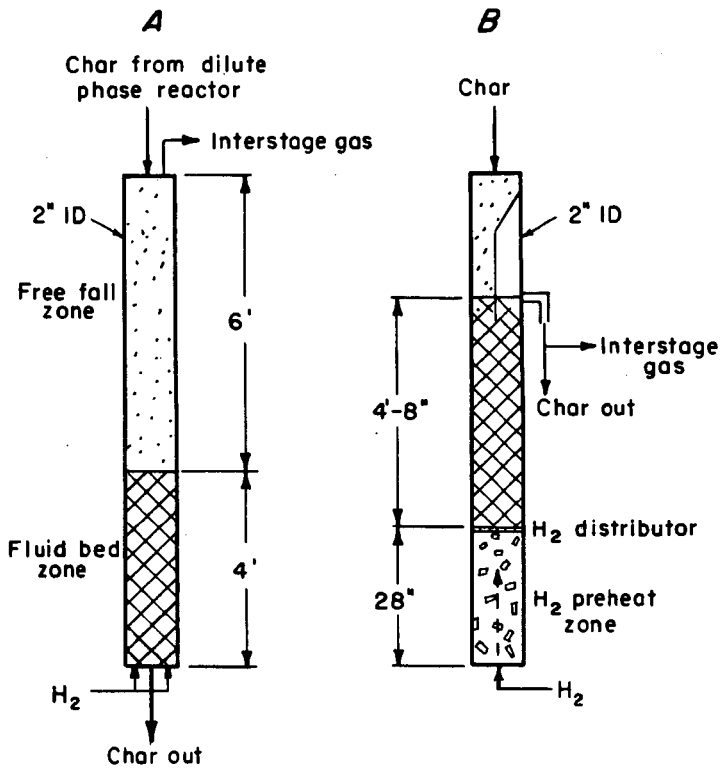


Figure 3—Schematics of fluid bed reactors

L-14051

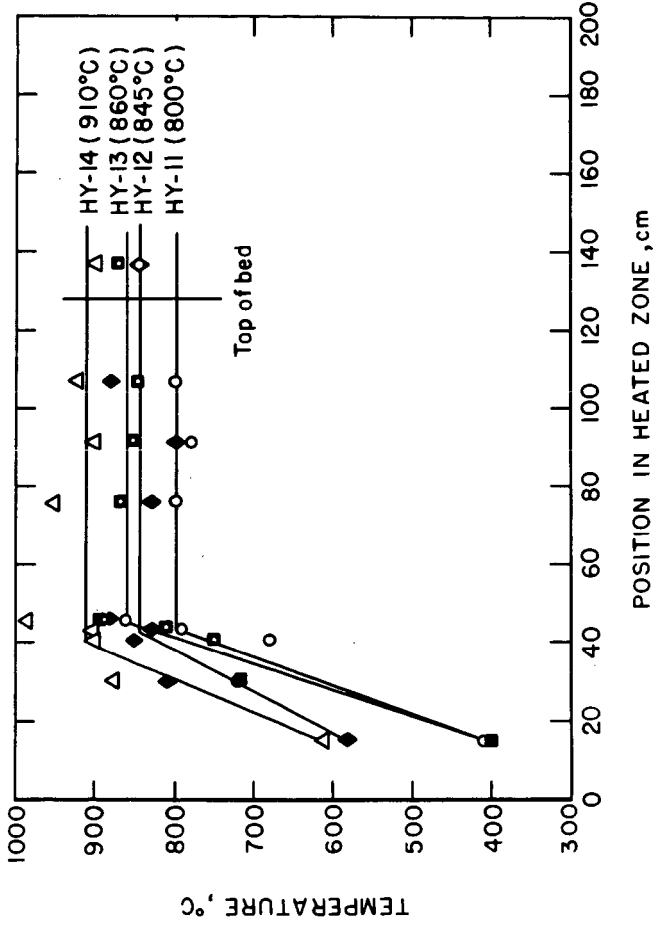


FIGURE 4 - Temperature profiles for scheme A fluid bed reactor.

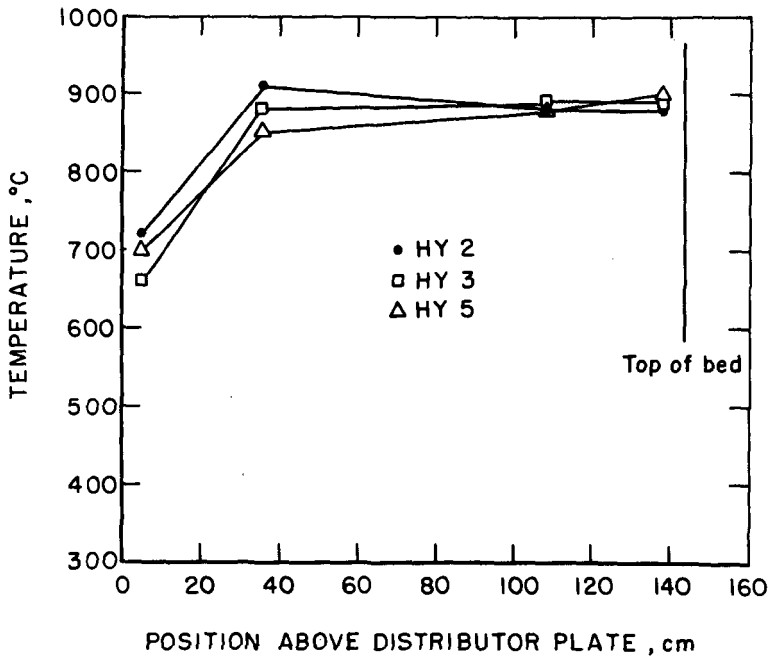


FIGURE 5 - Temperature profiles for scheme B fluid bed reactor.

L-14043

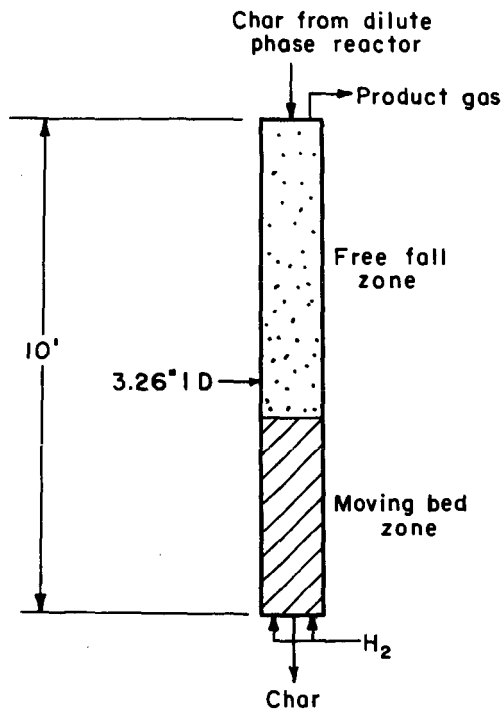


Figure 6—Schematic of moving bed reactor

L-14056

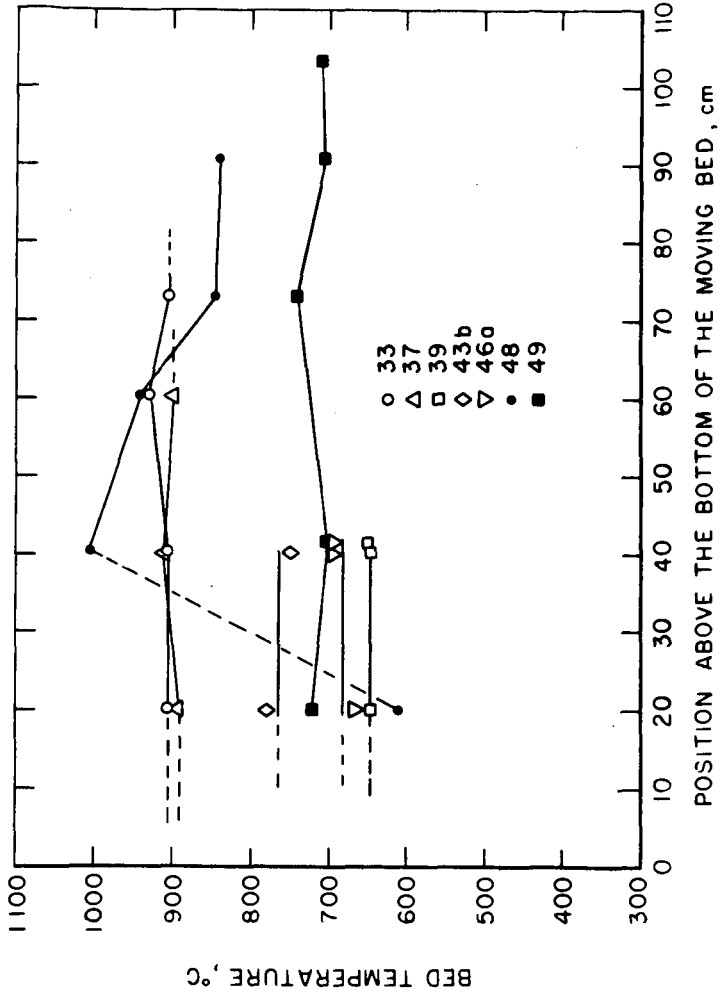


FIGURE 7 - Temperature profiles for the moving bed reactor

L-14044

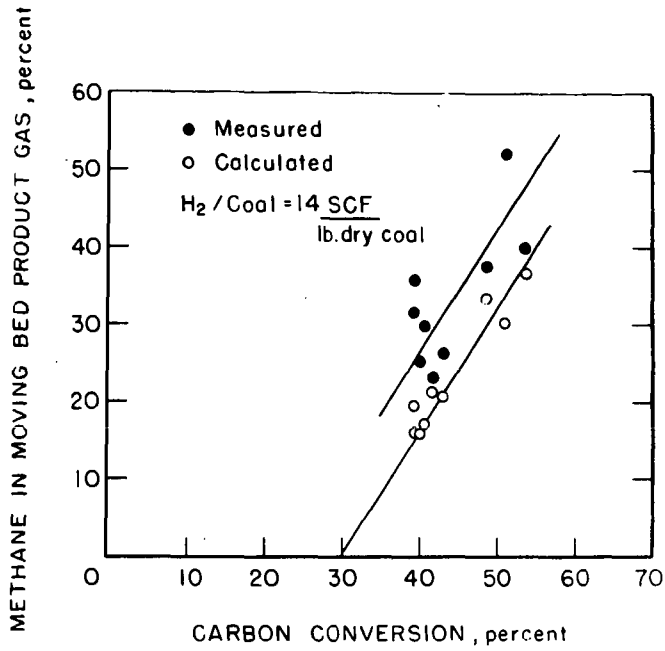


FIGURE 8 - Mixing effect on the moving bed product gas near the sampling point.

L-14042

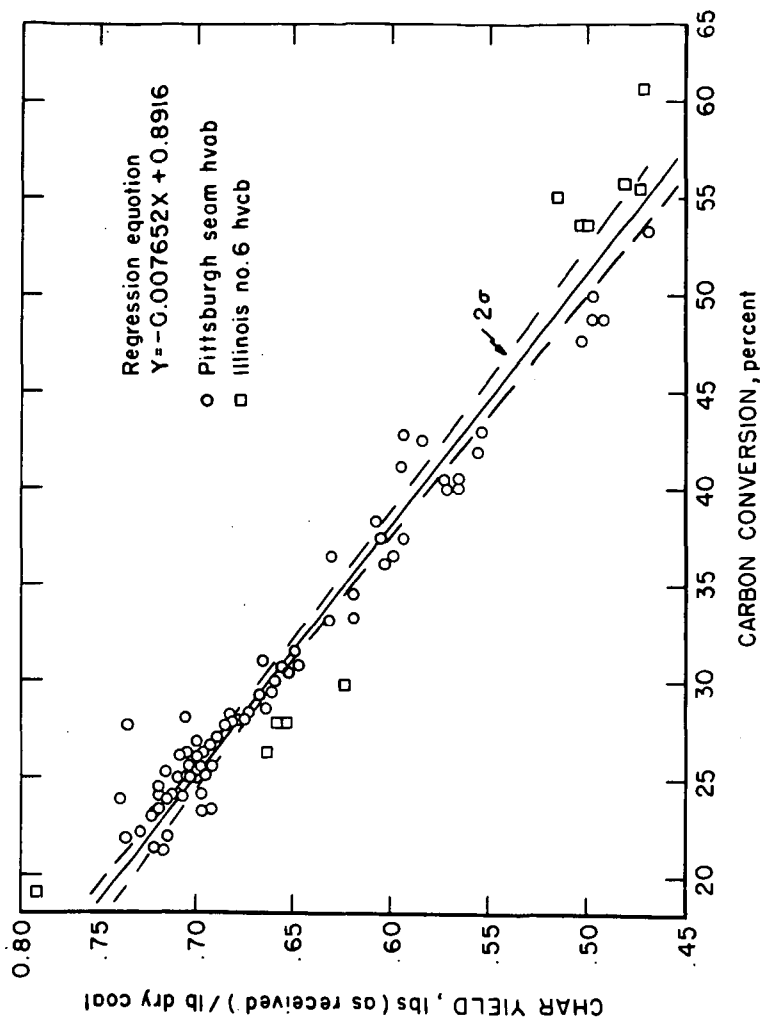


FIGURE 9 - Char yield as a function of carbon conversion during hydrogasification.

L-13708

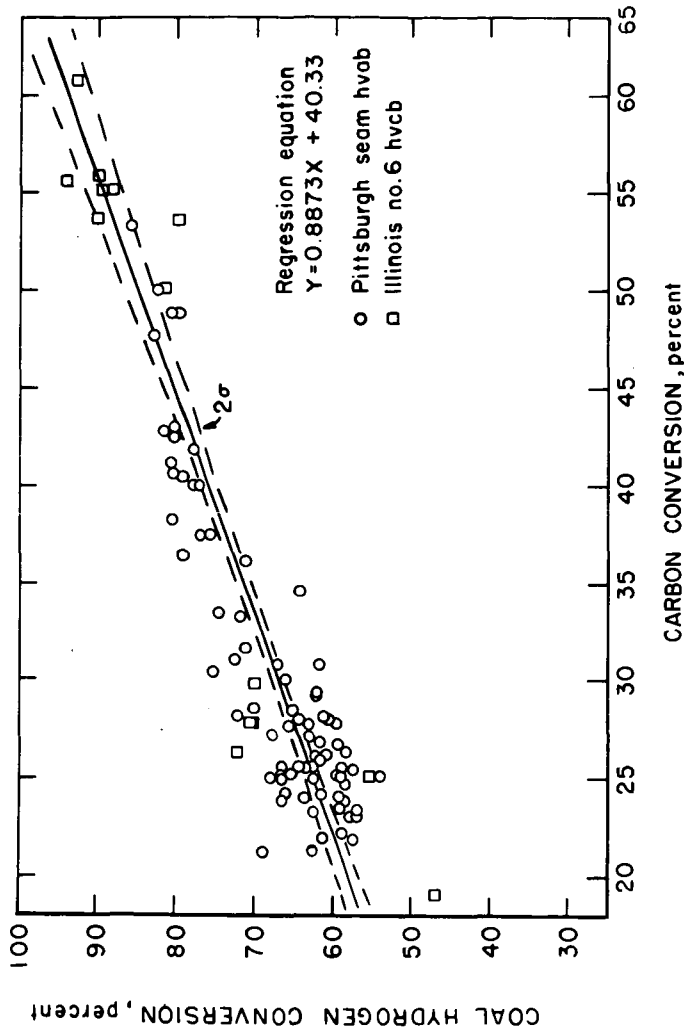


FIGURE 10 - Coal hydrogen conversion as a function of carbon conversion during hydrogasification.

L-13709

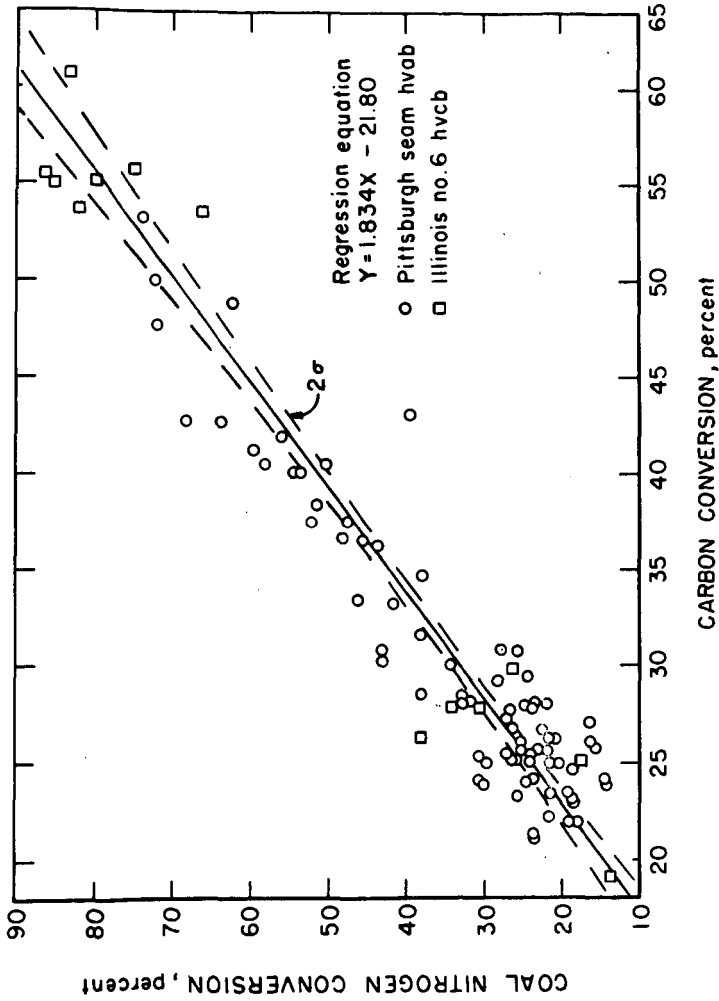


FIGURE II - Coal nitrogen conversion as a function of carbon conversion during hydrogasification.

L-13712

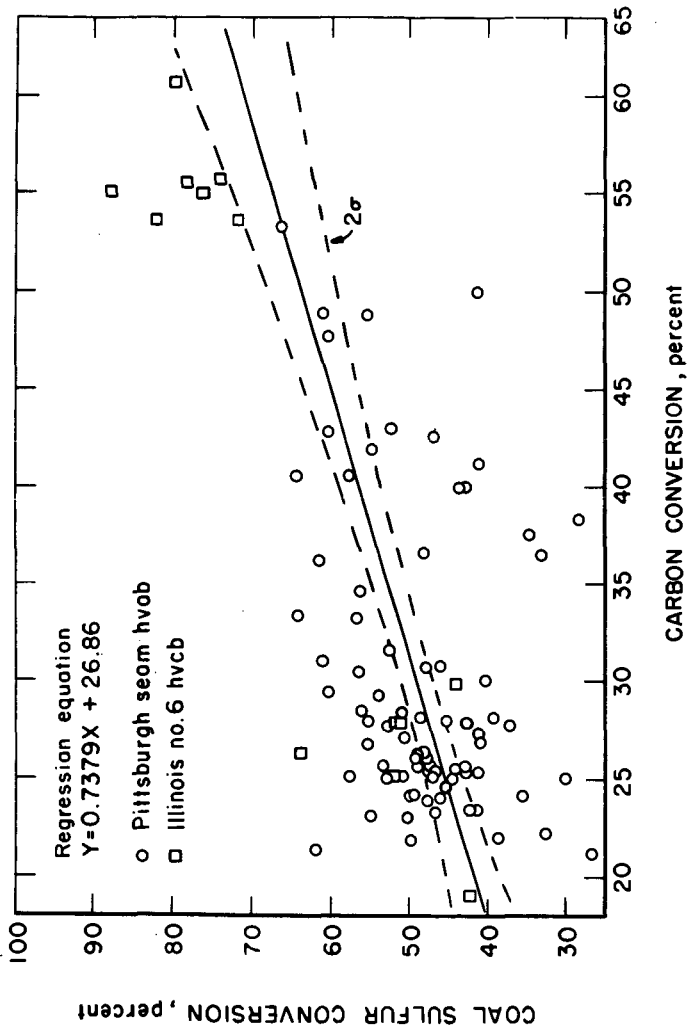


FIGURE 12 - Sulfur conversion as a function of carbon conversion during hydrogossification.

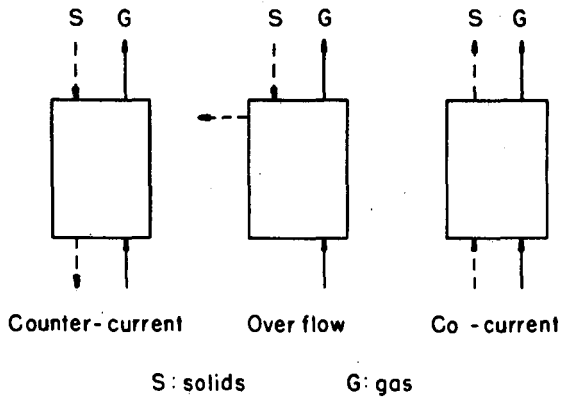


FIGURE 13- Modes of the fluidized bed operations.

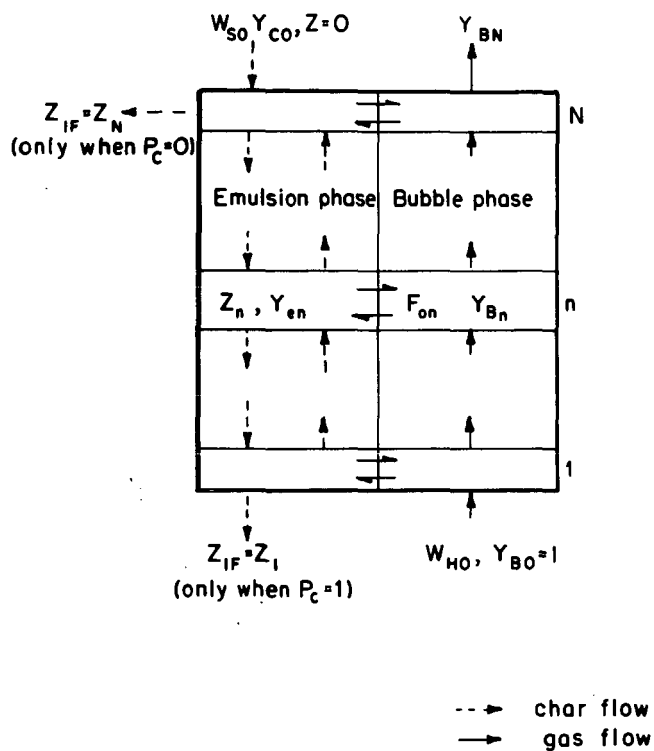


Figure 14 —Bubble assemblage model for fluidized char gasification

L-14046

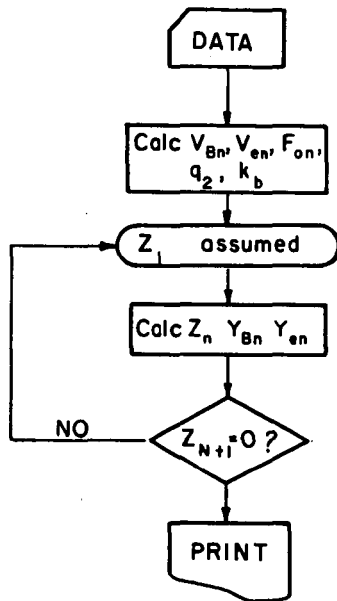


Figure 15 - Computer logic diagram

L-14049

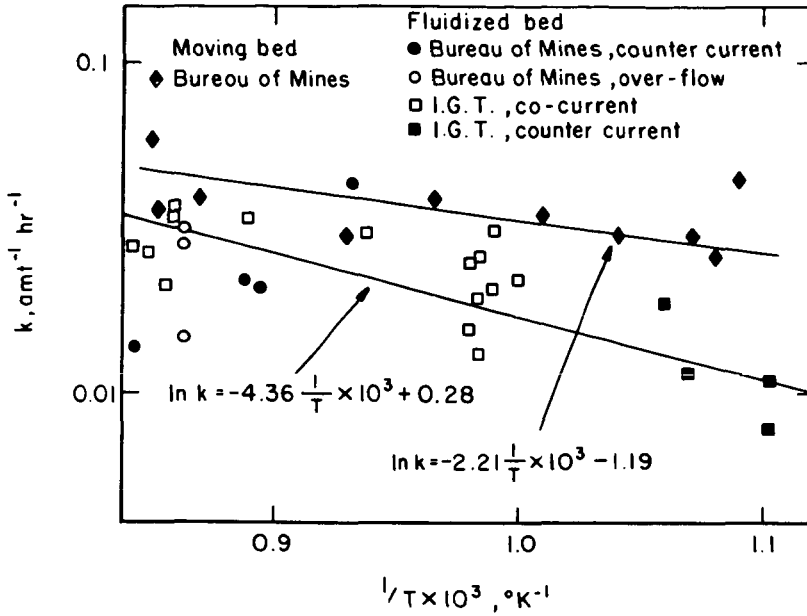


FIGURE 16 - Effect of average bed temperatures on rate constants for char hydrogasification

L-14047

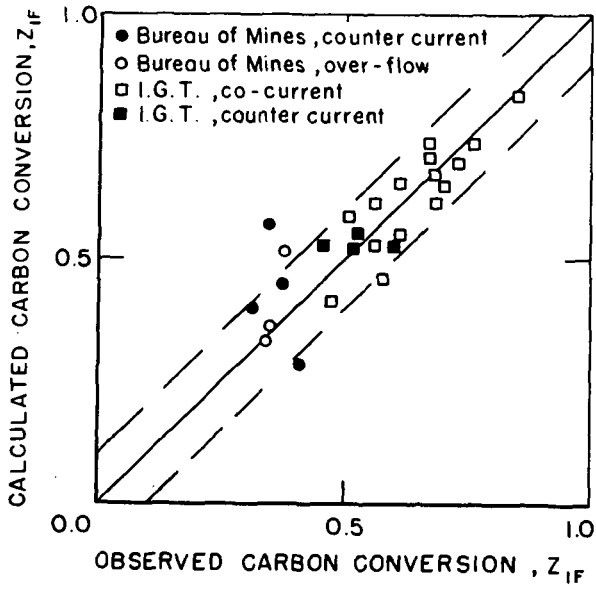


FIGURE 17- Comparison of calculated and observed carbon conversions in fluidized char hydrogasification experiments .

L-14048

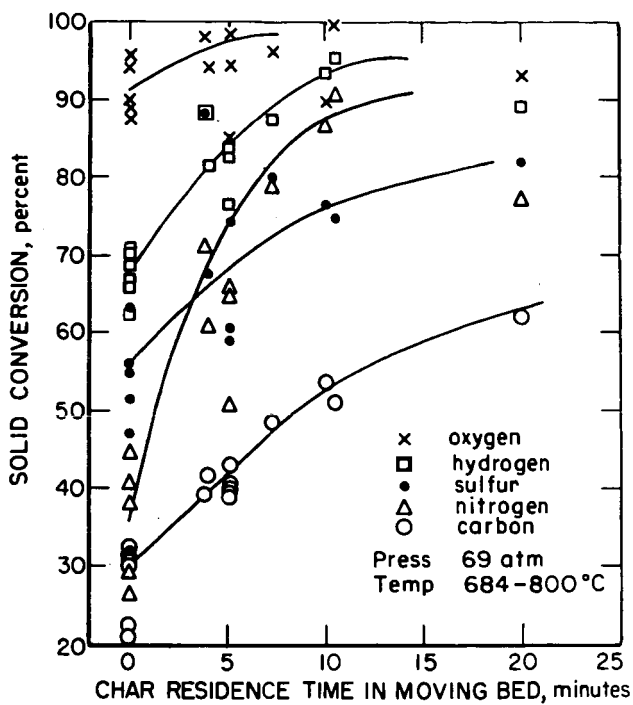


Figure 18 - Cool constituent conversion as function of residence time

L-13954

## (HYDRO) GASIFICATION OF BATTELLE TREATED COAL (BTC)

S. P. Chauhan, H. F. Feldmann, E. P. Stambaugh,  
and J. H. Oxley

Battelle Columbus Laboratories  
505 King Avenue, Columbus, Ohio 43201

INTRODUCTION

Conversion of coal to SNG is one of the options available for alleviating the critical supply shortage of natural gas. This gas supply problem is most extreme in our eastern industrial areas. However, the only commercial SNG plants using coal as a feed stock proposed thus far have been planned for the western states. A primary reason for using western coal is that the only commercially available technology that is being considered for SNG is Lurgi technology which works best with the western noncaking coals. Rapid expansion of a coal-based SNG industry in the west is limited by factors other than finding cooperative coal. For example, the issues of reclamation of strip-mined land in arid regions, potential water supply problems, as well as the reluctance of the residents to have these areas undergo rapid industrialization can be expected to have a retarding effect on the construction of coal-conversion plants.

Availability of water, large reserves of high-sulfur coals which cannot be burned without exceeding allowable SO<sub>2</sub> emission levels, proximity to areas where gas shortages are most severe, the availability of an existing industrial and mining base and adequate rainfall to insure reclamation of strip-mined land are all factors that should encourage the utilization of eastern coals as SNG feedstocks. However, the utilization of eastern coals is complicated by its highly agglomerating nature.

Another constraint on the development of an SNG from coal industry whether it is located East or West is the capital required to build these plants. Recent estimates place the investment required for building a plant that will produce approximately 280 x 10<sup>9</sup> SCF/day of pipeline gas from coal in the neighborhood of \$800 million.

Thus, there is a strong driving force to develop technology that will allow both the economic solution to the agglomeration problems that complicate the utilization of eastern coal and that allows the investment required to build these plants to be reduced.

One approach to lowering investment costs is by catalysis of the coal-steam-hydrogen reactions to allow the coal-steam reaction to occur at lower temperatures and the coal-hydrogen reaction at lower pressures. Numerous attempts have been made since the beginning of this century to catalyze the reaction of coal and other carbonaceous matter with steam (1-9). A few attempts have been made recently to catalyze the reaction of coal and other carbonaceous matter with hydrogen--called hydrogasification (8-12). However, it is of considerable importance to develop even better catalyst systems to promote both the hydrogasification and the steam-carbon reactions.

In this paper, we discuss the preliminary results of a novel treatment process that, in addition to enhancing the reactivity of coal to steam and hydrogen, eliminates the swelling and caking properties of even the most highly caking Eastern U.S. coals.

PROCESS DESCRIPTION

Battelle's process involves the chemical and physical incorporation of a suitable catalyst in coal.\* This process is the outgrowth of a development effort to reduce the sulfur content of coal by chemical extraction that has been supported by the Battelle Energy Program. Gasification tests of the BTC showed that it had a reactivity far greater than that predictable from the results of ongoing investigations described in the literature. In addition, BTC was found to be nonswelling and noncaking. Because of these promising results, a separate effort was undertaken to develop gasification concepts and to conduct experimental feasibility studies to establish the technical and economic feasibility of this approach for the production of SNG. The results of this study have exceeded our expectations and, we believe, provide the basis for a breakthrough in SNG technology.

The catalyst usually consists of a conventional gasification catalyst and a reagent that reacts with coal to alter and open up the structure of coal facilitating the penetration of the catalyst throughout the volume of coal. During the treatment, a significant amount of catalyst (normally 1 to 3 weight percent) chemically binds to the coal while a controlled quantity of catalyst is physically incorporated into the coal. The reagent used to alter the structure of coal can be reclaimed by washing of treated coal.

EXPERIMENTAL RESULTS

A large number of gasification experiments were conducted with hydrogen and steam to determine the effects of catalyst incorporation, using the Battelle process, on the reactivity and caking properties of coal, on the gas analysis, and on the physical and chemical characteristics of the char.

Most of the experiments were conducted on 70 percent minus 200 U.S. mesh coal from the Eastern United States, containing about 30 percent volatile matter. The process was found to be applicable to coarser coals, e.g., plus 25 U.S. mesh, also. In this paper, we discuss the results with lime (CaO) as a gasification catalyst using coal from the Montour mine (Pittsburgh Seam No. 8) sized to 70 percent minus 200 U.S. mesh. The reagent and the conditions for treatment will be disclosed at a later date\*. The BTC was washed prior to gasification to remove the reagent used during treatment.

The experiments were conducted in a thermobalance reactor, designed for high-pressure (1500 psig) and high-temperature (1200°C) operation, shown schematically in Figure 1. The reactor system is very similar to the one described by Gardner, et al (9). The use of the thermobalance reactor allows the monitoring of the mass of a sample as a function of time during reaction. In this manner, precise differential rate data can be obtained. The catalyst-impregnated coal was formed into 3/16-inch-diameter by 1/16-inch-long cylindrical pellets, without using a binder, since the sample container was made of 100-mesh stainless steel screen. During a run, a 2-gram sample of coal was lowered into the preheated reactor zone from the loading zone in a few seconds using a motor-operated windlass. Thus, the reaction time was precisely known. The gasification system included a steam condenser, a water trap, flowmeters, a methane-analyzer (IR), and a gas chromatograph (GC).

Prevention of Caking and Swelling

The Battelle treatment makes even the highly caking coals, e.g., coals with a free swelling index (FSI) greater than 6, completely noncaking. Figure 2 is a photograph comparing the swelling and caking of BTC with both raw coal and coal

---

\* Coal treated by the Battelle process is abbreviated in this paper as BTC. This process is described more fully in another paper titled "The Battelle Hydrothermal Coal Process" to be presented by E. P. Stambaugh at the 80th AIChE Meeting.

treated by impregnating it with CaO as is conventionally done. As can be seen, BTC containing 7.5 percent calcium (some of which was present as an oxide with the rest chemically bound to coal) did not swell, cake, or fuse together during hydrogasification or steam gasification while the conventionally-impregnated coal containing 14.5 weight percent calcium (20.3 percent CaO) swelled, caked, and severely fused together on steam gasification. The swelling and agglomeration of the conventionally-treated coal would have been even more extreme under hydrogasification conditions. The scanning electron micrographs of raw coal and BTC coal before and after gasification are compared in Figure 3. It can be seen that BTC does not expand or swell during hydrogasification while raw coal expands and swells severely.

The use of the Battelle process to make the coal noncaking is much more attractive than the existing state of the art which involves the preoxidation of coal or the use of rather complicated gasifiers to eliminate the need for preoxidation of coal which results in the loss of volatile matter, a reduction in the reactivity of coal, and subsequently a lowering of the efficiency of the SNG process. The Battelle process, on the other hand, involves no loss of volatile matter and substantially simpler reactor systems.

#### Hydrogasification Rates

The reactivities of BTC under various conditions relative to raw (untreated) coal were determined from the fractional conversion versus time data obtained from the pressurized thermobalance. The fractional conversion of coal on an ash-free basis can be defined as

$$x = 1 - \frac{(\text{mass of coal at any time}) - (\text{mass of the ash})}{(\text{initial mass of coal}) - (\text{mass of the ash})} \quad 1)$$

For the purpose of determining the effect of Battelle treatment on the reactivity of coal, relative to raw coal, one can define an average relative reactivity,  $R_x$ , for a given fractional conversion,  $x$ , as

$$R_x = \frac{t_{x, \text{raw}}}{t_{x, \text{BTC}}} \quad 2)$$

where  $t_{x, \text{raw}}$  and  $t_{x, \text{BTC}}$  are the time required for a fractional conversion,  $x$ , of raw and Battelle-treated coal, respectively.

BTC was found to have a much higher hydrogasification reactivity than raw coal. The data in Figure 4 show that the average rate of gasification at 850°C and 500 psig hydrogen pressure based on 70 percent conversion (moisture-free basis) of BTC containing 7.5 weight percent calcium, was about 40 times faster than the raw coal.

The BTC was found to be more than an order of magnitude more reactive than coal that was impregnated with catalyst by the conventional slurry mixing at room temperature, as shown in Figure 5.

The importance of the increased hydrogasification reactivity is that high concentrations of methane should be achievable in the raw product gas thereby reducing the amount of methane that has to be produced by methanation.

One of the most important results of this work from a process economics point of view is the reduced pressure at which the BTC can be hydrogasified compared to raw coal. Figure 4 shows that even at pressures of 150 psig the BTC is much more reactive than raw coal at 500 psig. Furthermore, comparison of methane yields by graphical integration of gas analysis data (Figure 6) indicate that the methane yield, defined as the ratio of the carbon converted to methane to the total carbon

gasified, of BTC at 250 psig is the same as for the raw coal at 500 psig.

Thus, because coal can be converted to methane at pressures much lower than had been previously thought possible, investment costs for SNG plants using BTC can be substantially reduced. In addition, the reliability of the plant should be significantly increased because of the lower pressure operation.

#### Steam Gasification Rates

Providing heat for the endothermic steam-carbon reaction is one of the factors that contributes substantially to the cost of SNG from coal. The reason for the costliness of this step is primarily that oxygen is usually used to combust part of the carbon to provide the heat. Thus, anything that can lower the temperature required for gasifying coal with steam will reduce oxygen requirements and, thereby, the SNG costs.

Experimental data show that the Battelle catalyst incorporation process allows a substantial reduction in gasification temperature over that required for either raw coal gasification or coal that contains alkali catalysts that are impregnated into the coal by conventional means. For example, Figure 7 compares the time required to achieve various gasification conversion levels for BTC, coal conventionally impregnated with CaO and raw coal all at 825°C. Clearly, the reactivity of BTC is substantially better than either of the others even though the BTC contains only about half the concentration of Ca as in the conventionally impregnated coal.

The effect of temperature on gasification rate is shown in Figure 8. Interpolation indicates that, with BTC, gasification rates at approximately 675°C are equivalent to those at 825°C with raw coal.

More important in reducing oxygen consumption than the lowering of sensible heat requirements is the higher methane yield that one expects from lower temperature operation and the catalysis of the carbon-hydrogen reaction. The higher ratio of methane to carbon oxides achievable at the lower temperature substantially reduces the endothermicity of the carbon-steam reaction.

#### Reactor Systems for (Hydro) Gasification)

BTC's important advantages (i.e., low temperature and pressure operability, and no swelling or caking) will have a very important impact not only on the reactor system that is developed for integration with the coal treatment step but also on other supporting operations. Obviously, BTC could be used in any of the reactor systems currently being developed. However, because of the noncaking nature of the BTC and its high reactivity a much simpler reactor system than more currently being developed for handling eastern coals should suffice.

#### CONCLUSIONS

The Battelle-treated coal (BTC) is a potentially superior gasification feedstock than raw (untreated) coal or coal impregnated in a conventional manner with catalysts.

The specific advantages of BTC demonstrated by this gasification study are:

1. The prevention of caking and swelling of coal during hydrogasification and steam gasification
2. High rates of steam gasification allowing steam gasification to proceed at substantially lower temperatures than with raw coal or coal treated with catalysts in a conventional manner

3. Rates of hydrogasification as high as 40 times those of raw coal and the maintenance of this high reactivity even at pressures as low as 250 psig.

Because of these advantages we believe that the development of a (hydro) gasification process based upon the use of BTC will result in a substantial lowering of both investment and operating costs as well as allow the reliable utilization of our large eastern U.S. coal reserves for the production of clean gaseous fuels.

#### ACKNOWLEDGMENTS

This work was supported by the Battelle Energy Program. The technical assistance provided by Dr. John F. Foster is greatly appreciated.

REFERENCES

- (1) Elliott, M. A., Preprints of Fuel Division, American Chemical Society Meeting, 19 (3), 140 (1974).
- (2) Kroger, C., Melhorn, Gunter, Brennstoff-Chem., 19, 257 (1938).
- (3) Kroger, C., Angew. Chem., 52, 129 (1939).
- (4) Lewis, W. K., Gilliland, E. R., Hipkin, H., Ind. Eng. Chem., 45, 1697 (1953).
- (5) Kislykh, V. I., Shishakov, N. V., Gaz. Prom., 5, 15 (1960).
- (6) Willson, W. G., et al., Coal Gasification, Advances in Chemistry Series 131, Edited by L. G. Massey, American Chemical Society, Washington, D.C., 1974, p. 203.
- (7) Haynes, W. P., Gasior, S. J., Forney, A. J., Coal Gasification, Advances in Chemistry Series 131, Edited by L. G. Massey, American Chemical Society, Washington, D.C., 1974, p. 179.
- (8) Renwick, R. T., Wentrcek, P. R., Wise, H., Fuels, 53, 274 (October 1974).
- (9) Gardner, N., Samuels, E., Wilks, K., Coal Gasification, Advances in Chemistry Series 131, Edited by L. G. Massey, American Chemical Society, Washington, D.C., 1974, p. 217.
- (10) Wood, R. E., Hill, G. R., Preprints of Fuel Division, American Chemical Society Meeting, 17 (1), August, 1972.
- (11) Dent, F. J., Blackburn, W. M. Millet, H. C., Trans. Inst. Gas Engrs., 87, 231 (1937).
- (12) Dent, F. J., Blackburn, W. M., Millet, H. C., Inst. Gas Engrs., Commun., 190, 69 (1938).

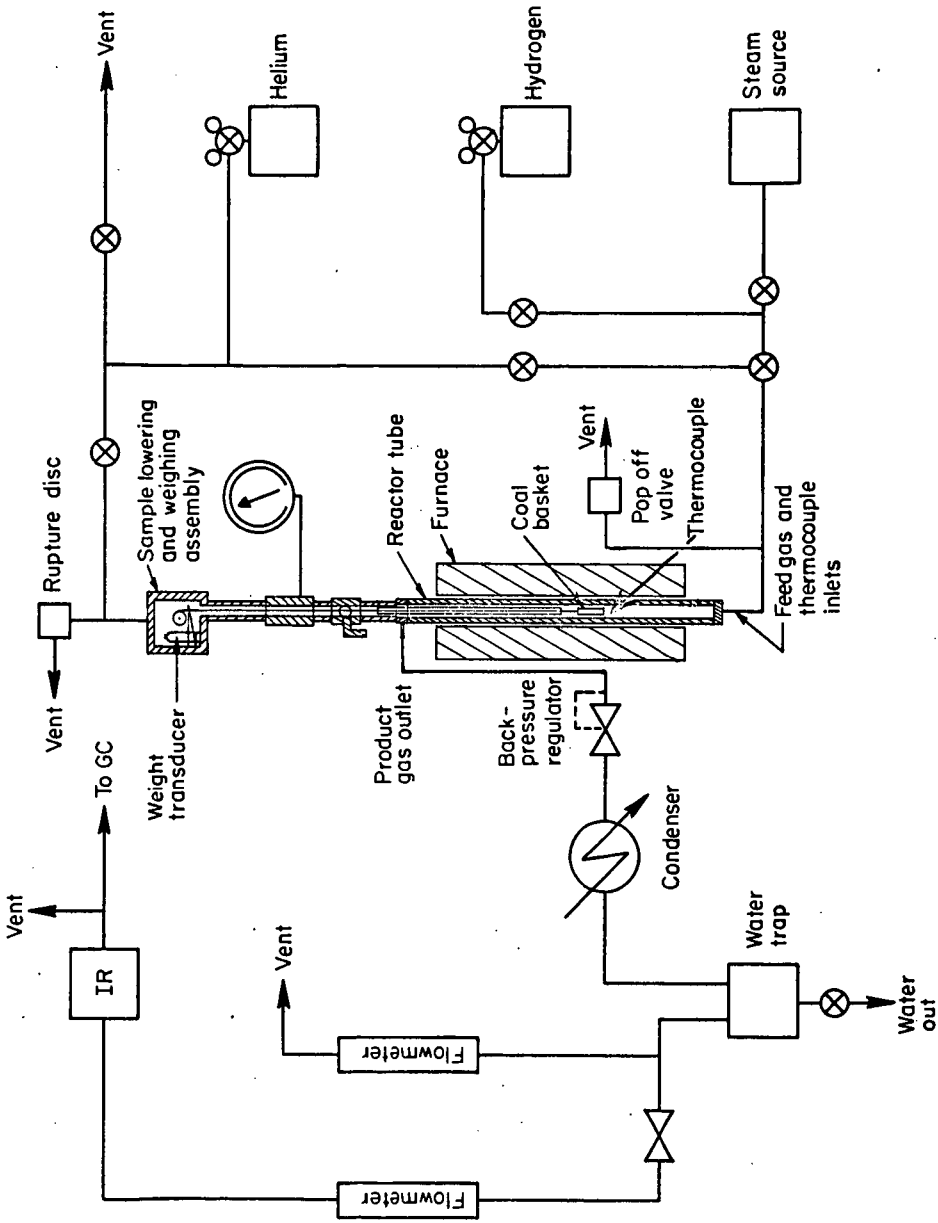


FIGURE 1. SCHEMATIC OF COAL GASIFICATION SYSTEM

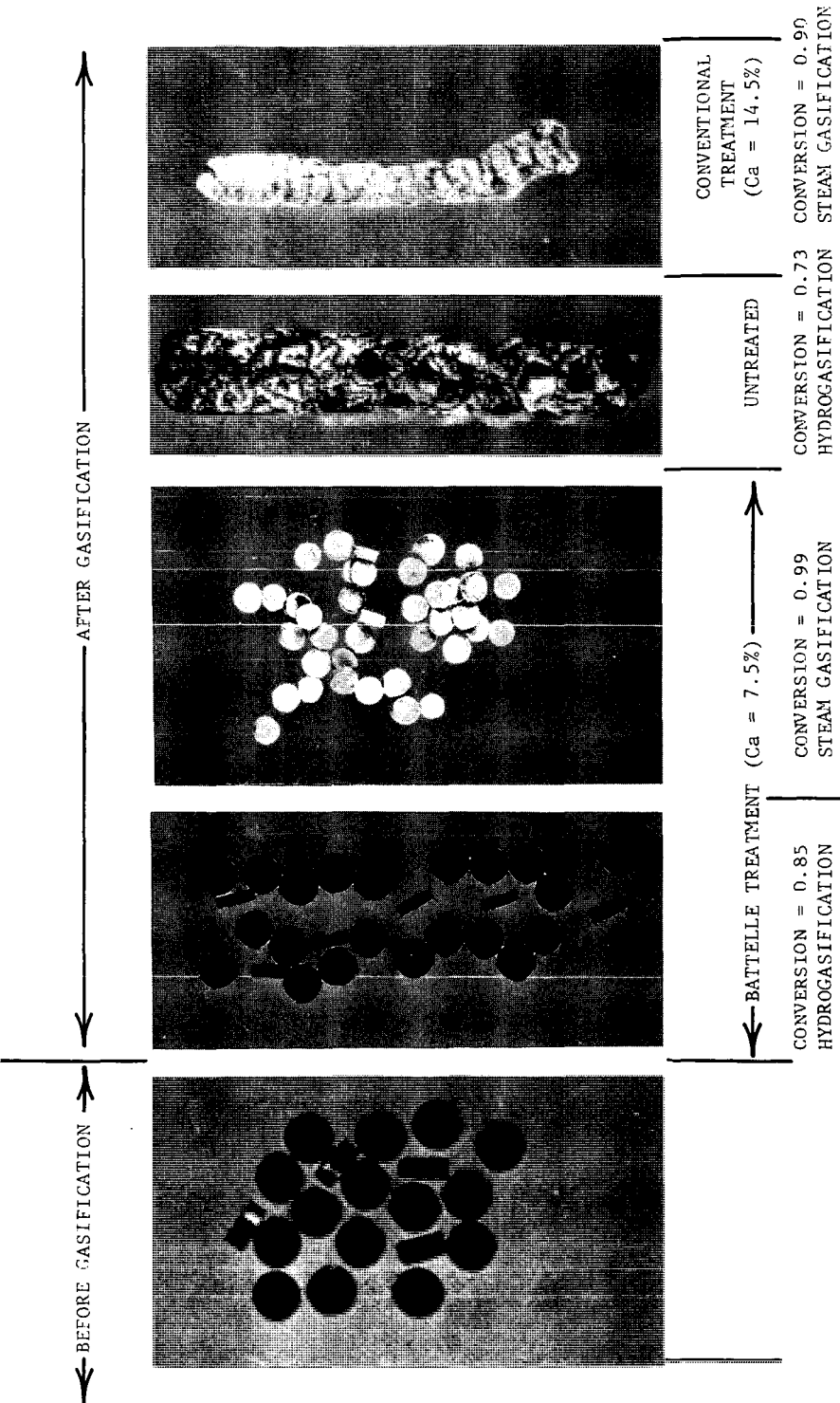
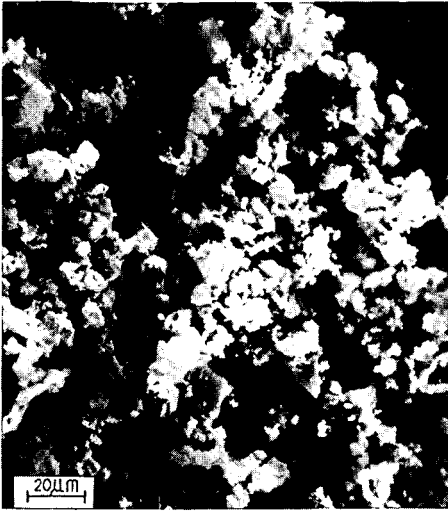


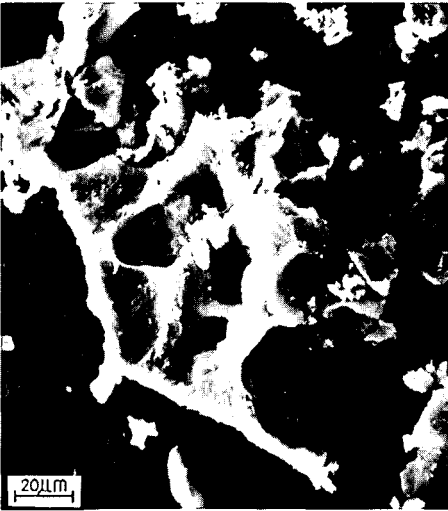
FIGURE 2. PHOTOGRAPHS OF TREATED AND UNTREATED COALS BEFORE AND AFTER GASIFICATION



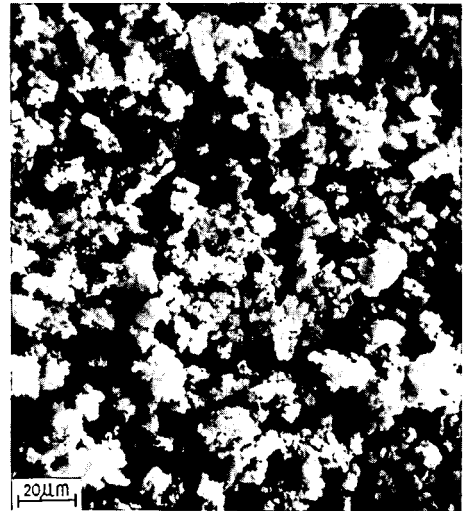
Raw Coal, Before Hydrogasification



BTC, Before Hydrogasification



Raw Coal, After Hydrogasification



BTC, After Hydrogasification

FIGURE 3. SCANNING ELECTRON MICROGRAPHS OF RAW COAL AND BTC BEFORE AND AFTER HYDROGASIFICATION

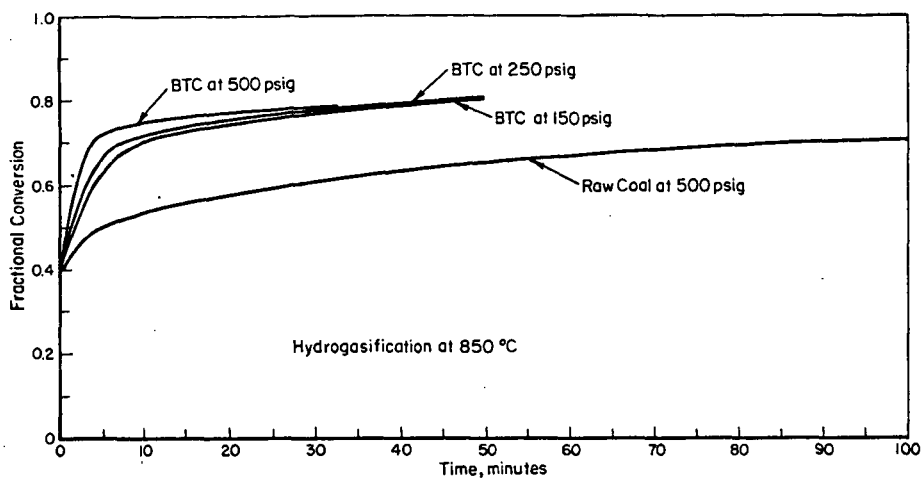


FIGURE 4. DEPENDENCE OF THE RATE OF HYDROGASIFICATION OF BTC ON PRESSURE

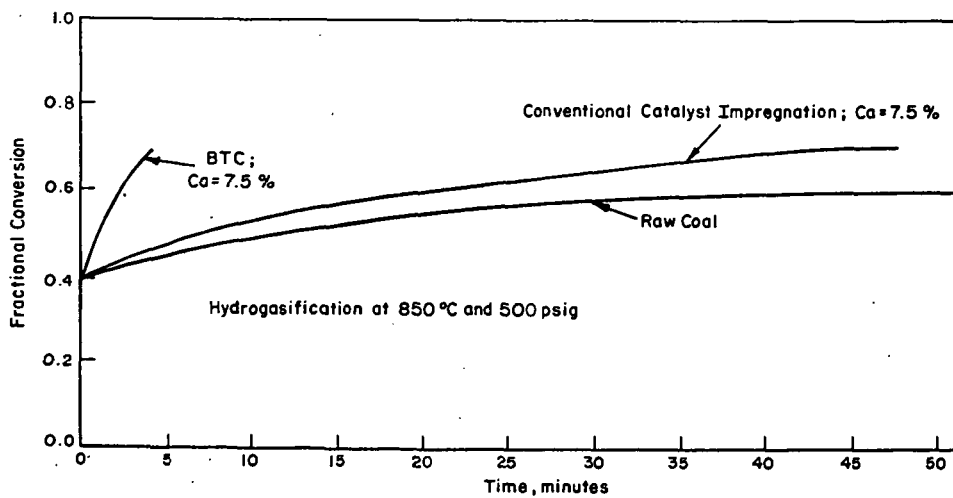


FIGURE 5. COMPARISON OF THE REACTIVITY OF BTC WITH RAW COAL AND A COAL THAT WAS CONVENTIONALLY IMPREGNATED WITH CATALYST

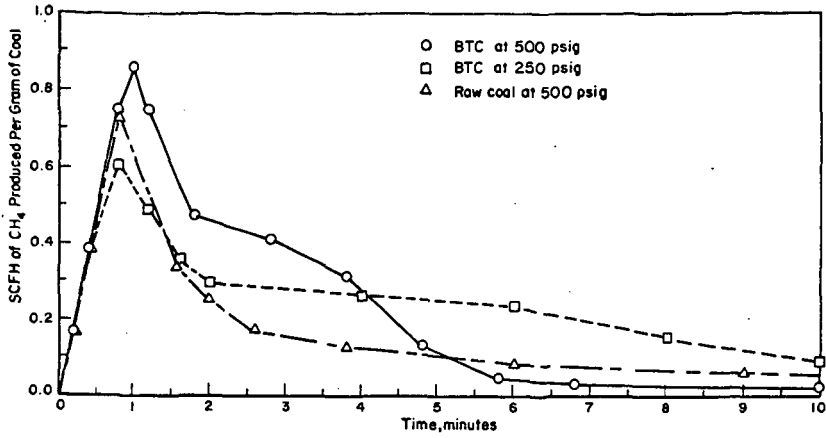


FIGURE 6. RATE OF METHANE PRODUCTION DURING HYDROGASIFICATION AT 850°C FOR COAL WEIGHING ONE GRAM (ASH-FREE) BEFORE GASIFICATION

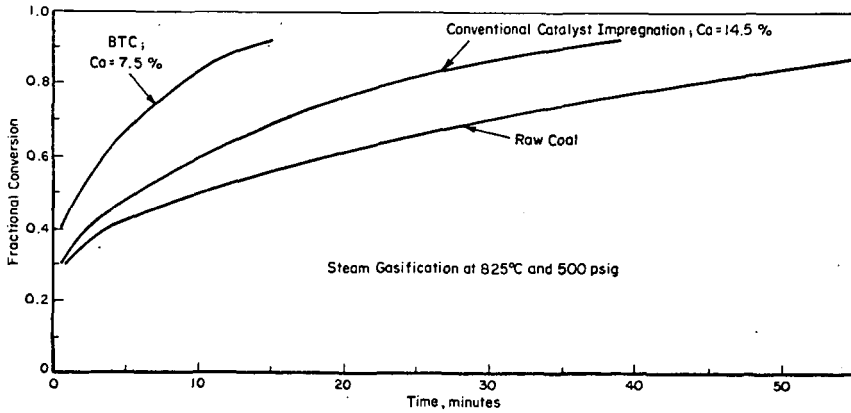


FIGURE 7. COMPARISON OF THE REACTIVITY OF BTC WITH RAW COAL AND A COAL THAT WAS CONVENTIONALLY IMPREGNATED WITH CATALYST

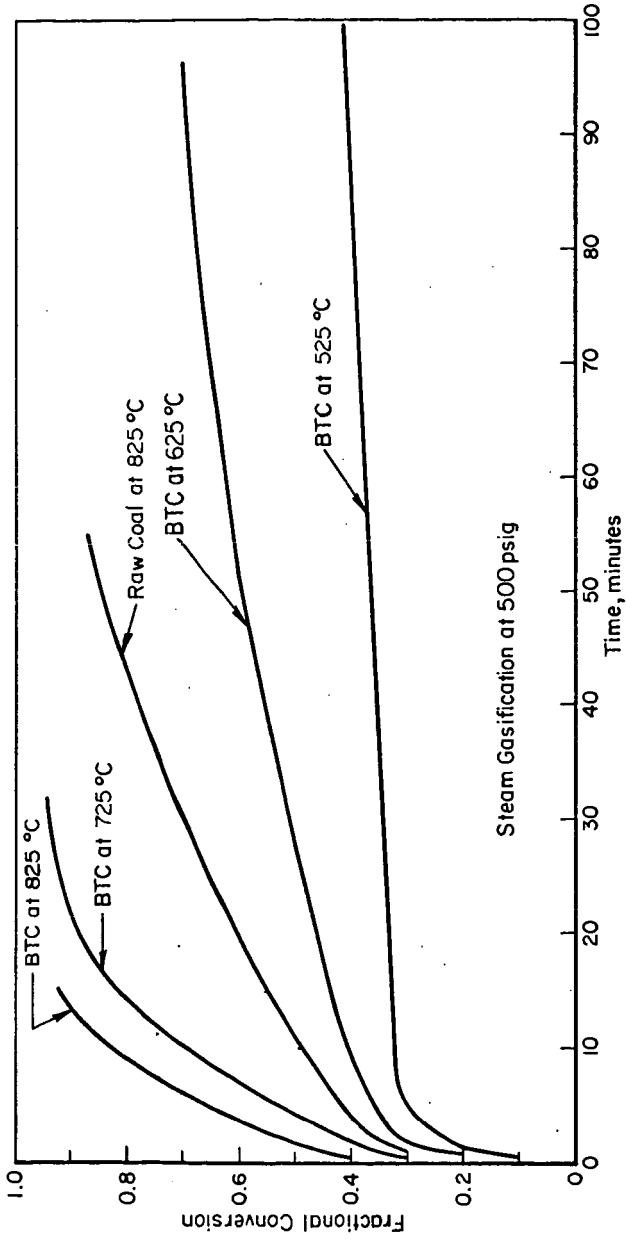


FIGURE 8. DEPENDENCE OF STEAM GASIFICATION RATE ON TEMPERATURE

## FACTORS AFFECTING THE THERMAL EFFICIENCY OF A GASIFICATION PROCESS

C. Y. Wen, P. R. Desai and C. Y. Lin

Department of Chemical Engineering, West Virginia University, Morgantown, WV 26506

Abstract - Two main factors affecting the thermal efficiency of the gasification process are the amount of methane formed in the gasifier and the kind of coal used. Thermal efficiencies are calculated for the various coal gasification processes having potential for commercialization. Another way of comparing different processes, based on the second law of thermodynamics considerations in terms of available work is introduced.

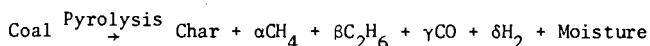
The results show that higher amounts of methane formed by direct methanation in the gasifier will result in higher thermal efficiency of the process. Thermal efficiency of Lurgi Process decreases considerably when higher ranking coals are used. The available work efficiency can be used not only for comparison but also to pinpoint inefficiencies inherent in certain process steps.

Introduction

Coal gasification processes for production of SNG can be divided into several individual sub-systems, such as coal preparation, pretreatment gasification, shift conversion, gas purification and methanation which may be followed by compression to desired pipeline gas pressure if necessary. As the products of gasification affect the overall thermal efficiency of the process greatly, gasification sub-system is described briefly in the following section.

Gasification

In gasification, coal is converted into gases that can be converted later into a pipeline quality gas having a heating value of more than 900 Btu/SCF. In a gasifier, following reactions take place:



Steam-char reaction is highly endothermic while water gas and hydrogasification reactions are exothermic. Heat required in reaction 1) can be supplied directly by coal-oxidation or indirectly by heating. (13)

The major factor affecting the thermal efficiency is the amount of methane formed in the gasifier. Amount of methane produced depends on pressure, temperature and the kind of gasifier used.

Effect of Methane Concentration in Gas from Gasifier on the Thermal Efficiency of the Process:

In Figure 1, heating value of the gas at the gasifier exit is plotted against the calculated values of overall thermal efficiency for various processes (2), (6). The results clearly show that when the amount of methane produced in the gasifier is higher, the thermal efficiency of the process is consistently higher. The reason for this is that the amount of hydrogen required to produce methane is less if hydrogen reacts with carbon in coal rather than with carbon in carbon monoxide or

dioxide as it occurs in methanator later on. Also the heat generated in the gasifier because of hydrogasification reaction can be utilized to carry out the carbon-steam endothermic reaction in the gasifier. This heat utilization is more efficient than utilization of heat recovered in the form of high pressure steam in methanation. In addition, heat generated due to hydrogasification reaction reduces the oxygen requirements reducing the consumption of energy in the oxygen plant. Coal contains certain amounts of aliphatic compounds and hydrogen in the form of volatile matter. This volatile matter decomposes into low hydrocarbon compounds such as methane, ethane, etc., by reacting with hydrogen during the pyrolysis and the initial stage of gasification. For example, in Lurgi Process using moving bed gasifier, coal and gas flows are countercurrent and hence, large amounts of hydrogen is contacted with coal in the devolatilization zone (top of the reactor) producing methane.

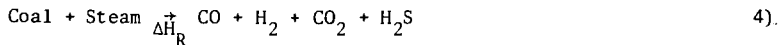
#### Effect of Temperature and Pressure on Methane Production:

Amount of methane produced decreases with increase in temperature, e.g., in Koppers-Totzek Process, due to high temperature (3200°F) very little methane is produced (3). And, therefore, intensive methanation is required. However, due to high temperature, tar and higher hydrocarbons decomposes into carbon monoxide and hydrogen eliminating complications in the purification section found in other lower temperature processes. Amount of methane produced increases with the increase in pressure. This increase in methane concentration continues at pressures above 400 psig. (used in Lurgi gasifiers) and quantitative data on this phenomenon have been reported by B.C.R.(4).

The other factor affecting the thermal efficiency is the kind of coal gasified. Coal can be classified into peat, lignite, sub-bituminous, bituminous, semi-bituminous and anthracite. Lignite and sub-bituminous coals are usually caking coals and form non-porous coke on heating.

#### Effect of Coal on the Efficiency of the Gasification Process:

In coal-steam reaction, theoretically the following two forms of reactions can take place.



Even though reaction 4 and 5 are extremes, they take place simultaneously in a gasifier with few exceptions. For example, in Koppers-Totzek gasifier reaction 4 occurs while in Hydrane gasifier reaction 5 occurs to large extent. Both of the above reactions are endothermic. Endothermicity of the reaction represents the amount of heat required to complete the reaction and in gasification, this heat is supplied by oxidation of coal with oxygen. The endothermicity of the reaction is different for different coal and since heat is supplied by oxidation of coal, it may be expected to be directly related to the efficiency of the process.

For three different coals, data shown in Table 1 were reported by Koppers company (3). These data show that the amount of oxygen and steam required for gasification increases with the increase in volatile matter. The data also show that the composition and the heating value of the gasifier product are almost similar in all cases and thus are nearly independent of kind of coal used. Carbon conversion is a function of reactivity of coal. Lignite and sub-bituminous coals can be converted almost completely while conversion of high volatile coals approaches 95%-97% (3). The same kind of data collected from trials at Westfield, Scotland, were reported by Lurgi for Montana, Illinois 5, Illinois 6 and Pittsburgh 8 coals.(1),(11)

TABLE 1 Effect of Coal on Gasifier Products, Koppers-Totzek Process (3)

Coal	Sub-bituminous Western	High Volatile B-Bituminous Illinois	High Volatile A-Bituminous Eastern
<u>Composition (wt. %)</u>			
C	56.76	61.94	69.88
H	4.24	4.36	4.90
O	13.18	6.73	7.05
N	1.01	0.97	1.37
S	0.67	4.88	1.08
Ash	22.14	19.12	13.72
Moisture	2.00	2.00	2.00
Heating Value BTU/lb.	9,888.	11,388.	12,696.
<u>Gasification</u>			
Oxygen required T/T of coal	0.649	0.704	0.817
Steam required T/T of coal	0.136	0.27	0.294
<u>Gas Composition</u> Dry Basis (Vol %)			
CO	58.68	55.38	55.90
CO <sub>2</sub>	7.04	7.04	7.18
H <sub>2</sub>	32.86	34.62	35.39
N <sub>2</sub>	1.12	1.01	1.14
H <sub>2</sub> S	0.28	1.83	0.35
COS	0.02	0.12	0.04
	<u>100.00</u>	<u>100.00</u>	<u>100.00</u>
Gas Heating value BTU/SCF	295.1	290.2	294.4
No. of moles/ton of coal	136.4	156.6	174.8
<u>Efficiency %</u>			
Heating value of gas/ Heating value of coal	77.3	75.8	77.0
Heating value of gas/ Heating value of coal + + coal used for pro- duction of steam and power required.	69.7	67.9	68.7

These data are shown in Table 2. It can be concluded that higher operating temperature is necessary with decreasing coal reactivity. Oxygen and steam consumptions increase with the decrease in coal rank. However, yield of methane remains fairly constant for different kinds of coal. It also shows that efficiency of gasification, allowing for the coal equivalent of steam and oxygen supplies, decreases substantially with the increase in coal rank.

The type of coal processes also affects the amount of water required in a gasification process. The factors affecting the water requirements are:

- a) Moisture content
- b) Reactivity of coal
- and c) Sulfur content of coal.

For a plant producing 250 MMSCF of pipeline gas, the total water requirement is roughly about 19,000 gpm. when lignite coal is used while for bituminous coal water required is about 22,500 gpm.

Thermal efficiency calculations done on the basis of first law of thermodynamics are useful for comparison of coal gasification processes. Another way of comparing different alternatives is to calculate energy utilization efficiency based on the second law of thermodynamics, which is defined as the ratio of total output of work equivalent in all outgoing streams to the total input. The main advantage of this approach is its ability to compare energy utilization efficiency of different processing schemes and alternatives, which may start from different energy resources and may produce different products, in a consistent way. It also pinpoints the inefficiencies inherent in certain process steps.

From second law of thermodynamics, the available work,  $de$ , can be expressed in terms of enthalpy change ( $dH$ ) and entropy change ( $ds$ ) as:

$$de = dH - T_0 ds$$

where  $T_0$  is the temperature of the surrounding.

For a closed system in equilibrium at  $T_0$ , when no work can be obtained from it in the given surroundings,

$$e = H - H_0 - T(S - S_0)$$

is the maximum amount of work which can become available from the system if it can exchange heat only with a heat reservoir at  $T_0$ . A process stream carrying  $\dot{n}$  moles of  $i$  per unit of time and performing work  $\dot{w}$  in the same time is equivalent to a flux of available work

$$\dot{e} = \sum_i \dot{n}_i e_i + \dot{w}$$

At steady state, for any system, the available work  $\dot{e}_{in}$  entering the system is always greater than or equal to that leaving the system.

$$\dot{e}_{in} \geq \dot{e}_{out}$$

Then, the available work efficiency  $\eta$  can be defined as

$$\eta = \dot{e}_{out} / \dot{e}_{in}$$

The fraction  $(1-\eta)$  is being lost due to irreversible processes causing an entropy production  $\sigma$

$$(1-n) \frac{Q}{T_{in}} = T_0 \sigma = I$$

Where I is the irreversible work associated with the entropy change.

The datum level used in available work efficiency calculations, is defined as one in which an existing substance, when in equilibrium with the surrounding, will have zero available work.

The bases used for calculations are air and water at 1 atm. and 25°C. Under these conditions, it may be assumed that available work from CO<sub>2</sub> and SO<sub>2</sub> is zero.

Table 2 Effect of coal on Gasifier Products  
Lurgi Process (1 )

Coal	Rosebud Montana	Illinois #5	Illinois #6	Pittsburgh #8
Composition wt %				
C	50.56	64.11	64.16	74.15
H	3.18	4.36	4.34	5.04
O	9.80	7.04	8.10	4.52
N	0.91	1.22	1.21	1.35
S	1.09	3.13	2.80	2.52
Ash	9.76	8.20	9.16	7.84
Moisture	24.70	11.94	10.23	4.58
	100.00	100.00	100.00	100.00
Heating value Btu/lb	8611.	11456.	11464.	13442.
<b>Gasification</b>				
Oxygen required	0.24	0.46	0.45	0.59
T/T of coal				
Steam required	1.25	2.25	2.51	3.24
T/T of coal				
<b>Gas composition</b>				
Dry Basis (%)				
CO	15.1	17.6	17.3	16.9
CO <sub>2</sub>	30.4	31.0	31.2	31.5
H <sub>2</sub>	41.1	38.8	39.1	39.4
N <sub>2</sub>	1.2	1.5	1.2	1.6
H <sub>2</sub> S	0.5	1.1	1.1	0.8
CH <sub>4</sub>	11.2	9.2	9.4	9.0
C <sub>2</sub> H <sub>6</sub>	0.5	0.5	0.7	0.7
C <sub>2</sub> H <sub>4</sub>	-	0.3	-	0.1
	100.0	100.0	100.0	100.0
<b>Gas heating value excluding</b>				
H <sub>2</sub> S Btu/SCF	239.	291.	290.	285.
No. of moles/ton of coal	212.6	160.6	158.	187.
<b>Efficiency %</b>				
Heating value of gas/ heating value of coal	79.9	77.5	75.8	75.3
Heating value of gas/ (Heating value of coal gasi-58.7 fied + coal used for produc- tion of steam and power re- quired)		52.8	50.9	48.8

Based on above datum level, the corresponding work equivalent of the chemical elements are calculated and are shown in Table 3.

Table 3 Available Work of Chemical Elements

Substance	State	$\epsilon$ at 25°C & 1 atm. Btu/mole
Coal*	Solid	224,460 (Btu/mole-C)
C	Solid	168,000'
S	Solid	127,560
O <sub>2</sub>	Gas	1,670
N <sub>2</sub>	Gas	250
H <sub>2</sub>	Gas	101,210
H <sub>2</sub> O	Gas	3,700
CO	Gas	109,780
CO <sub>2</sub>	Gas	0
CH <sub>4</sub>	Gas	348,570

\*Pittsburgh seam coal is used. Entropy of coal is about 4 cal/gmole-carbon °K.

Energy utilization efficiency based on available work and percentage distribution of irreversibility for different process steps of Lurgi, Koppers-Totzek and Hydrane Processes were calculated. The results are shown in Table 4.

Table 4 Evaluation of irreversible work distribution in the coal gasification processes to produce pipeline gas.

(Feed Coal = 1 ton basis, Pittsburgh seam)

	Lurgi-Gasifier	Koppers-Totzek Gasifier	Hydrane Process
Feed coal, available work x 10 <sup>6</sup> Btu	25.74	25.74	25.74
Product pipeline gas, available work x 10 <sup>6</sup> Btu	15.30	13.49	16.72
Irreversible lost work x 10 <sup>6</sup> Btu	10.44	12.25	9.02
Thermal eff.	64%	54%	72%
Available work eff.	59%	52%	65%
Irreversible lost work distribution, x 10 <sup>6</sup> Btu			
Gasifier	3.82	4.03	4.16
Heat exchanger and spray tower	0.96	1.06	0.81
Shift converter	0.33	1.41	0.30
Purification unit	1.16	1.28	1.05
Methanation unit	1.09	1.80	0.13
Oxygen plant	1.34	2.06	0.86
Steam and power plant	1.74	0.61	1.71

Acknowledgment

This work was supported partially by National Science Foundation and partially by ERDA.

References

1. Elgin, D. C., "Results of Trials of American Coals in Lurgi Pressure-Gasification Plant at Westfield, Scotland", proceedings of Sixth Synthetic Pipeline Gas Symposium, Chicago, Illinois, October 1974.
2. Feldmann, H. F., Wen, C. Y., Simon, W. H., Yavorsky, P. M., "Supplemental Pipeline Gas from Coal by the Hydrane Process", paper presented at the 71st National AIChE Meeting, Dallas, Texas, February 20-23, 1972.
3. Fransworth, J. F., Mitsak, D. M., Kamody, J. F., "The Production of Gas from Coal Through a Commercially Proven Process", Koppers Company, Inc., Pittsburgh, August, 1973.
4. Hendrickson, T. A., "Synthetic Fuels Data Handbook", pp. 168-182, Cameron Engineers, Inc., 1975.
5. Howard, H. C., Ind. & Eng. Chem. Vol. 44, No. 5, p. 1083, 1952.
6. Huebler, J., Lee, B. S., and Schora, F. C., Jr., "Hygas Coal Gasification Process", For Publication in the Handbook of Energy Technology, June, 1974.
7. Lowry, H. H., Chemistry of Coal Utilization, p. 208, p. 250-260.
8. Mazumdar, B. K., Coal Science, p. 475, 1966.
9. Mudge, L. K., Schietelbein, G. F., Li, C. T., and Moore, R. H., "The Gasification of Coal, A Batelle Energy Program Report, July, 1974.
10. Riekert, L., Chem. Eng. Sci., Vol. 29, p. 1613, 1974.
11. Rudolph, R. F. H., "Processing of American Coals in a Lurgi Gasifier", Proceedings of Sixth Synthetic Pipeline Gas Symposium, Chicago, Illinois, October, 1974.
12. University of Michigan, "Evaluation of Coal Conversion Processes to Provide Clean Fuels", Final Report, p. 376-379, Feb. 1974.
13. Wen, C. Y., "Optimization of Coal Gasification Processes", Interim Report to Office of Coal Research, 1972.

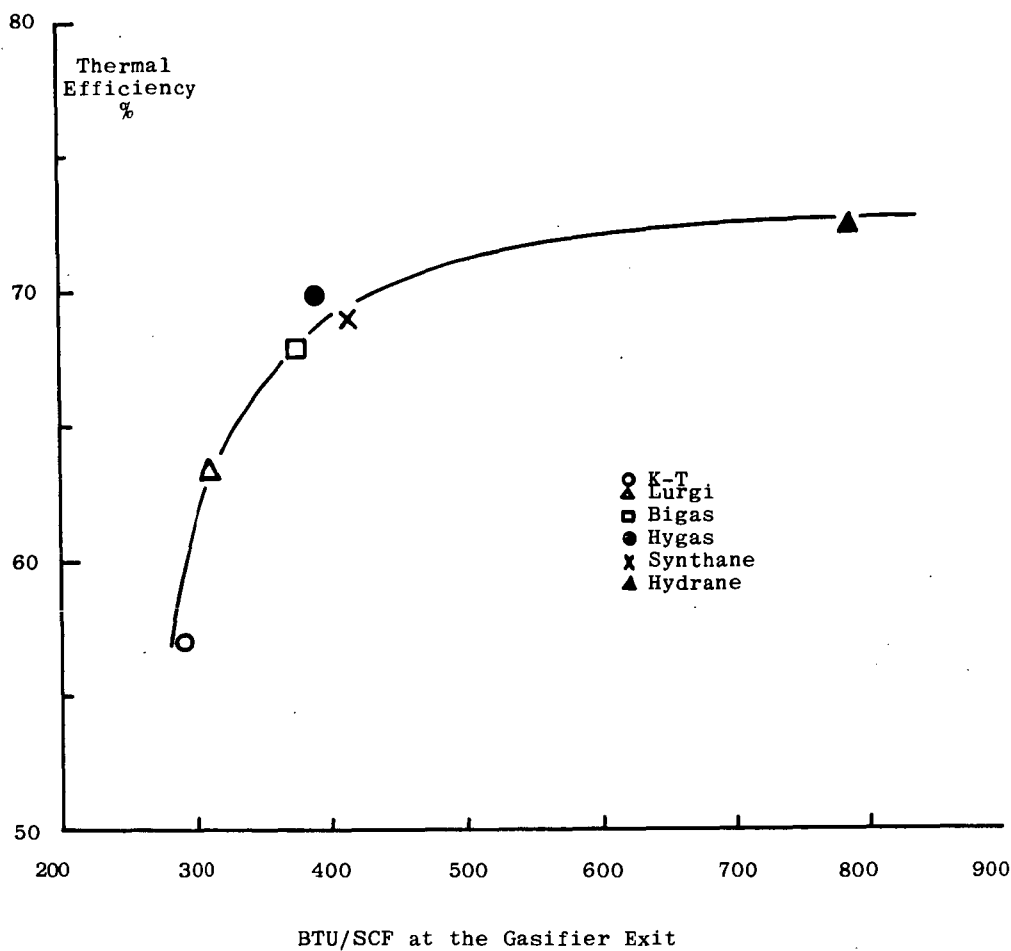


Figure 1 Effect of Amount of Methane Produced in the Gasifier on the Thermal Efficiency of the Process.

LABORATORY EVALUATION OF PROPERTIES  
OF FLY ASH-IRON OXIDE ABSORBENTS FOR H<sub>2</sub>S  
REMOVAL FROM HOT LOW-BTU GAS

E. C. Oldaker, A. M. Poston, Jr., and W. L. Farris, Jr.

U.S. Energy Research and Development Administration  
Morgantown Energy Research Center  
Morgantown, West Virginia

INTRODUCTION

The Morgantown Energy Research Center is conducting research on solid, regenerable absorbents to remove H<sub>2</sub>S from hot (1,000°-1,500°F) low-Btu fuel gas made by gasifying coal with air and steam. The heating value of low-Btu gas ranges from 100 to 150 Btu per cubic foot, which makes it uneconomical for long distance transport but is suitable for "on-site" utilization to fire powerplant or industrial boilers. Removal of the sulfur (largely H<sub>2</sub>S) from the gas while still hot affords two benefits for the utilization of low-Btu gas as a fuel. First, the gas can be directly fired in boilers and meet environmental standards concerning sulfur emissions to the atmosphere. Second, the sensible heat of the gas is retained, thereby increasing the overall thermal efficiency of the fuel.

The use of iron oxide to remove H<sub>2</sub>S from industrial gases has been practiced for many years. Coke oven gases have been desulfurized by fixed or fluid beds of iron oxide at temperatures up to 752°F (1). Abel et al. (2) and Shultz (3) reported the results of laboratory studies in which solid absorbents were used to remove H<sub>2</sub>S from hot, simulated and actual producer gas. Clay and Lynn (4) described the use of iron oxide supported on alumina to remove NO<sub>x</sub> and SO<sub>x</sub> from powerplant stack gases at temperatures approaching 1,000°F. They injected a stream of synthesis gas (CO + H<sub>2</sub>) to reduce the SO<sub>2</sub> to H<sub>2</sub>S and NO to N<sub>2</sub> before passing the flue gases over the catalyst.

Laboratory investigations are being directed toward developing a solid, regenerable absorbent composed of iron oxide supported on a matrix of fly ash which has both the absorption capacity and physical strength believed to be required for a commercial application in removing H<sub>2</sub>S from low-Btu fuel gases at temperatures above 1,000°F.

Mechanical problems involving attrition of the iron oxide leading to unacceptable carry-over and absorbent replacement, and plugging or fouling of system components were some of the shortcomings of previous work using iron oxide to remove H<sub>2</sub>S from various type gases. By supporting the iron oxide upon a matrix of fly ash, these problems are overcome. The development of a solid, pellet-sized absorbent having adequate surface area or pore volume which effectively removes H<sub>2</sub>S eliminates the need for fluidization and/or the use of very small iron oxide particles. Another advantage is the lower capital and operational costs when using a fixed bed for absorbing, in which continuous recycling and replacement of iron oxide is not required.

The process described herein is designed to remove H<sub>2</sub>S from raw producer gas above 1,100°F by passing it through a fixed bed of fly ash-iron oxide absorbents. The H<sub>2</sub>S reacts with the Fe<sub>2</sub>O<sub>3</sub> to form FeS and FeS<sub>2</sub>. When the absorbents are fully sulfided, the FeS+FeS<sub>2</sub> is easily returned to Fe<sub>2</sub>O<sub>3</sub> by passing air through the bed for a short period.

MATERIAL, EQUIPMENT AND PROCEDURES

Fly ash from a coal-fired powerplant near Morgantown, West Virginia, was used exclusively as supporting material for the fly ash-iron oxide absorbents. This fly ash was similar to the fly ash from three other local sources. A typical analysis

of the fly ash was:  $\text{SiO}_2$ -51.7%,  $\text{Al}_2\text{O}_3$ -24.6%,  $\text{Fe}_2\text{O}_3$ -15.9%,  $\text{CaO}$ -3.06%,  $\text{K}_2\text{O}$ -2.38%,  $\text{MgO}$ -0.94%,  $\text{TiO}_2$ -0.84%,  $\text{Na}_2\text{O}$ -0.66%, and  $\text{P}_2\text{O}_5$ -0.34%. The BET surface area was 0.95  $\text{m}^2/\text{gm}$ . The fly ash was dried and screened to remove agglomerates but was not otherwise processed.

The iron oxides used were Fisher Certified or MCB Technical Grade with BET surface areas of 10 and 8.5  $\text{m}^2/\text{gm}$  respectively. (These iron oxides were used to maintain consistent data throughout the investigations. Commercial iron oxides will be used for later tests.)

Laboratory grade, high-swelling bentonite (2 grams to 24 milliliters) of 63%  $\text{SiO}_2$  and 19%  $\text{Al}_2\text{O}_3$  content, and technical grade 40-42° Baume (3.22  $\text{SiO}_2/\text{Na}_2\text{O}$ ) sodium silicate solution, were used as additives to improve physical strength.

The dry ingredients were thoroughly mixed using a split-sleeve mixer, then transferred to a small portable-type cement mixer. Water was added to the mixture to obtain correct consistency for extrusion. The extrusion apparatus produced 3/16-inch diameter by 3/4-inch long extrudates through a multiple die arrangement at the end of a 2-inch diameter by 6-inch long barrel and auger. The solid extrudates were dried, then sintered at temperatures and times required. The crush strength (force applied across the diameter) was measured on a Tinius-Olsen testing machine.

Figure 1 is a flowsheet of the equipment used to conduct absorption and regeneration experiments with the iron oxide-fly ash absorbents. An entrainment carbonizer, used in previous coal carbonization research (5) was adapted to simulate on a small scale the production of hot, raw producer gas (containing coal-related tars and particulates) or clean, hot producer gas. Various gases to make up the producer gas were supplied from bottled gases metered into a manifold and into the gas preheater. Water was metered and injected into the gas preheater to simulate the amount of steam in actual producer gas.

When tars and particulates were required in the experiment, coal was fed into the carbonizer by a screw-type feeder. The coal entered the top of the carbonizer, 4-inch diameter by 18-inches high which was electrically heated, and was charred as it fell through; char and ash were removed through a lock hopper at the bottom. The outlet gas contained tars, light oils, and particulates and the gas make up was similar to actual producer gas. Eighty percent of the total gas passed through the absorption bed; the other 20% provided a sample of the input for analysis. The absorption vessel was 2-inches inside diameter by 45-inches long. A stainless steel screen 31-inches down from the top supported the absorbent bed. The vessel was externally heated by high temperature heating tapes. Both the vessel and heating tapes were covered with insulation to prevent excessive heat losses. Five internal thermocouples were used to monitor bed temperatures.

The input gas sample system consisted of a heated dust filter, an electrostatic precipitator, a water-cooled condenser, a silica gel trap and a dry gas meter. The input gas was analyzed for  $\text{H}_2\text{S}$  only using the Tutwiler method (6). The gas sample system following the absorption bed was identical to the input sample system except the gas stream passed through a bank of infra-red gas analyzers and was analyzed for  $\text{CO}$ ,  $\text{CO}_2$ ,  $\text{CH}_4$  and  $\text{H}_2$ .  $\text{H}_2\text{S}$  was again analyzed by the Tutwiler method.

On start-up, the preheater was heated to 950°F and the carbonizer chamber preheated to 1,300°F. The absorbent bed was heated to 1,100°F before starting the absorption period. The gas flow was allowed to proceed until a predetermined amount of  $\text{H}_2\text{S}$  was found in the gas passing through the absorption bed, usually 400 grains  $\text{H}_2\text{S}$  per 100 standard cubic feet of gas. The input  $\text{H}_2\text{S}$  concentration, as near as possible, was maintained at a level decided upon before the start of the experiment.  $\text{H}_2\text{S}$  concentrations much higher than normal producer gas were used to shorten the time required to complete an experiment. Results have been cross checked with those

made with producer gas  $H_2S$  concentrations and no major differences in results were obtained. Total gas flow through the system varied with the experiment and ranged from 25 to 35 scfh. When the predetermined  $H_2S$  concentration was reached, the input gases were turned off and a nitrogen purge started. The system was purged for 30 minutes with nitrogen to prepare the system for the regeneration cycle.

Figure 2 is a flow diagram for the absorption tests made using a 1,500 scfh side stream from the MERC stirred, fixed-bed gasifier (7). The gas was maintained at its exit temperature of  $1,100^{\circ}F$  by means of electric heaters and insulation surrounding the pipe. The hot gas was brought into contact with the iron oxide-fly ash absorbents in a 6-inch diameter, 4 foot high stainless steel absorber equipped with electric shell heaters and insulated for temperature control. The sulfided absorbents were regenerated by introducing air at  $70^{\circ}F$  into the 1-inch inlet of the absorber and piping the  $SO_2$ -rich gas to the stack through the 1-inch exit line. Inert gas was also piped into the absorber inlet for bed temperature control during regeneration. The complete system was maintained above  $1,000^{\circ}F$  to prevent condensation of the tar which would affect the absorbents or plug the lines to and from the absorber. The absorber contained 73 pounds of 3/16-inch diameter absorbents, composed of 25% iron oxide and 75% fly ash with 3%, by weight, of bentonite added as a binder. A space velocity (scfh gas/cu.ft. absorbent) of 1,900 was maintained throughout the tests.

#### EXPERIMENTAL RESULTS

Four important criteria must be met before an absorbent can be considered optimum for process consideration. The absorbent must be physically strong to withstand handling, loading and cyclic thermal degradation. The absorbent must have the necessary surface area containing iron oxide particles to effectively react with  $H_2S$  and provide enough absorptive capacity for economical operations. The absorbent should be regenerable so that material and replacement costs are at a minimum. Finally, and equally important, the absorbent should have a satisfactory life expectancy.

Absorbents containing additives such as bentonite, sodium silicate and magnesium sulfate were prepared and tested for their effect on physical strength. The addition of bentonite greatly increased both hardness and crushing strength. However, the addition of 3% bentonite caused a sharp decrease in  $H_2S$  absorption capacities. The data, as shown in Table 1, indicate that bentonite does not adversely effect absorption capacity until 1.5% is added and the lesser amounts are effective in providing strength to the absorbent. Sodium silicate also produced an extrudate having a crush strength of approximately 70 pounds per one centimeter length, as opposed to around 16 pounds for an untreated extrudate, without appreciable loss in absorption capacity. On the other hand, the addition of magnesium sulfate decreased the absorption capacity without benefiting the physical strength of the absorbent.

The variables effecting absorption capacity that were tested included porosity, amount of iron oxide contained in the absorbent and steam concentrations of the hot gas being desulfurized. Ten percent, by weight, of ordinary starch was added to and burned out from the fly ash-iron oxide absorbent mixture to determine if additional porosity could be obtained. This absorbent showed nearly twice the absorption capacity of the untreated absorbent; however, it did not develop the crush strength observed earlier with a similar absorbent containing 1% bentonite. After sintering for 2 hours, the absorbent showed a decrease in absorption capacity with very little increase in physical strength.

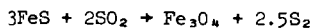
By adding varying amounts of iron oxide mixed with fly ash in preparing an absorbent mixture, it was found that 25% iron oxide with 75% fly ash showed the better absorption capacity. When 33% iron oxide was used, a significant decrease in absorption capacity was noted (2). When 13% iron oxide was used, the same significant decrease was observed. It is believed that particle size distribution of the iron

oxide and fly ash controls this phenomenon. Another disadvantage of higher amounts of iron oxide was the lesser physical strength indicated by noticeable amounts of absorbent degradation during testing while those at lesser percent were quite resistant to degradation.

Abel (2) reported that producer gas containing steam reduced the capacity of the absorbent to react with  $H_2S$ . At  $1,500^\circ F$  the absorption capacity was reduced about 25% in wet (8%) simulated gas. This phenomenon is not surprising since steam is a product of reaction in the absorption of  $H_2S$ . Tests performed under the present investigations using improved absorbents also showed reduced capacity. The water-gas shift reaction,  $CO + H_2O = CO_2 + H_2$ , occurred with the iron oxide-fly ash absorbent bed catalyzing the reaction to show an approximate shift of 2% for  $H_2$  and  $CO_2$ . This effect may be beneficial when the end use is feed stock for a methanation plant since the  $H_2/CO$  ratio is brought closer to the desired 3 to 1 value for the dry  $CO_2$ -free gas.

Regeneration of the sulfided absorbents was accomplished by using air or mixtures of air and nitrogen. Air regeneration at 12 scfh produced bed temperatures of  $1,700^\circ$  to  $1,900^\circ F$  in the zone of regeneration. Lower flow rates reduced temperatures  $100^\circ$ - $400^\circ F$ . Dilution of air with nitrogen had a similar effect.

At  $900^\circ F$  regeneration started immediately and proceeded rapidly, depending on the space velocity, to completion. The higher the rate of air introduction, that is, the greater the flow of oxygen, the higher the temperature of regeneration. The temperature increased and decreased rapidly as the zone of reaction passed through the bed and it was not known how much damage to the absorbent occurred at high temperatures for short durations. It was postulated to be around  $1,800^\circ F$  but a safer long-term maximum temperature for the absorbents should be  $1,500^\circ F$ . The dilution of the air with nitrogen was one method of controlling the maximum bed temperature without losing time in regeneration at lower flow rates. Figure 4 shows a typical temperature profile on regeneration using 12 scfh air flow rate compared with using 12 scfh air and 12 scfh nitrogen or a total of 24 scfh flow rate. Number 1 thermocouple is near the inlet while No. 5 thermocouple is located near the exit from the bed. TC-5 was consistently lower in all regenerations. This was believed to have been caused by the partial regeneration of the bed by unreacted oxygen from the main zone of regeneration with possibly some credit given to the endothermic reaction between  $FeS$  and  $SO_2$ . Elemental sulfur was found in the exit piping and valves. It would be produced according to the following reaction:



Sulfur balances calculated using the  $H_2S$  input versus  $SO_2$  in the outlet gas averaged about 95% recovery as  $SO_2$ . Several batches of regenerated absorbents were analyzed for total sulfur after several cycles of absorption and regeneration and the sulfur content was found to be less than 1%. This would indicate that very little sulfate was formed at the high regeneration temperatures used.

Regeneration was essentially completed in 120 minutes when the air flow rate was 12 scfh. At 6 scfh, regeneration required 190 minutes. A 1 to 1 mixture of air and nitrogen at 24 scfh flow rate required a regeneration time of 150 minutes. Since the normal absorption cycle required about 5 hours, enough time was available to use any of the above flow rates. Aside from critical temperature design criteria, another consideration was the  $SO_2$ -enrichment that was needed for downstream conversion or reduction. The  $SO_2$  concentration in the effluent gas approximated 11½-12% when using air for regeneration; however, when dilution gas was used, the  $SO_2$  concentration was proportionate to the amount of diluent used, being around 5½-6% at 1 to 1 dilution of air with nitrogen. Typical regeneration curves, depicted by Figure 5, showed that maximum  $SO_2$  concentration was reached in less than 5 minutes and dropped from maximum to base line in approximately 20 minutes. These time factors are noted for both air and diluted air regeneration schemes.

The life expectancy of a specific absorbent could only be determined with accuracy by continuous cycling until the absorption capacity dropped below acceptable limits or degradation and fusion caused operational problems. This was costly in terms of money and manpower. However, one absorbent bed has been through 30 absorption-regeneration cycles using simulated producer gas containing both coal-related tars and particulates to study the cyclic effect upon the absorbents. Absorbents used in this study were prepared by adding 10%, by weight, of starch to an absorbent mixture containing 25% iron oxide and 75% fly ash. The absorbent was sintered at 1,800°F for 30 minutes in an oxidizing atmosphere. The producer gas was maintained at 1,100°F throughout the absorption cycle at an average flow rate of 15 scfh. The H<sub>2</sub>S concentration in the inlet gas stream was maintained at 2% and the steam content between 7 and 11%.

Regeneration after each absorption cycle was accomplished by using a 12 scfh air flow rate for approximately 2 hours. The average absorption cycle lasted 5 hours. Figure 3 indicates the absorption capacity of each cycle. The increasing absorption capacity through the first few cycles was believed due to the result of burn-out of the residual starch during regeneration where temperatures approached 1,300°F for short periods. The continuing starch-char burnout would open more pores for better gas penetration to the iron oxide particles in the absorbent. After 30 cycles, the absorbent was in good condition without visible signs of deterioration or caking. Table 2 lists 6 of the 30 runs which were representative of the typical information computed from the raw data obtained during operations.

Abel (2) earlier reported that sintered pellets containing 25% iron oxide and 75% fly ash underwent 174 absorption-regeneration cycles using hot (1,000°-1,500°F), clean simulated producer gas without visible damage to the pellets or appreciable loss in absorptive activity. The absorption capacity averaged 8% for those tests conducted at 1,100°F. The pore volume reached a constant value of 0.12 cubic centimeters per gram after 30 absorption-regeneration cycles.

Four 15-hour absorption runs were completed using a 1,500 scfh sidestream of hot (1,100°F) raw producer gas made by gasifying high volatile bituminous coal with air and steam in a 42-inch stirred, fixed-bed gasifier (7). These runs were made primarily to demonstrate the feasibility of the process at much higher gas flow rates and at actual process conditions. The four 15-hour runs were completed successfully with an average absorption capacity of 8.25 wt.-pct. Ninety to 94% of the H<sub>2</sub>S was removed from the hot producer gas which averaged 0.5% H<sub>2</sub>S entering the absorber. Table 3 shows the data and run conditions for the 4 periods. The absorbents remained in good condition for the duration of the tests and were not adversely affected by the tars and particulates in the effluent gas. The tars could be tolerated if the absorber bed temperature remained above 1,000°F. The fine carbonaceous particulate accumulated in the absorber bed during absorption was burned off during the regeneration cycle. An insignificant amount of ash residue remained in the bed after regeneration which was determined by visual inspection of the bed after completion of the 4 cycles. Pressure drop across the bed increased to 8-9 psig at the end of the absorption periods but returned to 1.5 psig after regeneration of the absorbent bed.

#### CONCLUSION

The laboratory tests conducted thus far indicate that the fly ash-iron oxide absorbent containing bentonite is an adequate absorbent for removing H<sub>2</sub>S from raw producer gas at temperatures between 1,000°F and 1,500°F. The physical strength, expressed as the crush strength (measured across the diameter), of 50 to 100 pounds per one centimeter of length is considered adequate to withstand handling, transportation and placement of the absorbents. The absorbent is regenerable and has an average capacity of 10 wt.-pct. This amount of absorptive capacity coupled with an efficiency of 90-94% permits ample time "on line" and provides an effluent gas which meets the existing environmental air standards.

Thirty and 174 absorption-regeneration cycles were completed without visible deterioration or loss of absorptive capacity. Although not conclusive, these tests indicate that the absorbents could withstand many more cycles. Eventual pore closing by fusion due to long time thermal cycling and/or micron size particulate exposure needs to be investigated further. These two occurrences would be the most likely limiting factors on life expectancy of the absorbents.

Laboratory work is now being performed to find a suitable substitute for the fly ash so that higher temperatures and faster regeneration would be permissible. Finding cheaper sources of iron oxide and comparing results of these oxides should be investigated so that availability of iron oxide would be assured. Finally, a pilot plant hot gas cleanup facility should be operated so that its feasibility for commercial application would be demonstrated along with hardware development and scale-up design criteria established.

## REFERENCES

1. Reeve, L. Desulfurization of Coke-Oven Gas at Appleby-Frodingham. *J. Inst. Fuel*, vol. 31, No. 210, July 1958; pp. 319-324.
2. Abel, W. T., F. G. Shultz, and P. F. Langdon. Removal of Hydrogen Sulfide from Hot Producer Gas by Solid Absorbents. BuMines RI 7947; 1974, 23 pp.
3. Shultz, F. G. Removal of Hydrogen Sulfide from Simulated Producer Gas at Elevated Temperatures and Pressures. Proc. 2d International Conf. on Fluidized-Bed Combustion, Hueston Woods State Park, College Corner, Ohio, Oct. 4-7, 1970. U.S. Environmental Protection Agency, Office of Air Programs, 1972, pp. III-5-1--III-5-5.
4. Clay, D. T. and Scott Lynn. Iron-Catalyzed Reduction of NO by CO + H<sub>2</sub> in Simulated Flue Gas. General Motors Symposium on NO Reduction, Oct. 7-8, 1974.
5. Belt, R. J. and M. M. Roder. "Low Sulfur Fuel by Pressure Entrainment Carbonization of Coal," Chap. 11, pp. 121-134, *Pollution Control and Energy Needs*, R. M. Jameson and R. S. Spindt, *Advances in Chemistry Series 127*, ACS, Washington, D. C., 1973.
6. Altieri, V. J. *Gas Analyses and Testing of Gaseous Materials*, American Gas Assoc., New York, 1st Edition, 1945, pp. 339-340.
7. Oldaker, E. C., A. M. Poston, and W. L. Farrior. Removal of Hydrogen Sulfide from Hot Low-Btu Gas with Iron Oxide-Fly Ash Sorbents. MERC/TPR-75/1, Feb. 1975.

TABLE 1. - Effect of Bentonite on Absorption Capacity of Fly Ash-Iron Oxide Absorbent Using Apparatus Shown in Figure 1

Bentonite, percent	Gas flow rate, std. cu.ft./hr.	Run duration, hr.	Space velocity, vol/vol/hr	H <sub>2</sub> S absorption		
				Total, grains	Capacity wt.-pct.	Total absorbed, pct.
0.5	17.19	4.11	510	1290	11.94	96.3
1.0	15.30	5.75	454	1265	11.70	96.6
1.5	14.27	4.52	423	1134	10.5	97.2
3.0	17.58	3.15	521	678	6.28	94.1

Absorption temperature -- 1,100°F  
 Saturation point -- 400 grains/100 scf  
 Weight of absorbent -- 700 grams

TABLE 2. - Typical Data from Six of Thirty Absorption Capacity Tests (Figure 1) Using Same Fly Ash-Iron Oxide Absorbent Containing 10 Percent Starch

Gas flow rate, std. cu.ft./hr.	Run duration, hr.	Space velocity, vol/vol/hr	H <sub>2</sub> S absorption			Total quantities through bed	
			Total grains	wt.-pct.	Efficiency pct.	Tar, gms	Dust, gms
14.27	6.28	501	1118	10.35	92.5	31.5	.2
15.97	5.75	563	1193	11.04	95.0	30.8	.6
16.37	5.75	570	1180	10.92	93.5	28.2	.4
16.38	5.50	587	1135	10.51	93.1	33.5	.5
15.23	6.00	529	1159	10.73	94.2	32.3	.5
15.09	7.25	549	1332	12.33	92.2	33.4	.5

Absorption temperature -- 1,100°F  
 Saturation break-through point -- 400 gr/100 scf  
 Weight of absorbent -- 700 grams

TABLE 3. - Run Data Obtained During Four Absorption Periods Using Raw Producer Gas from MERC Producer (Figure 2)

	Run 1	Run 2	Run 3	Run 4
Volume of bed, cubic feet	0.785	0.785	0.785	0.785
Weight of absorbents, pounds	73	73	73	73
Gas flow rate, scfh	1,500	1,500	1,500	1,500
Space velocity, $\frac{\text{scfh}}{\text{cu. ft. absorbent}}$	1,910	1,910	1,910	1,910
Duration of run, hours	15.87	9.78	14.50	10.75
Inlet steam concentration, percent	8.5	3.3	3.1	6.3
Bed temperature, °F	1,085	1,085	1,085	1,085
Absorption capacity, weight-percent	9.19	6.17	8.35	9.29
H <sub>2</sub> S absorbed, grains	46,950	31,532	53,624	47,450
H <sub>2</sub> S absorbed when 150 grains = point of saturation, percent	83	83	81	86
-----				
H <sub>2</sub> S absorbed if 50 grains = point of saturation, percent	92.9	91.4	90.7	94.2

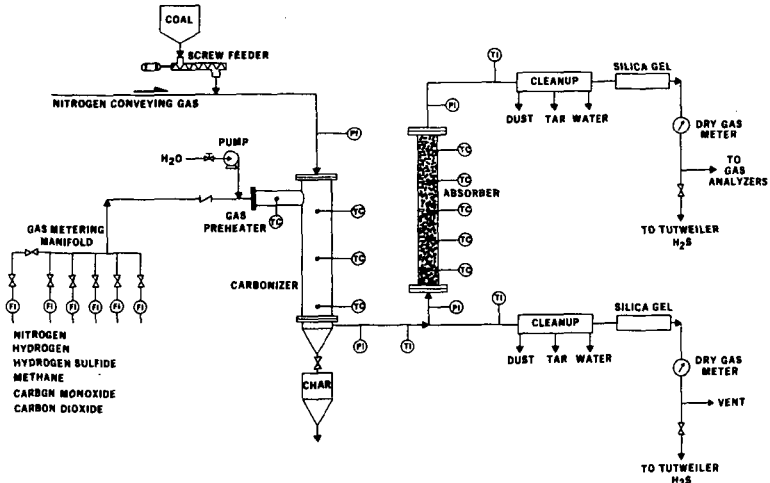


Figure 1. - Flow Diagram of Apparatus for Measuring Absorption Capacity

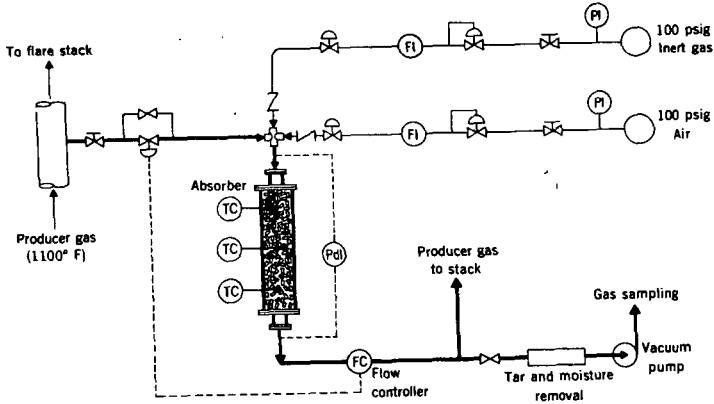


Figure 2. - Flow Diagram of Apparatus for Testing Solid Absorbents Using Hot Producer Gas

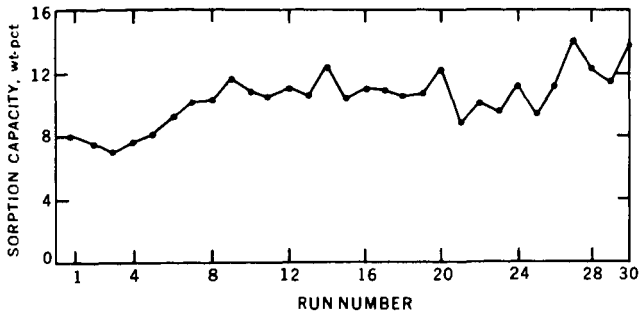


Figure 3. - Absorption Capacities Achieved During Thirty Absorption-Regeneration Test Runs Using the Same Absorbent, with Operating Conditions Listed in Table 2

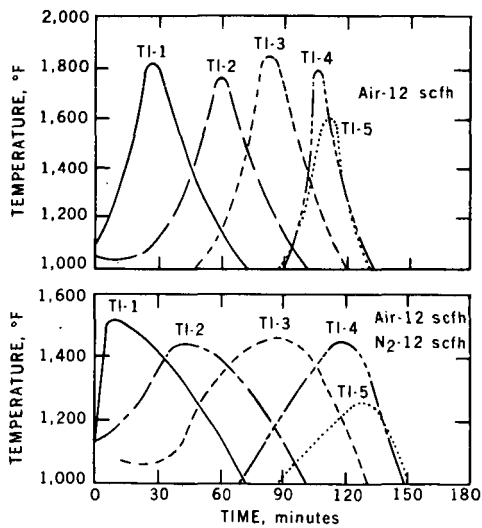


Figure 4. - Comparison of Bed Temperature Profiles With and Without Dilution Gas for Regeneration of Sulfided Absorbents

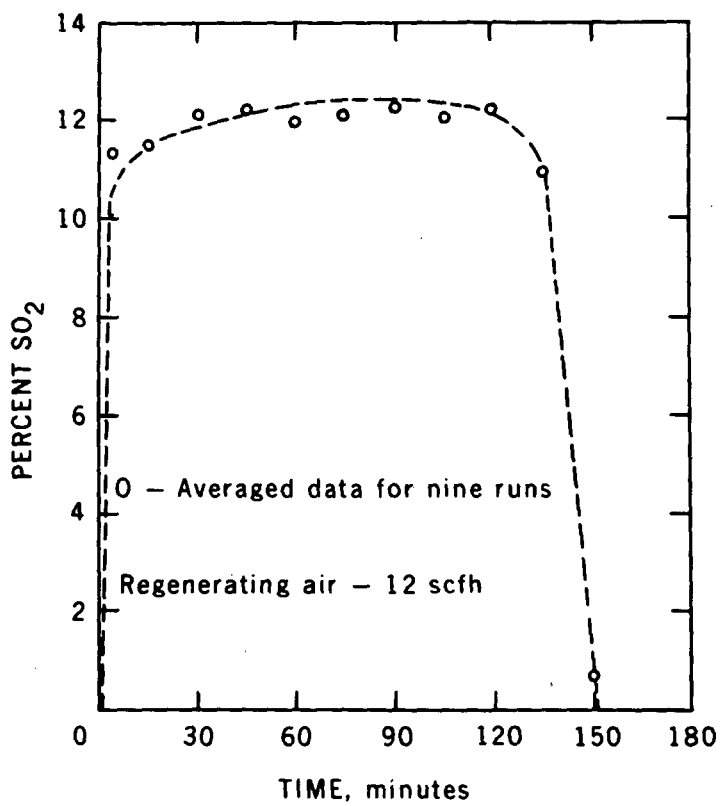


Figure 5. - Typical Curve Showing SO<sub>2</sub> Concentration in the Effluent Gas During Regeneration of the Sulfided Absorbents

INVESTIGATIONS ON THE REMOVAL OF HYDROGEN  
SULFIDE AT HIGH TEMPERATURE FROM COAL GAS

Keshava S. Murthy

Battelle's Columbus Laboratories  
505 King Avenue  
Columbus, Ohio 43201WHY HOT-GAS CLEANUP?

At current consumption levels, proven U.S. natural gas reserves are estimated to last 8 years.<sup>(1)\*</sup> Gasification of oils with negligible sulfur content is not feasible since the U.S. oil supply, slowly dwindling, is sufficient for only 10 years.<sup>(1)</sup> Thus, if continued gas supply is desired, coal gasification may be the only immediately feasible alternative.

Lurgi and Kopper-Totzek (K-T) gasifiers are among the older commercially proven processes. The Lurgi process produces low- or medium-Btu gases contaminated with varying amounts of sulfur compounds such as hydrogen sulfide (H<sub>2</sub>S) and carbonyl sulfide (COS). The Lurgi gas is at a higher pressure (350 psi) and lower temperature (750 to 1100 F depending on coal type) than K-T gas which is at 1 atmosphere and 2500 F. Both processes produce gas with a heating value (HHV) of 300 Btu/scf when using oxygen. The Lurgi process can also produce a 180 Btu/scf gas when air blown.

These medium- and low-Btu gases can be used in many ways. The high-pressure-low-temperature Lurgi gas, after removal of its H<sub>2</sub>S, tar, and dust content is well suited for synthesis of methane to produce substitute natural gas (SNG). Also, because of its high pressure, the gas can be desulfurized by any of the established wet processes, although this requires cooling the gas to 200 F or -50 F, depending on the liquid scrubbing process chosen. In contrast, if the gas is desulfurized and cleaned until free of particulates at close to the gasifier exit temperature, the sensible heat of the gas can be utilized to efficiently generate electric power in a combined-cycle power plant or to avoid the large heat-exchange hardware requirements in a SNG production scheme.

The K-T gas, at atmospheric pressure and 2500 F, needs compression to 450 psig and cooling before the wet desulfurization and subsequent methanation steps if SNG is the desired product. The prior compression and cooling may be less attractive compared with the direct utilization of the K-T gas in a power plant boiler if a means can be found to desulfurize and clean the crude gas at near gasifier exit temperature. In the latter event, the sensible heat of the medium-Btu gas (45 Btu/scf or 15 percent of its heating value) could be usefully employed. The K-T gasifier can gasify any type of solid fuel (caking coals, chars, petroleum coke, tar, oils, and slurries) and has quick startup and shutdown capabilities. The K-T gasifier is expected to be a suitable source of fuel gas to many power plants in western United States now using natural gas; the retrofit difficulties are estimated to be minimal. If the electric utility industry and other industrial markets now using over 65 percent of the natural gas supply convert to low-Btu gas, about 5 trillion cu ft (35 percent) of natural gas would be freed for other uses.<sup>(1)</sup>

Doubtless, the K-T gasifier--hot-gas-cleanup approach needs to compete with the emerging flue-gas desulfurization (FGD) processes which permit the use of sulfur containing coal. Currently, the FGD processes generate large volumes of secondary wastes, including sludges and liquid purge streams. A detailed evaluation of FGD versus the K-T gasifier--hot-gas-cleanup system may demonstrate the latter

\* References are listed at the end.

approach to be favorable, since it does not produce significant secondary wastes; the choice could be largely site specific.

If hot-gas-cleanup systems can be developed to remove sulfur compounds in crude gases, to less than the 0.1-ppm level, they may also be applicable to the SNG production processes. Significant savings appear possible by eliminating the cooling step or minimizing the degree of cooling and heat exchange.

The above arguments suggest that the development of a hot desulfurization process has merit. Also, as evidenced in the development of FGD processes and their wide but slow acceptance, a factor that favors the development of new systems is that when a well-proven system exists, the best use will be made of it. The Energy Research and Development Administration (ERDA) has been investigating hot-gas  $H_2S$ -removal techniques since 1967.<sup>(2)</sup> Others independently involved in the study are the University of Kentucky (since 1972), Air Products and Chemicals, Inc., and Conoco. Battelle's work began in 1974 as a result of funding under the Battelle Energy Program\* initiated early in 1973. This paper describes the results of the Battelle investigations on the development of sorbents for removal of  $H_2S$  at high temperature from coal gases.

#### EXPERIMENTAL FACILITY

The Battelle experimental facility is presented in Figure 1. It consists of a gas-mixing section, a preheater, and a fixed-bed tubular glass reactor. Both the reactor and preheater operate in the range 100 to 1800 F, and precise control of temperature of the gas and sorbent bed is possible. The preheater and reactor used are made of clear quartz tube, 50-mm ID. Quartz was chosen after stainless steel reactors (Types 304 and 446) were found to react severely with  $H_2S$ . No particular hazard was observed with the operation of the unit when the gases were properly scrubbed and vented.

#### EXPERIMENTAL PROCEDURES

Certified standard gas mixtures\*\* were used to obtain simulated coal gas of the following composition in volume percent:  $H_2$ , 17; CO, 26.0;  $CO_2$ , 5.0;  $N_2$ , 50.5; and  $H_2S$ , 1.5. The large amount of nitrogen suggests simulation of a low-Btu gas obtained by air-blown process. The gas does not resemble any actual producer gas exactly; the  $H_2S$  content is rather high and also free of the usual moisture, tar, and dust present in actual coal gases. The rationale for choice of this composition was that Battelle studies were designed to generate data for comparison with the results of ERDA studies.<sup>(2)</sup> A gas chromatographic analysis confirmed that actual gas composition was close to the desired values. Matheson flow controllers were helpful

---

\* Research described here was supported by The Battelle Energy Program (BEP). The Program has been established to carry out major R&D efforts aimed at developing practical solutions to some of the extremely serious energy shortage and utilization problems expected to exist in the United States during 1975-1995. Battelle Memorial Institute has allocated millions of its own funds to support this effort because of the importance of the energy problem to the nation. The primary emphasis of BEP is on the development of coal as a clean fuel source since coal holds the greatest promise for filling the gap between the U.S. energy requirements and the ability to meet these requirements in the time period of interest. Additional energy sources being investigated under the program include solar energy.

\*\* Matheson Gas Products, Joliet, Illinois, was the vendor.

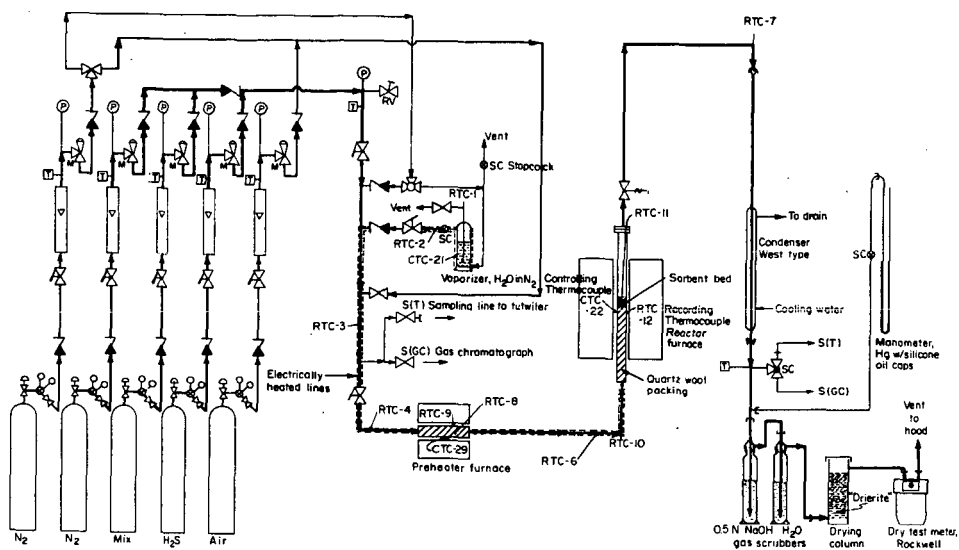


FIGURE 1. FLOW DIAGRAM OF THE HIGH-TEMPERATURE H<sub>2</sub>S-REMOVAL ASSEMBLY

in maintaining flow accuracy and precision to within  $\pm 3$  percent on the total flow.  $H_2S$  was fed as a 25 percent gas mixture in nitrogen and the  $H_2S$  in test gas was 950 grains/100 scf with a precision of  $\pm 10$  grains.

$H_2S$  in the inlet and outlet streams was measured by the Tutwiler method.<sup>(3)</sup> The method consists of grab sampling 100 cc of the gas in a glass bulb connected to a burette containing standard iodine solution. The gas, collected over starch solution, is titrated with the iodine to a blue end point. Each milliliter of the iodine solution (prepared by diluting 13.5 ml of 0.1 N solution to 100 ml with distilled water) is equivalent to 100 grains of  $H_2S$ /100 scf of gas. The method can detect  $H_2S$  as low as 2 grains/100 scf of gas, or  $3\frac{1}{2}$  ppm of  $H_2S$ .

The quartz preheater and reactor were packed with quartz wool to provide a heat-transfer surface. The test sorbent, 100-gram charge, was supported on a honeycomb structure made of quartz tube to provide even gas distribution. The sorbent bed was located  $\pm 2$  inches about the center of the reactor's length. The thermocouple tip was about 0.5 cm above the bed. The temperature profile through the bed indicated that the bed was nearly uniform in temperature, and the gas entered and exited the bed at nearly the reaction temperature. A 12-point recorder provided temperature read-out.

To insure a proper basis for comparison of results on sorbent performance, the experiments were performed at uniform operating conditions (1500 F reaction temperature, cold gas flow of 1 liter/min. at 70 F and 14.7 psia and 950 grains  $H_2S$ /100 scf). The cold-space velocity was 600 gas volumes per volume of bed per hour, equivalent to an operating GSV of 2000 V/V/hr varying slightly with bed volume. The acceptance run was terminated when the outlet-gas  $H_2S$  concentration approached 100 grains at an inlet-gas  $H_2S$  content of 950 grains. The regeneration run was ended when the sulfur dioxide in the regenerator gas dropped from 6 volume percent to 0.05 percent. Sulfur dioxide was also measured by the Tutwiler method. After one cycle of acceptance and regeneration, the sorbent was subjected to sieve analysis to determine attrition.

#### SORBENT PREPARATION

Sorbents were prepared utilizing CP or reagent-grade chemicals. These, as dry powder (-200 U.S. sieve), were weighed and mixed together with 1 gram each of starch, bentonite, and sodium silicate per 100 grams of the mixture. The resulting mix was made into a paste with distilled water. The paste was either pelletized or extruded. The pellets, after oven-drying at 250 F, were sintered at 1800 F (or 1600 F) for 2 hours. The sintered pellets were screened to -6 + 10 U.S. sieve mesh. The extrudates (1/8 inch in diameter and about 1/4 inch long) were also dried and sintered similarly and screened to remove all minus 10-mesh particles. The sorbent was free flowing and reasonably strong. The average density was about 0.9 cc/g.

#### EXPERIMENTAL RESULTS AND DISCUSSION

As a first step, five blank runs were performed with test gas. The reactor was not charged with sorbent. Results with Type 304 stainless steel and other reactor materials (Table 1) show that stainless steels are unsuitable as experimental reactors but that quartz resists  $H_2S$  attack satisfactorily. The steel reactor walls flaked off and thermocouple wells were damaged by corrosion.

TABLE 1. TEST RESULTS WITH BLANK REACTOR

Parameter	Stainless Steel		Quartz
	Type 304	Type 446	
Diameter (ID), inches	1.26	2.0	2.1
Length of Hot Zone, inches	16.0	16.0	16.0
Gas Flow Rate			
At 70F, 1 Atm, cm <sup>3</sup> /min	750	750	1000
H <sub>2</sub> S absorbed, percent			
At 1000 F	15 <sup>(a)</sup>	8	0
At 1500 F	90	90	5
Test Duration, hours			
At 1000 F	15	8	3
At 1500 F	27	10	4

- (a) During the first 11 hours, the removal was 99.5 percent; a gradual drop to 15 percent occurred in the next 4 hours. At 1500 F, no significant reduction in removal was observed.

### H<sub>2</sub>S Acceptance Experiments

With the quartz reactor (using quartz thermocouple wells), 21 experiments were conducted to study the H<sub>2</sub>S acceptance-regeneration characteristics of the 11 sorbents listed in Table 2. The USBM sorbent was provided by the Morgantown Energy Research Center (MERC).<sup>\*</sup> The fly ash used in the sorbent contained approximately 52 percent SiO<sub>2</sub>, 25 percent Al<sub>2</sub>O<sub>3</sub>, 15 percent Fe<sub>2</sub>O<sub>3</sub>, with the remainder being CaO, MgO, K<sub>2</sub>O, etc.<sup>(4)</sup> This sorbent was studied in four experiments to establish baseline performance data at 1500 F, since the reported desulfacity<sup>\*\*</sup> results obtained with stainless steel reactors<sup>(2)</sup> were suspected to be too high.

A comparison of data reported by USBM (now ERDA) with those obtained in BCL studies (Table 3) for three sorbents, including fly ash--iron oxide sorbent, indicates that the influence of H<sub>2</sub>S uptake by the reactor at 1500 F is a significant factor in the reported desulfacity results. Contrary to a reported increase in desulfacity at higher temperature, the BCL data establish that a significantly higher H<sub>2</sub>S removal occurs at 1000 F than at 1500 F. Thermodynamic considerations support these data in that the predicted equilibrium conversion is high (approaching 100 percent) at temperatures of 1000 F and higher. This is modified by the fact that the reaction is exothermic, hence lower temperatures permit actual realization of the predicted high conversion.<sup>(5)</sup>

The data in Table 3 also indicate a significantly low exit H<sub>2</sub>S concentration for all sorbents containing component X (used in BCL sorbents) at all temperatures. Also, BCL experiments show that pure iron oxide at 1000 F permits a very low exit-H<sub>2</sub>S concentration. In certain applications of coal gas, the low H<sub>2</sub>S level may be an advantage. A graphical comparison of the low exit H<sub>2</sub>S concentration of various sorbents is presented in Figure 2.

### Regeneration Results

A comparative plot of the regeneration curves of various sorbents is presented in Figure 3. All of these experiments were performed at uniform conditions of 1 liter/minute of air inflow at 70 F, 1 atm, and 1000 F sorbent bed temperature. The data do not provide conclusive evidence on comparative regeneration characteristics of the sorbents. This indicates that the need for further experimentation is more pronounced in the area of regeneration than in the area of H<sub>2</sub>S acceptance. The major ambiguity is in reference to Curves 5 and 6 for the regeneration of sorbent BCL 29 E. These two curves, which should have been closely similar because of replication of the same experiment, are obviously very different. However, while the sorbent in Curve 5 was regenerated immediately after the end of the acceptance run (with no overnight cooling of the sulfided sorbent), the sorbent in Curve 6 was cooled overnight between the acceptance and regeneration runs. Neither of these occurrences was deliberate.

Although the reasons for the superior regeneration characteristics of Curve 5 are not clear, this curve represents a desirable regeneration trend. The 3 percent SO<sub>2</sub> in exit gas for over 5 hours followed by a sudden concentration drop should help in further processing of the SO<sub>2</sub>-bearing gas to either sulfuric acid or sulfur. The sulfur balance, based on 23.7 grams of H<sub>2</sub>S absorbed by the sulfided

\* Courtesy of Ernest Oldaker, MERC, ERDA, Morgantown, West Virginia.

\*\* Desulfacity is defined as grams of H<sub>2</sub>S removed from the gas by 100 grams of sorbent charge, or weight percent H<sub>2</sub>S-removal capacity either at breakthrough or when exit gas H<sub>2</sub>S concentration reaches 100 grains/100 scf.

TABLE 2. LIST OF SORBENTS STUDIED

Sor bent Designation	Size	
	Pellet -6+10 U.S. Sieve	Extrudate, 1/8" Diam., 1/4" Long
USBM #0074*		3/16" diam. x 1/2" long
BCL #8WB**	X	
BCL #20	X	
BCL #20E		X
BCL #21	X	
BCL #23	X	
BCL #25E		X
BCL #26E		X
BCL #27E		X
BCL #28E		X
BCL #29E		X

\* U.S. Bureau of Mines Sorbent Batch No. 0074 contains 75 percent fly ash and balance iron oxide.

\*\* BCL (Battelle Columbus Laboratories) Sorbents. The composition of these Sorbents are withheld for proprietary reasons.

TABLE 3. COMPARISON OF DATA ON DESULFURIZATION\* (Weight Percent) AND CONCENTRATION OF H<sub>2</sub>S IN REACTOR EXIT GAS

Sorbent	USBM Reported Data in Stainless Steel Reactor (2), weight percent	BCL Data From Quartz Reactor, weight percent	H <sub>2</sub> S in Exit Gas, (BCL Data) grains/100 scf
USBM #0074			
At 1000 F	8.7	No data	No data
At 1500 F	41.1	19.0	22.5
BCL SWB			
At 1000 F	22	26.3	4.4
At 1500 F	Bed plugged	19.2	21.6
BCL 29E Extrudates**			
At 1000 F	Not studied	22.2	10.2
At 1500 F	Not studied	17.2	12.0
BCL 20			
Pellets, 1500F**	Not studied	21.9	8.3
Extrudates, 1500F	Not studied	21.0	10.0
BCL 21			
(Pure Component X), 1500 F	Not studied	21.0	8.0

Note: All the BCL experiments were conducted under nearly identical conditions: 1000 scf cm/min of gas flow at 70 F, atmosphere pressure, inlet H<sub>2</sub>S of 950 grain/scf, 100 grams of sorbent charge, and excellent temperature control.

\* Grams H<sub>2</sub>S removed by 100-g sorbent charge; see full definition on Page 6.

\*\* Both these sorbents contain Component X.

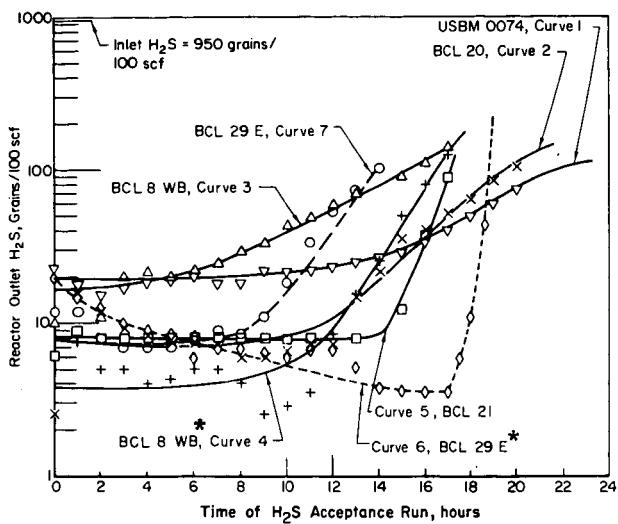
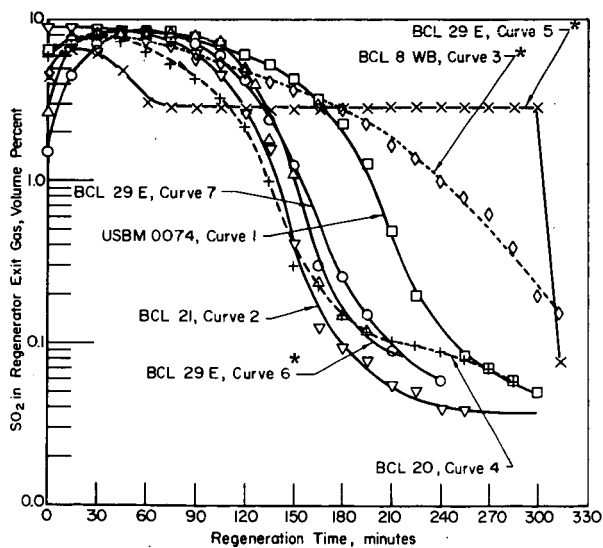
FIGURE 2.  $H_2S$  - ACCEPTANCE CURVES

FIGURE 3. SORBENT REGENERATION CURVES

\* For these runs,  $H_2S$  acceptance temperature was 1000 F, while for the remaining, it was 1500 F. All regeneration runs were done at 1000 F. Gas and air flow rates and all other conditions were the same for all runs shown here. Also, Regeneration Curves 5 and 6 are discussed on Page 6.

sorbent, indicates that 80 percent of the sulfur absorbed is accountable in the regenerator exit gas as  $\text{SO}_2$ . Also about 0.25 gram of sulfur was formed during regeneration, thus accounting for another 1 percent of the sulfur.

Sulfur balance calculations for Curve 1 (USBM 0074) show that 85 percent of the sulfur absorbed was accountable as  $\text{SO}_2$  in the regenerator exit gas. The formation of sulfur in the case of the sorbent represented by Curve 5 needs further evaluation to determine whether direct sulfur formation is possible during regeneration.

#### Studies on Sorbent Attrition

In an actual commercial processing scheme, sorbent attrition is an important property contributing to the rate of sorbent makeup required. If attrition occurs during  $\text{H}_2\text{S}$  removal, the coal gas will carry additional particulate load which may interfere with the utilization of the gas. Ideally, an attrition loss of zero is desirable. However, catalyst attrition-loss rates of 0.3 wt %/hr (0.09 lb/bbl feed) in fluidized-bed cracking are known to be tolerable. In high-temperature coal gas desulfurization, an attrition loss of, say, 1.0 lb/million scf of gas treated\* may be perhaps tolerable. It appears preferable that such loss occur during regeneration.

In the experiments reported here, the sorbents (fresh and after one cycle of acceptance-regeneration) were subjected to sieve analysis. The results are summarized in Table 4. Pure  $\text{Fe}_2\text{O}_3$  and pure Component X disintegrate as well as agglomerate, as the data show. However, when the two are mixed, there is neither disintegration nor agglomeration. The USBM sorbent showed considerable particle disintegration and flake formation on the extrudates. In the case of sorbent BCL 29 E, the fines formed in Experiment 36 were very high, while in Experiment 37, a replicate, no fines were formed at all. This could probably be due to the overnight cooling of the absorbed sorbent before regeneration in Experiment 37, whereas in Experiment 36, there was no time lag between the acceptance and regeneration runs. Once again these data indicate the need for further studies of the regeneration mode. The strength of sorbent BCL 20 appears better in comparison with that of most other sorbents.

#### $\text{H}_2\text{S}$ -Acceptance Thermodynamics

The performance of the mixture of  $\text{Fe}_2\text{O}_3$ -Component X is enhanced over the performance of individual components, particularly in regard to physical strength. While this is an accidental discovery, the actual reasons are speculative and Component X may be a stabilizing agent. The partial pressure of  $\text{H}_2\text{S}$  in the exit gas stream is lower for the mixture than for both pure  $\text{Fe}_2\text{O}_3$  and fly ash- $\text{Fe}_2\text{O}_3$  sorbent formulations.

The reaction mechanism of  $\text{H}_2\text{S}$  with Component X is not understood. Also free-energy data for component X are not available to compute equilibrium conversions. Experimental data at 1500 F show that the equilibrium conversion of  $\text{H}_2\text{S}$  with Component X is higher than with  $\text{Fe}_2\text{O}_3$ ; however, the effect of steam on  $\text{H}_2\text{S}$  conversion with Component X cannot be predicted, and actual experiments are needed to obtain the data.

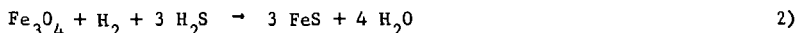
For  $\text{Fe}_2\text{O}_3$ , considerable thermodynamic data are available. According to ICI, fresh iron oxide ( $\text{Fe}_2\text{O}_3$ ) is converted to  $\text{Fe}_3\text{O}_4$  in the presence of hydrogen above 350 F.<sup>(6)</sup> Thus, in the range of 650 to 1500 F,  $\text{Fe}_3\text{O}_4$  is the sorbent.

\* At 10 wt % desulfuricity, for an inlet gas containing 280 grains/100 scf  $\text{H}_2\text{S}$  (0.45 vol %) this is equivalent to an attrition loss of 0.025 wt % per cycle.

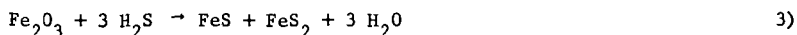
TABLE 4. SIZE ANALYSIS OF SELECTED SORBENTS TESTED

Average Particle Size	Grams of Sorbent in Size Mentioned													
	18, 23		20, 24		27, 28		29, 30		31		36		37	
	USBM	BCL	USBM	BCL	USBM	BCL	USBM	BCL	USBM	BCL	USBM	BCL	USBM	BCL
	0074	0074E	20	20E	21	21	26E	26E	29E(1)	29E(1)	36	36	37	37
<u>Fresh Sorbent</u>														
Pellet, 2680 $\mu$	100	100	100	--	100	--	100	--	100	--	--	--	--	--
Extrudate, 1/8" x 1/4" long	--	--	--	100 <sup>(5)</sup>	--	--	100	--	100	--	100	100	100	100
<u>Sorbent After Test Run</u>														
Total weight, all fractions	98.0	98.0	100.6	108.7	107.2	108.9	101.9	101.9	107.4	107.4	107.4	107.4	109.0	109.0
>2680 $\mu$ (agglomeration)	48.5	6.7	0	2.5	0	26.1	0	0	0	0	0	0	0	0
2680 $\mu$	38.1	78.3	98.6	102.8	106.9	44.5	100.4	100.4	31.0	31.0	31.0	31.0	107.9	107.9
1420 $\mu$	6.8	3.0	0.3	2.8	0.3	6.8	0.2	0.2	18.8	18.8	18.8	18.8	0.9	0.9
570 $\mu$	2.3	8.8	0.7	0.5	0	11.7	0.2	0.2	25.2	25.2	25.2	25.2	0.1	0.1
200 $\mu$	1.8	0.8	0.7	0.1	0	19.4	1.0	1.0	22.6	22.6	22.6	22.6	0.1	0.1
75 $\mu$	0.5	0.3	0.3	0	0	0.4	0.1	0.1	7.7	7.7	7.7	7.7	0	0
40 $\mu$	0	1.0	0.0	0	0	0	0	0	2.1	2.1	2.1	2.1	0	0
Fines formed ( $\leq 570$ )	4.6	10.9	1.7	0.6	0	31.5	1.3	1.3	57.6	57.6	57.6	57.6	0.2	0.2
Fused particles (>2680)	48.5	6.7	0	2.5	0	26.1	0	0	0	0	0	0	0	0
Finger crushing strength <sup>(3)</sup>	P	S	E	G	G	P	G	G	G	G	G	G	G	G
Free flowing tendency	S	S	G	G	E	P	E	E	E	E	E	E	E	E
Flaking tendency <sup>(4)</sup>	None	None	High	None	None	None	None	None	None	None	None	None	None	None

(1) Run 36 and 37 are same except for the difference in regeneration quality described before.  
 (2) A test run includes one cycle of one acceptance run and one regeneration run.  
 (3) P = poor, S = satisfactory, G = good, E = excellent.  
 (4) Flaking is observable only on extrudates. The extrudates were covered with thin flakes.  
 (5) 3/16-inch diameter and 1/4-inch long extrudates.



According to this reaction, each mole of  $\text{Fe}_2\text{O}_3$  reacts with 2 moles of  $\text{H}_2\text{S}$ ; the theoretical desulfacity is 40 percent by weight. However, USBM reports that the following reaction takes place:



on this basis the desulfacity of  $\text{Fe}_2\text{O}_3$  would be 60 percent by weight. The amount of water evolved by either reaction is the same. Actual experimental data on the fly ash +  $\text{Fe}_2\text{O}_3$  sorbent (64 grams  $\text{H}_2\text{S}$  removed per 100 grams  $\text{Fe}_2\text{O}_3$ ) support the USBM reaction mechanism (2) which can be utilized for computing the equilibrium conversions.

For Reaction 3), the standard free-energy change ( $\Delta F^\circ$  at 25 C and 1 atmosphere) is -26,270 cal/g-mole. Thus, the equilibrium constant

$$K = \exp\left(\frac{-\Delta F^\circ}{RT}\right) = 1.85 \times 10^{19} \text{ at } 25 \text{ C.}$$

K at 1000 F (537 C) can be computed using the equation

$$\frac{d \ln K}{dT} = \frac{\Delta H^\circ}{RT^2},$$

where  $\Delta H$ , the heat of reaction can be shown to be substantially constant over the temperature range under study. Thus,

$$K_{1000 \text{ F}} = 8.6 \times 10^9.$$

The high K value indicates that conversions are very high and approach 100 percent. These reactions are heterogeneous and the change in number of moles of gas is zero. Therefore, there should be no effect of pressure on conversion.

The above calculations for  $\text{Fe}_2\text{O}_3$  also hold for other dry oxides. Thus,  $\text{BaO}$ ,  $\text{CaO}$ ,  $\text{CoO}$ ,  $\text{Cu}_2\text{O}$ ,  $\text{Na}_2\text{O}$ ,  $\text{NiO}$ , and  $\text{ZnO}$  all show high equilibrium conversions. Two oxides ( $\text{MgO}$  and  $\text{ZrO}_2$ ) show positive standard free-energy changes, indicating thermodynamic infeasibility. Regeneration (reaction with oxygen) of the sulfides of all these sorbents is thermodynamically feasible.

#### Effect of Steam on Conversion

Coal gases usually contain steam, at least 10 percent by volume. Since steam is a product of the reaction of oxides with  $\text{H}_2\text{S}$ , the presence of steam in feed gas can reduce  $\text{H}_2\text{S}$  conversion. For the iron oxide sorbent, calculations show that at 1000 F ( $K = 8.6 \times 10^9$ ), for a gas containing 5000 ppm  $\text{H}_2\text{S}$  and 10 percent steam, the equilibrium  $\text{H}_2\text{S}$  content in exit gas is 4.6 ppm based on the USBM reaction mechanism. If the ICI reaction is used, the equilibrium  $\text{H}_2\text{S}$  in exit gas is >300 ppm. These calculations cannot be made for Component X since thermodynamic data are not available. Further, the behavior of a mixture of materials reactive with  $\text{H}_2\text{S}$  as a sorbent in presence of steam is more complex than thermodynamics can predict.

### A CONCEPTUAL PROCESSING SCHEME

It is important not only to have a good sorbent but also a processing scheme in which it can be used. Many processing schemes can be visualized to desulfurize hot coal gases. One such scheme is presented in Figure 4. The sorbent (pellets or extrudates) moves at a slow rate in a moving bed and discharges into a fluidized-bed regenerator. Air acts as the fluidizing medium and supplies the oxygen for the sulfide oxidation. The scheme has the advantages of a continuous process but reduces attrition problems during H<sub>2</sub>S removal. Thus, no dust particles are introduced into the hot gas stream. This scheme is intended mainly for atmospheric pressure gases like K-T gas. The design of the H<sub>2</sub>S-acceptance zone can be critical to the successful performance of the process.

### CONCLUSIONS

A good desulfurizing sorbent should regenerate well, have a long life (activity) and high desulfacity. The SO<sub>2</sub> concentration in regenerator exit gas should be high with a sharp breakthrough. Also, the equilibrium H<sub>2</sub>S concentration in exit gas during acceptance should be low, even in the presence of steam in feed gas. The attrition resistance should be high.

The fly ash--Fe<sub>2</sub>O<sub>3</sub> sorbent did not show as good a resistance to attrition as BCL 20 sorbent. The BCL 20 sorbent showed lower exit equilibrium H<sub>2</sub>S concentration and performed better at 1000 F than at 1500 F. The superior performance at lower temperature is in accordance with the thermodynamic rule that for exothermic reactions, the attained equilibrium conversion is higher at lower temperature. The addition of Component X improved the sorbent composition.

In conclusion, in this study, an effort has been made to define properties of a good sorbent, develop such a sorbent and conceptualize a processing scheme for its use. The commercial feasibility of the process can be demonstrated by using the sorbent in such a scheme over a number of acceptance-regeneration cycles. The following recommendations are made toward achieving that end.

### RECOMMENDATIONS

The use of high-temperature H<sub>2</sub>S removal technology should be investigated for the following cases.

- Low-Btu gasification and gas utilization in electric power plants
- Packaged coal-gasification plants (medium- and low-Btu gases)
- Synthetic natural-gas production.

High-temperature H<sub>2</sub>S removal is a novel technology with good potential to compete with other desulfurizing processes. An overall process engineering and economic study of the novel technology vis-a-vis other processes (like Rectisol) is needed. Also needed is an experimental program to develop solid sorbents that can remove H<sub>2</sub>S to less than 1-ppm levels. Both the Process engineering/economics study and the experimental program to screen sorbents should proceed concurrently. Intense efforts are needed to explore the full potential of this emerging technology and measure its impact on the national energy needs.

### ACKNOWLEDGEMENTS

This work was supported by the Battelle Energy Program (BEP). The encouragement and cooperation of Dr. Frank G. Dawson and Mr. Jack G. Conner of BEP and Mr. Herman Feldmann, Dr. James E. Flinn, and Dr. Edward W. Ungar of BCL are sincerely appreciated.

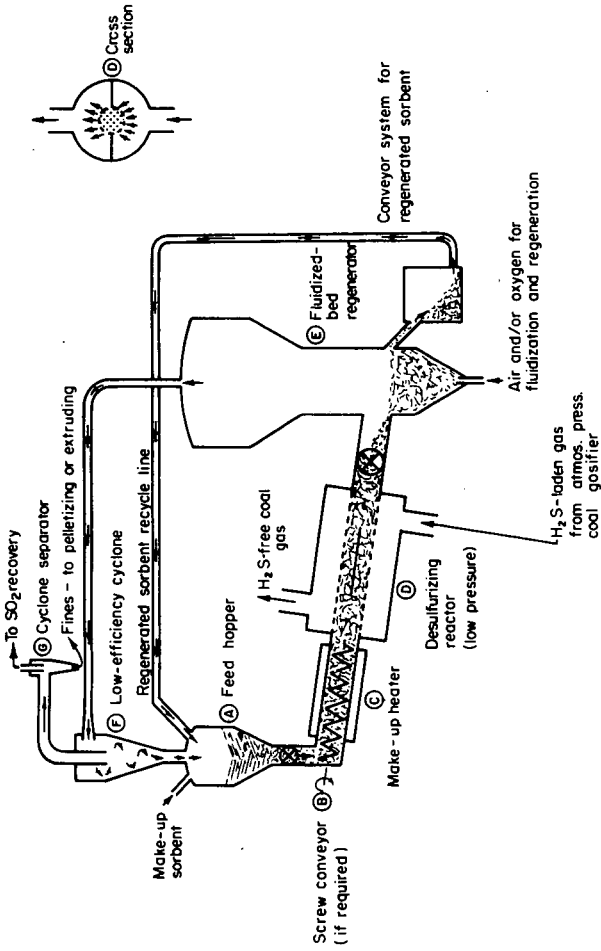


FIGURE 4. CONCEPTUAL PROCESS SCHEME FOR HIGH-TEMPERATURE, SOLID-GAS REACTION IN A MOVING BED WITH REGENERATION IN A FLUIDIZED BED

REFERENCES

- (1) "Report of the Cornell Workshops on The Major Issues of a National Energy Research and Development Program", Published by Cornell University, Ithaca, New York (December, 1973), p 76.
- (2) Abel, W. T., et al., "Removal of Hydrogen Sulfide from Hot Producer gas by solid Sorbents", RI 1947, Morgantown Energy Research Center, ERDA (1974).
- (3) Seil, Gilbert., E., DRY BOX PURIFICATION OF GAS, American Gas Association, New York, New York (1943), p 54.
- (4) Oldaker, E. C., et al., "Removal of Hydrogen Sulfide from Hot Low-Btu gas with Iron Oxide-Fly Ash Sorbents", Report No. MERC/TPR-75/1, ERDA, MERC, Morgantown, West Virginia (February, 1975).
- (5) Levenspiel, O., CHEMICAL REACTION ENGINEERING, 2nd Edition, John Wiley & Sons, Inc., New York (1972), p 215.
- (6) CATALYST HANDBOOK, Imperial Chemical Industries, Ltd., Distributed by Springer-Verlag, Inc., New York (1970), p 53.

## SEPARATION OF COAL HYDROGASIFICATION GASES BY PERMSELECTIVE MEMBRANES

W. J. Schell

Chemico Process Plants Co.  
El Monte, California 91734

### INTRODUCTION

It has been recognized for many years that non-porous polymer films exhibit a higher permeability toward some gases than towards others. As early as 1831 (1), investigations were reported on the phenomenon of enrichment of air with rubber membranes; however, not until 1950 (2) had the practical possibility of this and other gas separations with permselective membranes been seriously studied. Weller and Steiner (2, 3) in their classic papers, demonstrated the feasibility of separating oxygen from air and described practical processes for separation of hydrogen and helium from methane. Although their results were highly valuable in the development of the science of membrane separation, the calculated membrane area requirements for industrial processes were enormous.

The technical breakthrough in the application of membranes to gas separation came with the development of a process for preparing cellulose acetate membranes in a state which retains the permselective characteristics of ordinary cellulose acetate but which yields vastly increased gas permeability. These cellulose acetate membranes are prepared from a solution of the polymer which is cast on a smooth surface, partially dried then set or gelled in an ice-water bath. At this stage the membranes are heated in water to improve their selectivity characteristics and are then dried by a solvent exchange technique. The reason for the highly permeability values, together with the permselective characteristics of ordinary cellulose acetate, is the formation of an "active" layer on the air-dried surface of the membrane. This active layer has characteristics similar to those of ordinary cellulose acetate and has a thickness of the order of 0.1 micrometer ( $\mu\text{m}$ ) or less, whereas the total membrane thickness may range from approximately 75 to 125  $\mu\text{m}$ . Thus, the membranes are said to be asymmetric. The major portion of the membrane is an open-pore sponge-like support structure through which gases may flow freely. The permeability and selectivity characteristics of these membranes are functions of casting solution composition, film casting conditions, and post-treatment and are relatively independent of total membrane thickness.

### GAS SEPARATION THEORY

The steady state mass flux ( $J_i$ ) of component  $i$  through a homogeneous film of uniform thickness separating two gaseous phases is given by Fick's "First Law" of diffusion:

$$J_i = -D_i \frac{dC_i}{dx} = \text{constant} \quad 1)$$

where  $D_i$  = local diffusivity ( $\text{cm}^2/\text{sec}$ )  
 $C_i$  = local concentration of component  $i$   
 $x$  = the distance through the film

This relationship can be simplified when the gases do not chemically associate with each other and when the gases are sparingly soluble in the membrane material. In such cases, the diffusivity of the permeating gas is constant through the film and the solubility of the gas at the membrane surface is essentially directly proportional to its partial pressure in the gas phase adjacent to that surface, i. e., Henry's Law applies:

$$C_i = k_i P_i \quad 2)$$

where  $k_i$  is the solubility parameter and  $P_i$  is the partial pressure.

If we let superscript I refer to the high pressure or upstream side of the membrane and superscript II refer to the low pressure or downstream side of the membrane, Equation 1, after integration between  $C_i^I$  at  $x = 0$  and  $C_i^{II}$  at  $x = l$ , becomes:

$$J_i = \frac{k_i D_i (P_i^I - P_i^{II})}{l} \quad 3)$$

The product  $k_i D_i$  is termed the permeability coefficient ( $\bar{P}_i$ ) of the membrane for component i. This coefficient is independent of membrane thickness and pressure differential and the frequently used units are, cc(STP)-cm/cm<sup>2</sup>-sec-cm Hg. Another parameter of interest is the permeability rate, defined as  $\bar{P}_i/l$ , which is a measured characteristic of a given membrane with units, cc(STP)/cm<sup>2</sup>-sec-cm Hg. The total pressures,  $P^I$  and  $P^{II}$ , are given by the sums,  $P_i^I + P_j^I$  and  $P_i^{II} + P_j^{II}$ , respectively.

The ratio of fluxes of two gases through a membrane is given by:

$$J_i = \frac{\bar{P}_i (P_i^I - P_i^{II})}{\bar{P}_j (P_j^I - P_j^{II})} \quad 4)$$

The ratio  $\bar{P}_i/\bar{P}_j$  is defined as the ideal separation factor for component i with respect to component j in the membrane and is written  $\alpha_{i/j}$ .

From the previous discussion it can be seen that, if component i is the more permeable, increasing  $P_i^I$ , either by increasing the total pressure or the concentration of component i, will result in a higher membrane permeability rate. In addition, higher values for  $\alpha_{i/j}$  result in greater efficiency in gas separation.

If we define a permselectivity of the membrane to component i with respect to component j by  $\sigma_{ij}$ ,

$$\sigma_{ij} \equiv \frac{P_j^I P_i^{II}}{P_i^I P_j^{II}} \quad 5)$$

it can be shown from Equations 4 and 5 that:

$$\sigma_{ij} = \alpha_{i/j} \frac{P_j^I}{P_i^I} \frac{(P_i^I - P_i^{II})}{(P_i^I - P_j^{II})} \quad 6)$$

It can be seen from Equation 6 that as  $P^{II} \rightarrow 0$  or  $P^I/P^{II} \rightarrow \infty$ , the permselectivity of the membrane approaches the ideal separation factor, i. e.:

$$\lim_{P^{II} \rightarrow 0} \sigma_{ij} = \alpha_{i/j} \quad 7)$$

It is evident then that by increasing the feed pressure to product pressure ratio,  $P^I/P^{II}$ , an increase in the efficiency of the separation of the gas mixture is obtained.

Other system variables that will have an effect on the separation process are temperature and relative humidity of the gas. Usually an increase in temperature increases the permeability and decreases the separation factor. The effect of relative humidity is variable and has not been reported in the literature to any great extent.

#### MEMBRANES AND MEMBRANE SYSTEMS

The casting solutions for preparation of the membranes discussed herein contain cellulose diacetate, cellulose triacetate, acetone, dioxane, methanol and acetic acid or maleic acid. The solution is cast at a thickness of 0.010 in. and is gelled in ice water. The resulting membranes are heat-treated in water at 85 to 98°C for several minutes and are then dried by solvent exchanging the water with organic solvents followed by evaporation of the remaining solvent. Drying is necessary for application to gas separation and this procedure serves to prevent the membrane from shrinking and losing its asymmetric character upon removal of water.

The gas permeability measurements for the flat membranes were made in circular (2.93 cm<sup>2</sup> membrane area or 0.0316 ft<sup>2</sup>) test cells. Single gases at 23 to 25°C were brought into contact with the dense active layer side of the membrane at a regulated pressure of 15 to 750 psig, causing a portion of the gas to permeate through the membrane. The permeate gas was removed from the opposite side of the membrane at atmospheric pressure. The permeation rates were measured either by the displacement of a soap bubble in a 5 ml gas buret or with a wet-test meter. The measured permeation rates and separation factors for the single gases with flat-sheet membranes are shown in Table 1, measured at 100 psi pressure differential, along with literature values for 0.001-in. cellulose acetate films. It can be seen that the permeation rates of the asymmetric membranes range from 600 to over 1000 times those of the films while essentially retaining the selectivity for gases. The membranes exhibit an exceptionally high permeation rate for hydrogen and helium and are particularly permselective for hydrogen relative to carbon monoxide and methane. This evidence confirms the continuity of the thin active layer and demonstrates the improvement in membrane separation technology.

Cellulose acetate membrane modules have been manufactured in our facilities for several years now for use in water desalination. These modules have a spiral-wound configuration (6) that has the advantage of compactness and low cost. For example, the dimensions of such a module are 4-in. in diameter by 3-ft in length containing approximately 70 ft<sup>2</sup> of membrane. Development of similar modules with dry membrane for gas separation will provide gas permeability rates of the order of 3200 - 9500 SCFH at 750 psig for hydrogen.

TABLE I

## PERMEABILITY PROPERTIES OF FLAT CELLULOSE ACETATE MEMBRANES AND FILMS

	Permeability*, $\frac{\text{cc(STP)} \times 10^8}{\text{cm}^2 \text{-sec-cm Hg}}$				Separation Factor, $\alpha$							
	H <sub>2</sub>	CO <sub>2</sub>	O <sub>2</sub>	CO	CH <sub>4</sub>	N <sub>2</sub>	He/CH <sub>4</sub>	H <sub>2</sub> /N <sub>2</sub>	H <sub>2</sub> /CH <sub>4</sub>	CO <sub>2</sub> /CO	CO <sub>2</sub> /CH <sub>4</sub>	O <sub>2</sub> /N <sub>2</sub>
Film, 0.001-in. thick (4)	53.5	-	-	-	0.55	0.55	97	-	-	-	-	-
Film, 0.001-in. thick (5)	19.7	20-24	2.8-3.5	-	-	0.7-0.95	-	~25	-	-	-	~4.0
Membrane, Sample 1	32,400	28,000	15,800	2110	606	583	486	55	58	48	46	27
Membrane, Sample 2	32,800	29,310	16,100	2110	612	601	467	55	63	49	48	27
Membrane, Sample 3	33,900	28,600	16,400	2230	639	627	506	54	57	46	45	26

\*A permeability of 30,000 cc(STP)  $\times 10^{-8}$  /cm<sup>2</sup>-sec-cm Hg corresponds to 0.184 SCFH/ft<sup>2</sup> membrane/psi pressure differential.

## APPLICATION OF MEMBRANE SYSTEM TO COAL UTILIZATION PROCESSES

The feasibility of adapting permselective membranes to coal utilization processes is described in the following paragraphs. Two processes were chosen from contract reports to the U. S. Department of Interior (7, 8).

In the two processes, the membrane separation units described are assumed to have the permeability and separation properties of the asymmetric cellulose acetates described previously in Table 1. It is also assumed throughout that all gas streams will have been pretreated for removal of acid gases. The resulting feed gases may then be considered to be a two-component system of hydrogen and methane-carbon monoxide (carbon monoxide and methane have similar permeabilities) and a computer program can be used to predict the permeate stream compositions.

### Hydrogasification of Lignite

Figure 1 is a schematic diagram showing how membrane gas separators could be used to advantage in processing the gas from the hydrogasification of lignite. In this case the desired product is high Btu pipeline gas and the membrane separations are incorporated into the Institute of Gas Technology overall Process Block Flow Diagram (7) in order to reduce the size of several pieces of equipment and to produce 4% more methane with a higher Btu value.

The Prepurification Unit I effluent gas is cooled to 100°F to remove water and is then fed (Figure 1) into a spiral wound membrane separation unit which separates almost all of the hydrogen from the carbon monoxide and methane. The carbon monoxide and methane stream then has about 65% of the volume of the original stream and can be fed to a carbon monoxide shift reactor where the low concentration of hydrogen enables the reaction to be shifted further to the right ( $\text{CO} + \text{H}_2\text{O} \rightleftharpoons \text{CO}_2 + \text{H}_2$ ), therefore consuming considerably less steam than otherwise required. The overall result is that the carbon monoxide shift reactor size is reduced and the heat load of the waste heat recovery unit is reduced. The hydrogen-bearing permeate stream comes from the membrane unit at low pressure and must be compressed and cooled before it is sent to the Prepurification Unit II. After removal of carbon dioxide and the trace of hydrogen sulfide, the hydrogen stream is fed to the methanation unit where carbon monoxide is converted into methane.

The second membrane separation unit processes the effluent gas after waste heat recovery by removing most of the 4.4% hydrogen and recycling it back to the methanation unit. The recovered hydrogen allows about a 4% increase in the volume of methane produced and an increase in the Btu value of the pipeline gas.

The cost of the membrane units is believed to be small in comparison with the savings to be gained by reducing the size of the carbon monoxide shift reactor and waste heat recovery unit and reducing the amount of steam consumed so that the overall plant should be less costly. In addition, the incorporation of the membrane separators should allow greater variation in operating conditions and compositions of intermediate gas streams.

### Coal Oil Hydrogenation

Membrane gas separation may also be applied to coal oil hydrogenation such as the Coal Oil Energy Development (C. O. E. D.) process (8). The hydrogenation unit is fed C. O. E. D. oil from the pyrolysis unit along with a mixture of fresh and recycle hydrogen. The membrane separator removes most of the methane

and heavier hydrocarbons from the recycle hydrogen stream at high pressure. The one-pass membrane unit operating at 1050 psig increases the recycle hydrogen concentration from 43% to over 90%, with the accompanying improvement in the hydrogenation efficiency and reduction in size of the hydrogenation unit. The methane and hydrocarbon gas stream contains less than 2% hydrogen and after extraction of the higher hydrocarbons would be ideal for pipeline gas.

#### REFERENCES

1. J. V. Mitchell, J. Roy. Inst., 2, 101, 307 (1831).
2. Sol Weller and W. A. Steiner, J. Appl. Phys., 21, 279 (1950).
3. Sol Weller and W. A. Steiner, Chem. Eng. Prog., 46, 585 (1950).
4. P. K. Gantzel and U. Merten, Ind. Eng. Chem. Process Des. Develop., 9, 331 (1970).
5. Modern Plastics Encyclopedia, Oct. (1969).
6. U.S. Patent #3,417,870 by D. T. Bray, Assignment to Secretary of the Interior.
7. Institute of Gas Technology, Chicago, Ill., "Cost Estimate of a 500 Billion Btu/Day Pipeline Gas Plant via Hydrogasification and Electrothermal Gasification of Lignite," Office of Coal Research, R&D Report No. 22, Interim No. 4, pgs. 6-7, Contract No. 14-01-0001-381.
8. FMC Corporation, Princeton, New Jersey, "Char Oil Energy Development," Appendice I, Table XV, RSIS2, Office of Coal Research, Washington, D.C., Contract No. 14-01-001-235.

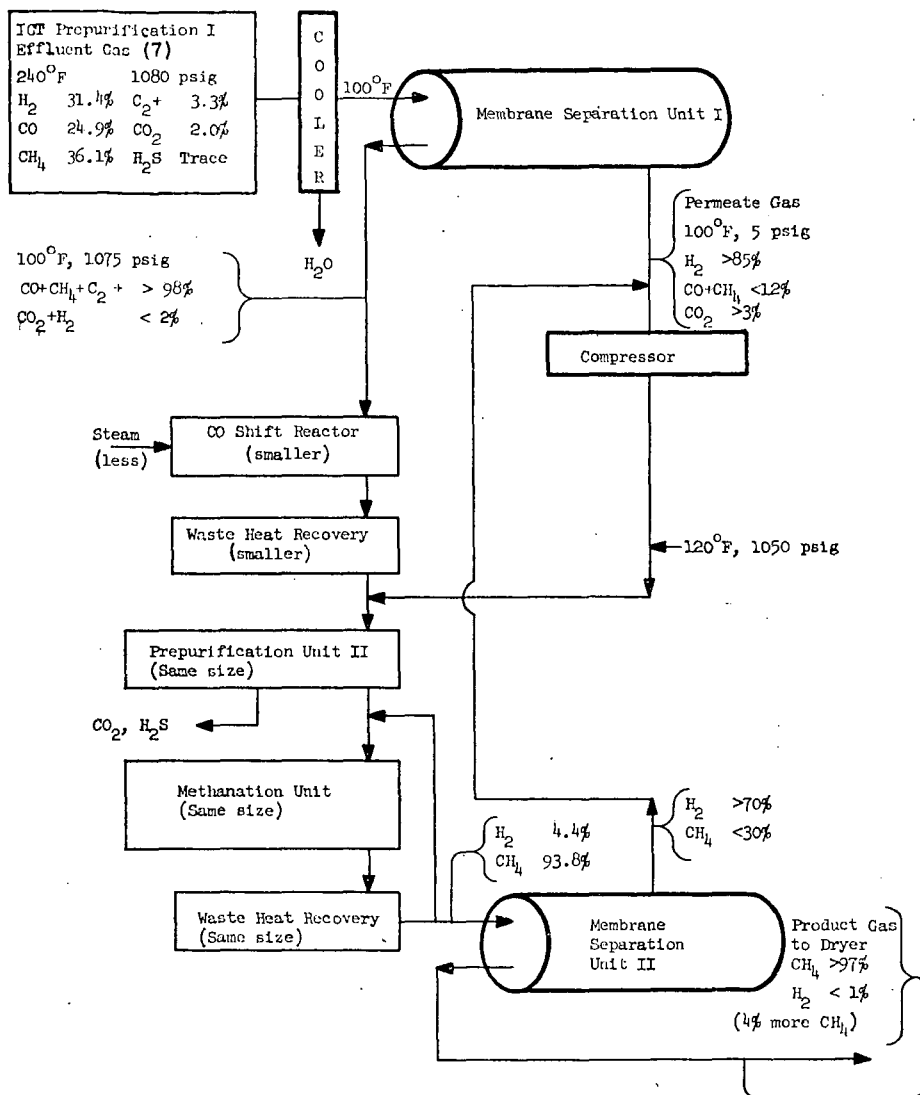


Figure 1. SCHEMATIC - APPLICATION OF MEMBRANE GAS SEPARATIONS IN A LIGHT GAS HYDROGASIFICATION PROCESS

## COMBINED POWER CYCLE USING LOW

## BTU GAS PRODUCED FROM THE KELLOGG MOLTEN SALT

## COAL GASIFICATION PROCESS

C. A. KUMAR, L. D. FRALEY, S. E. HANDMAN

RESEARCH &amp; ENGINEERING DEVELOPMENT

THE M. W. KELLOGG COMPANY

HOUSTON, TEXAS

INTRODUCTION

In recent years, it has become increasingly important to look for alternate sources of energy on a commercially feasible basis. In the midst of the present energy crisis, coal remains the most abundant source of energy in this country. However, the time honored techniques used to convert coal into electrical power no longer satisfy the needs of the power industry. Also, the public and the industry alike have grown to be ecology conscious; there is an ever increasing emphasis on burning "clean" fuel. A direction now established for increasing the economics of power generation is to exploit the use of a combined gas turbine-steam turbine power cycle. The relatively inexpensive gas turbine extends operation into the higher temperature range (presently 1950°F) and the temperature limit on gas turbine development has yet to be established. However, the gas turbine requires a clean fuel, natural gas or clean liquids. Low Btu fuel obtained from The M.W. Kellogg Molten Salt Coal Gasification Process, currently under development, when used in conjunction with a gas turbine-steam turbine combined power cycle system provides for an efficient method of generating electrical power from high sulfur, high ash coal while minimizing environmental pollution.

DISCUSSION

Gasification of coal using Kellogg's Molten Salt Process has been described in detail elsewhere (1, 2, 3). The overall process converts the heating value of high sulfur coal to fuel gas with a lower heating value of 100 to 150 Btu/SCF at a conversion efficiency of around 90% with most of the sulfur retained by the melt. The gasifier is set to operate at 260 psia and 1700°F and compressed air is used to partially burn coal to produce the fuel gas at these conditions.

The work to develop the Kellogg Molten Salt Coal Gasification Process for SNG (Substitute Natural Gas) has been modified to develop a process that is compatible with the combined cycle concept. (See Figure 1.)

There are four systems in the process:

1. Gasifier --a single pressure vessel where molten sodium carbonate catalyzes the partial oxidation of coal by air to produce a raw fuel gas. A typical composition is shown in Table 1.
2. Coal and Carbonate Feed --supply coal and make-up sodium carbonate at pressure to the gasifier.
3. Gas Conditioning --a series of heat exchanges and gas washes make the raw gas compatible with a gas turbine.
4. Carbonate Recycle --the stream which purges ash from the gasifier is approxi-

mately 70% sodium carbonate and 8% sodium sulfide. The system recovers the sodium for recycling to the gasifier.

### COMBINED POWER CYCLE

The overall efficiency of a combined cycle power plant burning low Btu gas produced from the Kellogg process is dependent on the coal gasification efficiency--including the salt cleanup and regeneration--and the temperature-pressure conditions in the steam generation system. Salt recovery technique thus is one of the key features in the performance of this cycle. The sensible heat from the melt purge (@ 1700°F) is used to preheat the air supply to the gasifier (to 990°F). (See Figure 2.) Most of the salt is recovered by evaporation as carbonate for recycle and the heat for evaporation is provided from the gas turbine exhaust. Sulfur retained by the melt is converted to hydrogen sulfide by carbonation and then recovered as elemental sulfur in a nearby Claus plant.

The fuel gas leaving the gasifier is cooled in a series of heat exchangers to a temperature of around 175°F before being sent to a scrubber. The major part of this heat is utilized for the production of steam and BFW heat for the steam system (2400 psia/1000°F/1000°F) as well as for reheating the scrubbed fuel gas back to 500°F before being sent into the gas turbine. The scrubbing operation provides the CO<sub>2</sub> needed for carbonation of the salt, while scrubbing with water eliminates sodium. The only fixed nitrogen in the fuel is a trace of NH<sub>3</sub> and thus the fuel gas produced is quite clean. Also, sodium carbonate being a catalyst gasifies coal completely without the production of associated coal distillates. For example, using Ohio Clarion High Sulfur (4.65%) Coal in the Kellogg process, it has been determined that more than 90% of sulfur is retained by melt for recovery later. This results in 0.78 lb SO<sub>2</sub>/MMBtu in the flue gas without any scrubbing to remove SO<sub>2</sub>.

The gasification system distributes the heating value of the coal into four parts. (See Table 2.)

The sensible heat in the fuel gas is available at various temperature levels. This requires a close integration with the steam system of the combined cycle so that it is used in the most efficient manner.

The number and type of interfaces just described mean that the gasifier and combined cycle must be tightly integrated if the overall system is to be very efficient.

Figure 2 shows the result of just such an integration. A commercially available gas turbine with 1950°F inlet temperature and a 2400 psia/1000°F/1000°F steam cycle were used. The match up between the steam cycle and sensible heat, both in the fuel gas and flue gas, is shown in Figure 3.

These curves show that the heat interchanges are arranged in such a fashion that minimum temperature differentials of around 40°F are observed at the pinch points. This, along with the fact that heat available at the gasifier level is limited to steam generation, has required that BFW heating and steam generation be done in more than one step. The distribution of power among various components for a 120 eMW net plant is shown in Table 3.

It is estimated that integration of a gas turbine combined power cycle (with fully loading the gas turbine in conjunction with a 2400 psia/1000°F/1000°F steam system) with the Kellogg Molten Salt Coal Gasification process generates power at a net heat rate of around 9500 Btu/kw-hr or lower using available equipment (HHV).

UTILIZATION OF LOW ASH COAL

(e.g., Pittsburgh Seam Coal with 5.2% ash-1.3%S) Incorporating minor changes in the purge recycle and the power cycle discussed above, the molten salt process can be very effectively used with low ash coal. It is estimated that such a process would have a gasifier efficiency of over 95% with a 0.45 lb/MMBtu of SO<sub>2</sub> in the flue gas without any scrubbing. The overall efficiency of such a combined cycle power plant utilizing the low ash coal is estimated around 40% (8500 Btu/kwh based on HHV).

ECONOMICS

Any attempt at economic analysis in these days must be based more on underlying fundamentals of a system rather than on numbers.

However, in Table 4 is an attempt at a current analysis. This compares the cost of power generated by a conventional power plant equipped with a stack gas scrubber to the gasifier - combined cycle system. Both systems were considered to have an efficiency of 36%. Coal was assumed to be 20\$/ton, the conventional plant to cost 400\$/kw plus 55\$/kw for a scrubber. The gasifier - combined cycle system was estimated to be 375\$/kw. These parameters reflect the conditions at the end of 1974. Table 4 shows an 11% advantage for the gasifier - combined cycle system. This can be considered marginal since it is a system currently under development.

STATUS OF THE PROCESS

Extensive work has been done in testing the containment of the molten sodium carbonate bath for the production of high Btu pipeline quality gas (SNG). Basic data on the gasification process have been reported. Low Btu coal gasification is essentially an outcome of the Kellogg Molten Salt process for the production of SNG and as such most of the work done for the SNG process can easily be extended to the production of low Btu gas.

Thus, incorporating a combined cycle in conjunction with the Kellogg Molten Salt process, currently under development, for the production of low BTu gas, provides for a relatively easy way of obtaining power with the following advantages:

1. The Molten Salt gasifier will handle any type of coal including caking coals without pretreatment.
2. The catalytic action of the molten sodium carbonate promotes complete gasification of coal without the production of associated coal distillates, thus eliminating downstream fouling and some of the pollution control facilities that would otherwise be required.
3. The catalytic effect of sodium carbonate allows gasification at lower temperatures permitting higher gasification efficiency.
4. The system provides clean fuel gas for use in a gas turbine.
5. In the next five to ten years gas turbines possibly will be available with inlet temperatures of 2500°F and 3000°F. The power cycle efficiency in these cases are estimated to be 46% and 49%, respectively, based on HHV and low ash coal. And finally,
6. It is estimated that power plants using 3000°F inlet to gas turbine result in about 47% reduction in power costs compared to a conventional cycle (Table 4)

263  
REFERENCES

1. Cover, A.E., W.C. Schreiner, and G.T. Skaperdas, "The Kellogg Coal Gasification Process", paper presented at American Chemical Society Meeting, Washington, D.C., Sept. 1971.
2. Cover, A.E., W.C. Schreiner, and G.T. Skaperdas, "Kellogg's Coal Gasification Process", Chemical Engineering Progress, March 1973.
3. Cover, A.E., and W.C. Schreiner, "The Kellogg Molten Salt Process", paper presented at the 4th Conference on Synthetic Fuels from Coal, Oklahoma State University, Stillwater, Oklahoma, May 1974.

TABLE 1  
COAL AND FUEL GAS COMPOSITION

## COAL PROXIMATE ANALYSIS

% ASH	16.87
% VOLATILE	39.44
% FIXED CARBON	<u>43.69</u>
	100.00
% SULFUR	4.65
% MOISTURE	3.43
HIGHER HEATING VALUE - 11273 BTU/LB	

## FUEL GAS ANALYSIS

	WGT. FRACTION
N <sub>2</sub>	0.614
H <sub>2</sub> O	.02
CO <sub>2</sub>	.04
CO	.31
CH <sub>4</sub>	.006
H <sub>2</sub>	.01
H <sub>2</sub> S	<u>.0002</u>
	1.00
HIGHER HEATING VALUE - 137 $\frac{\text{BTU}}{\text{SCF}}$	

TABLE 2  
 DISTRIBUTION OF HIGHER HEATING VALUE  
 IN COAL AFTER GASIFICATION

1. FUEL GAS TO GAS TURBINE		
	HHV	72.5%
	NET SENSIBLE HEAT GAIN	1.8
2. STEAM GENERATED BY FUEL GAS		16.6
3. ASH PURGE LOSS		
	NET SENSIBLE HEAT LOSS	1.9
	COMBUSTIBLE (C, S)	6.7
4. SCRUBBER LOSS		<u>0.5</u>
		100%

GASIFIER EFFICIENCY (1) + (2) = 90.9%

TABLE 3  
DISTRIBUTION OF POWER FOR 120 e MW PLANT  
(REFER TO FIG. 1.) e

GAS TURBINE	69.3
STEAM TURBINE	<u>61.2</u>
GROSS	130.5 e MW
AUXILIARIES	6.5
BOOSTER COMPRESSOR	<u>4.0</u>
	10.5 e MW

POWER OUT (NET) = 120 e MW

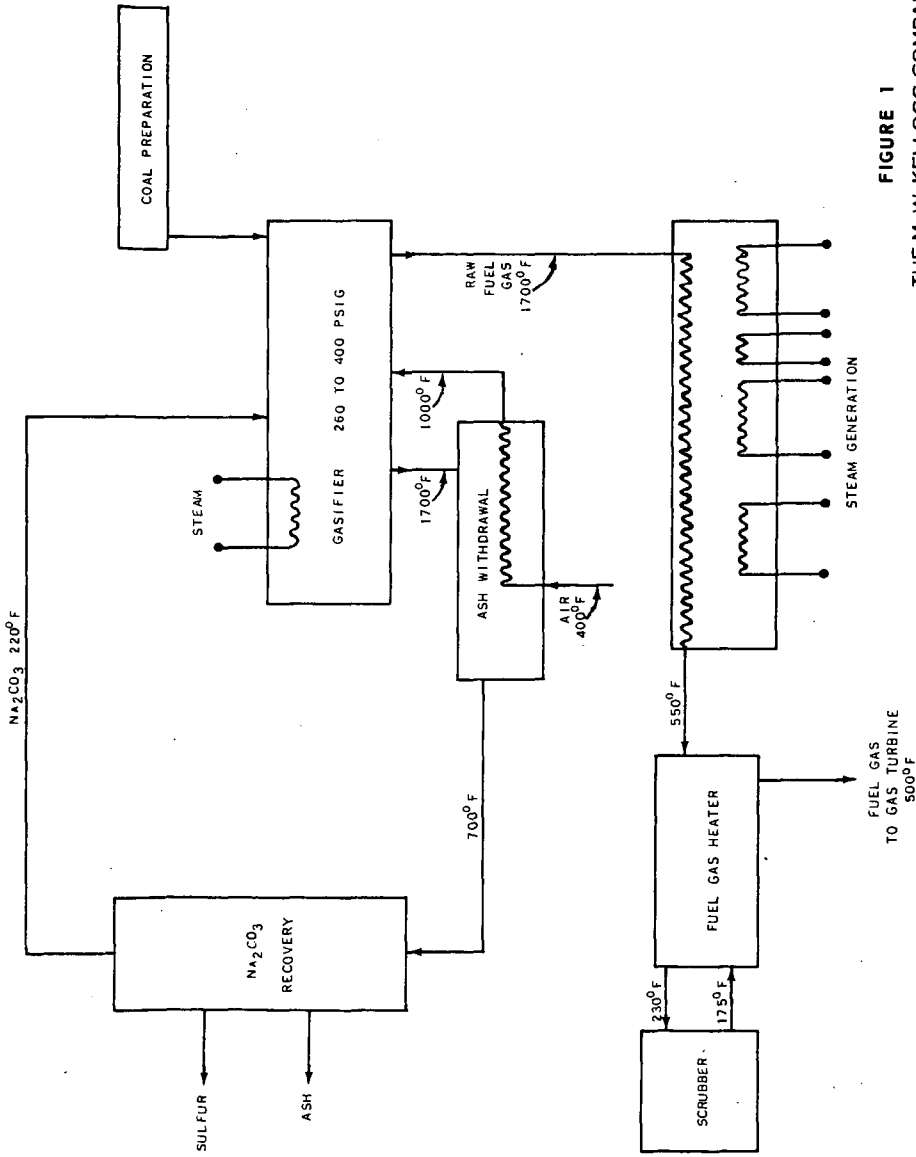
OVERALL EFFICIENCY = 36%

TABLE 4  
COMPARISON OF POWER COST FOR 480 MW CONVENTIONAL PLANT  
WITH SCRUBBER VS. GASIFIER COMBINED CYCLE PLANT

	CONVENTIONAL WITH SCRUBBER		GASIFIER COMBINED CYCLE	
CAPITAL	15.8	MILLS KWHR	13.0	MILLS KWHR
LABOR	0.3		0.3	
OPERATING	<u>10.6</u>		<u>10.7</u>	
TOTAL	26.7		24.0	

FUTURE PLANTS  
w/3000°F Inlet to  
Gas Turbine

9.2	MILLS
0.2	KWHR
8.8	
<u>18.2</u>	



**FIGURE 1**  
**THE M. W. KELLOGG COMPANY**  
A DIVISION OF PHILIPPIAN INCORPORATED  
**MOLTON SALT COAL GASIFICATION**

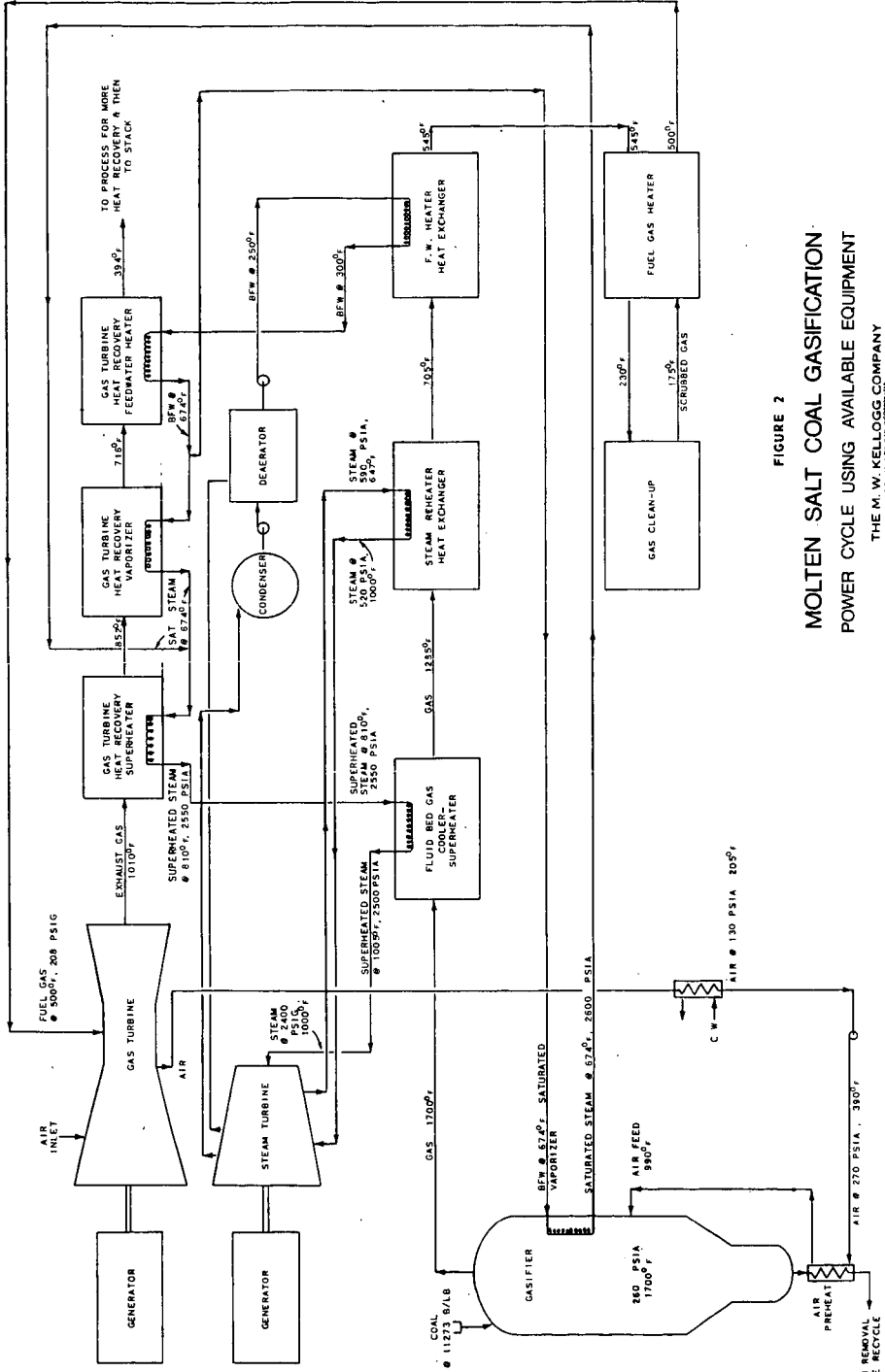
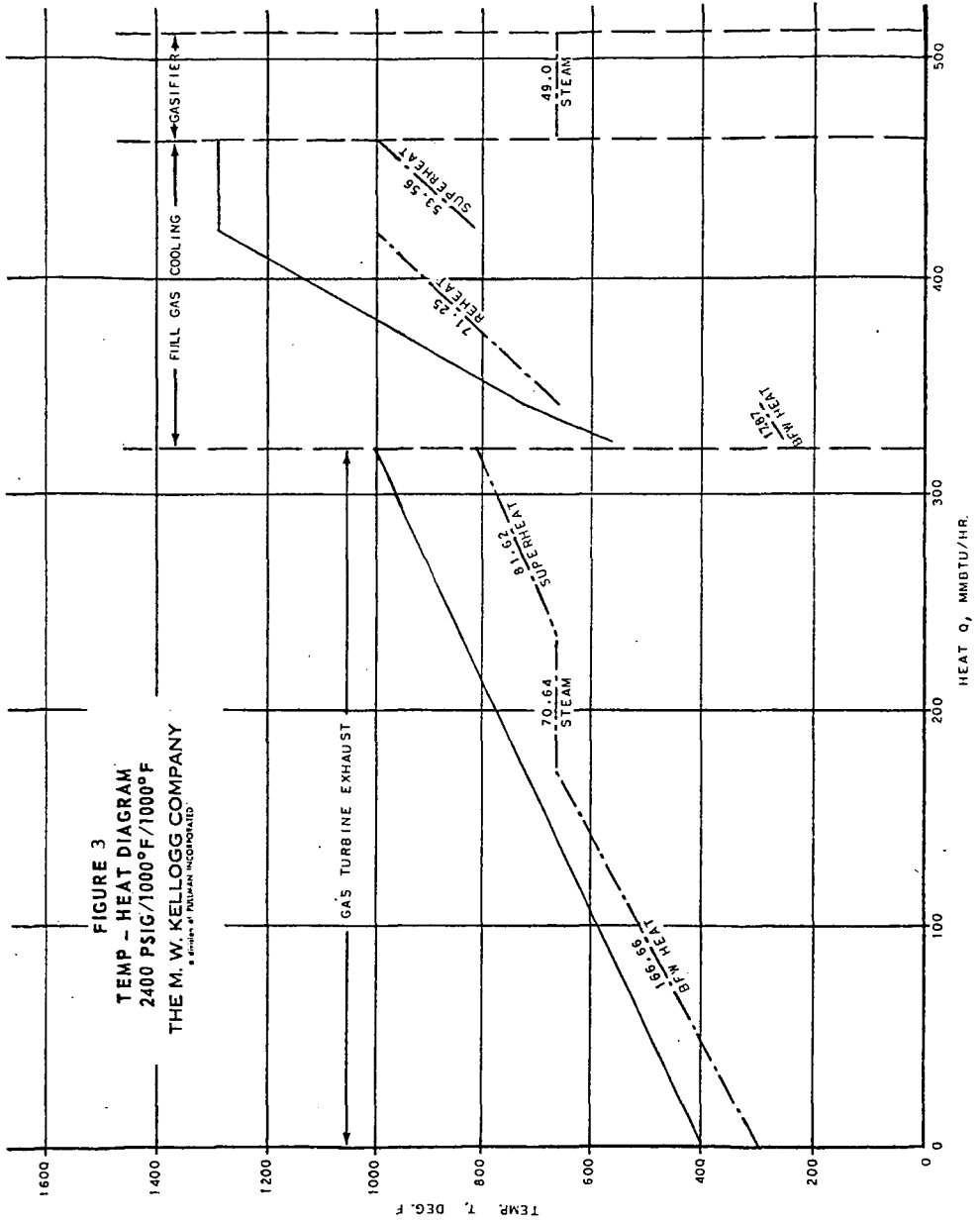


FIGURE 2  
**MOLTEN SALT COAL GASIFICATION  
 POWER CYCLE USING AVAILABLE EQUIPMENT**  
 THE M. W. KELLOGG COMPANY



INTERACTION OF MOLTEN SODIUM CARBONATE WITH COAL ASH  
COMPONENTS - ALUMINUM OXIDE. A. J. Darnell, Atomics  
International Division of Rockwell International Corporation, 8900 DeSoto  
Avenue, Canoga Park, CA 91304

A fundamental study is being made of the coal ash-melt interactions in relation to gasification of coal in molten sodium carbonate. In the present paper, the interaction of alumina with molten sodium carbonate is discussed. Alumina reacts with molten sodium carbonate to form sodium aluminate ( $\text{NaAlO}_2$ ) and carbon dioxide, i. e.,  $\text{Al}_2\text{O}_3(\text{s}) + \text{Na}_2\text{CO}_3(\text{l}) \rightarrow 2\text{NaAlO}_2(\text{s}) + \text{CO}_2(\text{g})$ . The sodium aluminate formed is very refractory (mp  $>1700^\circ\text{C}$ ) and is only sparingly soluble (10-20 ppm) in molten sodium carbonate. The sodium aluminate forms a protective coating around the unreacted alumina which slows down further reaction with the molten sodium carbonate. The rate of the reaction between  $\text{Al}_2\text{O}_3$  and  $\text{Na}_2\text{CO}_3$  has been examined over the temperature range  $900^\circ$  to  $1100^\circ\text{C}$  under an atmosphere of  $\text{CO}_2$  and with alumina particles ranging in size from  $1\ \mu$  to  $300\ \mu$ . Temperature cycling did not affect the protective nature of the coating of  $\text{NaAlO}_2$  on  $\text{Al}_2\text{O}_3$  even though sodium aluminate is known to undergo a solid phase transition at  $470^\circ\text{C}$ . This was demonstrated in tests in which the temperature was cycled from ambient to  $900^\circ\text{C}$  and in tests in which the temperature was held at  $900^\circ\text{C}$ . Identical rate loss curves were obtained in the two sets of tests.

Supported by U.S. Energy Research and Development Administration.